NONLOCAL PLASTICITY MODELS FOR LOCALIZED FAILURE

THÈSE N^{O} 2887 (2003)

PRÉSENTÉE À LA FACULTÉ ENVIRONNEMENT NATUREL, ARCHITECTURAL ET CONSTRUIT

Institut de structures

SECTION DE GÉNIE CIVIL

ÉCOLE POLYTECHNIQUE FÉDÉRALE DE LAUSANNE

POUR L'OBTENTION DU GRADE DE DOCTEUR ÈS SCIENCES

PAR

Simon ROLSHOVEN

Dipl.- Ing. Physikalische Ingenieurwissenschaft, TU Berlin, Allemagne
et de nationalité allemande

acceptée sur proposition du jury:

Dr M. Jirásek, directeur de thèse
Prof. A. Curnier, rapporteur
Prof. F. Frey, rapporteur
Prof. M. Geers, rapporteur
Prof. J. Planas, rapporteur

Lausanne, EPFL
2003

nonlocal
simon rolshoven 05
localization
plasticity
failure
concrete
normalized plastic strain
normalized coordinate x/l
0
1
2
3
4
5
6
7
8
9
L
e
x
z

Abstract

In quasi-brittle materials such as concrete, failure is preceded by highly localized deformation patterns. Localized failure is caused by strain softening, which cannot be described by classical local models, because they lack a length scale. Mathematically, the use of such models leads to ill-posed boundary value problems. If properly formulated, nonlocal models can provide a sound description of strain softening and model the complete failure process of quasi-brittle materials.

A bifurcation analysis is performed for a number of nonlocal plasticity models of the gradient and integral type, and the load-displacement response up to complete failure is computed. The nonlocal models are constructed mainly as enhancements of the standard small-strain, rate-independent, isotropic local plasticity model. Most nonlocal models respond in a physically appropriate manner at initial bifurcation, but for some models, the plastic zone widens at later stages of the loading process, and stresses remain at a spuriously high level.

For the integral format of two nonlocal models selected for further development, the Vermeer–Brinkgreve model and the ductile damage model, the bifurcation analysis is extended to hardening and the two-dimensional, plane strain setting. For both models, the enhancement is based on a modified hardening law, which depends in a specific way on the local hardening variable and its nonlocal counterpart. The analysis determines the range of material parameters for which the solution is regular and provides an analytical expression for the initial distribution of the rate of plastic strain. The use of the Vermeer–Brinkgreve model is restricted to softening, while the ductile damage model can be used for hardening and softening.

An efficient and robust iterative numerical algorithm for the stress return of integral-type nonlocal models that use the local and nonlocal hardening variable in the yield function is developed and implemented. Due to weighted averaging, the stress return is a coupled nonlinear complementarity problem. It is solved by a Jacobi-like iterative technique, derived in a rigorous manner for a special case and generalized based on a physical interpretation of the resulting equations.

In view of the numerical modeling of concrete, the nonlocal enhancement is applied to plasticity models with pressure-dependent yield functions and non-associated flow rules. Simulations of laboratory tests demonstrate that the nonlocal model regularizes localization due to softening and non-associated plastic flow. Neither the load-displacement response nor the propagation of the process zone depend in a spurious manner on the computational grid. For eccentric compression of a prismatic column under plane strain conditions, the trend for the size effect on structural strength and post-peak response is correctly predicted.

Kurzfassung

Dem Versagen quasi-spröder Materialien wie Beton geht eine starke Lokalisierung der Deformation voraus, die durch Entfestigung verursacht wird. Die Verwendung klassischer lokaler Modelle führt zu mathematisch schlecht gestellten Randwertproblemen, weil lokale Modelle keinen Längenparameter enthalten. Richtig formulierte nichtlokale Modelle hingegen können den gesamten Verformungsprozess quasi-spröder Materialien beschreiben.

Für eine Reihe von nichtlokalen Plastizitätsmodellen vom Gradienten- und Integraltyp wird eine eindimensionale Bifurkationsanalyse durchgeführt und die Spannungs-Dehnungs-Antwort bis zum Versagen untersucht. Die nichtlokalen Modelle basieren auf dem ratenunabhängigen, isotropen Plastizitätsmodell für kleine Deformationen. Bei der Bifurkation von der homogenen Lösung zeigen die meisten nichtlokalen Modelle physikalisch sinnvolles Verhalten; bei einigen Modellen kommt es jedoch in der Folge zur Ausdehnung der plastischen Zone. Die Spannung verbleibt in diesen Fällen trotz wachsender Dehnung auf zu hohem Niveau.

Das Vermeer-Brinkgreve-Modell und das Ductile-Damage-Modell werden für die weitere Entwicklung ausgewählt und unter Berücksichtigung von Verfestigung einer Bifurkationsanalyse im ebenen Verzerrungszustand unterzogen. Beiden Modellen gemeinsam ist die nichtlokale Erweiterung durch eine Fließfunktion, die in geeigneter Weise von der lokalen und der nichtlokalen Verfestigungsvariablen abhängt. Die Analyse liefert Kriterien für reguläre Lösungen und einen analytischen Ausdruck für die initiale Verteilung der plastischen Dehnrate. Bei geeigneter Wahl der Parameter kann das Ductile-Damage-Modell sowohl für Entfestigung als auch für Verfestigung verwendet werden, das Vermeer-Brinkgreve-Modell ist jedoch auf Entfestigung beschränkt.

Ein effizienter und robuster iterativer Algorithmus für den *stress return* nichtlokaler Modelle, bei denen die Fließfunktion von der lokalen und der nichtlokalen Verfestigungsvariable abhängt, wird vorgestellt und implementiert. Aufgrund der gewichteten Mittelung ist der *stress return* ein gekoppeltes nichtlineares Komplementärproblem, welches durch eine Art Jacobi-Iteration gelöst wird. Der Algorithmus wird für einen Sonderfall rigoros hergeleitet und anschliessend durch physikalische Interpretation der Ergebnisse verallgemeinert.

Im Hinblick auf die Modellierung von Beton wird die nichtlokale Erweiterung auf Plastizitätsmodelle mit druckabhängigen Fließfunktionen und nicht-assoziierten Fließregeln angewendet. Die numerische Simulation einfacher Experimente zeigt, dass die nichtlokalen Modelle die Lokalisierung aufgrund von Entfestigung und nicht-assoziiertem Fluss regularisieren. Weder die Last-Verschiebungs-Antwort noch die Entwicklung der Prozesszone hängen in unnatürlichem Maße von der Diskretisierung ab. Der Trend für den Größeneffekt der Strukturfestigkeit einer prismatischen Säule unter exzentrischer Kompression wird richtig vorausgesagt.

Version abrégée

La rupture des matériaux quasi-fragiles comme le béton est précédée de déformations fortement localisées. La cause de cette localisation est l'adoucissement. Celui-ci ne peut pas être décrit par des modèles locaux classiques, car ils ne contiennent pas de longueur interne. Appliqués à l'adoucissement, ces modèles mènent à des problèmes mathématiquement mal posés. Par contre, le choix des modèles non locaux permet de décrire d'une manière rigoureuse l'adoucissement et la désintégration complète des matériaux quasi-fragiles.

Les solutions de bifurcation possible sont étudiées pour un grand nombre de modèles non locaux, et la réponse force-déplacement est calculée numériquement jusqu'à la rupture. Les modèles non locaux sont conçus comme extensions de la plasticité classique isotrope pour petites déformations et indépendante du temps. Pour la plupart des modèles, on démontre un comportement physiquement réaliste à la bifurcation initiale, mais pour certains d'entr'eux, la taille de la zone plastique grandit par la suite et les contraintes restent trop élevées.

Pour deux modèles selectionnés, les formulations de type intégral du modèle de Vermeer & Brinkgreve et du modèle d'endommagement ductile, l'analyse de bifurcation est étendue au cas de l'écrouissage et de la déformation plane. Les deux modèles utilisent un critère de plasticité qui dépend d'une manière spécifique de la variable d'écrouissage et sa valeur non locale. La variable d'écrouissage non locale, obtenue par intégration spatiale pondérée, introduit une longueur interne. L'analyse donne une expression analytique pour la taille initiale de la zone plastique ainsi que la gamme de paramètres pour laquelle la solution est régulière. Le modèle de Vermeer & Brinkgreve est restreint essentiellement à l'adoucissement, tandis que le modèle d'endommagement ductile s'utilise pour l'adoucissement et l'écrouissage.

Un algorithme numérique efficace et stable est developpé et mis en œuvre pour des modèles non locaux du type intégral qui utilisent la variable d'écrouissage et sa valeur non locale dans le critère de plasticité. L'intégration pondérée de la variable d'écrouissage fait que le retour à la surface de plasticité est un problème complémentaire non linéaire couplé. Ce système est résolu par une méthode itérative du type Jacobi, laquelle est construite d'une manière rigoureuse pour un cas spécifique avant d'être généralisée de par l'interprétation physique du résultat.

Dans le but de modéliser le béton, la formulation non locale est appliquée à des modèles de plasticité non-associés dont le critère de plasticité dépend de la pression. Des simulations d'essais de laboratoire démontrent que les modèles non locaux régularisent la localisation due à l'adoucissement et à l'écoulement non-associé. La réponse force-déplacement ainsi que la propagation de la zone de plasticité ne dépendent pas anormalement du maillage. Dans le cas de la compression d'une colonne avec excentricité sous conditions de déformations planes, la tendance de l'effet de taille dans la résistance de la structure est correctement reproduite.

Acknowledgements

The research presented in this thesis was carried out at the Laboratory of Structural and Continuum Mechanics (LSC), headed by Prof. F. Frey, at the Swiss Federal Institute of Technology, Lausanne. I would like to thank Prof. F. Frey for the opportunity to work on this project.

I would like to express my deepest gratitude to my supervisor Dr. Milan Jirásek for valuable ideas and suggestions, and for numerous fruitful discussions.

I am grateful to the committee members, Prof. A. Curnier, Prof. F. Frey, Prof. M. Geers, Prof. J. Planas, and the president of the jury, Prof. M. Hirt, for their interest in this thesis, critical comments and suggestions.

I would like to thank my former colleague B. Patzák, the designer of OOFEM, the computer program the models were implemented in, for providing this excellent tool and for support in learning C++. My colleague P. Grassl deserves my gratitude for critical and stimulating discussions.

I thank the present and former collaborators of the LSC, St. Bordas, St. Commend, C. Falla Luque, P. Krawczyk, X. Nguyen, B. Rébora, B. Seem, M. Studer, and Th. Zimmermann, for making the LSC a nice and friendly place.

A very special note is reserved for Marie-Soleil: Thank you for encouraging me, for understanding, and simply for being there. And for the only color picture in this thesis.

The author gratefully acknowledges the financial support of the Swiss National Science Foundation under project FNS 2100-057062.99/1 and FNS 2000-068045.02/1.

Contents

List of selected symbols **xv**

1 Introduction **1**
1.1 Problem . . . 1
1.2 Literature survey . . . 1
1.3 Aim . . . 3
1.4 Outline . . . 3

2 Size effect and nonlocality **5**
2.1 Experimental evidence for size effect . . . 5
2.2 Nonlocal continuum models . . . 8
2.3 Nonlocal averaging . . . 10
2.4 Local plasticity . . . 12
2.5 Localization of plastic strain in a bar . . . 14

3 Gradient plasticity models **17**
3.1 General assumptions . . . 17
3.2 Classification . . . 17
3.3 Gradient models and nonlocality . . . 19
3.4 Strain-gradient elasticity . . . 20
3.5 Strain-gradient plasticity model of Chambon et al. . . . 22
3.5.1 Model description . . . 22
3.5.2 Bifurcation from a uniform state . . . 23
3.5.3 Evolution of plastic region . . . 26
3.6 Strain-gradient plasticity model of Fleck and Hutchinson . . . 30
3.6.1 Model description . . . 30
3.6.2 Localization analysis . . . 31
3.7 Mechanism-based strain-gradient plasticity . . . 31
3.7.1 Model description . . . 31
3.7.2 Localization analysis . . . 33
3.8 First-gradient plasticity model of Schreyer and Chen . . . 36
3.8.1 Model description . . . 36
3.8.2 Localization analysis . . . 36
3.9 Second-gradient plasticity model of Aifantis . . . 38
3.9.1 Model description . . . 38
3.9.2 Localization analysis . . . 38

3.9.3 Nonlinear softening . . . 39
3.9.4 Influence of a physical boundary . . . 42
3.10 Aifantis model with first and second gradients . . . 43
3.11 Gradient elastoplasticity . . . 46
3.12 Ductile damage model of Geers and coworkers . . . 47
3.12.1 Model description . . . 47
3.12.2 Bifurcation from a uniform state . . . 48
3.12.3 Evolution of plastic region . . . 52
3.13 Overview of gradient plasticity models . . . 53

4 Integral-type nonlocal plasticity models 55
4.1 General assumptions . . . 55
4.2 Model with nonlocal softening variable . . . 55
4.2.1 Model description . . . 55
4.2.2 Plastic region far from the boundary . . . 55
4.2.3 Plastic region close to the boundary . . . 58
4.3 Vermeer–Brinkgreve model . . . 59
4.3.1 Motivation . . . 59
4.3.2 Model description . . . 61
4.3.3 Plastic region far from the boundary . . . 62
4.3.4 Plastic region close to the boundary . . . 63
4.3.5 Nonlinear softening . . . 64
4.4 Models motivated by ductile damage . . . 65
4.4.1 Ductile damage model of Geers and coworkers . . . 66
4.4.2 Nonlocal Gurson model . . . 68
4.5 Models with nonlocal stress and nonlocal strain . . . 71
4.6 Model with nonlocal plastic strain . . . 72
4.6.1 Model description . . . 72
4.6.2 Localization analysis . . . 73
4.6.3 Locking mechanism . . . 74
4.7 Thermodynamics with internal variables . . . 74
4.7.1 Thermodynamic framework for local plasticity . . . 75
4.7.2 Thermodynamic framework for nonlocal plasticity . . . 76
4.8 Models with double nonlocal averaging . . . 79
4.8.1 Models with nonlocal elastic part . . . 79
4.8.2 Models with local elastic part . . . 81
4.8.3 Model of Borino and coworkers . . . 81
4.8.4 Model of Svedberg and Runesson . . . 82
4.9 Nilsson's model . . . 86
4.9.1 Model description . . . 86
4.9.2 Localization analysis . . . 88
4.9.3 Dissipation properties . . . 89
4.10 Dissipation properties of models with simple averaging . . . 90
4.11 Overview of integral-type nonlocal model . . . 91
4.12 Choice of a nonlocal model . . . 93

5 Nonlocal models with hardening **95**
5.1 Motivation . . . 95
5.2 One-dimensional bifurcation analysis . . . 95
5.3 Consequences of the bifurcation analysis . . . 98
5.4 Bifurcation analysis under plane strain conditions . . . 99
5.4.1 Plasticity model . . . 99
5.4.2 Analysis . . . 99
5.4.3 Discussion . . . 102
5.5 A convenient hardening law . . . 103
5.6 Uniaxial tensile test . . . 105

6 Stress return for nonlocal plasticity **107**
6.1 Motivation . . . 107
6.2 Local Drucker–Prager plasticity model . . . 107
6.2.1 Model equations . . . 107
6.2.2 Stress return algorithm for the regular case . . . 109
6.2.3 Stress return algorithm for the vertex case . . . 110
6.3 Nonlocal extension of the Drucker–Prager model . . . 111
6.4 Stress return for the Vermeer–Brinkgreve model . . . 112
6.5 General nonlocal stress return . . . 114
6.6 Efficient implementation . . . 116

7 Examples with nonlocal Drucker–Prager model **117**
7.1 Biaxial compression under plane strain . . . 117
7.1.1 Test geometry and material parameters . . . 117
7.1.2 Discussion of results for aligned meshes . . . 120
7.1.3 Discussion of results for misaligned meshes . . . 122
7.2 Triaxial compression under plane strain . . . 122
7.2.1 Motivation . . . 122
7.2.2 Test geometry and material parameters . . . 124
7.2.3 Discussion . . . 126
7.3 Eccentric compression . . . 126
7.3.1 Motivation . . . 126
7.3.2 Test series . . . 127
7.3.3 Numerical model . . . 128
7.3.4 Material model and calibration . . . 129
7.3.5 Discussion . . . 131

8 Nonlocal Rankine plasticity with examples **135**
8.1 Nonlocal Rankine plasticity model . . . 135
8.2 Three-point bending test . . . 137
8.2.1 Test geometry and model parameters . . . 137
8.2.2 Discussion . . . 138

9 Conclusions **143**

List of selected symbols

σ	stress (scalar)
ε, ε_{p}	strain (scalar), plastic strain (scalar)
$\boldsymbol{\sigma}$, $\boldsymbol{s}$	stress tensor and its deviatoric part
$\boldsymbol{\varepsilon}$, $\boldsymbol{e}$	strain tensor and its deviatoric part
$\boldsymbol{\varepsilon}_{\mathrm{p}}$, $\boldsymbol{e}_{\mathrm{p}}$	plastic strain tensor and its deviatoric part
f	yield function
$F(\boldsymbol{\sigma})$	equivalent stress
$\boldsymbol{f}$	derivative of yield function with respect to stress
g	flow potential
$\boldsymbol{g}$	flow direction
λ	plastic multiplier
κ, $\bar{\kappa}$, $\hat{\kappa}$	hardening variable, its nonlocal average, and $\hat{\kappa} = m\bar{\kappa} + (1-m)\kappa$
m	parameter of the Vermeer–Brinkgreve model
$\alpha(r)$	weight function for spatial weighted average
R	interaction radius of the bell-shaped weight function
σ_{Y}	yield stress in uniaxial tension
τ_{Y}	yield stress in shear
$h(\kappa)$	local hardening law
$h_{\mathrm{NL}}(\kappa, \bar{\kappa})$	general nonlocal hardening law
H_{L}	local hardening modulus
H_{NL}	nonlocal hardening modulus
$h_1(\bar{\kappa})$	nonlocal function in the hardening law for ductile damage model
$h_2(\kappa)$	local function in the hardening law for ductile damage model
σ_0	initial yield stress in uniaxial tension
τ_0	initial yield stress in shear
H	hardening modulus, parameter of the linear hardening law
κ_{c}	parameter of the exponential softening law
$\boldsymbol{D}$, $\boldsymbol{C}$	elastic stiffness tensor, elastic compliance tensor
E, ν, G, K	Young's modulus, Poisson's ratio, shear modulus, bulk modulus
c_ϕ, c_ψ	dilatancy coefficient, friction coefficient
$\delta(x - x_0)$	Dirac distribution
$\langle \cdot \rangle$	positive part operator
$\| \cdot \|$	Euclidean norm
I_1, J_2	first invariant, second deviatoric invariant

Chapter 1

Introduction

1.1 Problem

The classical models for plasticity, based on the standard continuum theory and constitutive equations that are *simple* in the sense of Noll (1972), fail to provide an objective description of localized material failure. For sufficiently strong softening or non-associated flow rules, ellipticity of the governing differential equations is lost, and the boundary value problem becomes ill-posed. The problem admits irregular solutions with the rate of plastic strain localized into a set of zero measure, i.e., a curve in two dimensions or a surface in three dimensions.

Deviations of the observed material behavior from the prediction of the standard theories typically appear only if the characteristic wavelength of the deformation field becomes comparable to the intrinsic length of the material. This length depends on the characteristic size and spacing of major heterogeneities in the microstructure. In the elastic range, this happens only in special cases, e.g., in the immediate vicinity of a crack tip, or during the propagation of short waves. However, once the material response becomes highly nonlinear, deviations from local theory are amplified and may lead to size effects that cannot be predicted or explained by standard theories.

The actual width of the zone of localized plastic strain is related to the heterogeneous material microstructure. It can be correctly predicted only by so-called *nonlocal* models that have a parameter with the dimension of length. This length scale is absent from standard theories of plasticity, and should be introduced by an appropriate enhancement. A properly formulated nonlocal theory has a regularizing effect, i.e., it acts as a *localization limiter* that restores the well-posedness of the boundary value problem and prohibits solutions with the plastic strain rate localized into a set of zero measure.

1.2 Literature survey

In the past, a number of enhanced plasticity models have been proposed. They all contain at least one length scale. Depending on the way the length scale is introduced into the model, they are traditionally divided into *gradient* models that work with differential operators and *integral-type* nonlocal models that use spatial weighted averages.

A number of gradient plasticity models are based on the elastic strain-gradient the-

ory, which has its roots in the pioneering work of Toupin (1962) and Mindlin (1965). This framework enriches the kinematic description of the continuum by strain gradients, and from thermodynamic arguments, the model also contains their thermodynamic conjugates, the so-called double stresses. Probably the first extension of strain-gradient theory to plasticity was proposed by Dillon and Kratochvil (1970), but this model was not meant to serve as a localization limiter. In the context of the couple-stress theory, Fleck and Hutchinson (1993) developed a flow theory of strain-gradient plasticity. Later, the theory was reformulated in the context of the general strain-gradient theory (Fleck and Hutchinson 1997), which takes into account not only the microcurvatures (rotation gradients) but also the stretch gradients. A key ingredient of this model is the dependence of the yield function on both the stress and the double stress. Chambon et al. (1998) proposed an elastoplastic extension that shares some similarities with the Fleck–Hutchinson model, but for this model the yield function depends only on the stress.

A second group of gradient models enriches the conventional plasticity theory by gradients of internal variables. In the historically first model of this type, the yield stress is a function of the hardening variable and its first and second gradient (Aifantis 1984). The special case where the yield stress depends only on the hardening variable and its second gradient became widely popular and its theoretical formulation and numerical implementation was later developed by a number of authors (Coleman and Hodgdon 1985; Mühlhaus and Aifantis 1991; Vardoulakis and Aifantis 1991; de Borst and Mühlhaus 1992; Pamin 1994; de Borst and Pamin 1996; Comi and Perego 1996; Li and Cescotto 1996; Ramaswamy and Aravas 1998). A model using only the hardening variable and its first gradient has been proposed by Schreyer and Chen (1986) and Schreyer (1990). Drawing inspiration from implicit gradient damage models (Peerlings, de Borst, Brekelmans, and de Vree 1996), Geers, Engelen and coworkers proposed an implicit gradient plasticity model based on the concept of ductile damage (Geers, Engelen, and Ubachs 2001; Engelen, Geers, and Baaijens 2003). An essential component of this model is an enrichment of the yield stress. The yield stress depends on the hardening variable and an additional quantity, which can be interpreted as a nonlocal hardening variable, implicitly defined by the field of the hardening variable in the whole body through a Helmholtz-type differential equation.

Zervos et al. (2001) proposed a model that belongs to both groups. It can be interpreted as a strain-gradient theory with the yield stress dependent on the hardening variable and its second gradient.

Although some preliminary ideas can be traced back to the late 19th century (Duhem 1893), the development of modern nonlocal constitutive models of the integral type, i.e. using weighted spatial averages, started in the 1960s (Rogula 1965; Kröner 1966; Kunin 1966; Eringen 1966). These and other early studies on nonlocal elasticity, often motivated by homogenization of the atomic theory of Bravais lattices, aimed at a better description of phenomena taking place in crystals on a scale comparable to the range of interatomic forces. They showed that nonlocal continuum models approximately reproduce the dispersion of short elastic waves and improve the description of interactions between crystal defects such as vacancies, interstitial atoms and dislocations.

The first extension of integral-type nonlocal models to plasticity was proposed by Eringen. He developed nonlocal formulations of isotropically hardening plasticity in strain space (Eringen 1981), perfect plasticity with associated flow, and deformation theory of

plasticity (Eringen 1983). Eringen and Ari (1983) applied these models to simulations of the yielding zone at a fracture front. However, Eringen's formulation was not meant to serve as a localization limiter. The averaging operator was applied to the total strain tensor, which could lead to spurious instabilities (zero energy modes), as shown later in the slightly different context of an imbricate continuum (Bažant and Chang 1984).

In the context of continuum damage mechanics, Pijaudier-Cabot and Bažant (1987) proposed to apply nonlocal averaging to variables that are related to the inelastic processes and that can only grow or remain constant. This idea paved the way to formulations that work with nonlocal averages of internal variables or their conjugate thermodynamic forces. Development of such formulations for damage models is relatively straightforward, because the concerned variable driving the dissipative process (e.g., the damage energy release rate, or the equivalent strain) is usually directly related to the total strain and thus can easily be evaluated in a displacement-driven finite element procedure. In plasticity, however, the problem is more delicate, since the concerned variable is typically the accumulated plastic strain, which must be computed from the consistency condition that has no longer a local character.

The first nonlocal plasticity model aiming at an objective description of localization was proposed by Bažant and Lin (1988). In the past decade, several other nonlocal formulations of softening plasticity were advanced (Leblond et al. 1994; Vermeer and Brinkgreve 1994; Brinkgreve 1994; Nilsson 1994; Strömberg and Ristinmaa 1996; Planas et al. 1996; Svedberg 1996; Nilsson 1997; Svedberg and Runesson 1998; Polizzotto et al. 1998; Borino et al. 1999; Borino and Failla 2000).

1.3 Aim

The aim of this thesis is to find a regularized plasticity model for strain-softening materials that acts as a localization limiter, both for localization due to softening and due to non-associated plastic flow. A robust numerical algorithm should be developed and implemented, and the model should finally be used for the analysis of plain concrete. Based on a detailed analysis of the existing regularized plasticity models, formulations that are suitable for extensions to multiple dimensions and for applications to real problems should be identified, and the drawbacks of certain theoretically appealing formulations should be pointed out.

1.4 Outline

Chapter 2 is an introduction to size effect, continuum models with internal length scales and nonlocal averaging. The local plasticity framework is presented, and the basic problems of a local plasticity model under softening are explained in the one-dimensional setting.

Models that work with gradients are analyzed in Chapter 3, while integral-type nonlocal models are scrutinized in Chapter 4. The analysis is restricted to the one-dimensional setting and softening without initial hardening. The integral-type nonlocal models retained for further development are described in Sections 4.3 and 4.4, and further reading requires knowledge of the basic results presented in these sections.

For the selected integral-type nonlocal model, a bifurcation analysis for the case of hardening and for plane strain conditions is presented in Chapter 5. The concept for nonlocal enhancement is applied to the Drucker–Prager plasticity model in Chapter 6. This model serves as an example for the detailed description of the stress return algorithm for nonlocal plasticity models of this type.

Simple laboratory tests are analyzed with the nonlocal Drucker–Prager model in Chapter 7, including bi- and triaxial compression under plane strain and eccentric compression under plane strain. The nonlocal Rankine plasticity model, suitable for tensile failure of concrete, and its application to a three-point bending test are presented in Chapter 8.

The conclusions of the thesis are drawn in Chapter 9.

Chapter 2

Size effect and nonlocality

2.1 Experimental evidence for size effect

In uniaxial compression tests, plain concrete prisms of different length and same cross-sectional area show a size-dependent response (van Mier 1984, Chapter 4.4). Three different specimens of length $L = 50$, 100 and 200 mm, and same rectangular cross-sectional area $A = 100 \times 100\,\text{mm}$ were tested. They were supported at one end by a stiff brush that allowed lateral slip, and loaded with an axial force applied over a similar brush at the other end. This experimental setup limits the constraints introduced by the boundaries and thereby guarantees the one-dimensional character of the experiments. To allow post-peak measurements, the experiment was performed under displacement control.

For the pre-peak regime, i.e. before the maximum load has been reached, the nominal stress (load divided by cross-sectional area) is a unique function of nominal strain (top displacement divided by length), and does not depend on the specimen's length, see Fig. 2.1a. In the post-peak regime however, the response changes significantly with the length, and the structural response tends from ductile to brittle for increasing specimen length. If the nominal stress is plotted as a function of the top displacement in the post-peak (top displacement minus its value at peak) instead, the curves match within the experimental scatter, see Fig. 2.1b.

At peak load, the deformation pattern changes from macroscopically homogeneous deformation to localized shear bands or cracks. The structure experiences macroscopic *strain softening*, i.e. the nominal stress decreases with increasing nominal strain.

Under the assumption that the lateral dimensions have a negligible influence, which is justified due to the boundary conditions (a stiff brush which allows for lateral sliding), a dimensional analysis of the physical problem reveals that a mathematical model describing this phenomenon must contain a material parameter with the dimension of length. The dimensional analysis based on the Π-theorem by Buckingham follows the standard procedure, cf. e.g. Görtler (1975). The Π-theorem states that if $f(x_1, x_2, ..., x_n) = 0$ holds for dimensional parameters x_i, then the relation can be equivalently written as $f^\star(\Pi_1, \Pi_2, ..., \Pi_m) = 0$ with $m = n - q$ dimensionless parameters Π_i. Here, f represents the unknown functional relation between the parameters and q is the number of involved independent units.

Assume first that the governing parameters are the stress σ, top displacement Δu,

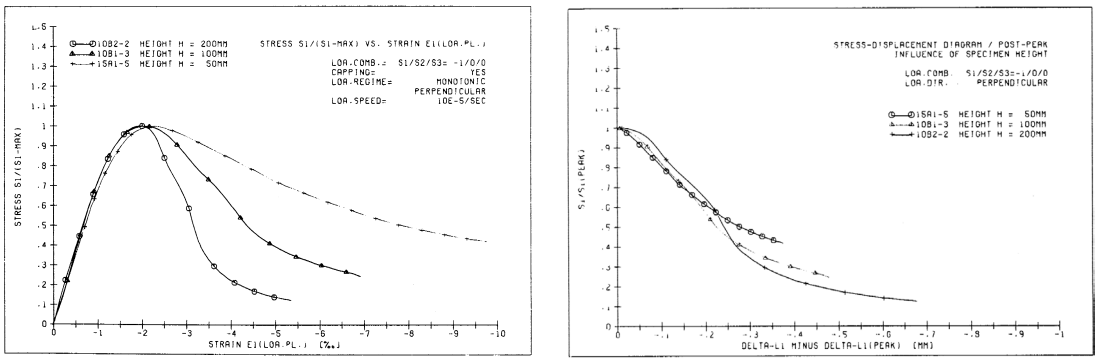

(a) (b)

Figure 2.1: Concrete prisms of varying length: Nominal stress as a function of (a) nominal strain and (b) top displacement minus its value at peak. Figures taken from van Mier (1984).

length L, and p additional material parameters E_i with the dimension of stress, e.g. the elastic modulus, initial yield stress etc. The physical process can then be described by

$$f\left(\sigma, \Delta u, L, E_1, E_2, \ldots, E_p\right) = 0 \tag{2.1}$$

In the present case, the number of dimensional parameters is $n = p + 3$, the independent units are Newton and meter, so $q = 2$, and the physical problem is thus controlled by $m = p + 1$ dimensionless parameters.

Possible sets of dimensionless parameters are generated based on the dimensionless *Ansatz* in form of the potential product

$$\Pi = \sigma^a (\Delta u)^b L^c \prod_{i=1}^{p} E_i^{d_i} \tag{2.2}$$

where the exponents a, b, c, and d_i have to satisfy

$$a + \sum_{i=1}^{p} d_i = 0 \tag{2.3}$$

$$-2a + b + c - 2\sum_{i=1}^{p} d_i = 0 \tag{2.4}$$

to make the right-hand side of Eq. (2.2) dimensionless. In general, $p + 1$ exponents can be chosen independently. The specific choice influences the resulting set of dimensionless parameters, which is nonunique. Nevertheless, every obtained set is sufficient to describe the physical process and is in this sense complete.

Choosing c and d_1 as dependent exponents, Equations (2.3) and (2.4) are written as

$$d_1 = -a - \sum_{i=2}^{p} d_i \tag{2.5}$$

$$c = -b \tag{2.6}$$

Setting e.g. $a = b = d_2 = \ldots = d_n = 1$, Eq. (2.2) can be expressed by the product

$$\Pi = \left(\frac{\sigma}{E_1}\right)\left(\frac{\Delta u}{L}\right)\prod_{i=2}^{p}\left(\frac{E_i}{E_1}\right) \tag{2.7}$$

of $m = p + 1$ dimensionless parameters σ/E_1, $\Delta u/L$, and E_2/E_1, E_3/E_1, ..., E_p/E_1. According to the Buckingham theorem, the functional dependence can then be described by the dimensionless function

$$f^\star\left(\frac{\sigma}{E_1}, \frac{\Delta u}{L}, \frac{E_2}{E_1}, \frac{E_3}{E_1}, \ldots, \frac{E_p}{E_1}\right) = 0 \tag{2.8}$$

For one specific material, the parameters E_i/E_1 are constants, and the functional dependence

$$f^\star_{\mathrm{M}}\left(\frac{\sigma}{E_1}, \frac{\Delta u}{L}\right) = 0 \tag{2.9}$$

must be expected. This simply means that if σ/E_1 is plotted as a function of $\Delta u/L$, a unique curve should be obtained. For the uniaxial compression test, this is obviously satisfied in the pre-peak regime, but not for the post-peak, see Fig. 2.1a.

It can be inferred that some control parameter is missing in the initial set. Motivated by the fact that during post-peak failure, localized deformation modes of characteristic size appear, assume that the physical process can be desribed by

$$f\left(\sigma, \Delta u, L, E_1, E_2, \ldots E_p, l\right) = 0 \tag{2.10}$$

with an additional material parameter l that has the dimension of length, the *internal length scale*. Following the same procedure for the dimensional analysis, an additional dimensionless parameter $\Delta u/l$ is obtained (for a specific choice of the exponents). For one specific material, the problem is described by

$$f^\star_{\mathrm{M}}\left(\frac{\sigma}{E_1}, \frac{\Delta u}{L}, \frac{L}{l}\right) = 0 \tag{2.11}$$

in dimensionless parameters.

In the pre-peak range of the experiments, σ/E_1 is obviously a function of $\Delta u/L$, and the strain at peak, $\Delta u_{\mathrm{peak}}/L$, is a constant. For the post-peak, σ/E_1 is a unique function of $(\Delta u - \Delta u_{\mathrm{peak}})/l = (\Delta u/L - \Delta u_{\mathrm{peak}}/L)\, L/l$, see Fig. 2.1b. Both functional dependencies can be described by $f^\star_{\mathrm{M}}$ in Eq. (2.11). In conclusion, a properly formulated model containing a parameter with the dimension of length can in principle describe the observed phenomenon.

The dependence of the physical process on a parameter with the dimension of length is an example of *size effect*. Here, the size effect influences only the post-peak response. For more complex geometrically similar structures, a size effect on the nominal structural strength, i.e. on the peak load divided by a structural dimension (for two-dimensional similarity) or its square (for three-dimensional similarity), is observed, cf. Bažant and Planas (1998). The structural strength reduces with increasing size, and the overall response tends from ductile to brittle.

Size effects have also been observed for hardening materials and even in the elastic range. For porous materials such as foams and human bones (Lakes 1986), size effects

on the torsional and bending stiffness contradicting the standard elasticity theory were measured. Clearly pronounced size effects on the yield stress and hardening curve were observed in tests of metals on the millimeter and micrometer scales, e.g. bending of thin beams (Richards 1958; Stolken and Evans 1998), torsion of thin wires (Morrison 1939; Fleck et al. 1994) and micro-indentation (Nix 1989; Ma and Clarke 1995; Poole et al. 1996).

For concrete, size effect is typically accompanied by localized deformation patterns and reduction of transmitted stress. The typical size and spacing of these patterns depends on the heterogeneous material microstructure, which controls the length scale of a properly formulated material model. For concrete, the length scale is related to the size and spatial distribution of the aggregates; for metals, the length scale depends on the dislocation density.

To describe localization with a continuum model, the maximum stress supported by the material point must decrease with increasing strain, a phenomenon called strain softening. Mathematically, the description of strain softening is a complex task, closely related to material models with internal length scales, or *nonlocal* continuum models.

2.2 Nonlocal continuum models

Classical mechanical continuum models, used in many engineering applications, rely on the assumption that the stress at a certain material point can be uniquely determined from the history of the strain (first-order deformation gradient) at that point only. Individual material points are supposed to interact only with their immediate neighbors, and the mechanical part of the interaction is fully described by the usual symmetric stress tensor, i.e. interaction is restricted to the effect of the standard balance equations. Force interaction at finite distance is excluded (except for externally applied body forces), same as the dependence on higher-order gradients of the displacement field.

The concept of internal variables further reduces the functional dependence on the strain history. It replaces the dependence on the strain history by dependence on the current values of strain and additional internal variables at the given time and material point. Again, this dependence is usually strictly local, and gradients of the internal variable fields or their values at other material points are not taken into account. The same holds for the evolution equations that specify the rates of internal variables.

In this classical concept, the material is described by the same continuum model at an arbitrary (small) scale. In physical reality however, the effects of heterogeneity and discontinuous microstructure become nonnegligible on a sufficiently small scale for any given material. For metals, this scale is in the order of microns, but for concrete and other highly heterogeneous composite materials, it is substantially larger. If the strain distribution is sufficiently smooth, as is often the case in the elastic regime, the standard local theory provides a good approximation and no important deviations from the actual behavior can be observed. After strain localization, the characteristic wave length of the deformation field becomes much shorter and this activates nonlocal effects, i.e. interaction between material points.

Constitutive models formulated within the classical framework of simple nonpolar materials (Noll 1972) are called *strictly local*, because they are invariant with respect to

scaling of the spatial coordinates. They lack a length scale that would reflect the typical size and spacing of characteristic microstructural features; therefore, they are inherently incapable of describing size effects of the transitional type that are experimentally observed if the characteristic wave length of the deformation pattern becomes comparable with the intrinsic material length scale.

In the context of plasticity, classical models fail to describe strain localization due to softening or non-associated flow in a mathematically rigorous way. Their application in the post-critical regime leads to ill-posed boundary value problems, which admit solutions with discontinuous displacement fields and the deformation localized into a set of measure zero. Such solutions correspond to perfectly brittle failure, with zero energy dissipation, which does not reflect physical reality.

The remedy has been sought in various enrichments that incorporate, at least in a simplified way, some information about the material heterogeneity on the mesoscopic or microscopic levels. If properly formulated, they act as *localization limiters*, i.e. the localization of the strain field, still present, is limited to a region of nonzero size.

Examples of such enrichments are additional kinematic variables (e.g. independent micropolar rotations in unconstrained Cosserat-type theories), weighted spatial averages, or higher-order gradients. Enriched models can be classified according to the type of enrichment:

- *Models with enrichment of the kinematic description*, e.g. strain-gradient models that characterize the deformation at a material point not only by the conventional strain (related to the displacement gradient) but also by the strain gradient (related to the second gradient of displacement). Generally, these models can also take into account second or higher-order gradients of strain, or weighted spatial averages (described in detail in Sec. 2.3) of strain.

- *Models with enrichment of the constitutive equations* which use gradients or weighted spatial averages of internal variables or their thermodynamic conjugates.

Common to both classes is the presence of at least one length scale. Consequently, these models are not invariant with respect to scaling of the spatial coordinates. In a broad sense, materials which contain a length scale will be called *nonlocal*.

A mathematical definition of nonlocality (Rogula 1982) is based on the properties of the operator A in the abstract representation of any physical problem

$$Au = f \tag{2.12}$$

where f is the given excitation and u the unknown response. Operator A is called *local* if for any open set O and for any two functions u and v that are equal in O, the images Au and Av are also equal in O. Differential operators are local in this sense, while problems described by integrodifferential equations are nonlocal. Models which are local in the sense of Rogula but do contain a length scale will be called *weakly nonlocal*, while models which are nonlocal in the sense of Rogula will be called *strongly nonlocal*.

To construct a regularized plasticity model for strain-softening materials, material models that enrich only the constitutive equations are particularly attractive. Often, size effect is restricted to the softening regime, and the elastic response can be conveniently described by a standard local model. The internal variables, typically the plastic strain

and the hardening variable, are linked to the inelastic process. The enhanced material model can easily be formulated such that the length scale is activated only in the inelastic regime, and the elastic response of the material is not altered.

Depending on the type of operator that is applied to the internal variables (or conjugate thermodynamic forces), two classes are distinguished:

- *Gradient models* that apply differential operators.
- *Integral-type nonlocal models* that use weighted spatial averages.

Models that formally work with gradients, either strain-gradient models that enrich the kinematic description or gradient models that enrich only the constitutive law, are discussed in Chapter 3. A number of integral-type nonlocal models, most of them specifically conceived as regularized material models for strain softening, are scrutinized in Chapter 4.

2.3 Nonlocal averaging

The weighted spatial average, or nonlocal average, of a local field $\kappa(\boldsymbol{x})$ is defined by the integral

$$\bar{\kappa}(\boldsymbol{x}) = \int_{\mathcal{V}} \alpha(\boldsymbol{x}, \boldsymbol{\xi}) \kappa(\boldsymbol{\xi}) \mathrm{d}\boldsymbol{\xi} \tag{2.13}$$

where α is a suitable weight function, $\mathcal{V}$ is the spatial domain representing the body (finite or infinite), and the superimposed bar marks the nonlocal quantity. For an infinite, macroscopically homogeneous and isotropic body, the weight function depends only on the distance $r = \|\boldsymbol{x} - \boldsymbol{\xi}\| \geq 0$ and can be expressed as $\alpha(\boldsymbol{x}, \boldsymbol{\xi}) = \alpha_\infty(\|\boldsymbol{x} - \boldsymbol{\xi}\|) = \alpha_\infty(r)$.

For a finite body, the weight function is usually adjusted such that the nonlocal field corresponding to a constant local field remains constant even in the vicinity of a boundary. This is guaranteed if the weight function satisfies the normalizing condition

$$\int_{\mathcal{V}} \alpha(\boldsymbol{x}, \boldsymbol{\xi}) \mathrm{d}\boldsymbol{\xi} = 1 \quad \forall \boldsymbol{x} \in \mathcal{V} \tag{2.14}$$

and the simplest way to achieve that is to set

$$\alpha(\boldsymbol{x}, \boldsymbol{\xi}) = \frac{\alpha_\infty(\|\boldsymbol{x} - \boldsymbol{\xi}\|)}{\int_{\mathcal{V}} \alpha_\infty(\|\boldsymbol{x} - \boldsymbol{\zeta}\|) \mathrm{d}\boldsymbol{\zeta}} \tag{2.15}$$

Commonly used nonlocal weight functions are the Gauss-like function

$$\alpha_\infty^{\mathrm{Gauss}}(r) = \frac{1}{c_{\mathrm{Gauss}}} \exp\left(-\frac{r^2}{2l^2}\right) \tag{2.16}$$

where the scaling factor c_{Gauss} depends on the problem dimension, and is given by $c_{\mathrm{Gauss}} = \sqrt{2\pi}\, l$ for one dimension, $2\pi l^2$ for two dimensions, and $\sqrt{\pi^3/2}\, l^3$ for three dimensions. Unless stated otherwise, all results in this thesis are computed with the bell-shaped truncated polynomial function

$$\alpha_\infty^{\mathrm{bell}}(r) = \begin{cases} \dfrac{1}{c}\left(1 - \dfrac{r^2}{R^2}\right)^2 & \text{if} \quad |r| \leq R \\ 0 & \text{if} \quad |r| \geq R \end{cases} \tag{2.17}$$

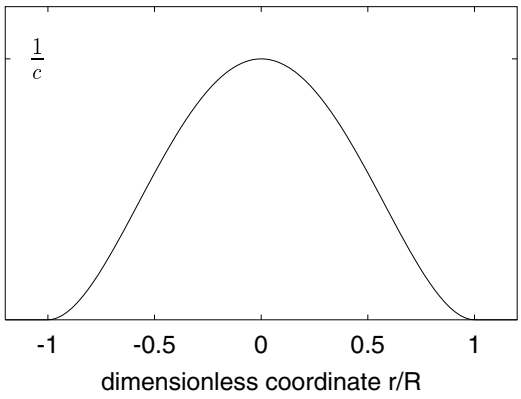

Figure 2.2: Nonlocal weight function $\alpha_\infty^{\text{bell}}(r)$.

plotted in Fig. 2.2. The scaling factor c is given by $c = 16R/15$ for one dimension, $\pi R^2/3$ for two dimensions, and $32\pi R^3/105$ for three dimensions.

The weight function always contains at least one parameter with the dimension of length, e.g., the length scale l in (2.16) or the interaction radius R in (2.17). This parameter incorporates in the simplest possible way some information about the material microstructure into the model. The value of the length scale parameter is related to the intrinsic material length, which is dictated by the size and spacing of dominant heterogeneities.

The Gauss-like weight function (2.16) has an unbounded support, which means that the nonlocal interaction theoretically takes place at an arbitrary long distance. Since the decay of $\alpha_\infty^{\text{Gauss}}$ with increasing r/l is very fast, in practical applications it is possible to truncate the function at a finite distance. The bell-shaped function (2.17) has a bounded support and vanishes at distances r exceeding the interaction radius R.

The operator transforming the local field into a nonlocal field can be called the *regularization operator* $\mathcal{R}$. This means that if $\bar{f}$ is the nonlocal average of f, evaluated according to (2.13), then $\bar{f} = \mathcal{R}(f)$. The thermodynamically motivated nonlocal plasticity models proposed by Polizzotto et al. (1998) and Svedberg (1996), discussed in Sections 4.7 and 4.8, use the *adjoint operator* $\mathcal{R}^*$, defined by the identity

$$\int_{\mathcal{V}} f\, \mathcal{R}^*(g)\, \mathrm{d}\boldsymbol{x} = \int_{\mathcal{V}} \mathcal{R}(f)\, g\, \mathrm{d}\boldsymbol{x} \tag{2.18}$$

that must hold for any functions f and g for which the integrand on the right-hand side is integrable. The field transformed by the adjoint operator $\mathcal{R}^*$ is denoted by a superposed tilde, i.e., $\widetilde{g} = \mathcal{R}^*(g)$.

To derive an explicit formula for the transformation of g into $\widetilde{g}$, rewrite the right-hand side of (2.18) as $\int_{\mathcal{V}} \bar{f} g \mathrm{d}\boldsymbol{x}$ and expand $\bar{f}$ according to its definition (2.13):

$$\begin{aligned}
\int_{\mathcal{V}} \bar{f}(\boldsymbol{x}) g(\boldsymbol{x}) \mathrm{d}\boldsymbol{x} &= \int_{\mathcal{V}} \int_{\mathcal{V}} \alpha(\boldsymbol{x}, \boldsymbol{\xi}) f(\boldsymbol{\xi}) \mathrm{d}\boldsymbol{\xi}\, g(\boldsymbol{x}) \mathrm{d}\boldsymbol{x} \\
&= \int_{\mathcal{V}} f(\boldsymbol{\xi}) \int_{\mathcal{V}} \alpha(\boldsymbol{x}, \boldsymbol{\xi}) g(\boldsymbol{x}) \mathrm{d}\boldsymbol{x} \mathrm{d}\boldsymbol{\xi} \\
&= \int_{\mathcal{V}} f(\boldsymbol{x}) \int_{\mathcal{V}} \alpha(\boldsymbol{\xi}, \boldsymbol{x}) g(\boldsymbol{\xi}) \mathrm{d}\boldsymbol{\xi} \mathrm{d}\boldsymbol{x}
\end{aligned} \tag{2.19}$$

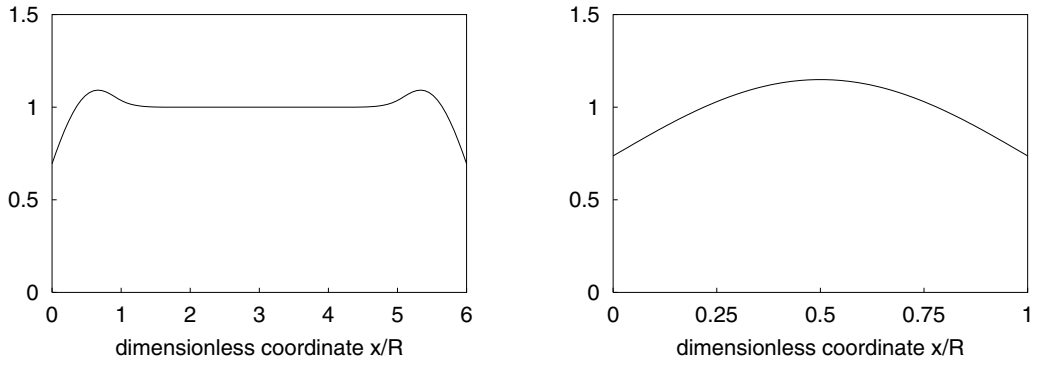

(a) (b)

Figure 2.3: Function $\widetilde{1}$ obtained by integrating the scaled weight function α with respect to its first argument; the total length of the bar is (a) $L = 6R$, (b) $L = R$.

This is equal to $\int_{\mathcal{V}} f(\boldsymbol{x})\widetilde{g}(\boldsymbol{x})\mathrm{d}\boldsymbol{x}$ if

$$\mathcal{R}^*(g)(\boldsymbol{x}) \equiv \widetilde{g}(\boldsymbol{x}) = \int_{\mathcal{V}} \alpha(\boldsymbol{\xi}, \boldsymbol{x}) g(\boldsymbol{\xi}) \mathrm{d}\boldsymbol{\xi} \tag{2.20}$$

The resulting formula reveals that the adjoint operator $\mathcal{R}^*$ is also a nonlocal averaging operator, but with the reversed order of the arguments of weight function α. The operation defined in (2.20) is called *dual averaging*.

In cases when $\alpha(\boldsymbol{x}, \boldsymbol{\xi})$ depends only on $r = |\boldsymbol{x} - \boldsymbol{\xi}|$, there is no difference between standard (primary) averaging and dual averaging; in other words, the regularization operator $\mathcal{R} = \mathcal{R}^*$ is self-adjoint. If the weight function is scaled according to (2.15), the symmetry is broken, and dual averaging does not preserve a constant field. For a one-dimensional example, $g(\xi) \equiv 1$ is transformed into

$$\widetilde{1}(x) = \int_{\mathcal{L}} \alpha(\xi, x)\, \mathrm{d}\xi = \int_{\mathcal{L}} \frac{\alpha_\infty(\xi - x)}{\int_{\mathcal{L}} \alpha_\infty(\xi - \zeta)\, \mathrm{d}\zeta}\, \mathrm{d}\xi \tag{2.21}$$

where $\mathcal{L}$ represents the one-dimensional integration domain. As shown in Fig. 2.3, the function $\widetilde{1}(x)$ is equal to 1 only sufficiently far from the boundary. For a weight function with bounded support, the thickness of the boundary layer in which $\widetilde{1}(x)$ is different from 1 is twice the interaction radius. For a weight function with unbounded support, $\widetilde{1}(x)$ is theoretically non-constant over the entire domain, but at a sufficient distance from the boundary the deviation of $\widetilde{1}(x)$ from 1 is not discernible.

2.4 Local plasticity

In a one-dimensional setting, standard small-strain local plasticity with linear isotropic hardening is described by the elastic stress-strain law

$$\sigma = E(\varepsilon - \varepsilon_{\mathrm{p}}) \tag{2.22}$$

hardening law

$$q = -H\kappa \tag{2.23}$$

and evolution laws for the internal variables

$$\dot{\varepsilon}_{\mathrm{p}} = \dot{\lambda}\frac{\partial f(\sigma,q)}{\partial \sigma} \tag{2.24}$$

$$\dot{\kappa} = \dot{\lambda}\frac{\partial f(\sigma,q)}{\partial q} \tag{2.25}$$

with loading-unloading conditions

$$\dot{\lambda} \geq 0, \qquad f(\sigma,q) \leq 0, \qquad \dot{\lambda}\, f(\sigma,q) = 0 \tag{2.26}$$

Here, σ is the stress, ε is the (total) strain, ε_{p} is the plastic strain, E is the elastic modulus, H is the plastic modulus (positive for hardening and negative for softening), κ is the hardening variable, q is the dissipative force conjugate to κ, $\dot{\lambda}$ is the rate of the plastic multiplier, and

$$f(\sigma,q) = |\sigma| - \sigma_0 + q \tag{2.27}$$

is the yield function. Initially, the variables κ and q have zero values, and so the parameter σ_0 is the initial yield stress. A superimposed dot denotes the derivative with respect to time.

From the thermodynamic point of view, Equations (2.22)–(2.23) are the state laws that can be derived under certain additional assumptions from the free-energy potential

$$\rho\psi(\varepsilon,\varepsilon_{\mathrm{p}},\kappa) = \tfrac{1}{2}E(\varepsilon-\varepsilon_{\mathrm{p}})^2 + \tfrac{1}{2}H\kappa^2 \tag{2.28}$$

and Equations (2.24)–(2.26) are the complementary laws that can be derived from the dual dissipation potential $\phi^*(\sigma,q)$ defined as the indicator function of the set of plastically admissible states; for a detailed discussion, see e.g. Jirásek and Bažant (2002, Chapter 23).

The basic equations (2.22)–(2.26) are written in a form that reveals a certain symmetry in the state laws and complementary laws. Making use of the particular definition of the yield function (2.27), it is possible to replace $\partial f/\partial\sigma$ in (2.24) by $\operatorname{sgn}\sigma$ and $\partial f/\partial q$ in (2.25) by 1. The latter equation then turns into the identity $\dot{\kappa} = \dot{\lambda}$, and so the rate of the plastic multiplier can be eliminated from the basic equations. From the flow rule (2.24), rewritten as $\dot{\varepsilon}_{\mathrm{p}} = \dot{\lambda}\operatorname{sgn}\sigma$ and combined with the condition $\dot{\lambda} \geq 0$, it then follows that $\dot{\kappa} = \dot{\lambda} = |\dot{\varepsilon}_{\mathrm{p}}|$, which gives to the hardening variable κ the physical meaning of cumulative plastic strain. To give a clear physical meaning also to the variable that controls the size of the elastic domain, the current yield stress is defined as $\sigma_{\mathrm{Y}} = \sigma_0 - q$, and the hardening law, Eq. (2.23), is rewritten as $\sigma_{\mathrm{Y}} = \sigma_0 + H\kappa$. After all these adjustments, the basic equations reduce to

$$\sigma = E(\varepsilon - \varepsilon_{\mathrm{p}}) \tag{2.29}$$

$$\sigma_{\mathrm{Y}} = \sigma_0 + H\kappa \tag{2.30}$$

$$\dot{\varepsilon}_{\mathrm{p}} = \dot{\kappa}\operatorname{sgn}\sigma \tag{2.31}$$

$$\dot{\kappa} \geq 0, \quad f(\sigma,\sigma_{\mathrm{Y}}) \leq 0, \quad \dot{\kappa}\, f(\sigma,\sigma_{\mathrm{Y}}) = 0 \tag{2.32}$$

where the yield function is now given by

$$f(\sigma,\sigma_{\mathrm{Y}}) = |\sigma| - \sigma_{\mathrm{Y}} \tag{2.33}$$

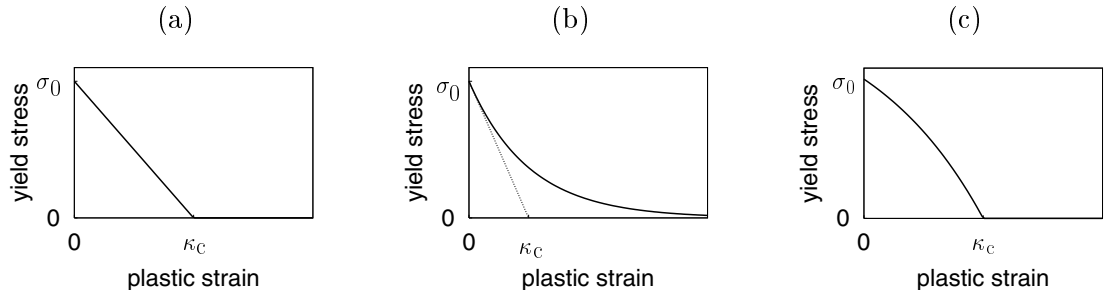

Figure 2.4: Softening laws: (a) linear, (b) exponential softening law as an example of a nonlinear law with positive curvature, (c) nonlinear with negative curvature.

Under tensile yielding, there is no difference between the plastic strain and the cumulative plastic strain, i.e., $\varepsilon_{\mathrm{p}} \equiv \kappa$.

Whenever only softening is considered, κ is called the softening variable and Eq. (2.30) the softening law. They are called hardening variable and hardening law if the term hardening is used in the general sense, including both hardening and softening.

The localization analysis of particular models presented in Chapters 3 and 4 usually starts with the simplest case of linear softening (Fig. 2.4a), but the ramifications to nonlinear softening (Fig. 2.4b,c) are also discussed. In the nonlinear case, the softening law Eq. (2.30) is replaced by

$$\sigma_{\mathrm{Y}} = \sigma_0 + h(\kappa) \tag{2.34}$$

where h is a suitably chosen function that defines the evolution of the drag stress (difference between the current and initial yield stress). A nonlinear hardening law in the form

$$\sigma_{\mathrm{Y}} = \sigma_0 + \left[\exp\left(-\frac{\kappa}{\kappa_{\mathrm{c}}}\right) - \sigma_0\right] \tag{2.35}$$

will be called exponential softening. The meaning of parameter κ_{c} is clear from Fig. 2.4b.

In fact, a rigorous description of 'linear' softening requires a bilinear function h, because the current yield stress cannot decrease below zero. When the softening variable exceeds the failure threshold $\kappa_{\mathrm{c}} = -\sigma_0/H$, the current yield stress is kept equal to zero rather than formally evaluated as negative; see Fig. 2.4a. The corresponding softening function can be described as

$$h(\kappa) = \langle \sigma_0 + H\kappa \rangle - \sigma_0 \tag{2.36}$$

where $\langle \ldots \rangle$ is the positive part operator, defined as $\langle x \rangle = \max(0, x)$. Nevertheless, this type of softening is still called linear softening.

2.5 Localization of plastic strain in a bar

To illustrate the basic localization properties of various nonlocal plasticity models, they are analyzed for a simple uniaxial tensile test of a prismatic bar, fixed at one end and loaded by an applied displacement at the opposite end (Fig. 2.5). Before the peak of the uniaxial stress-strain curve is reached, the solution is unique and the strain distribution remains uniform along the bar. The peak is a multiple bifurcation point, beyond which

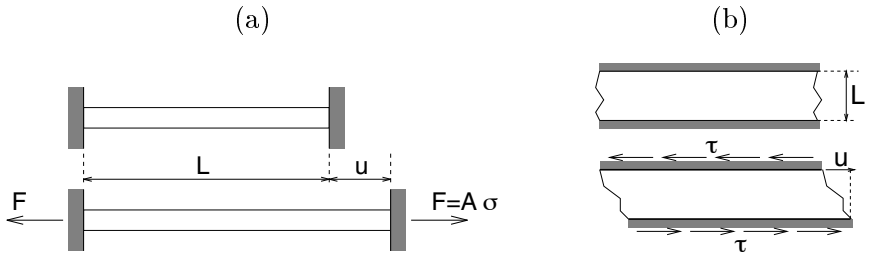

Figure 2.5: (a) Bar under uniaxial tension, (b) shear layer.

the uniform solution becomes unstable. The aim of the analysis is to study different types of nonuniform solutions that can appear after bifurcation.

The standard (local) plasticity model is not suitable for softening, because the governing equations admit infinitely many solutions with a nonuniform strain distribution and arbitrarily small dissipation after peak stress. The stress remains uniform and decreases, but plastic yielding does not need to occur simultaneously at all sections of the bar. The plastic zone I_p can become arbitrarily small and the bar can fail at an arbitrarily small dissipation. These physically inadmissible properties of the theoretical solutions are the source of pathological sensitivity of the numerical results to the computational grid, as amply documented in the literature (Bažant 1976).

The case when the plastic region is far from the clamped supports (physical boundary of the one-dimensional model) and the case when it is close to one of the supports are analyzed separatly. For nonlocal models, the plastic region is typically localized into a narrow band (sometimes even into a single cross section). The solution of the first case can often be constructed as if the bar were infinite, while for the latter case, boundary effects influence the response. For integral-type nonlocal models, these boundary effects are due to the specific form of the nonlocal average operator close to the boundary, for gradient models; they are caused by the adopted boundary conditions.

Suppose that the plastic zone I_p starts at a certain distance a from the boundary. The boundary influences the averaging operator only through the denominator in formula (2.15) that defines the weight function α. Furthermore, for a weight function with a bounded support, this scaling is only activated if the distance a is smaller than twice the support radius, $2R$. Thus, if no boundary scaling is performed or if $a \geq 2R$, the solution is the same as for an infinite domain, and it is symmetric with respect to the center of the plastic region.

For a weight function with an unbounded support, like the Gaussian function (2.16), the boundary affects the theoretical solution at an arbitrarily large distance. In a numerical solution, however, the support is bounded; the 'numerical' support radius R depends on the computer precision. For sufficiently large values of a, the numerical solution is the same as for an infinite domain.

To keep the discussion simple, the one-dimensional localization problem is interpreted here as a uniaxial tensile test. For purely deviatoric plastic flow, the results are also valid for localization in a shear layer under pure shear, i.e. when only the shear stress is nonzero. It is sufficient to replace the normal stress by shear stress, normal strain by engineering shear strain, Young's modulus by shear modulus, etc.

Chapter 3

Gradient plasticity models

3.1 General assumptions

This chapter compares and evaluates gradient-type extensions of the conventional plasticity theory. Attention is focused on the ability of individual formulations to act as localization limiters, i.e. to regularize the boundary value problem in the presence of softening and to prevent localization of inelastic strain increments into a set of zero measure. To keep the presentation simple and to highlight the essential properties of the investigated models, only the static, rate-independent response in the small-strain range and in the one-dimensional setting is considered. These restrictions permit an analytical or semi-analytical treatment of the problem, while the basic characteristics of the solutions remain valid in the general, multi-dimensional case.

3.2 Classification

The broad class of gradient theories can be divided into two groups:

- *Strain-gradient models*, which characterize the deformation at a material point not only by the conventional strain (related to the displacement gradient) but also by the strain gradient (related to the second gradient of displacement). In a general case, these models can also take into account second or higher-order gradients of strain.

- *Models with gradients of internal variables*, some of which also incorporate the gradients of the dissipative forces conjugate to the internal variables.

The fundamental difference between these two groups of models is that strain gradients considered as additional observable state variables are conjugate to higher-order stresses that enter the equilibrium equations, while gradients of internal variables are conjugate to certain dissipative thermodynamic forces that can enter the evolution equations for internal variables but do not appear in the equilibrium (momentum balance) equations. Thus the latter group of theories modifies only the constitutive description while the kinematic and equilibrium equations remain standard. In thermodynamic terms, one could say that the theories with gradients of internal variables enrich only the free-energy potential and

the dissipation potential, while the strain-gradient theories require also generalizations of the external and internal work expressions. Of course, certain models may have a mixed character. For instance, Zervos et al. (2001) proposed a model that can be interpreted as a strain-gradient theory with softening law enriched by the second gradient of an internal variable.

The initial response of a model with gradients of internal variables is governed by standard elasticity, while the response of strain-gradient models deviates from standard models already in the elastic regime. In the elastic regime, the internal variables do not evolve and remain equal to their initial values (usually zero), and so their gradients vanish. The elastic response of strain-gradient models is described by the nowadays classical strain-gradient elasticity theory pioneered by Toupin (1962) and Mindlin (1965).

The terminology used in the literature on gradient-enriched material models is not unified, which presents a potential source of misunderstanding. Gradient theories are often classified according to the order of the enrichment terms and are called first-gradient theories, second-gradient theories, etc. But this terminology should be used only when the context is clear, because it can lead to confusion. First of all, it is important to know on which field the gradient operators act. For instance, the basic version of strain-gradient elasticity enriches the free-energy potential by dependence on the first gradient of strain. Since the strain itself is the symmetric part of the displacement gradient, the strain gradient is directly related to the second gradient of the displacement field. So one can imagine that this theory is called a first- or second-gradient theory, depending on the interpretation.

Another potential source of misunderstanding is hidden in the fact that enrichments of the observable state variables inevitably lead to modifications of the corresponding balance laws, and the same is true for the internal variables and corresponding evolution equations if the theory is formulated within a thermodynamic framework. For instance, in strain-gradient elasticity the strain gradient is work-conjugate to the so-called double stress, and the second gradient of the double stress appears in the momentum balance equation. When the basic equations are combined and the momentum balance is written in terms of displacements, it turns out to be a fourth-order differential equation, i.e., its order increases by 2 as compared to the standard theory. So even though the enrichment of the kinematic part of the model is of the first order, duality induces another first-order enrichment of the equilibrium equation and the resulting effect is of the second order. On the other hand, some theories postulate the enrichment of the constitutive equations directly, without using the thermodynamic framework, and then two dual first-order enrichments are presented as one second-order enrichment. A typical example is the phenomenological gradient plasticity of Aifantis (1984), which incorporates in the hardening law the dependence on the second gradient of cumulative plastic strain. It is therefore considered as a second-gradient theory, but the same constitutive model could be constructed from a thermodynamically based theory with free energy dependent on the first gradient of cumulative plastic strain (Svedberg 1996; Svedberg and Runesson 1997).

3.3 Gradient models and nonlocality

In Chapter 2, the notions of strong and weak nonlocality have been introduced. While certain gradient models are strongly nonlocal, others are only weakly nonlocal. This depends on the way in which the gradients are introduced into the model. This can be done either in an *explicit* or *implicit* manner.

Explicit models enrich the governing equations directly by gradients of the local state variables or thermodynamic forces. The dependence on the gradients makes the stress response of one material point depend on the behavior of a neighborhood of that point, but the neighborhood can be arbitrarily small. This is why such models are *weakly nonlocal*.

Implicit models also work with higher-order gradients but do not insert them directly into the constitutive equations. The differential operators are not applied to the local internal variable field, f, but they implicitly define a nonlocal field, $\bar{f}$, constructed e.g. as the solution of the Helmholtz-type differential equation

$$\bar{f} - c\nabla^2 \bar{f} = f \qquad \text{in } V \tag{3.1}$$

where ∇^2 is the Laplace operator, V is the domain occupied by the body of interest, and c is a material parameter with the dimension of length squared.

To uniquely specify $\bar{f}$, Eq. (3.1) must be supplemented by appropriate boundary conditions. The precise form of these conditions is not obvious, but it seems reasonable to require that the transformation should not alter a constant field. If $f(\boldsymbol{x}) = f_0 = \text{const.}$, then $\bar{f}(\boldsymbol{x}) = f_0$ satisfies the differential equation (3.1), and it should also satisfy the boundary conditions, independently of the value of f_0. Clearly, it is not possible to use the Dirichlet boundary conditions, but every constant field satisfies the homogeneous Neumann boundary conditions

$$\boldsymbol{n} \cdot \boldsymbol{\nabla} \bar{f} = 0 \qquad \text{on } \partial V \tag{3.2}$$

where $\boldsymbol{\nabla}$ is the gradient operator, ∂V is the boundary of the domain V, and $\boldsymbol{n}$ is the unit vector normal to the boundary. For an infinite domain, the boundary conditions are replaced by the requirement that the solution must remain bounded.

Implicit gradient models that incorporate a transformed field defined as the solution of a boundary value problem such as (3.1)–(3.2) have been developed e.g. by Peerlings et al. (1996), Peerlings et al. (1998), and (Geers et al. 2001; Engelen et al. 2003). In contrast to explicit gradient models, they are *strongly nonlocal*, because the value of the solution $\bar{f}$ at a given point $\boldsymbol{x}$ depends on the values of the right-hand side f in the entire body, and so the stress at $\boldsymbol{x}$ depends on the state of the entire body.

The implicit gradient models can be equivalently written in an integral nonlocal format (Peerlings et al. 1996). Taking the one-dimensional case as an example, the domain V in the boundary value problem (3.1)–(3.2) reduces to an interval $\mathcal{L}$. The Green function of this BVP is a function $G(x,\xi)$ that satisfies the differential equation

$$G(x,\xi) - c\,\frac{\partial^2 G(x,\xi)}{\partial x^2} = \delta(x-\xi) \qquad \forall x \in \mathcal{L} \tag{3.3}$$

and the boundary conditions

$$\frac{\partial G(x,\xi)}{\partial x} = 0 \qquad \forall x \in \partial\mathcal{L} \tag{3.4}$$

The symbol δ in (3.3) denotes the Dirac distribution. Since $\int_{\mathcal{L}} \delta(x-\xi) f(\xi)\,\mathrm{d}\xi = f(x)$, the solution of (3.1)–(3.2) can be written as

$$\bar{f}(x) = \int_{\mathcal{L}} G(x,\xi) f(\xi)\,\mathrm{d}\xi \tag{3.5}$$

Consequently, the transformed field $\bar{f}$, implicitly defined as the solution of the boundary value problem, is a weighted spatial average of the local field f, with the Green function playing the role of the weight function. So, the implicit gradient models are equivalent to *integral-type nonlocal models* with special weight functions; see Bažant and Jirásek (2002) for a review on integral nonlocal models and Jirásek and Rolshoven (2003) for a comparative study on localization properties of integral-type nonlocal plasticity models.

For instance, if the problem is solved on the infinite interval $\mathcal{L} = (-\infty, \infty)$, the boundary conditions (3.4) are replaced by the condition that the solution must remain bounded, and the Green function is given by

$$G(x,\xi) = \frac{1}{2\sqrt{c}} \exp\left(-\frac{|x-\xi|}{\sqrt{c}}\right) \tag{3.6}$$

The graph of $G(x,\xi)$ as a function of the normalized coordinate $x/\sqrt{c}$ for fixed $\xi = 0$ is shown in Fig. 3.1.

The Green function has similar properties to the weight functions commonly used by nonlocal integral models—it depends only on the distance $r = |x-\xi|$, is non-negative and monotonically decreases with increasing distance. It also satisfies the normalizing condition $\int_V G(\boldsymbol{x},\boldsymbol{\xi})\,\mathrm{d}\boldsymbol{\xi} = 1$ because, for $f(\boldsymbol{x}) \equiv 1$, the solution of the boundary value problem (3.1)–(3.2) is $\bar{f}(\boldsymbol{x}) \equiv 1$.

The only property of the Green function (3.6) deviating from the typical properties of weight functions commonly used by integral models is that it is not continuously differentiable at $x = \xi$. This is because its first derivative at that point must jump by $-1/c$, due to the presence of the Dirac distribution on the right-hand side of (3.3). In three dimensions, the Green function even becomes unbounded at the origin—it has a singularity of the $1/r$ type (Zauderer 1989).

3.4 Strain-gradient elasticity

The elastic strain-gradient theory has its roots in the pioneering work of Toupin (1962) and Mindlin (1964). The linear version of strain-gradient elasticity is derived from a quadratic free-energy potential that depends not only on the strain but also on the strain gradient. In one dimension, the free energy per unit mass ψ can be expressed as

$$\rho\psi(\varepsilon,\eta) = \tfrac{1}{2}E\varepsilon^2 + \tfrac{1}{2}El^2\eta^2 \tag{3.7}$$

where ρ is the mass density, $\eta = \varepsilon'$ is the spatial derivative of strain and l is a material parameter with the dimension of length.

For an elastic material, the dissipation density $\mathcal{D} = \mathcal{P}_{\mathrm{int}} - \rho\dot{\psi}$ must vanish. Since the rate of free energy density depends not only on the strain rate but also on the strain gradient rate (which is *locally* independent of the strain rate), the standard expression for

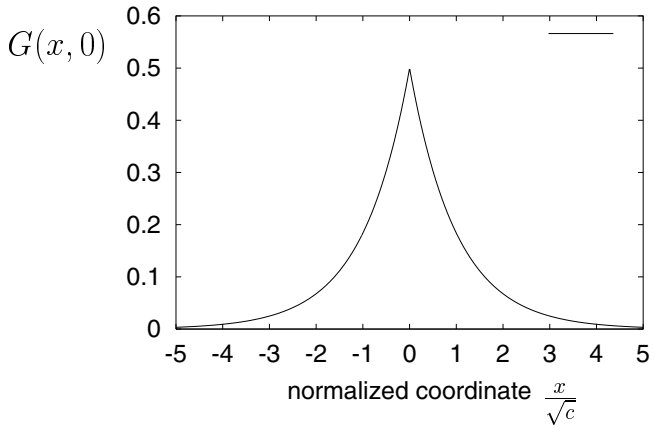

Figure 3.1: Green function of the Helmholtz equation in one dimension.

the internal power $\mathcal{P}_{\text{int}} = \sigma\dot{\varepsilon}$ must be enriched by a term $\chi\dot{\eta}$ where χ, called the double stress, is the thermodynamic force conjugate to the state variable η.

The state equations are obtained from the condition that $\mathcal{D} = 0$ for any combination of rates $\dot{\varepsilon}$ and $\dot{\eta}$. They consist of the standard stress-strain law of linear elasticity

$$\sigma = \rho\frac{\partial\psi}{\partial\varepsilon} = E\varepsilon \tag{3.8}$$

and an additional linear elastic law

$$\chi = \rho\frac{\partial\psi}{\partial\eta} = El^2\eta \tag{3.9}$$

that links the double stress to the strain gradient. The higher-order elastic modulus El^2 has a physical dimension that differs from Young's modulus E by the square of the intrinsic length parameter l. For $l = 0$, standard elasticity is recovered as a special case.

The state variables ε and η are linked to the displacement field by the kinematic equations

$$\varepsilon = u' \tag{3.10}$$
$$\eta = u'' \tag{3.11}$$

and the corresponding static equations follow from duality. Integrating by parts the internal power for the entire bar (taken per unit cross-sectional area) leads to

$$\begin{aligned} P_{\text{int}} &= \int_{\mathcal{L}} \mathcal{P}_{\text{int}} = \int_{\mathcal{L}} (\sigma\dot{u}' + \chi\dot{u}'')\,\mathrm{d}x \\ &= \int_{\partial\mathcal{L}} n\left[(\sigma - \chi')\dot{u} + \chi\dot{u}'\right]\mathrm{d}(\partial\mathcal{L}) - \int_{\mathcal{L}} (\sigma' - \chi'')\dot{u}\,\mathrm{d}x \end{aligned} \tag{3.12}$$

where ∂L is the boundary of the interval $\mathcal{L} = (0, L)$ and n is the unit "normal" to this boundary. Of course, in one dimension ∂L consists of two points, 0 and L, and n is a scalar equal to -1 on the left boundary and to 1 on the right boundary. The formal presentation with integrals over the boundary (which reduce to sums over the

boundary points) emphasizes the general structure of the theory and allows easy extensions to multiple dimensions.

The standard expression for the external power (per unit cross-sectional area) supplied by body forces b and surface tractions t is

$$P_{\text{ext}} = \int_{\mathcal{L}} b\dot{u}\,\mathrm{d}x + \int_{\partial\mathcal{L}} t\dot{u}\,\mathrm{d}(\partial\mathcal{L}) \tag{3.13}$$

Substituting this into the power equality $P_{\text{ext}} = P_{\text{int}}$ and considering that the displacement rate must satisfy the essential (kinematic) boundary conditions but otherwise is arbitrary, results into the general form of the equilibrium equation

$$\sigma' - \chi'' + b = 0 \tag{3.14}$$

and the boundary conditions

$$u = \bar{u} \quad \text{or} \quad n(\sigma - \chi') = t \quad \text{on } \partial\mathcal{L} \tag{3.15}$$

$$u' = \bar{\varepsilon} \quad \text{or} \quad \chi = 0 \quad \text{on } \partial\mathcal{L} \tag{3.16}$$

where $\bar{u}$ is the prescribed displacement, $\bar{\varepsilon}$ is the prescribed strain, and $\bar{t}$ is the prescribed traction. The expression for the external power could contain additional nonstandard boundary forces acting on the displacement gradients, but such higher-order tractions are usually assumed to vanish.

In the absence of body forces, the equilibrium equation (3.14) can be written as

$$(\sigma - \chi')' = 0 \tag{3.17}$$

Due to the contribution of the double stress χ, the distribution of stress σ is not necessarily uniform. The quantity that remains uniform in space is $\sigma - \chi'$, sometimes called the *total* stress, while σ is more specifically called the *Cauchy* stress. From the boundary condition (3.15b) it follows that $\sigma - \chi'$ is equal to the traction $t = F/A$ applied at the right boundary (where $n = 1$). So the reaction force F in the support is related to the total stress and not to the Cauchy stress.

Probably the first extension of strain-gradient theory to plasticity, proposed by Dillon and Kratochvil (1970), was based on the elastic theory with second gradients of strain (Mindlin 1965). Higher-order effects were loosely motivated by dislocation interactions and activated only after the onset of plastic flow. The main purpose of the Dillon–Kratochvil model was to reflect the formation of nonuniform deformation patterns on the microscopic level in hardening metals. In the subsequent sections, more recent formulations of strain-gradient plasticity that can serve as localization limiters will be presented and analyzed.

3.5 Strain-gradient plasticity model of Chambon et al.

3.5.1 Model description

Chambon et al. (1998) proposed a localization limiter based on the theory of continua with microstructure. They discussed a rather general framework, but the specific formulation they finally used can be considered as an elastoplastic extension of strain-gradient elasticity (Toupin 1962; Mindlin 1964).

The extension is based on the assumption that the yield function depends only on σ, and not on χ. Thus, the yield function as well as loading-unloading conditions and softening law remain the same as in standard plasticity. Under the assumption of associated flow, plastic deformation is described only by the classical plastic strain. Consequently, the constitutive part of the model consists of standard plasticity (2.29)–(2.33) and the higher-order elastic law (3.9). Note that, on the constitutive level, the stress-strain relation is fully decoupled from the relation between the double stress and the strain gradient. The elastic constitutive equation for double stresses (3.9) remains valid without any plastic correction. The double stress is linked to the stress by the equilibrium equation (3.14) and the strain gradient is linked to the strain by the compatibility equation $\eta = \varepsilon'$ that follows from the kinematic equations (3.10)–(3.11).

3.5.2 Bifurcation from a uniform state

Chambon et al. (1998) outlined the general approach to an analytical solution of their model in one dimension. For comparison with other gradient-type formulations, it is useful to provide the specific solution of the one-dimensional localization problem and discuss the main localization properties of Chambon's model.

To analyze the bifurcation from a uniform state, the equilibrium equation (3.17) is first integrated in space and then rewritten in the rate form

$$\dot{\sigma}(x) - \dot{\chi}'(x) = \dot{t} \tag{3.18}$$

Since the stress-strain law is given by the standard equations of plasticity (Sec. 2.4), the stress rate can be expressed as $\dot{\sigma} = E\dot{\varepsilon}$ in the elastic region and $\dot{\sigma} = E_t\,\dot{\varepsilon}$ in the plastic region, in which $E_t = EH/(E+H) < 0$ is the tangent elastoplastic modulus. The rate of the double stress is easily expressed from (3.9). Substituting all this into (3.18), gives

$$E\dot{\varepsilon}(x) - El^2\dot{\varepsilon}''(x) = \dot{t} \qquad \text{for } x \in I_\mathrm{e} \tag{3.19}$$

$$E_t\,\dot{\varepsilon}(x) - El^2\dot{\varepsilon}''(x) = \dot{t} \qquad \text{for } x \in I_\mathrm{p} \tag{3.20}$$

where the elastic region I_e is characterized by $\dot{\varepsilon} \le 0$ and the plastic region I_p is characterized by $\dot{\varepsilon} \ge 0$. The above differential equation has the general solution

$$\dot{\varepsilon}(x) = \frac{\dot{t}}{E} + C_1 \cosh\frac{x}{l} + C_2 \sinh\frac{x}{l} \qquad \text{for } x \in I_\mathrm{e} \tag{3.21}$$

$$\dot{\varepsilon}(x) = \frac{\dot{t}}{E_t} + C_3 \cos\frac{\alpha x}{l} + C_4 \sin\frac{\alpha x}{l} \qquad \text{for } x \in I_\mathrm{p} \tag{3.22}$$

where

$$\alpha = \sqrt{-\frac{E_t}{E}} = \sqrt{-\frac{H}{E+H}} \tag{3.23}$$

is a positive parameter that depends only on the ratio between the softening modulus and the modulus of elasticity, and C_i, $i = 1, 2, 3, 4$, are integration constants. If the elastic region or plastic region consists of several disjoint intervals, the integration constants are of course different in each contiguous part.

To obtain a valid solution, it is necessary to find the regions I_e and I_p and determine the integration constants such that the solution satisfies the boundary conditions at both end

sections of the bar and the appropriate continuity conditions at the internal elastoplastic boundaries. In general, one should enforce continuity of u, u', χ and $\sigma - \chi'$. In the present simple case, continuity of $\sigma - \chi'$ is satisfied automatically and continuity of u would be used to obtain the displacement field by integration of the strain field but does not need to be considered when solving for the strains only. So it is sufficient to enforce continuity of u' and χ, which is equivalent to continuity of ε and ε'. On each external boundary, only one of conditions (3.16) is enforced. In the homogeneous one-dimensional setting, it would be physically unrealistic to prescribe the value of strain on the boundary, so the condition to be used is $\chi = 0$, which is equivalent to $\varepsilon' = 0$.

The size and location of the elastic and plastic regions are not given in advance; they must be determined such that the solution is admissible. Recall that, according to the loading-unloading conditions, the strain rate is nonnegative in I_p and nonpositive in I_e. Since, for the present model, the strain must be continuous, these conditions imply that each internal elastoplastic boundary is in the regime of neutral loading, with a vanishing strain rate. This provides a sufficient number of additional conditions that make it possible to determine the exact location of the elastoplastic boundaries.

However, the number of elastic and plastic intervals must be selected first. This is a typical situation in one-dimensional localization analysis. The choice is not unique, but the most interesting solutions are those for which the plastic strain localizes into one single interval, which can form either at one bar end, or in the interior of the bar. The number of elastic intervals is then 1 or 2, resp.

Consider first the case of localization at the left end. The bar domain $\mathcal{L} = [0, L]$ is divided into the plastic region $I_\mathrm{p} = [0, L_\mathrm{p}]$ and the elastic region $I_\mathrm{e} = [L_\mathrm{p}, L]$, where L_p is the size of the plastic region, still to be determined. Imposing conditions $\dot\varepsilon'(0) = 0$ and $\dot\varepsilon(L_\mathrm{p}) = 0$ on the general solution (3.22) and conditions $\dot\varepsilon(L_\mathrm{p}) = 0$ and $\dot\varepsilon'(L) = 0$ on the general solution (3.21), a family of particular solutions described by

$$\dot\varepsilon(x) = \begin{cases} \dfrac{\dot t}{E_t}\left(1 - \dfrac{\cos\dfrac{\alpha x}{l}}{\cos\dfrac{\alpha L_\mathrm{p}}{l}}\right) & \text{for } x \in I_\mathrm{p} \equiv [0, L_\mathrm{p}] \\ \dfrac{\dot t}{E}\left(1 - \dfrac{\cosh\dfrac{L - x}{l}}{\cosh\dfrac{L - L_\mathrm{p}}{l}}\right) & \text{for } x \in I_\mathrm{e} \equiv [L_\mathrm{p}, L] \end{cases} \tag{3.24}$$

is obtained. This family is parameterized by the unknown length L_p, which can be determined from the condition of continuity of $\dot\varepsilon'$ at $x = L_\mathrm{p}$. The resulting equation has the form

$$\tan\frac{\alpha L_\mathrm{p}}{l} + \alpha\tanh\frac{L - L_\mathrm{p}}{l} = 0 \tag{3.25}$$

Since an equation of this type plays an important role for this and several other models, it is useful to introduce a function $\lambda_\mathrm{p}(\alpha, \lambda) = L_\mathrm{p}/l$, defined implicitly as the smallest positive solution of the transcendental equation

$$\tan\alpha\lambda_\mathrm{p} + \alpha\tanh(\lambda - \lambda_\mathrm{p}) = 0 \tag{3.26}$$

where $\lambda = L/l$, see Fig. 3.2.

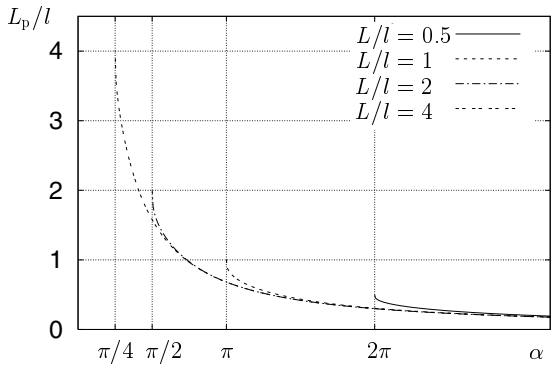

Figure 3.2: Normalized plastic zone size $\lambda_p = L_p/l$ as a function of α for different values of the normalized bar length $\lambda = L/l$.

For any fixed α, λ_p is a decreasing function of λ and for $\lambda \to \infty$ it approaches its minimum possible value,

$$\lim_{\lambda\to\infty} \lambda_p(\alpha, \lambda) \equiv \lambda_{p,\infty}(\alpha) = \frac{\pi - \arctan\alpha}{\alpha} \tag{3.27}$$

In terms of function λ_p, the size of the plastic region solved from Eq. (3.26) can be written as $L_p = l\lambda_p(\alpha, L/l)$.

For very long bars, L_p tends to its limit value $L_{p,\infty} = l\lambda_{p,\infty}(\alpha) = (l/\alpha)(\pi - \arctan\alpha)$. This limit length is proportional to the characteristic length l, but it also depends on the ratio H/E. For very steep softening, when H is close to its minimum admissible value, $-E$, parameter α is very large and the plastic region can become arbitrarily small. For mild softening, when the absolute value of H is small, parameter α is close to zero and the plastic region can become arbitrarily large.

In a finite bar, the size of the plastic region is increasing with decreasing bar length, and if the theoretical size of the plastic region solved from Eq. (3.25) is larger than the actual bar length, localization is impossible. The critical bar length below which bifurcation cannot take place,

$$L_{\min} = \frac{\pi l}{\alpha} \tag{3.28}$$

can be obtained from Eq. (3.25) by setting $L_p = L = L_{\min}$ and looking for the smallest positive solution.

The foregoing derivations were based on the assumption that the plastic region forms around one of the bar ends. Another possible localization pattern is a plastic region inside the bar, separated from the bar ends by two elastic intervals. It turns out that solutions of this type are symmetric with respect to the middle section and that each of them can be constructed by combining two solutions with localization around the boundary of a bar of length $L/2$; see Fig. 3.3. Such solutions exist only if the bar length exceeds $2L_{\min} = 2\pi l/\alpha$. The size of the plastic region is then given by $L_p = 2l\lambda_p(\alpha, L/2l)$.

For bar lengths between $L_{\min}$ and $2L_{\min}$, the plastic strain localizes into a region adjacent to one of the bar ends (which end will attract the plastic region is decided by

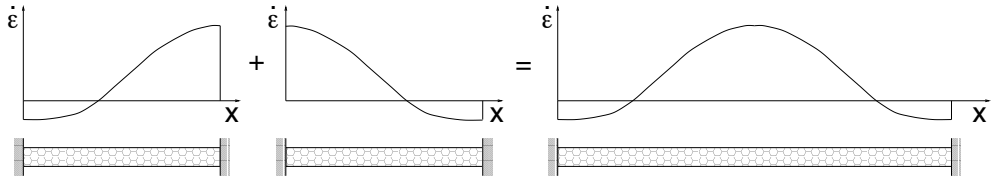

Figure 3.3: Symmetric solution obtained by combining two solutions localized at the boundary.

random imperfections). For bar lengths that exceed $2L_{\min}$, there are multiple localization patterns and their number increases with increasing bar length but always remains finite.

According to the criterion proposed by Bažant (1988) and based on thermodynamic arguments, the actual solution (stable under displacement control) is that which leads to the steepest slope of the resulting load-displacement diagram or, equivalently, to the algebraically largest tangent compliance. In the present context, the load is the traction t and the displacement is the total bar elongation. Integrating the strain rate along the bar, the elongation rate

$$\dot{u}^s(L) = \dot{t}\left\{\frac{L}{E} + \frac{2l}{\alpha H}\left[\alpha\lambda_{\mathrm{p}}\left(\alpha, \frac{L}{2l}\right) - \tan\left(\alpha\lambda_{\mathrm{p}}\left(\alpha, \frac{L}{2l}\right)\right)\right]\right\} \tag{3.29}$$

for the symmetric solution and

$$\dot{u}^b(L) = \dot{t}\left\{\frac{L}{E} + \frac{l}{\alpha H}\left[\alpha\lambda_{\mathrm{p}}\left(\alpha, \frac{L}{l}\right) - \tan\left(\alpha\lambda_{\mathrm{p}}\left(\alpha, \frac{L}{l}\right)\right)\right]\right\} \tag{3.30}$$

for the solution localized at the boundary is obtained. Inspection of Equations (3.29)–(3.30) reveals that $\dot{u}^s(L)$ can be obtained from the expression for $\dot{u}^b(L)$ simply by doubling the characteristic length l.

So, to decide which solution will actually occur, the dependence of the compliance on the characteristic length needs to be studied , with all other parameters kept fixed. The structural compliance $C = \dot{u}(L)/\dot{t}$ can be expressed as a sum of the elastic compliance, $C_{\mathrm{e}} = L/E$, and the plastic compliance, C_{p}. The relative plastic compliance $\Gamma_{\mathrm{p}} = C_{\mathrm{p}}/C_{\mathrm{e}}$ depends only on the parameters α and $\lambda = L/l$:

$$\Gamma_{\mathrm{p}}(\alpha, \lambda) = \frac{1+\alpha^2}{\lambda\alpha^3}[\tan(\alpha\lambda_{\mathrm{p}}(\alpha, \lambda)) - \alpha\lambda_{\mathrm{p}}(\alpha, \lambda)] \tag{3.31}$$

In Fig. 3.4, Γ_{p} is plotted as a function of α for several fixed values of λ. The graph shows that the plastic compliance is an increasing function of λ, which can be proven rigorously, based on the fact that λ_{p} is a decreasing function of λ and that $\tan(\alpha\lambda_{\mathrm{p}}) - \alpha\lambda_{\mathrm{p}}$ is a negative increasing function of λ_{p} in the range of interest, $\pi - \arctan\alpha < \alpha\lambda_{\mathrm{p}} \leq \pi$. Consequently, for any $L > 2L_{\min}$, the plastic compliance corresponding to the solution localized at the boundary is larger than the plastic compliance corresponding to the symmetric solution, and the plastic strain tends to localize at the boundary.

3.5.3 Evolution of plastic region

The foregoing analysis referred to the rates at the onset of localization, i.e., at first bifurcation from a uniform state. Since the solution depends only on the dimensionless ratios

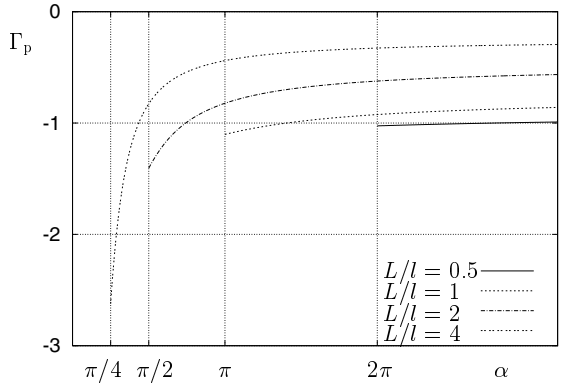

Figure 3.4: Dimensionless plastic compliance $\Gamma_p = C_p/C_e$ as a function of parameter α for several fixed values of dimensionless bar length $\lambda = L/l$.

L/l and H/E, it remains valid as long as these ratios do not change. Clearly, L and E are constant parameters, and the internal length l is normally considered as a constant as well. The softening modulus H should be interpreted as the derivative of the yield stress with respect to the cumulative plastic strain, and it is constant if the softening law is linear. In this case, the solution remains valid if the rates are replaced by finite increments with respect to the state at bifurcation. The size of the plastic zone and the shape of the plastic strain profile therefore remain constant and the plastic strains at all points of the plastic region grow proportionally to the applied increment of bar elongation (displacement of the right end if the left end is fixed).

For nonlinear softening laws, the solution of the rate problem changes during the localization process and it cannot be constructed analytically. However, if the solution were artificially kept uniform until a certain state in the post-peak range and only then the bifurcation were allowed, the plastic region would localize into an interval whose length can be obtained from the foregoing formulae with H replaced by the current (tangent) softening modulus $H_t = \mathrm{d}h/\mathrm{d}\kappa$ and α computed correspondingly. This indicates that if the magnitude of the softening modulus decreases during the softening process, the plastic region is expected to expand. Some limited expansion of the plastic region would be acceptable, but the problem is that as the current softening modulus tends to zero, the size of the plastic region grows without any bounds. The bar then cannot fail by yielding of its limited segment but every section must sooner or later start yielding. This is a spurious, nonphysical effect, which is typically accompanied by stress locking, manifested by a nonvanishing residual resistance of the structure even at very large applied elongations. A model exhibiting this kind of behavior cannot correctly predict complete failure.

Similar pathological effects can be expected for the full form of the linear softening law, Eq. (2.36), with a cut-off at zero residual yield stress. The analytical solution with a constant size of the plastic region remains valid only if the softening modulus is constant across the entire plastic region, which is true as long as the maximum plastic strain remains below the critical level κ_c. The sudden jump of the tangent softening modulus from a constant negative value to zero at the critical plastic strain level can be expected to produce qualitatively similar locking effects as the gradual decrease of the tangent

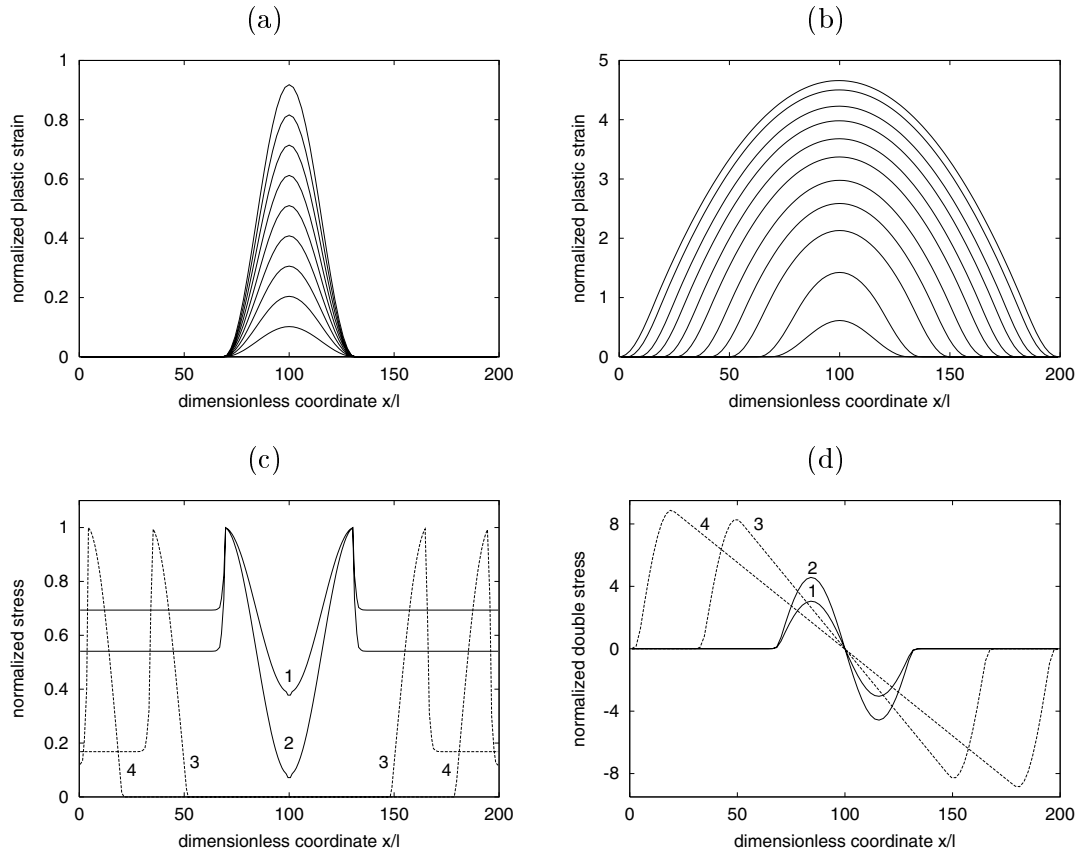

Figure 3.5: Chambon's model with linear softening: evolution of (a) plastic strain profiles at early stages of softening, (b) plastic strain profiles at late stages of softening, (c) stress profiles, (d) double stress profiles.

softening modulus characteristic of nonlinear softening laws.

Numerical calculations confirm this simplified and partially intuitive analysis. In the case of a linear softening law with cut-off at zero stress, the plastic zone is indeed initially of constant size; see the evolution of plastic strain profiles in Fig. 3.5a and the profiles of stress and double stress marked as 1 and 2 in Fig. 3.5c,d. The (Cauchy) stress distribution is nonuniform, with two maxima at the elastoplastic boundaries, where the stress σ remains at the initial yield stress level σ_0, and a minimum at the center of the plastic zone. In the elastic zones, the stress decreases with increasing distance from the elastoplastic boundary and asymptotically approaches a constant level. The size of the transition layers is in the order of the characteristic length l. The reason why these layers appear so small in Fig. 3.5c is that, for the selected model parameters, the initial plastic zone size L_p is about 60 times larger than l. The example has been computed with $H/E = -0.01$ and $L/l = 200$, which gives $\alpha = \sqrt{-H/(E+H)} = 0.1005$ and $L_\mathrm{p} = 2l\lambda_\mathrm{p}(\alpha, L/2l) = 2l\lambda_\mathrm{p}(0.1005, 100) = 60.52\,l$.

When the maximum plastic strain at the center of the plastic zone attains its critical value $\kappa_\mathrm{c} = -\sigma_0/H$, the yield stress at that point vanishes. Upon further loading, an initially small interval with zero yield stress forms at the center of the plastic zone, and the plastic zone starts expanding; see Fig. 3.5b. Typical profiles of stress and double stress

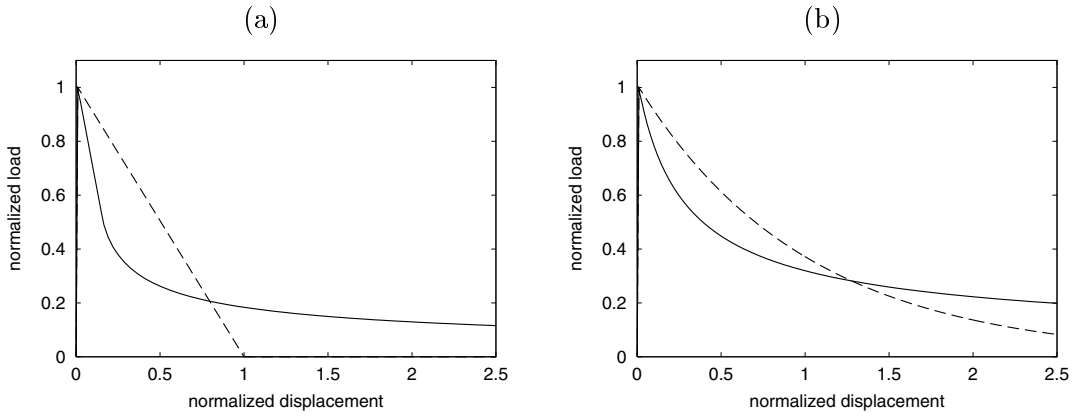

Figure 3.6: Load-displacement diagrams for Chambon's model with (a) linear softening, (b) exponential softening; the solid curves correspond to the actual (localized) solutions while the dashed curves correspond to the unstable uniform solutions.

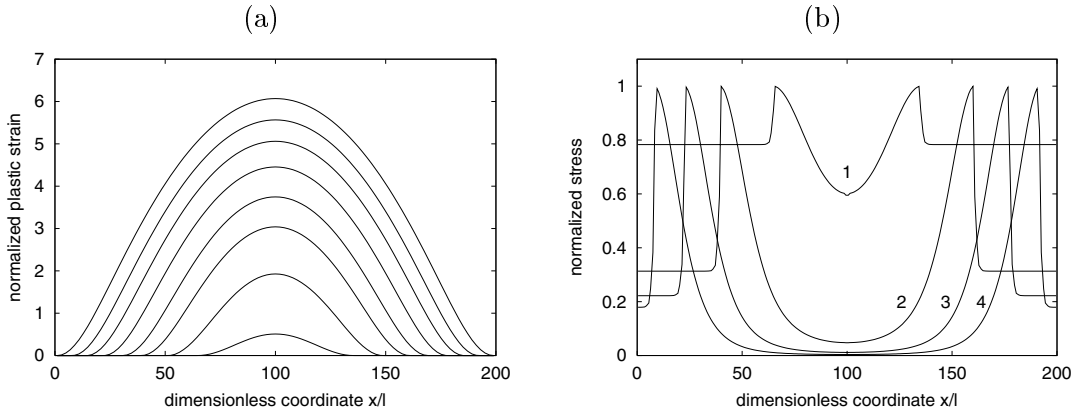

Figure 3.7: Chambon's model with exponential softening: evolution of (a) plastic strain profiles, (b) stress profiles.

corresponding to this loading stage are shown in Fig. 3.5c,d and marked by labels 3 and 4. The maximum Cauchy stress at the moving elastoplastic boundaries is still equal to the initial yield stress. The reaction at the bar end (equal to the total stress $\sigma - \chi'$) decreases only slowly with increasing bar elongation. The load-displacement curve, shown in Fig. 3.6a, even crosses the dashed curve that would correspond to the (unstable) uniform solution. The total work needed to completely break the bar (given by the area under the load-displacement diagram) is larger than in the absence of localization. This is clearly a pathological locking effect.

For a nonlinear softening law with a decreasing magnitude of the tangent softening modulus, the expansion of the plastic zone starts right away after localization. This is documented for the exponential softening law, Eq. (2.35) in Fig. 3.7. At later stages of the softening process, high residual reactions are obtained even for large bar elongations, and the load-displacement diagram eventually crosses that corresponding to the unstable uniform solution; see Fig. 3.6b.

3.6 Strain-gradient plasticity model of Fleck and Hutchinson

3.6.1 Model description

Fleck et al. (1994) and Fleck and Hutchinson (1993) proposed two extensions of the couple-stress theory to the nonlinear range. The model described in the first article can be interpreted as a deformation theory of plasticity. In general, the deformation theory of plasticity cannot realistically describe unloading, and so it would not be appropriate for the description of localization phenomena. In this approach, the free energy was defined as a power function of the combined strain, which is a scalar measure of the strain and the local curvatures (gradients of the rotational part of the displacement gradient). Once this measure was defined, the stress-strain relations were easily obtained as the state laws. No internal variables were used and the dissipation was not considered.

A more realistic model is provided by the flow theory of strain-gradient plasticity, which was first proposed by Fleck and Hutchinson (1993) in the context of the couple-stress theory. It was later reformulated by Fleck and Hutchinson (1997) in the context of the general strain-gradient theory, which takes into account not only the microcurvatures (rotation gradients) but also the stretch gradients. This is the model to be analyzed next.

In contrast to the model of Chambon et al. (1998), the yield condition is assumed to depend not only on the standard (Cauchy) stress but also on the double stress. The yield function is defined as

$$f(\sigma, \chi; \kappa) = \Sigma(\sigma, \chi) - [\sigma_0 + h(\kappa)] \tag{3.32}$$

where

$$\Sigma(\sigma, \chi) = \sqrt{\sigma^2 + \frac{\chi^2}{l_\mathrm{p}^2}} \tag{3.33}$$

is the overall effective stress. Since σ and χ have different physical dimensions, the definition of Σ must contain a scaling parameter l_p related to the internal structure of the material. This plastic characteristic length is in general different from the characteristic length used by the elastic strain-gradient theory, which will be from now on denoted as l_e. The elastic laws read

$$\sigma = E\left(\varepsilon - \varepsilon_\mathrm{p}\right) \tag{3.34}$$

$$\chi = E l_\mathrm{e}^2 \left(\eta - \eta_\mathrm{p}\right) \tag{3.35}$$

where ε_p is the usual plastic strain and η_p is the plastic part of the strain gradient, considered as an independent internal variable. Note that $\eta = \varepsilon'$ is the strain gradient, but η_p has no direct relation to the derivative of the plastic strain, ε_p'.

Within an associated framework, the evolution laws for plastic strain ε_p, plastic strain gradient η_p and hardening variable κ are

$$\dot{\varepsilon}_\mathrm{p} = \dot{\lambda}\frac{\partial f}{\partial \sigma} = \dot{\lambda}\frac{\sigma}{\Sigma} \tag{3.36}$$

$$\dot{\eta}_\mathrm{p} = \dot{\lambda}\frac{\partial f}{\partial \chi} = \dot{\lambda}\frac{\chi}{l_\mathrm{p}^2 \Sigma} \tag{3.37}$$

$$\dot{\kappa} = \dot{\lambda}\frac{\partial f}{\partial(-\sigma_\mathrm{Y})} = \dot{\lambda} \tag{3.38}$$

Under plastic loading, the rate of the plastic multiplier $\dot{\lambda}$ can be determined from the consistency condition $\dot{f} = 0$. After substitution of Equations (3.34)–(3.38) into the consistency condition and algebraic manipulations, the resulting expression reads

$$\dot{\lambda} = E\Sigma \frac{\sigma\dot{\varepsilon} + \chi\dot{\eta}l_{\mathrm{e}}^2/l_{\mathrm{p}}^2}{H\Sigma^2 + E(\sigma^2 + \chi^2 l_{\mathrm{e}}^2/l_{\mathrm{p}}^4)} \tag{3.39}$$

3.6.2 Localization analysis

At the first bifurcation from a uniform state, the problem is completely identical with the bifurcation problem for Chambon's model, and its solution is therefore exactly the same as discussed in Sec. 3.5.2. The stress is constant along the bar and the double stress vanishes (this is the unique elastic solution satisfying the appropriate boundary conditions). Consequently, Eq. (3.39) reduces to $\dot{\lambda} = E\dot{\varepsilon}/(E+H)$, the evolution laws give $\dot{\varepsilon}_{\mathrm{p}} = \dot{\lambda}$ and $\dot{\eta}_{\mathrm{p}} = 0$, and the rates of stress and double stress are $\dot{\sigma} = E_t\dot{\varepsilon}$ and $\dot{\chi} = El_{\mathrm{e}}^2\dot{\eta}$ where $E_t = EH/(E+H)$ is the tangent modulus of standard elastoplasticity.

As soon as a nonuniform strain profile develops, the evolution is in general different from that predicted by Chambon's model. Double stresses build up and the rate of the plastic strain gradient becomes nonzero. For the limit case when $l_{\mathrm{p}} \to \infty$, the Fleck–Hutchinson model reduces to Chambon's model, with $l = l_{\mathrm{e}}$.

As follows from the foregoing analysis, the initial size of the plastic region is controlled by the ratio H/E and the elastic characteristic length l_{e}. The subsequent evolution is not amenable to an analytical solution but it can be studied numerically. Fig. 3.8 shows the evolution of the strain profile for the same value of l_{e} but two different values of l_{p}, namely $l_{\mathrm{p}} = 2\,l_{\mathrm{e}}$ and $l_{\mathrm{p}} = 5\,l_{\mathrm{e}}$ (with $H/E = -0.01$ and $L = 200\,l_{\mathrm{e}}$). Even though the initial size of the plastic zone $L_{\mathrm{p}} = 60.52\,l_{\mathrm{e}}$ is in both cases the same and the strain profiles during the initial stage of localization are very similar (Fig. 3.8 top), the plastic zone at late stages of the softening process is wider for larger l_{p} (Fig. 3.8 bottom).

3.7 Mechanism-based strain-gradient plasticity

3.7.1 Model description

Fleck–Hutchinson strain-gradient theories of plasticity are physically motivated by the concept of statistically stored and geometrically necessary dislocations, but their essence remains phenomenological. A micromechanically based strain-gradient law for the flow strength of materials, derived from the Taylor hardening model by Nix and Gao (1998), serves as the basis of a group of theories called the mechanism-based strain-gradient (MSG) plasticity.

The original MSG model (Gao et al. 1999; Huang et al. 2000) is a nonlinear extension of the Toupin-Mindlin theory, interpreted as deformation theory of plasticity. The stress and double stress are considered as functions of the strain and strain gradient, without any internal variables that could describe irreversible processes. Localization analysis of the shear layer problem using the deformation theory of MSG plasticity was presented by Shi et al. (2000).

Since deformation theories are usually inappropriate for loading programs that deviate from proportionality, attention is restricted to the recently formulated flow theory of MSG

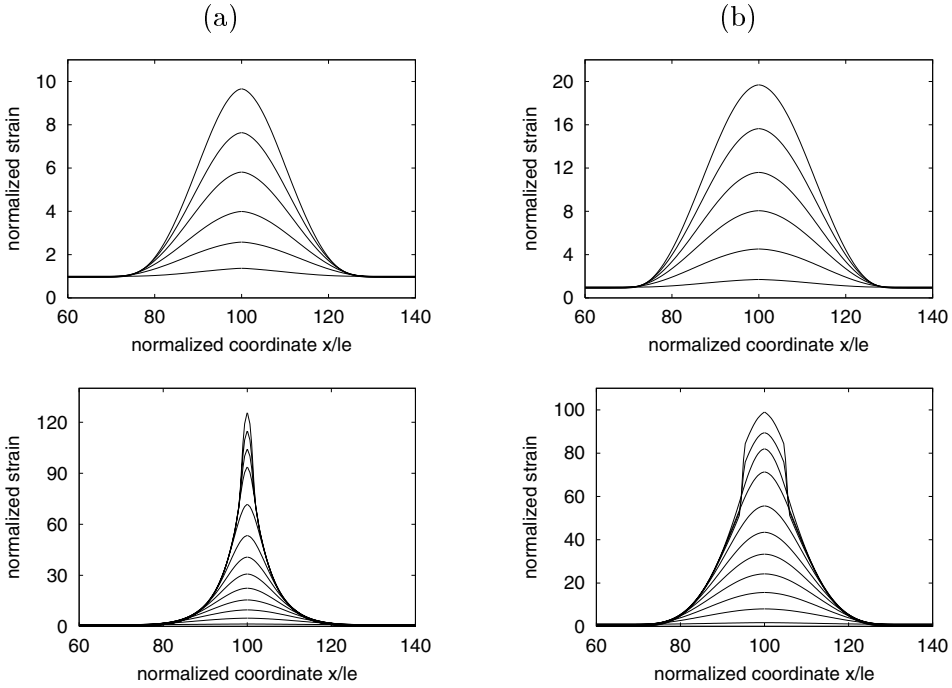

Figure 3.8: Fleck–Hutchinson model with linear softening: Evolution of the strain profile for (a) $l_\mathrm{p} = 2\,l_\mathrm{e}$, (b) $l_\mathrm{p} = 5\,l_\mathrm{e}$.

plasticity (Qiu et al. 2003). The hardening law is considered in the form

$$\sigma_\mathrm{Y} = \sqrt{\left[\sigma_0 + h(\kappa)\right]^2 + 3\alpha_\mathrm{T}^2 b E^2 |\eta|} \tag{3.40}$$

where h is a function describing the hardening law $\sigma_\mathrm{Y} = \sigma_0 + h(\kappa)$ in the absence of strain gradients, α_T is the Taylor factor with values between 0.1 and 0.5, and b is the Burgers vector (spacing between neighboring atoms in the crystal lattice). This and all subsequent equations refer to the shear layer problem, but for easier comparison with other models the notation corresponding to the tensile test is used here. In the present context, E should be interpreted as the shear modulus of elasticity, κ as the cumulative value of engineering plastic shear strain, σ as the shear stress, σ_Y as the yield stress in shear, ε as the engineering shear strain, and η as its derivative in the direction perpendicular to the boundaries of the layer.

The dependence of the yield stress on the magnitude of the strain gradient η (in multiple dimensions replaced by a suitable scalar measure of the strain-gradient tensor) is supposed to reflect the influence of geometrically necessary dislocations. The yield function preserves its classical form , Eq. (2.33), i.e., it takes into account only the Cauchy stress σ but not the double stress χ. The consistency condition $\dot\sigma = \dot\sigma_\mathrm{Y}$ combined in the usual way with the elastic stress-strain law, Eq. (2.29), leads to the following expressions for the rates of cumulative plastic strain and of stress:

$$\dot\kappa \;=\; \frac{\sigma_\mathrm{Y}\dot\varepsilon - 1.5\alpha_\mathrm{T}^2 b E n \dot\eta}{\sigma_\mathrm{Y} + hH/E} \tag{3.41}$$

$$\dot{\sigma} = \frac{hH\dot{\varepsilon} + 1.5\alpha_{\mathrm{T}}^2 bE^2 n\dot{\eta}}{\sigma_{\mathrm{Y}} + hH/E} \tag{3.42}$$

Here, $H = \mathrm{d}h/\mathrm{d}\kappa$ is the (standard) plastic modulus, and n is a signed unity defined by $n = \mathrm{sgn}\,(\eta)$ if $\eta \neq 0$, $n = \mathrm{sgn}\,(\dot{\eta})$ if $\eta = 0$.

In MSG plasticity, the rate of double stress is derived by first-order averaging over the mesocell of size l_ε. After simplifications that correspond to the one-dimensional case, the complicated tensorial expression given in Qiu et al. (2003) reduces to

$$\dot{\chi} = \frac{El_\varepsilon^2}{12}\frac{hH\dot{\eta}}{E\sigma_{\mathrm{Y}} + hH} + \frac{\chi(e\sigma_{\mathrm{Y}}\dot{\kappa} - \dot{\sigma})}{\sigma_{\mathrm{Y}} + hH/E} \tag{3.43}$$

where

$$e = \frac{H}{h} + \frac{1}{H}\frac{\mathrm{d}H}{\mathrm{d}\kappa} \tag{3.44}$$

Equations (3.41)–(3.43) apply to plastic loading. Elastic unloading is characterized by $\dot{\kappa} = 0$, $\dot{\sigma} = E\dot{\varepsilon}$ and $\dot{\chi} = E(l_\varepsilon^2/12)\dot{\eta}$.

3.7.2 Localization analysis

At bifurcation from a uniform state, the double stress χ vanishes and therefore the second term in Eq. (3.43) drops out. The strain gradient η also vanishes, and the yield stress is $\sigma_{\mathrm{Y}} = \sigma_0 + h(\kappa)$. Taking all this into account, and substituting Equations (3.42)–(3.43) and $\dot{\eta} = \dot{\varepsilon}'$ into the rate form of the equilibrium equation, Eq. (3.18), the second-order differential equation

$$\dot{\varepsilon} - \frac{\beta l_\varepsilon}{2\sqrt{3}}|\dot{\varepsilon}'| - \frac{l_\varepsilon^2}{12}\dot{\varepsilon}'' = \frac{\dot{t}}{E_t} \tag{3.45}$$

is obtained. Here, $E_t = EH/(E + H)$ is the elastoplastic modulus and

$$\beta = -\frac{3\sqrt{3}\alpha_{\mathrm{T}}^2 bE^2}{H\sigma_{\mathrm{Y}} l_\varepsilon} \tag{3.46}$$

is a dimensionless parameter. The negative sign in the definition (3.46) has been selected such that β is positive for softening ($H < 0$), which is the major interest in this study. However, Eq. (3.45) is valid even for hardening, characterized by a negative value of β. In the special case of perfect plasticity ($H = 0$), the elastoplastic modulus E_t vanishes and Eq. (3.45) must be written in a different way.

Independently of the sign of plastic modulus H, the characteristic equation of (3.45) has two real roots, one positive and one negative:

$$\lambda_1 = \frac{-\sqrt{3}n\beta + \sqrt{3\beta^2 + 12}}{l_\varepsilon}, \qquad \lambda_2 = \frac{-\sqrt{3}n\beta - \sqrt{3\beta^2 + 12}}{l_\varepsilon} \tag{3.47}$$

Therefore, the general solution of Eq. (3.45) has the form

$$\dot{\varepsilon}(x) = \frac{\dot{t}}{E_t}\left[1 + C_1\exp(\lambda_1 x) + C_2\exp(\lambda_2 x)\right] \tag{3.48}$$

on each interval with a constant value of $n = \mathrm{sgn}\,(\dot{\varepsilon}')$, i.e., on each interval where the strain rate does not change its sign.

The foregoing derivation applies to the plastic region. In the elastic region, the constitutive equations of linear strain-gradient elasticity $\dot{\sigma} = E\dot{\varepsilon}$ and $\dot{\chi} = E(l_\varepsilon^2/12)\dot{\eta}$ substituted into Eq. (3.18) lead to

$$\dot{\varepsilon} - \frac{l_\varepsilon^2}{12}\dot{\varepsilon}'' = \frac{\dot{t}}{E} \tag{3.49}$$

and the general solution is

$$\dot{\varepsilon}(x) = \frac{\dot{t}}{E}\left[1 + C_3 \exp(\lambda_3 x) + C_4 \exp(-\lambda_3 x)\right] \tag{3.50}$$

where $\lambda_3 = -2\sqrt{3}/l_\varepsilon$.

Now, a solution with plastic strain increments localized in an interval $I_\mathrm{p} = [0, L_\mathrm{p}]$, adjacent to the boundary of the shear layer at $x = 0$, is seeked. To simplify the problem, assume that the layer is sufficiently thick compared to the thickness of the localized zone, so that the analysis can be performed on a semi-infinite interval $[0, \infty)$. The boundary condition at the elastic boundary is replaced by the requirement that the strain must remain bounded as $x \to \infty$, which implies that the integration constant C_4 must vanish. On the plastic boundary (at $x = 0$), $\chi = 0$, and on the elastoplastic interface (at $x = L_\mathrm{p}$) continuity of strain and double stress is enforced. Note that continuity of the strain gradient is not required. The boundary conditions specified above correspond at the same time to a localized shear band of thickness $2L_\mathrm{p}$ with symmetric strain distribution, placed in an infinite (or sufficiently large) body such that $x = 0$ corresponds to the center of the band.

Boundary condition $\chi(0) = 0$ and continuity conditions for $\varepsilon(x)$ and $\chi(x)$ at $x = L_\mathrm{p}$ lead to a set of three linear equations, from which it is possible to determine the integration constants. To simplify the subsequent derivations, the symbol $\mu = H/E$, $e_i = \exp(\lambda_i L_\mathrm{p})$, $i = 1, 2, 3$, and

$$\Lambda_{12} = \lambda_1\lambda_2(e_1 - e_2) \tag{3.51}$$

$$\Lambda_3 = \lambda_3(\lambda_1 e_2 - \lambda_2 e_1) \tag{3.52}$$

$$\Lambda = \mu\Lambda_{12} + (1 + \mu)\Lambda_3 \tag{3.53}$$

are introduced. The integration constants can then be expressed in the simple form

$$C_1 = \frac{\lambda_2\lambda_3}{\Lambda} \tag{3.54}$$

$$C_2 = -\frac{\lambda_1\lambda_3}{\Lambda} \tag{3.55}$$

$$C_3 = \frac{\Lambda_{12}}{e_3\Lambda} \tag{3.56}$$

Note that the size of the plastic region, L_p, is still undetermined. For an arbitrary $L_\mathrm{p} > 0$, a formal solution that satisfies the equilibrium equation and the boundary and continuity conditions can be constructed. However, the solution is admissible only if it also satisfies the loading-unloading conditions $\dot{\kappa}(x) \geq 0$ for $0 \leq x \leq L_\mathrm{p}$ and $\dot{\sigma}(x) - \dot{\sigma}_\mathrm{Y}(x) \leq 0$ for $L_\mathrm{p} \leq x$.

Since

$$\dot{\sigma}(x) - \dot{\sigma}_\mathrm{Y}(x) = \dot{t}\left[1 + (1 - n\beta\mu)C_3 \exp(\lambda_3 x)\right] \tag{3.57}$$

and λ_3 is negative, the condition $\dot{\sigma}(x) - \dot{\sigma}_{\mathrm{Y}}(x) \leq 0$ written for $x \to \infty$ implies that the traction rate $\dot{t}$ must not be positive. Provided that $\dot{t} < 0$, condition $\dot{\sigma}(x) - \dot{\sigma}_{\mathrm{Y}}(x) \leq 0$ is satisfied for all $x \geq L_{\mathrm{p}}$ if it is satisfied at $x = L_{\mathrm{p}}$, which is the case if

$$1 + (1 - n\beta\mu)C_3 e_3 \geq 0 \tag{3.58}$$

This is equivalent to

$$\frac{(1+\mu)(\Lambda_{12} + \Lambda_3) - n\beta\mu\Lambda_{12}}{\Lambda} \geq 0 \tag{3.59}$$

A nonnegative value of the plastic strain rate

$$\dot{\kappa}(x) = \frac{\dot{t}}{H}\left[1 + \left(1 - \frac{\beta n \mu \lambda_1}{\lambda_3}\right) C_1 \exp(\lambda_1 x) + \left(1 - \frac{\beta n \mu \lambda_2}{\lambda_3}\right) C_2 \exp(\lambda_2 x)\right] \tag{3.60}$$

at $x = L_{\mathrm{p}}$ is guaranteed if

$$\frac{(1 - n\beta)\Lambda_{12} + \Lambda_3}{\Lambda} \leq 0 \tag{3.61}$$

The signed unity n is defined as the sign of the strain gradient rate in the plastic region, and can be evaluated as

$$n = \operatorname{sgn} \dot{\varepsilon}'(L_{\mathrm{p}}) = \operatorname{sgn}\left(\frac{\dot{t}}{E_t}(C_1 e_1 \lambda_1 + C_2 e_2 \lambda_2)\right) = \operatorname{sgn}\left(\frac{\dot{t}}{\Lambda E_t}\lambda_1\lambda_2\lambda_3(e_1 - e_2)\right) \tag{3.62}$$

Under the usual assumption that $1 + \mu > 0$, i.e., $E + H > 0$, which excludes snapback in the stress-strain diagram under uniform strain, and with $\dot{t} < 0$, $\lambda_1 > 0$, $\lambda_2 < 0$, $\lambda_3 < 0$, $e_1 = \exp(\lambda_1 L_{\mathrm{p}}) > \exp(\lambda_2 L_{\mathrm{p}}) = e_2$, and $\operatorname{sgn} E_t = \operatorname{sgn} \mu$, the signed unity simplifies to

$$n = -\operatorname{sgn}\mu \ \operatorname{sgn}\Lambda \tag{3.63}$$

According to the definition of β, Eq. (3.46), $\operatorname{sgn}\beta = -\operatorname{sgn}\mu$, and so $\operatorname{sgn}(\beta n) = \operatorname{sgn}\Lambda$.

Now conditions (3.59) and (3.61) can be discussed. Recall that Λ_{12} and Λ_3 are negative. Λ must not be zero, otherwise the integration constants would tend to infinity.

1. If Λ is negative, then βn is negative and the numerator in Eq. (3.61) is negative; consequently, this condition is violated.

2. If Λ is positive, then βn is positive. Inequalities (3.59) and (3.61) rewritten for the numerators only can be combined to get

$$\mu \leq -\frac{\Lambda_{12} + \Lambda_3}{(1 - n\beta)\Lambda_{12} + \Lambda_3} \tag{3.64}$$

   However, since βn is now positive, the right hand side in Eq. (3.64) is smaller than -1. Values of $\mu = H/E$ smaller than -1 are not allowed because the material model would exhibit snapback in the stress-strain diagram under uniform strain.

In summary, with $\mu > -1$ it is impossible to satisfy conditions (3.59) and (3.61) simultaneously, and the solution of the localization problem is never admissible. From the foregoing analysis it follows that the bifurcation problem does not admit solutions with plastic yielding localized into a layer of finite thickness. Even for softening, localization cannot take place and the solution remains uniform. So the enhancement of the softening law by the strain-gradient term cannot be used as a localization limiter in the usual sense, because it would completely exclude localization, even into a finite interval.

3.8 First-gradient plasticity model of Schreyer and Chen

3.8.1 Model description

Schreyer and Chen (1986) proposed an explicit gradient plasticity model with the current yield stress dependent not only on the cumulative plastic strain (softening variable), κ, but also on its first spatial gradient, $\boldsymbol{\nabla}\kappa$. In the isotropic case, the dependence on a tensor can enter only through its invariants, and a first-order tensor has only one (independent) invariant—its norm. In one dimension, the norm of the gradient, $\|\boldsymbol{\nabla}\kappa\|$, reduces to the absolute value of the first derivative, $|\kappa'|$. According to the gradient model proposed by Schreyer and Chen, constitutive equations (2.29)–(2.33) remain valid, except for the softening law, Eq. (2.30), which is replaced by $\sigma_{\mathrm{Y}} = \sigma_0 + h(\kappa, \kappa')$.

The original form of the hardening-softening function was relatively complicated, but in a later paper Schreyer (1990) postulated the softening law in the simple form

$$\sigma_{\mathrm{Y}} = \sigma_0 + H\left[\kappa + (l\kappa')^2\right] \tag{3.65}$$

where $H < 0$ is the softening modulus and l is a material parameter with the dimension of length. Due to the presence of the second power, the yield stress depends only on the magnitude of κ' but not on its sign, as dictated by the condition that the softening process must be independent of the selected orientation of the coordinate axis. At the onset of yielding, $\kappa = 0$ and $\sigma_{\mathrm{Y}} = \sigma_0$, and once κ becomes positive, σ_{Y} drops below σ_0.

3.8.2 Localization analysis

The current yield stress at all points of the plastic zone I_{p} must be equal to the stress, which is constant along the entire bar due to the equilibrium condition. Setting $\sigma_{\mathrm{Y}}(x) = \sigma =$ const. for all $x \in I_{\mathrm{p}}$ and substituting Eq. (3.65), the nonlinear differential equation

$$\kappa + l^2(\kappa')^2 = \frac{\sigma - \sigma_0}{H} \qquad \text{in } I_{\mathrm{p}} \tag{3.66}$$

for the unknown distribution of the softening variable κ is obtained. Schreyer (1990) showed that this equation admits solutions of the form

$$\kappa(x) = \frac{\sigma - \sigma_0}{H} - \left(\frac{x - x_0}{2l}\right)^2 \tag{3.67}$$

where x_0 is an arbitrary point that corresponds to the center of the plastic zone, see Fig. 3.9.

From the condition $\kappa(x) > 0$ for all $x \in I_{\mathrm{p}}$ it follows that the plastic zone is an interval of length $L_{\mathrm{p}} = 4l\sqrt{(\sigma - \sigma_0)/H}$ centered at x_0. Note that if compressive yielding is excluded (which is a reasonable assumption in a uniaxial tensile test), the softening variable κ is identical with the plastic strain ε_{p}. Eq. (3.67) means that the distribution of plastic strain would be parabolic, and the size of the plastic zone would grow as shown in Fig. 3.9. The unlimited expansion of the plastic zone is certainly not very physical, but this problem could perhaps be handled by a suitable modification of the softening law, e.g., by making the parameter l decrease as a function of the cumulative plastic strain.

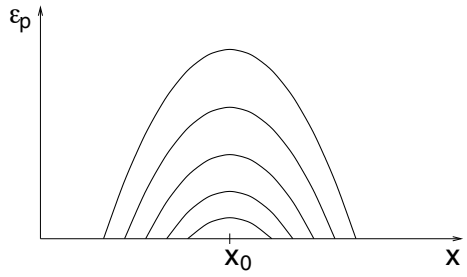

Figure 3.9: Evolution of the plastic strain profile according to the model of Schreyer and Chen.

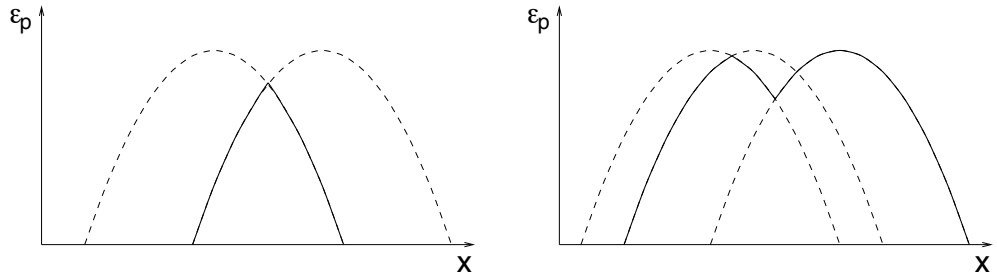

Figure 3.10: Possible nonsmooth plastic strain profiles admitted by the model of Schreyer and Chen.

Anyhow, the model suffers by another, more fundamental deficiency: The solution described by Eq. (3.67) and plotted in Fig. 3.9 is not the only possible type of solution. At any point of the plastic zone, it is possible to switch from a solution given by Eq. (3.67) with a certain value of x_0 to another solution given by the same general formula but with a different value of x_0; see Fig. 3.10. The combined solution satisfies the differential equation (3.66) at all points of the plastic zone except for those points at which the derivative κ' has a jump. But still, the derivatives from the left and from the right at these points exist and they both satisfy the differential equation. The point at which the derivative κ' has a jump can be seen as an internal boundary between two plastic regions. As for the elasto-plastic boundaries, continuity of κ' is not enforced at this point. The solution could be required to be continuously differentiable everywhere, but the only admissible solution would then be $\kappa(x) = (\sigma - \sigma_0)/H = \text{const.}$, i.e., the solution with uniform strain and with a plastic zone extending over the entire bar length.

It must be concluded that the present model does not provide a mathematically clean regularization of the problem. This is probably the reason why, to the best of the author's knowledge, a successful numerical implementation of this model has not been reported in the literature.

3.9 Second-gradient plasticity model of Aifantis

3.9.1 Model description

A widely popular second-gradient plasticity model was inspired by the ideas of Aifantis (1984), and its theoretical formulation and numerical implementation was later developed by a number of authors (Coleman and Hodgdon 1985; Mühlhaus and Aifantis 1991; Vardoulakis and Aifantis 1991; de Borst and Mühlhaus 1992; Pamin 1994; de Borst and Pamin 1996; Comi and Perego 1996; Li and Cescotto 1996; Ramaswamy and Aravas 1998). In the simplest version of that model, the softening law, Eq. (2.30) is enriched by a term proportional to the second gradient of the softening variable. For a one-dimensional model with linear softening, this law is written as

$$\sigma_{\mathrm{Y}} = \sigma_0 + H[\kappa + l^2\kappa''] \tag{3.68}$$

where l is a material parameter with the dimension of length. The square brackets emphasize that the enclosed term is not the argument of a function H (as may the parentheses suggest), but is only multiplied by the constant H.

3.9.2 Localization analysis

The enrichment of the softening law by the second derivative of the cumulative plastic strain regularizes the problem and prevents localization of plastic strain into an arbitrarily small region. Inside the plastic zone I_{p}, the consistency condition $\dot{f} = \dot{\sigma} - \dot{\sigma}_{\mathrm{Y}} = 0$ with $\dot{\sigma}_{\mathrm{Y}}$ evaluated from Eq. (3.68) leads to the differential equation

$$\dot{\kappa} + l^2\dot{\kappa}'' = \frac{\dot{\sigma}}{H} \qquad \text{in } I_{\mathrm{p}} \tag{3.69}$$

for the unknown rate of the softening variable $\dot{\kappa}(x)$. Due to static equilibrium, the stress rate is uniform along the entire bar, and so the right-hand side of Eq. (3.69) is constant. The general solution of this differential equation reads

$$\dot{\kappa}(x) = \frac{\dot{\sigma}}{H} + C\cos\frac{x - x_0}{l} \tag{3.70}$$

where C and x_0 are integration constants. Eq. (3.70) is valid inside the plastic zone, where the rate $\dot{\kappa}$ must be positive.

Since $\dot{\kappa}$ must be continuously differentiable and must vanish outside the plastic zone, both $\dot{\kappa}$ and $\dot{\kappa}'$ must vanish at the elasto-plastic interface. In general, the plastic zone could consist of several intervals, but the most localized solution with a contiguous plastic zone is known to be the stable one. If the plastic zone is located inside the bar, it is separated from the elastic part by two cross sections with unknown coordinates x_l and x_r. Interface conditions $\dot{\kappa}(x_l) = 0$, $\dot{\kappa}(x_r) = 0$, $\dot{\kappa}'(x_l) = 0$ and $\dot{\kappa}'(x_r) = 0$ provide four equations for four unknown parameters—the integration constants C and x_0 and the coordinates x_l and x_r.

It turns out that, in the idealized case of a bar with perfectly uniform properties, these conditions are not independent, which is related to the fact that the plastic zone can be located anywhere along the bar (its actual position depends on random imperfections). Fixing the value of x_0, the other constants are uniquely determined and the solution reads

$$\dot{\kappa}(x) = \frac{\dot{\sigma}}{H}\left(1 + \cos\frac{x - x_0}{l}\right) \qquad \text{for } x \in (x_0 - \pi l, x_0 + \pi l) \tag{3.71}$$

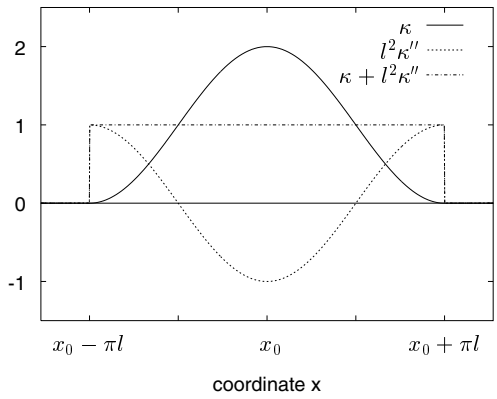

Figure 3.11: Distribution of plastic strain κ for the explicit gradient plasticity model on an infinite domain; κ and κ'' are such that $\kappa + l^2\kappa''$ is constant.

The plastic zone is the interval of length $L_\mathrm{p} = 2\pi l$ centered at x_0.

It is interesting to note that the size of the localized plastic zone is directly proportional to the internal length parameter l and independent of all the other material parameters, including the plastic modulus H. Eq. (3.71) is valid not only at the initial bifurcation from a uniform strain state, but also at later stages of the deformation process. Consequently, it can be integrated with respect to time, to get the distribution of plastic strain

$$\varepsilon_\mathrm{p}(x) = \kappa(x) = \frac{\sigma - \sigma_0}{H}\left(1 + \cos\frac{x - x_0}{l}\right) \tag{3.72}$$

corresponding to the stress level σ attained in the softening regime. This plastic strain profile is graphically illustrated in Fig. 3.11, along with the distribution of $l^2\kappa''$ and the constant sum $\kappa + l^2\kappa''$. The ordinates are normalized by the factor $H/(\sigma - \sigma_0)$.

3.9.3 Nonlinear softening

There are at least two ways of generalizing Eq. (3.68) to the case of nonlinear softening, and their influence on the solution in the nonlinear case is substantially different. One can either apply the nonlinear softening function h on the enriched softening parameter $\kappa + l^2\kappa''$, or apply h only on κ and modify the yield stress by a separate additive term $g\kappa''$ where $g < 0$ is a material parameter. If g is identified with Hl^2, both enrichments reduce in the linear case to the same softening law, Eq. (3.68).

For the first type of nonlinear softening law,

$$\sigma_\mathrm{Y} = \sigma_0 + h(\kappa + l^2\kappa'') \tag{3.73}$$

the differential equation for the rate of the softening variable still has the form (3.69), provided that H is interpreted as the tangent softening modulus (derivative of h) evaluated for the current value of $\kappa + l^2\kappa''$. It is easy to see that the analysis of the linear case remains valid—the size of the plastic zone does not depend on H and therefore does not vary during the deformation process, and the plastic strain distribution is given by a slightly

generalized form of Eq. (3.72), namely

$$\varepsilon_{\mathrm{p}}(x) = \kappa(x) = h^{-1}(\sigma - \sigma_0)\left(1 + C\cos\frac{x - x_0}{l}\right) \tag{3.74}$$

where h^{-1} is the inverse function of h.

The second type of nonlinear softening law in the form

$$\sigma_{\mathrm{Y}} = \sigma_0 + h(\kappa) + g\kappa'' \tag{3.75}$$

is actually that suggested in the original paper by Aifantis (1984). The corresponding differential equation for the rate of the softening variable reads

$$H(\kappa)\dot{\kappa} + g\dot{\kappa}'' = \dot{\sigma} \tag{3.76}$$

where $H \equiv \mathrm{d}h/\mathrm{d}\kappa$ is variable but g is not. Solution (3.71) remains valid only at the bifurcation from a uniform strain state, when $\kappa = 0$ along the bar and thus $H(\kappa) = H(0) = H_0$ is constant in space. At later stages of the localization process, the variation of H results into changes of the plastic strain distribution. Intuitively it can be expected that, for softening curves with gradually decreasing magnitude of the post-peak slope, the increase of the "variable characteristic length" $\sqrt{g/H(\kappa)}$ leads to an expansion of the plastic zone. This is confirmed by numerical simulations of localization with an exponential softening law, Eq. (2.35) and Fig. 2.4b, where $H_0 = \kappa_{\mathrm{c}}/\sigma_0$ is the initial softening modulus (at $\kappa = 0$). The initial size of the plastic zone is $2\pi\sqrt{g/H_0}$ (Fig. 3.12a) but later the plastic zone grows (Fig. 3.12b). This is a sign of locking effects that are apparent from the load-displacement diagram in Fig. 3.12c.

As already mentioned, both extensions (3.73) and (3.75) reduce to the same basic formulations in the linear case. However, as explained in Sec. 2.4, a linear softening law in the true sense of the word has only a limited range of validity.

For the first formulation, Eq. (3.73), the complete expression for the yield stress can be written as

$$\sigma_{\mathrm{Y}} = \left\langle \sigma_0 + H\left[\kappa + l^2\kappa''\right]\right\rangle \tag{3.77}$$

where $\langle\ldots\rangle$ are McAuley brackets denoting the positive part. The jump to a vanishing softening modulus occurs at all points of the plastic zone at the same time, because the expression $\kappa + l^2\kappa''$ is constant along the plastic zone. This jump occurs when the current yield stress in the plastic zone vanishes, which means that the stress transmitted by the bar vanishes as well. The subsequent evolution of plastic strain is not unique, because $\kappa + l^2\kappa''$ does not need to be constant along the plastic zone. This would lead to numerical instabilities in a finite element solution, caused by the singularity of the tangent stiffness matrix. From the physical point of view, it is essential that no stresses are generated at increasing strain, which is guaranteed because yielding continues at zero stress. Thus the model can describe the complete loss of material resistance without any artificial locking effects. Numerical problems could be circumvented by transition to a discontinuous description (discrete crack), removal of fully softened elements from the model, or stabilization by a very small nonzero plastic modulus.

For the second formulation, Eq. (3.75), the complete expression for the yield stress reads

$$\sigma_{\mathrm{Y}} = \langle\sigma_0 + H\kappa\rangle + Hl^2\kappa'' \tag{3.78}$$

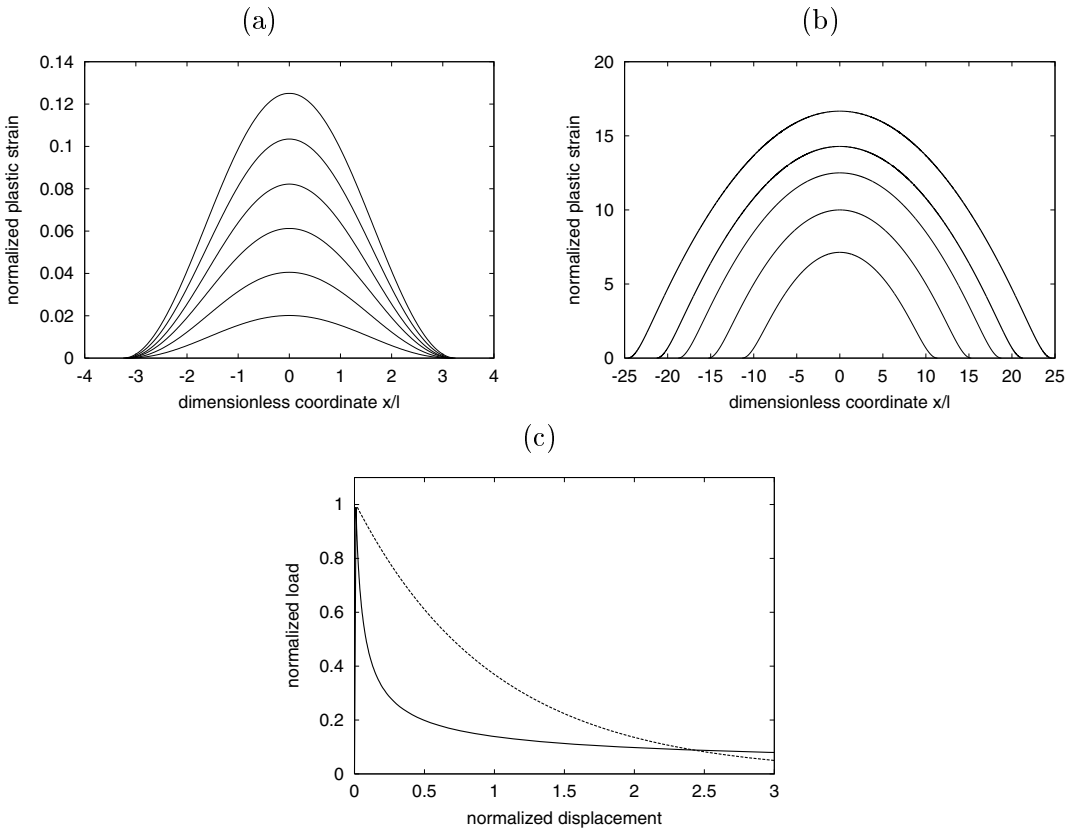

Figure 3.12: Localization simulated with a nonlinear extension of the Aifantis softening law in the form (3.75): (a) evolution of plastic strain profile at early stages of softening, (b) evolution of plastic strain profile at late stages of softening, (c) load-displacement diagram for the localized solution (solid curve) and the unstable uniform solution (dashed curve).

where Hl^2 is used instead of g, so that the equation can be directly compared to Eq. (3.77). In this case, the softening modulus changes when the softening variable κ reaches its critical value κ_c, which does not happen at all points in the plastic zone simultaneously. According to Eq. (3.72), the maximum plastic strain is attained in the middle of the plastic zone, at $x = x_0$:

$$\varepsilon_p(x_0) = \kappa(x_0) = \frac{2(\sigma - \sigma_0)}{H} \tag{3.79}$$

The softening variable $\kappa(x_0)$ reaches its critical value $\kappa_c = -\sigma_0/H$ already at stress level $\sigma = \sigma_0/2$. For stress levels lower than $\sigma_0/2$, $\kappa(x)$ exceeds κ_c in an interval of length L_c located at the center of the plastic zone. In this interval, the term in the Macauley brackets on the right-hand side of Eq. (3.78) vanishes, and the consistency and equilibrium conditions imply that the second derivative of $\kappa(x)$ must be constant, i.e., the distribution of plastic strain is quadratic. By enforcing C_1-continuity and the condition $\kappa = \kappa_c$ at the internal boundary between the interval with quadratic distribution of plastic strain and the remaining part of the plastic zone (in which the solution still has the general form (3.72), but with a variable value of x_0), it is possible to obtain analytical expressions for

$$L_c = \frac{2l}{\sigma}\sqrt{\sigma_0(\sigma_0 - \sigma)} \tag{3.80}$$

$$L_p = 2\pi l + L_c - 2l \arctan\frac{L_c}{2l} \tag{3.81}$$

As σ approaches zero, both L_c and L_p tend to infinity. This confirms that, for softening law (3.78), the plastic zone eventually expands over the entire bar, which is accompanied by strong locking effects.

3.9.4 Influence of a physical boundary

An additional boundary condition is needed for κ on the physical boundary, and the response of the model depends strongly on the applied condition. Often, the boundary condition is chosen as $\kappa = 0$, but $\kappa' = 0$ or any linear combination $a\kappa + bnl\kappa' = 0$ is also possible from the mathematical point of view. Here, a and b are given dimensionless constants, and n is the component of the unit "vector" representing the outer normal to the boundary. For the present one-dimensional problem, $n = -1$ on the left boundary (at $x = 0$) and $n = 1$ on the right boundary (at $x = L$).

If $\kappa = 0$ is adopted, all plastic flow is prohibited on the boundary, see Fig. 3.13. This implies that even if an imperfection is placed right next to the physical boundary, the localization zone is not centered over this imperfection, but its center is located at a distance πl from the boundary. The plastic zone is repulsed by the boundary.

If $\kappa' = 0$ is chosen, plastic strain may reach its maximum directly on the physical boundary, see Fig. 3.13. The length of the localization zone is reduced to one half, $L_p^b = L_p/2 = l\pi$, and the total dissipation is in this case also divided by two. Physically, this is the solution that would actually appear whenever the imperfection is within a distance of up to πl of the boundary. One can say that the localization zone is attracted by the boundary.

Finally, using the Robin-type boundary condition $a\kappa + bnl\kappa' = 0$ gives a solution where a part of the solution on an infinite bar is cut off. The Dirichlet and Neumann conditions are recovered as special cases with $b = 0$ and $a = 0$, respectively.

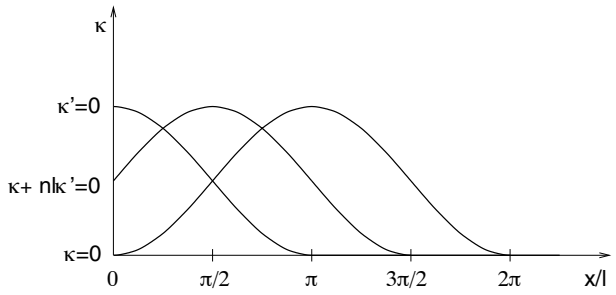

Figure 3.13: Plastic strain distribution for the explicit gradient plasticity model on a finite domain with different boundary conditions.

3.10 Aifantis model with first and second gradients

Certain generalized forms of the softening law (3.68) proposed in the literature use an additional enrichment by a first-gradient term (Aifantis 1984; Aifantis 1992; Aifantis 1995). As already explained in Sec. 3.8.1, in the isotropic case the first gradient of cumulative plastic strain should enter only through its invariant, i.e., its norm, which in the one-dimensional case reduces to the absolute value of κ'.

First, consider the simple extension of the softening law in the form

$$\sigma_{\mathrm{Y}} = \sigma_0 + H\left[\kappa + 2cl|\kappa'| + l^2\kappa''\right] \tag{3.82}$$

where c is a dimensionless parameter, positive or negative. Localized solutions of the one-dimensional problem exist if $|c| < 1$ and they have the form

$$\kappa(x) = \kappa_\sigma\left[1 + \left(\cos\frac{2\pi(x-x_0)}{L_{\mathrm{p}}} - \frac{cL_{\mathrm{p}}}{2\pi l}\sin\frac{2\pi|x-x_0|}{L_{\mathrm{p}}}\right)\exp\frac{c(2|x-x_0|-L_{\mathrm{p}})}{2l}\right] \tag{3.83}$$

where $x \in [x_0 - L_{\mathrm{p}}/2, x_0 + L_{\mathrm{p}}/2]$, $\kappa_\sigma = (\sigma - \sigma_0)/H$ is the plastic strain that would correspond to the given stress level σ in the local version of the model (with no gradient terms), and

$$L_{\mathrm{p}} = \frac{2\pi l}{\sqrt{1-c^2}} \tag{3.84}$$

is the length of the plastic zone, which again remains constant during plastic flow (provided that c is not variable). For $c = 0$ the solution (3.72) of the basic model with second gradient only is recovered.

For fixed length parameter l, the size of the plastic zone monotonically increases with increasing absolute value of c and tends to infinity as c tends to 1 or -1. This means that the enrichment of Eq. (3.68) by the first gradient of cumulative plastic strain leads to a larger plastic zone, independently of the sign of the first-gradient term.

The added term also modifies the shape of the plastic strain profile, but this time the sign does play a role. Fig. 3.14 shows the dimensionless plastic strain κ/κ_σ as a function of the dimensionless coordinate $(x - x_0)/l$ for different values of parameter c. The area under the graph is the plastic bar elongation divided by the normalizing factor $l\kappa_\sigma$. If

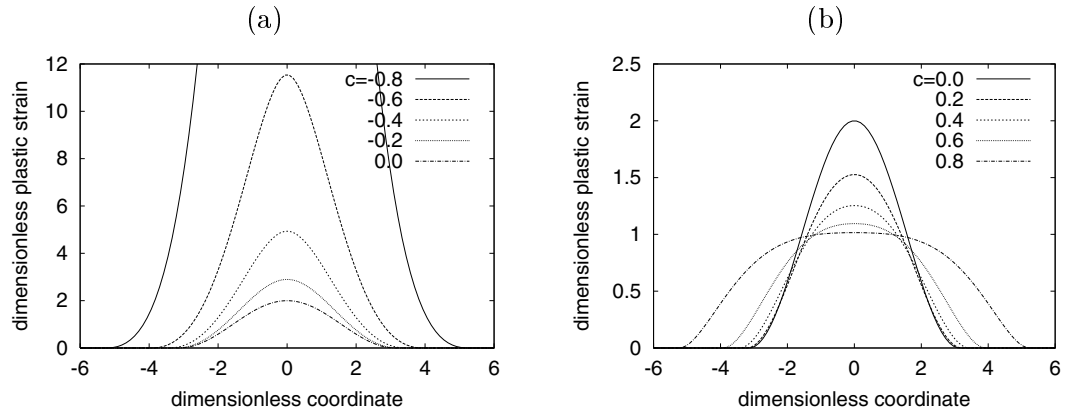

Figure 3.14: Plastic strain profiles for Aifantis model with added linear first-gradient term multiplied by a (a) negative coefficient, (b) positive coefficient.

this area is large, the bar responds in a ductile manner. For negative c (Fig. 3.14a), the maximum value of κ and the area under the graph both increase, which indicates that the response of the bar is more ductile than for the basic model with second gradient only ($c = 0$). For positive c (Fig. 3.14b), the maximum value of κ decreases and the area under the graph first slightly decreases and, for c larger than 0.6, it increases. The response of the bar is somewhat more brittle than for the basic model with second gradient only.

The softening law (3.82) contains gradient terms of different orders, but all of them are positively homogeneous of degree 1. Consequently, the size of the plastic zone and the shape of the plastic strain profile remain constant during softening.

The softening law originally proposed by Aifantis (1984) contained a term proportional to the squared norm of the first gradient. For the present purpose, it is convenient to write it in the form

$$\sigma_{\mathrm{Y}} = \sigma_0 + H\left[\kappa + \tfrac{1}{2}c(l\kappa')^2 + l^2\kappa''\right] \tag{3.85}$$

The corresponding nonlinear differential equation

$$\kappa + \tfrac{1}{2}c(l\kappa')^2 + l^2\kappa'' = \kappa_\sigma \tag{3.86}$$

was studied (in a different context) by Aifantis and Serrin (1983). Based on their results, it is possible to show that the ascending branch of the localized plastic strain profile satisfies the relation

$$cl\frac{\mathrm{d}\kappa}{\mathrm{d}x} = \sqrt{2\left(1 + c\kappa_\sigma\right)\left(1 - e^{-c\kappa}\right) - 2c\kappa} \tag{3.87}$$

The maximum value of plastic strain at the center of the plastic zone, $\kappa_{\max}$, can be obtained by looking for the positive solution of the nonlinear equation

$$c\kappa_{\max} = (1 + c\kappa_\sigma)(1 - e^{-c\kappa_{\max}}) \tag{3.88}$$

It is easy to see that for $1 + c\kappa_\sigma > 0$ this equation has exactly one nonzero solution which is always positive, while for $1 + c\kappa_\sigma \leq 0$ it has no nonzero solution. This indicates that if the coefficient c multiplying the square of the first gradient in Eq. (3.86) is positive (or zero), the plastic strain is bounded for any fixed value of the loading parameter $\kappa_\sigma =$

$(\sigma-\sigma_0)/H$, while if the coefficient is negative, the plastic strain blows up as κ_σ approaches $-1/c$. During the softening process, parameter κ_σ varies from zero to $\kappa_c = -\sigma_0/H$. If this final value of κ_σ at complete softening to zero stress does not exceed $-1/c$, the plastic strain profile still remains bounded. The resulting constraint on parameter c is $c \geq -1/\kappa_c = H/\sigma_0$.

For small values of κ_σ, i.e., at the early stage of localization, the shape of the plastic strain profile is close to the harmonic function Eq. (3.72) and κ_{max} is close to $2\kappa_\sigma$. The quadratic first-gradient term becomes important as κ_σ increases. Numerical solutions of Eq. (3.87) shown in Fig. 3.15 indicate that the size of the plastic zone increases and the plastic profile changes its shape. The graphs are plotted in terms of normalized plastic strain $c\kappa$ and dimensionless spatial coordinate x/l for different values of the rescaled loading parameter $c\kappa_\sigma$. The actual size of plastic zone at full softening to zero residual yield stress depends on the product $c\kappa_c = -c\sigma_0/H$. For instance, if $c = 1/\kappa_c$, the plastic zone grows from the initial size $2\pi l$ only slightly, approximately to $7\,l$, but if $c = 30/\kappa_c$, the final size of the plastic zone is $16\,l$. As already explained, if c is negative and exceeds in magnitude $1/\kappa_c$, the plastic strain in the middle of the plastic zone blows up when $c\kappa_\sigma = -1$, i.e., at stress level $\sigma = \sigma_0 - H/c$. This is again accompanied by locking effects: The total bar elongation tends to infinity as σ approaches the critical level from above, which means that the load-displacement curve asymptotically approaches a horizontal line at nonzero load level as the applied displacement is increased.

It is interesting to note that, for positive c and large κ_σ, the plastic strain profile is close to the parabolic shape that already appeared in the Sec. 3.8. Indeed, it is easy to verify that the quadratic function

$$\kappa(x) = \kappa_\sigma + \frac{1}{c} - \frac{(x-x_0)^2}{2cl^2} \tag{3.89}$$

is a solution of differential equation (3.86). However, this solution does not satisfy the continuity requirements, because its derivative does not vanish at the points where $\kappa(x) = 0$. Still, Eq. (3.89) is a very good approximation to the actual solution inside the plastic zone, with the exception of narrow boundary layers at the elastoplastic boundary. Right at the boundary, both κ and κ' vanish and $\kappa'' = \kappa_\sigma$. With increasing distance from the boundary, the importance of the zeroth- and first-order terms increases and they become dominant. The second derivative quickly approaches a constant value $1/cl^2$, and the solution of Eq. (3.86) becomes close to the solution of Eq. (3.66) with characteristic length $l\sqrt{c/2}$ and with the right-hand side increased by $1/c$.

For large values of c (and small values of l), the present model could be considered as a stabilized version of Schreyer's model. Even though the presence of the second derivative has in this case a negligible effect on the values of plastic strain and on the load-displacement diagram, it is essential from the mathematical point of view, because it enforces a regular solution. Indeed, solutions of the type depicted in Fig. 3.10 would now be inadmissible, because the second derivative at the points of slope change would be unbounded.

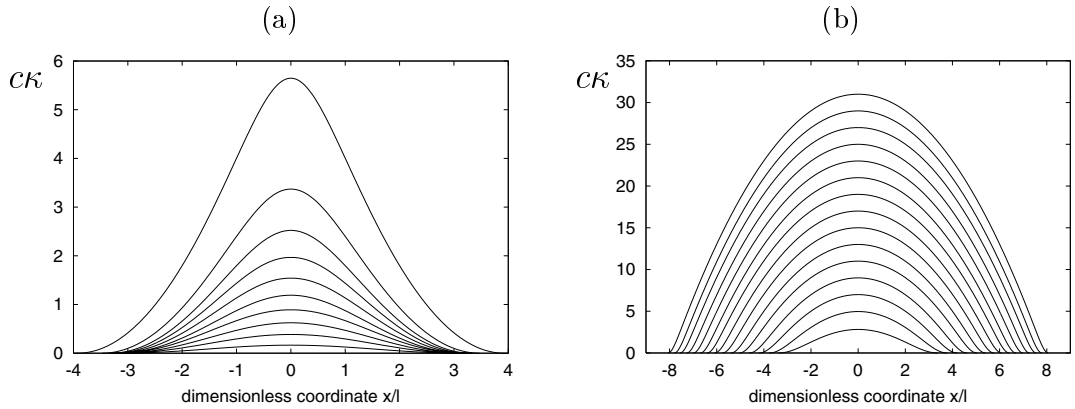

Figure 3.15: Evolution of plastic strain profiles for Aifantis model with added quadratic first-gradient term multiplied by a (a) negative coefficient, (b) positive coefficient.

3.11 Gradient elastoplasticity

Zervos et al. (2001) proposed a model that can be interpreted as a strain-gradient theory with softening law enriched by the second gradient of an internal variable, and they called it gradient elastoplasticity. In this theory, the higher-order elastic law links the double stress to the gradient of the elastic strain, and the yield condition is formulated for the total stress $\sigma - \chi'$, with the current yield stress σ_{Y} dependent on the cumulative plastic strain and its second gradient. Strictly speaking, Zervos et al. (2001) considered the second-gradient term as originating from kinematic hardening-softening, but for the present purpose of one-dimensional localization analysis their softening law can be reinterpreted as isotropic.

In the one-dimensional setting, the elastic part of the constitutive equations is written as

$$\sigma = E(\varepsilon - \varepsilon_{\mathrm{p}}) \tag{3.90}$$

$$\chi = El_{\mathrm{e}}^2(\varepsilon' - \varepsilon_{\mathrm{p}}') \tag{3.91}$$

and the yield function as

$$f(\sigma, \chi', \sigma_{\mathrm{Y}}) = |\sigma - \chi'| - \sigma_{\mathrm{Y}} \tag{3.92}$$

with the current yield stress given by

$$\sigma_{\mathrm{Y}} = \sigma_0 + H\kappa - El_{\mathrm{p}}^2\kappa'' \tag{3.93}$$

The last equation follows the original notation of Zervos et al. (2001) but, if the plastic modulus H is a negative constant, the softening law can be written in the equivalent form (3.68) with $l = l_{\mathrm{p}}\sqrt{-E/H}$.

Note that the higher-order elastic law (3.91) differs from those used by other plastic extensions of strain-gradient elasticity. Chambon's model does not consider any plastic part of the strain gradient and links the double stress to the gradient of the total strain. The Fleck–Hutchinson flow theory considers the plastic part of the strain gradient as an independent internal variable whose evolution is governed by a corresponding flow rule. In the present theory, the plastic part of the strain gradient is set equal to the gradient of plastic strain, so that the flow rule needs to be specified for the plastic strain only.

Replacing $\varepsilon - \varepsilon_\mathrm{p}$ by ε_e and combining Equations (3.90) and (3.91), an expression for the total stress

$$\sigma - \chi' = E(\varepsilon_\mathrm{e} - l_\mathrm{e}^2 \varepsilon_\mathrm{e}'') \tag{3.94}$$

in terms of the elastic strain and its second derivative is obtained. If the higher-order boundary condition reads $\chi = 0$, for the present model it can be rewritten as $\varepsilon_\mathrm{e}' = 0$. The equilibrium condition $\sigma(x) - \chi'(x) = t = \text{const.}$ combined with Eq. (3.94) gives a second-order differential equation for ε_e, and the particular solution satisfying the boundary condition $\varepsilon_\mathrm{e}' = 0$ at both bar ends is simply $\varepsilon_\mathrm{e}(x) = t/E = \text{const.}$

So the distribution of elastic strain remains uniform independently of the plastic processes, and the double stress vanishes. Consequently, the Cauchy stress σ remains uniform and the distribution of plastic strain can be obtained in the same way as for the Aifantis model, with exactly the same solution , Eq. (3.72). Of course, this is true only under the aforementioned assumptions of a homogeneous prismatic bar (or homogeneous shear layer under isochoric plastic flow) with vanishing body forces and higher-order tractions. Nevertheless, this example illustrates the close relationship between the gradient elastoplasticity of Zervos et al. (2001) and the traditional Aifantis model. Based on the correspondence, one can also expect locking effects if Eq. (3.93) is generalized to the nonlinear form with $H\kappa$ replaced by a convex function $h(\kappa)$ and the second-gradient term kept unchanged.

3.12 Ductile damage model of Geers and coworkers

3.12.1 Model description

Drawing inspiration from implicit gradient damage models (Peerlings et al. 1996), Geers, Engelen and coworkers proposed an implicit gradient plasticity model based on the concept of ductile damage (Geers et al. 2001; Engelen et al. 2003; Geers 2003; Geers et al. 2003). Softening is assumed to be driven by a transformed softening variable $\bar{\kappa}$, defined as the solution of a Helmholtz-type differential equation (valid for the entire body), which in the one-dimensional setting reduces to

$$\bar{\kappa} - l^2 \bar{\kappa}'' = \kappa \tag{3.95}$$

As usual, l is a material parameter with the dimension of length. The solution must satisfy the Neumann-type boundary conditions $\bar{\kappa}' = 0$ imposed at both end sections of the bar. As already discussed in Sec. 3.3, this implicit definition of $\bar{\kappa}$ is equivalent to weighted spatial averaging of the local softening variable κ with the Green function of the corresponding boundary value problem playing the role of the weight function. Therefore, $\bar{\kappa}$ will be referred to as the nonlocal softening variable.

An essential component of the model proposed by Geers et al. (2001) is the hardening-softening law written in the multiplicative form

$$\sigma_\mathrm{Y} = [1 - \omega_\mathrm{p}(\bar{\kappa})](\sigma_0 + H_\mathrm{L0}\kappa) \tag{3.96}$$

where the plastic modulus H_L0 is a positive constant, and the term $\sigma_0 + H_\mathrm{L0}\kappa$ represents linear plastic hardening of the bulk material. Due to the growth and coalescence of voids, the effective yield stress $\sigma_0 + H_\mathrm{L0}\kappa$ is reduced by a scalar factor $1 - \omega_\mathrm{p}$, similar to the reduction of the effective stress in continuum damage mechanics. While the hardening

process is driven by the local value of the cumulative plastic strain, the degradation of yield stress due to ductile damage is driven by the nonlocal cumulative plastic strain.

The damage variable ω_p grows from 0 to 1, but the onset of ductile damage does not need to coincide with the onset of yielding. In the simplest case, the dependence of ω_p on $\bar{\kappa}$ is described by a piecewise linear law,

$$\omega_\mathrm{p}(\bar{\kappa}) = \begin{cases} 0 & \text{for} \quad \bar{\kappa} \leq \kappa_\mathrm{i} \\ \dfrac{\bar{\kappa} - \kappa_\mathrm{i}}{\kappa_\mathrm{c} - \kappa_\mathrm{i}} & \text{for} \quad \kappa_\mathrm{i} \leq \bar{\kappa} \leq \kappa_\mathrm{c} \\ 1 & \text{for} \quad \bar{\kappa} \geq \kappa_\mathrm{c} \end{cases} \tag{3.97}$$

in which κ_i and κ_c are material parameters that specify the damage threshold and the (nonlocal) plastic deformation at complete damage (i.e., at zero residual yield stress), respectively; see Fig. 3.16a left. Alternatively, Geers et al. (2001) proposed the exponential damage law (Fig. 3.16a right)

$$\omega_\mathrm{p}(\bar{\kappa}) = \begin{cases} 0 & \text{for} \quad \bar{\kappa} \leq \kappa_\mathrm{i} \\ 1 - \exp\left(-\dfrac{\bar{\kappa} - \kappa_\mathrm{i}}{\kappa_\mathrm{c} - \kappa_\mathrm{i}}\right) & \text{for} \quad \kappa_\mathrm{i} \leq \bar{\kappa} \end{cases} \tag{3.98}$$

which gives a more realistic shape of the stress-strain law for materials such as concrete, characterized by a long tail of the softening curve; cf. Fig. 3.16d.

3.12.2 Bifurcation from a uniform state

As long as the damage variable ω_p remains equal to zero, the material is either elastic, or plastically hardening, and the strain distribution in a simple one-dimensional tensile test remains uniform. Depending on the choice of the specific ductile damage law, bifurcation can take place either right away at the onset of damage growth, or later, when a certain critical state is reached.

At incipient localization, all variables characterizing the material state are still uniformly distributed along the bar. It is easy to see that if $\kappa(x) = \kappa^* = \text{const.}$, then $\bar{\kappa}(x) = \kappa^*$ satisfies the differential equation (3.95) and the homogeneous Neumann boundary conditions. The plastic strain rate $\dot{\kappa}$ and its nonlocal counterpart $\dot{\bar{\kappa}}$ are linked by the rate form of Eq. (3.95),

$$\dot{\bar{\kappa}} - l^2 \dot{\bar{\kappa}}'' = \dot{\kappa} \tag{3.99}$$

Suppose that the plastic strain rate localizes in a plastic region I_p. The consistency condition $\dot{f} \equiv \dot{\sigma} - \dot{\sigma}_\mathrm{Y} = 0$ provides an additional equation linking the local and nonlocal plastic strain rates. Indeed, differentiating Eq. (3.96) leads to

$$\dot{\sigma}_\mathrm{Y} = (1 - \omega_\mathrm{p}) H_{\mathrm{L}0} \dot{\kappa} - \omega_\mathrm{p}'(\sigma_0 + H_{\mathrm{L}0}\kappa)\dot{\bar{\kappa}} = H_\mathrm{L}\dot{\kappa} + H_\mathrm{NL}\dot{\bar{\kappa}} \tag{3.100}$$

where $\omega_\mathrm{p}' \equiv \mathrm{d}\omega_\mathrm{p}/\mathrm{d}\bar{\kappa}$ is the derivative of the damage function, $H_\mathrm{L} = (1 - \omega_\mathrm{p}) H_{\mathrm{L}0}$ and $H_\mathrm{NL} = -(\sigma_0 + H_{\mathrm{L}0}\kappa)\omega_\mathrm{p}' = -(\kappa_0 + \kappa)\omega_\mathrm{p}' H_{\mathrm{L}0}$ can be considered as the current "local" and "nonlocal" plastic modulus, resp., and $\kappa_0 = \sigma_0 / H_{\mathrm{L}0}$ is a constant parameter introduced for convenience. Substituting Eq. (3.99) into the consistency condition

$$\dot{\sigma} = H_\mathrm{L}\dot{\kappa} + H_\mathrm{NL}\dot{\bar{\kappa}} \tag{3.101}$$

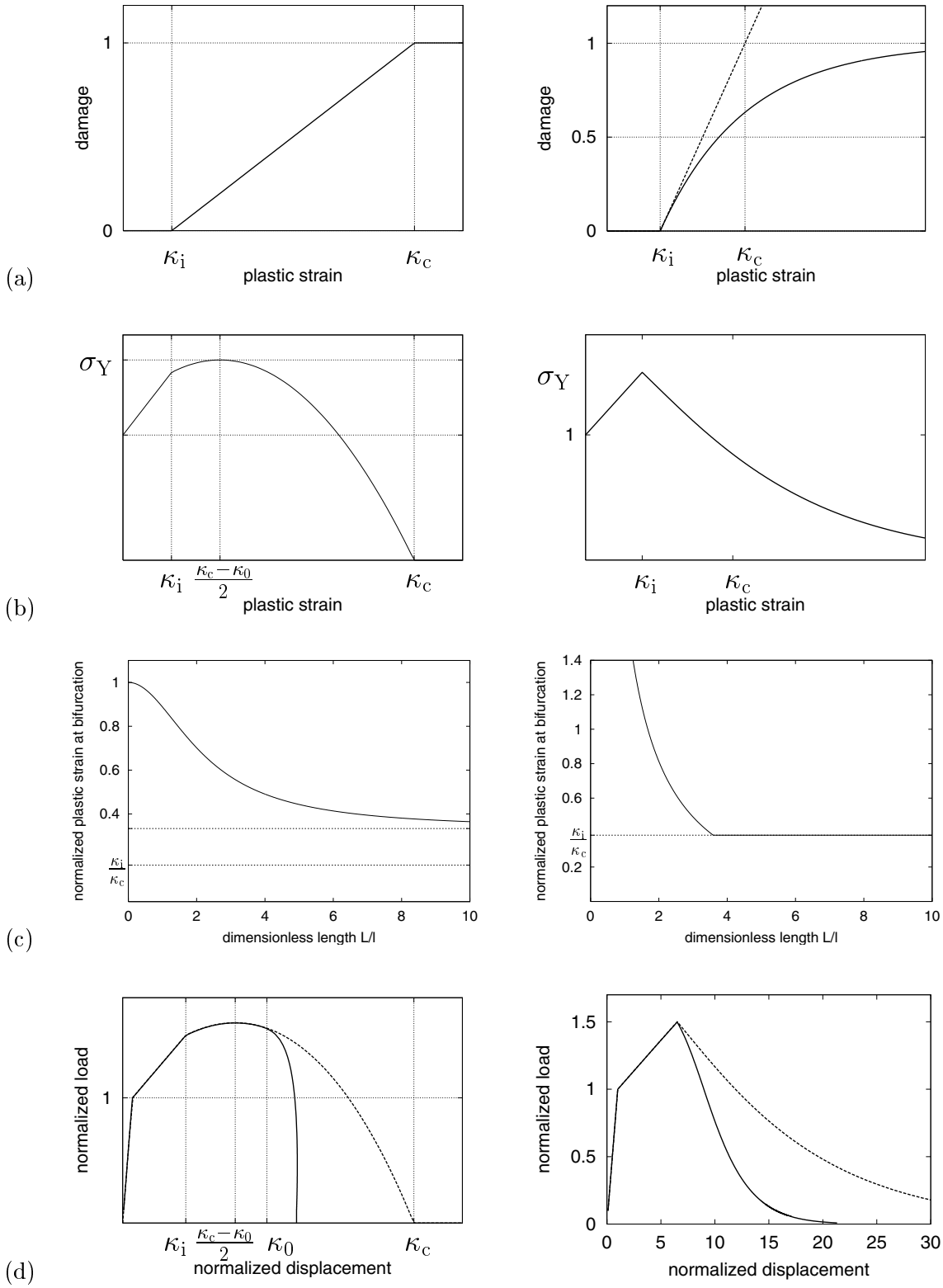

Figure 3.16: Illustration of implicit gradient plasticity model with a linear (left) or exponential (right) damage law: (a) damage law, (b) yield stress as a function of plastic strain in a uniform state, (c) dependence between the plastic strain at bifurcation and the bar length, (d) stress-elongation diagram for uniform response (dashed) and localized response (solid).

the local rate $\dot{\kappa}$ can be eliminated. In the plastic region I_p, the nonlocal rate $\dot{\bar{\kappa}}$ can then be computed from the differential equation

$$(H_\mathrm{L} + H_\mathrm{NL})\dot{\bar{\kappa}} - H_\mathrm{L} l^2 \dot{\bar{\kappa}}'' = \dot{\sigma} \tag{3.102}$$

In the elastic region, $\dot{\kappa}$ vanishes and the governing differential equation for the nonlocal rate,

$$\dot{\bar{\kappa}} - l^2 \dot{\bar{\kappa}}'' = 0 \tag{3.103}$$

is obtained directly from Eq. (3.99).

The solution of (3.102)–(3.103) must be continuously differentiable and must satisfy the boundary conditions $\dot{\bar{\kappa}}'(0) = 0$ and $\dot{\bar{\kappa}}'(L) = 0$. It is easy to show that if $H_\mathrm{L} + H_\mathrm{NL}$ is positive, the problem admits only a uniform solution $\dot{\kappa}(x) = \dot{\bar{\kappa}}(x) = \dot{\sigma}/(H_\mathrm{L} + H_\mathrm{NL})$. The yield stress is still growing and localization is impossible. The plastic region extends over the entire bar. Suppose now that $H_\mathrm{L} + H_\mathrm{NL}$ is negative, and that the plastic region extends from 0 to L_p and the elastic region from L_p to L. The general solution of (3.102)–(3.103) is then

$$\dot{\bar{\kappa}}(x) = \begin{cases} \dfrac{\dot{\sigma}}{H_\mathrm{L} + H_\mathrm{NL}} + C_1 \cos\dfrac{\alpha x}{l} + C_2 \sin\dfrac{\alpha x}{l} & \text{for } x \in I_\mathrm{p} \equiv [0, L_\mathrm{p}] \\ C_3 \cosh\dfrac{x}{l} + C_4 \sinh\dfrac{x}{l} & \text{for } x \in I_\mathrm{e} \equiv [L_\mathrm{p}, L] \end{cases} \tag{3.104}$$

where C_i, $i = 1, 2, 3, 4$, are integration constants, and

$$\alpha(\kappa, \bar{\kappa}) = \sqrt{-1 - \frac{H_\mathrm{NL}(\kappa, \bar{\kappa})}{H_\mathrm{L}(\bar{\kappa})}} = \sqrt{\frac{(\kappa + \kappa_0)\omega_\mathrm{p}'(\bar{\kappa})}{1 - \omega_\mathrm{p}(\bar{\kappa})} - 1} \tag{3.105}$$

is a parameter that depends on the current state.

It is possible to show that the local rate $\dot{\kappa}(x)$ is continuous at the elastoplastic interface, otherwise the unloading condition $\dot{\sigma} \le \dot{\sigma}_\mathrm{Y}$ would be violated in a part of the elastic domain adjacent to that interface. Imposing condition $\dot{\kappa}(L_\mathrm{p}) \equiv \dot{\bar{\kappa}}(L_\mathrm{p}) - l^2 \dot{\bar{\kappa}}''(L_\mathrm{p}) = 0$ and the boundary conditions on the general solution (3.104), a family of particular solutions of the form

$$\dot{\bar{\kappa}}(x) = \begin{cases} \dfrac{\dot{\sigma}}{H_\mathrm{L} + H_\mathrm{NL}} \left(1 + \dfrac{H_\mathrm{L}}{H_\mathrm{NL}} \dfrac{\cos\dfrac{\alpha x}{l}}{\cos\dfrac{\alpha L_\mathrm{p}}{l}} \right) & \text{for } x \in I_\mathrm{p} \equiv [0, L_\mathrm{p}] \\ \dfrac{\dot{\sigma}}{H_\mathrm{NL}} \dfrac{\cosh\dfrac{L - x}{l}}{\cosh\dfrac{L - L_\mathrm{p}}{l}} & \text{for } x \in I_\mathrm{e} \equiv [L_\mathrm{p}, L] \end{cases} \tag{3.106}$$

is obtained.

The initial size of the plastic region is determined from the condition of continuity of $\dot{\bar{\kappa}}'$ at $x = L_\mathrm{p}$, which turns out to lead to the same equation (3.25) as obtained for Chambon's model in Sec. 3.5. Consequently, the size of the plastic region is again formally given by $L_\mathrm{p} = l\lambda_\mathrm{p}(\alpha, L/l)$, only the meaning of parameter α is now different. The general

results regarding the size of the plastic region and the minimum bar length needed to induce localization remain valid. However, in view of the modified expression for α, their physical interpretation must be reconsidered.

For Chambon's model, parameter α depends only on the ratio of the tangent elastoplastic modulus to the modulus of elasticity. For the present model, α is given by Eq. (3.105) and depends on the ratio between the local and nonlocal tangent moduli. At bifurcation from a uniform state, the distribution of plastic strain is still uniform along the bar, and there is no difference between κ and $\bar{\kappa}$. Using the expressions $\omega_{\mathrm{p}}(\bar{\kappa}) = (\bar{\kappa} - \kappa_{\mathrm{i}})/(\kappa_{\mathrm{c}} - \kappa_{\mathrm{i}})$, $\omega'_{\mathrm{p}}(\bar{\kappa}) = 1/(\kappa_{\mathrm{c}} - \kappa_{\mathrm{i}})$ that hold for the piecewise linear damage law (3.97) and for the range $\kappa_{\mathrm{i}} \leq \kappa < \kappa_{\mathrm{c}}$, α is evaluated as

$$\alpha(\kappa, \bar{\kappa}) = \sqrt{\frac{(\kappa + \kappa_0)\omega'_{\mathrm{p}}(\bar{\kappa})}{1 - \omega_{\mathrm{p}}(\bar{\kappa})} - 1} = \sqrt{\frac{\kappa + \bar{\kappa} + \kappa_0 - \kappa_{\mathrm{c}}}{\kappa_{\mathrm{c}} - \bar{\kappa}}} \tag{3.107}$$

The value of α is real if $\kappa + \bar{\kappa}$ is not less than $\kappa_{\mathrm{c}} - \kappa_0$. Depending on the combination of model parameters, this can happen either right at the onset of damage (at $\kappa = \bar{\kappa} = \kappa_{\mathrm{i}}$) or later. Suppose that $2\kappa_{\mathrm{i}} + \kappa_0 < \kappa_{\mathrm{c}}$. In this case, the yield stress is still increasing after the onset of damage, and it reaches its maximum at $\kappa = \bar{\kappa} = (\kappa_{\mathrm{c}} - \kappa_0)/2$; see Fig. 3.16b left. At this state, the corresponding value of α is zero, and the size of the plastic region predicted by bifurcation analysis is infinite. This represents the theoretical onset of localization in an unbounded domain. Note that the condition $\alpha = 0$ is equivalent to $H_{\mathrm{L}} + H_{\mathrm{NL}} = 0$ (in general, not only for the linear damage law), and so the localization in an infinite bar starts at peak stress.

For a finite bar, bifurcation is postponed if the theoretical size of the plastic region $L_{\mathrm{p}} = l\lambda_{\mathrm{p}}(\alpha, L/l)$ exceeds the actual bar length L. Since λ_{p} is an increasing function of α and α is an increasing function of κ, the plastic strain at bifurcation,

$$\kappa_{\mathrm{b}} = \frac{\kappa_{\mathrm{c}} - \kappa_0 + \left(\frac{\pi l}{L}\right)^2 \kappa_{\mathrm{c}}}{2 + \left(\frac{\pi l}{L}\right)^2} \tag{3.108}$$

can be computed from the condition $L = \pi l/\alpha(\kappa_{\mathrm{b}}, \kappa_{\mathrm{b}})$.

For the exponential damage law (3.98), $\omega'_{\mathrm{p}}(\bar{\kappa}) = [1 - \omega_{\mathrm{p}}(\bar{\kappa})]/(\kappa_{\mathrm{c}} - \kappa_{\mathrm{i}})$ holds and

$$\alpha(\kappa, \bar{\kappa}) = \sqrt{\frac{(\kappa + \kappa_0)\omega'_{\mathrm{p}}(\bar{\kappa})}{1 - \omega_{\mathrm{p}}(\bar{\kappa})} - 1} = \sqrt{\frac{\kappa + \kappa_0 + \kappa_{\mathrm{i}} - \kappa_{\mathrm{c}}}{\kappa_{\mathrm{c}} - \kappa_{\mathrm{i}}}} \tag{3.109}$$

Note that, in this particular case, α happens to be independent of $\bar{\kappa}$. For an infinite bar, localization starts at $\kappa = \bar{\kappa} = \kappa_{\mathrm{c}} - \kappa_{\mathrm{i}} - \kappa_0$. For a finite bar of length L, the plastic strain at bifurcation is

$$\kappa_{\mathrm{b}} = \left(\frac{\pi l}{L} + 1\right)(\kappa_{\mathrm{c}} - \kappa_{\mathrm{i}}) - \kappa_0 \tag{3.110}$$

The dependence between the bar length and the plastic strain at bifurcation is illustrated in Fig. 3.16c. If the plastic strain at bifurcation κ_{b} computed from Eq. (3.108) or (3.110) is smaller than the plastic strain at the onset of damage, κ_{i}, bifurcation takes place at $\kappa = \kappa_{\mathrm{i}}$ and the size of the localized plastic region is immediately smaller than the bar length. This happens if the hardening curve has a sharp peak; see Fig. 3.16b right.

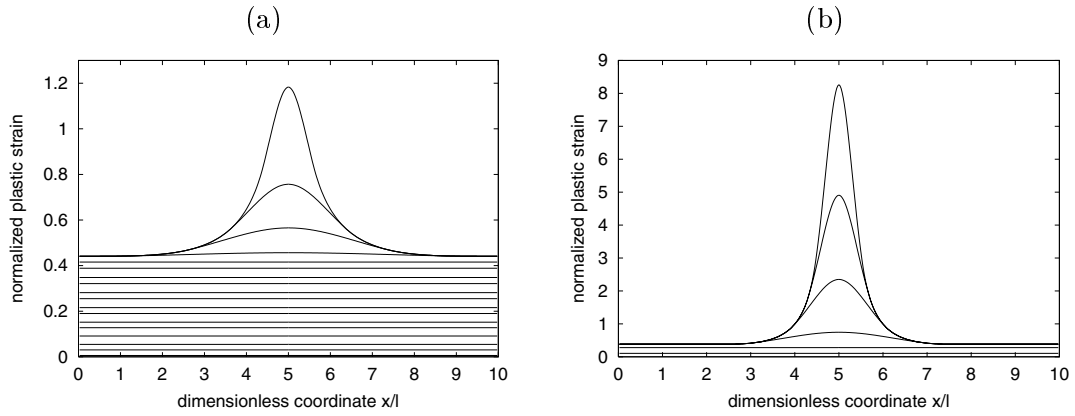

Figure 3.17: Ductile damage model: Evolution of plastic strain for the (a) linear and (b) exponential damage law.

3.12.3 Evolution of plastic region

The rate solution derived in the previous section would be valid for finite increments if parameter α remained constant across the localized plastic region. This was discussed already for Chambon's model in Sec. 3.5.3. For Chambon's model, α is given by Eq. (3.23) and depends only on the ratio of the tangent elastoplastic modulus to the modulus of elasticity. So the parameter α and, consequently, the size of the plastic region L_{p}, remain constant for linear softening.

For the present model, α given by Eq. (3.105) in general depends on both the local and nonlocal values of cumulative plastic strain. Consequently, the size of the plastic region and the distribution of plastic strain rates are expected to evolve during the localization process. For the exponential damage law (3.98), α given by Eq. (3.110) turns out to depend only on the local value, κ, and it increases with increasing κ. Since larger values of α correspond to smaller sizes of the plastic region, it can be expected that the plastic region tends to shrink during the loading process. This is confirmed by numerical simulations, see Fig. 3.17b. For the linear damage law (3.97), α given by Eq. (3.108) depends on both κ and $\bar{\kappa}$ but is still an increasing function of either of them if the other one is kept fixed. Consequently, the plastic region tends to shrink for this law as well; see Fig. 3.17a.

It is interesting to note that, even for a perfect bar, the position of the plastic zone is not arbitrary. In the examples presented here, the solutions are always symmetric with a localized zone in the middle of the bar, surrounded by two elastic zones that extend to the bar ends. Solutions localized at one boundary can be constructed from the symmetric ones by cutting the bar in the middle. If the plastic strain localizes into a single interval detached from the boundaries, this interval is always located exactly in the middle of the bar.

An implicit gradient formulation with hardening-softening law (3.96) does not suffer spurious locking effects, at least not for the commonly used damage laws. The plastic zone is shrinking and the stress transmitted by the bar tends to zero faster than for the unstable homogeneous solution. The model can safely be used for simulations of the complete failure process.

model	sec.	stress-strain laws		yield function
Chambon	3.5	$\sigma = E\,(\varepsilon - \varepsilon_{\rm p})$	$\chi = El^2\eta$	$f(\sigma,\kappa) = \sigma - [\sigma_0 + h(\kappa)]$
F&H	3.6	$\sigma = E\,(\varepsilon - \varepsilon_{\rm p})$	$\chi = El^2\,(\eta - \eta_{\rm p})$	$f(\sigma,\chi,\kappa) = \Sigma(\sigma,\chi) - [\sigma_0 + h(\kappa)]$
MSG	3.7	$\sigma = E\,(\varepsilon - \varepsilon_{\rm p})$	(3.43)	$f(\sigma,\kappa,\eta) = \sigma - [\sigma_0 + h(\kappa,\eta)]$
GEP	3.11	$\sigma = E\,(\varepsilon - \varepsilon_{\rm p})$	$\chi = El^2(\eta - \varepsilon'_{\rm p})$	$f(\sigma,\chi,\kappa) = $ $= \lvert\sigma - \chi'\rvert - [\sigma_0 + h(\kappa,\kappa'')]$

Table 3.1: Overview of strain-gradient plasticity models

model	sec.	softening law
local	2.4	$\sigma_{\rm Y} = \sigma_0 + h(\kappa)$
Schreyer	3.8	$\sigma_{\rm Y} = \sigma_0 + H\,[\kappa + (l\kappa')^2]$
second-gradient model of Aifantis	3.9	$\sigma_{\rm Y} = \sigma_0 + H\,[\kappa + l^2\kappa'']$
Aifantis (first and second gradients)	3.10	$\sigma_{\rm Y} = \sigma_0 + H\,[\kappa + 2cl\lvert\kappa'\rvert + l^2\kappa'']$
Aifantis (first and second gradients)	3.10	$\sigma_{\rm Y} = \sigma_0 + H\,[\kappa + \frac{1}{2}c(l\kappa')^2 + l^2\kappa'']$
ductile damage	3.12	$\sigma_{\rm Y} = \sigma_0 + h(\kappa,\bar\kappa)$

Table 3.2: Overview of gradient plasticity models using gradients of internal variables.

3.13 Overview of gradient plasticity models

A number of gradient plasticity models have been scrutinized in this chapter, see Tables 3.1 and 3.2 for an overview. Of course, these simple tables provide only the basic orientation; they cannot cover all the specific details of different formulations. For the strain-gradient models, Table 3.1 shows the stress-strain laws and the general format of the yield function. For the gradient plasticity models that make use of gradients of internal variables, the stress-strain relations and the evolution equations keep the standard form of the local model. The enhancement is introduced through the softening law, and the various formulations are compared in Table 3.2.

The main results can be summarized as follows:

1. Strain-gradient models based on the elastic strain-gradient theory provide regular solutions at the initial bifurcation, with the exception of the mechanism-based strain-gradient plasticity for which no localization occurs. At late stages of the softening process, Chambon's model nevertheless suffers locking, i.e. high residual stresses at increasing strain. For the Fleck–Hutchinson model, the model response at later stages has not been completely understood by the author.

2. Apart from Schreyer's model, the gradient plasticity models using gradients of internal variables efficiently regularize the initial bifurcation. For suitably formulated softening laws, the response at late stages of the softening process remains objective. Schreyer's model suffers serious mathematical problems and cannot be used for a regularized description of softening.

3. The numerical solution of strain-gradient models as well as explicit gradient models using gradients of internal variables leads to certain difficulties. Strain-gradient models require the independent interpolation of displacement and strain. Since the displacement field needs to be interpolated by a C^1-continuous function, the spatial

discretization with finite elements is difficult for multiple dimensions. For explicit gradient models using gradients of internal variables, continuity requirements on the internal variable field lead to similar problems.

4. The implicit gradient plasticity model motivated by ductile damage, which is strongly nonlocal, regularizes the problem both at the initial bifurcation and at later stages of the loading process in an objective manner. The numerical solution requires a two-field interpolation, but the discretized fields need to be only C^0-continuous.

Chapter 4

Integral-type nonlocal plasticity models

4.1 General assumptions

This chapter presents a detailed analysis of the existing integral-type nonlocal formulations, illustrates their regularizing effect, and compares their fundamental properties. To keep the presentation simple, attention is, as for the gradient models in Chapter 3, restricted to small-strain theory and to localization problems that allow a one-dimensional description (localization in a bar under uniaxial tension or in a semi-infinite layer under shear). Nevertheless, many important conclusions can be extended to the general case.

4.2 Model with nonlocal softening variable

4.2.1 Model description

Perhaps the simplest nonlocal plasticity model can be constructed if the softening law (2.30) is reformulated as

$$\sigma_{\mathrm{Y}} = \sigma_0 + H\bar{\kappa} \tag{4.1}$$

where the local softening variable κ is simply replaced by its nonlocal counterpart $\bar{\kappa}$. All other equations remain the same. Degradation of the yield stress is driven by the nonlocal average of the cumulative plastic strain. For brevity, this model will be called *basic nonlocal model* in the following.

4.2.2 Plastic region far from the boundary

The most interesting part of the solution of the bifurcation problem is the distribution of the softening variable κ and the size of the plastic zone, i.e. the part of the bar where $\dot{\kappa} > 0$. In a uniform bar and in the absence of body forces, the stress is uniform (at any stage of a quasistatic loading process), and the limit elastic state is reached simultaneously by all the material points. Assuming that the bar is divided into a plastic region $I_{\mathrm{p}} = (a, b)$ and an elastic region I_{e}, possible solutions with localized plastic strain are seeked. First, consider the case when the plastic region is sufficiently far from the boundary, so that the weight function α_∞ can be used without any adjustments.

To obtain an equation for the softening variable, start with the consistency condition in the plastic region, which states that the rate of the yield function $\dot{f} = \dot{\sigma}\,\mathrm{sgn}\,\sigma - \dot{\sigma}_\mathrm{Y}$ vanishes in I_p. In the extension test, the stress σ is positive, and so $\mathrm{sgn}\,\sigma = 1$. One could also postulate that the material can yield only in tension and drop the absolute value operator already from the yield function (2.33). Substituting the rate form of Equations (4.1) and (2.13) into the consistency condition $\dot{f} = 0$, the rate of the softening variable must satisfy the equation

$$\int_a^b \alpha_\infty(x-\xi)\dot{\kappa}(\xi)\mathrm{d}\xi = \frac{\dot{\sigma}}{H} \qquad \forall x \in (a,b) \tag{4.2}$$

The integration limits have been set to a and b because $\dot{\kappa}$ vanishes outside I_p.

Planas et al. (1994) showed that, for a wide class of weight functions, Eq. (4.2) does not admit any bounded solution $\dot{\kappa}$. Equation (4.2) is a Fredholm integral equation of the *first kind* for the unknown function $\dot{\kappa}$, and it is known that the solution of such equations often does not exist, at least not within a 'reasonable' space of functions, even if the right-hand side is very regular; see e.g. Baker (1977). To explain the main idea of the proof, first assume that the weight function is continuously differentiable. As already explained, $\dot{\sigma}$ and H do not depend on the spatial coordinate x. Differentiating Eq. (4.2) with respect to x leads to

$$\int_a^b \alpha'_\infty(x-\xi)\dot{\kappa}(\xi)\mathrm{d}\xi = 0 \qquad \forall x \in (a,b) \tag{4.3}$$

where $\alpha'_\infty \equiv \mathrm{d}\alpha_\infty/\mathrm{d}r$ is the derivative of the weight function. Suppose that $\dot{\kappa}$ is an integrable function, and recall that it is positive in I_p. The left-hand side of Eq. (4.3) is the convolution of an integrable function $\dot{\kappa}$ with a continuous function α'_∞, and is therefore continuous for all x. Continuity implies that Eq. (4.3) must also hold for x located at the boundary of I_p. Setting $x = b$ gives

$$\int_a^b \alpha'_\infty(b-\xi)\dot{\kappa}(\xi)\mathrm{d}\xi = 0 \tag{4.4}$$

If the weight function is strictly decreasing with increasing distance between the source and target points, $\alpha'_\infty(r) < 0$ for $0 < r < R$ where $R > 0$ is the interaction radius. Because $\dot{\kappa}(x) > 0$ in (a,b), the integral in Eq. (4.4) must be negative, which is a contradiction showing that, under the given assumptions, no integrable positive function $\dot{\kappa}(x)$ can satisfy Eq. (4.2).

After some technical adjustments, the proof can be extended to weight functions that are only piecewise continuous, provided that their derivative exists and is bounded everywhere except for a finite number of points. If the derivative is unbounded but integrable, no bounded solution $\dot{\kappa}(x)$ can exist. However, an essential assumption is still that the derivative is nonpositive for $r > 0$ and that there exists an interval $(0, R_0)$ in which it is negative.

Only for weight functions that are constant in some neighborhood of the origin, most notably for the uniform weight function, Eq. (4.2) has regular solutions. If $\alpha'_\infty(r) = 0$ for $r \in (-R_0, R_0)$, then a uniform plastic strain rate $\dot{\kappa}(x)$ on any interval (a,b) of length $b - a \leq R_0$ is transformed into a nonlocal plastic strain rate that is uniform on the same interval, and thus there exists a localized solution with a bounded plastic strain rate.

In summary, localized solutions with the plastic strain rate described by a bounded function exist only for very special weight functions. For typical bell-shaped weight functions, localization of plastic strain into a zone of nonzero thickness is impossible. This does not mean that the plastic strain cannot localize at all.

Localized patterns can appear, but they are not sufficiently regular so as to be described by usual functions. A typical plastic strain distribution of this kind is given by

$$\kappa(x) = \varepsilon_{\mathrm{p}}(x) = \frac{\sigma - \sigma_0}{H\alpha_\infty(0)}\,\delta(x - x_{\mathrm{s}}) \tag{4.5}$$

where x_{s} is the localization point (determined by random imperfections), and δ denotes the Dirac distribution, see Fig. 4.1. The corresponding nonlocal field

$$\bar{\kappa}(x) = \int_{\mathcal{L}} \alpha(x,\xi)\kappa(\xi)\mathrm{d}\xi = \frac{\sigma - \sigma_0}{H\alpha_\infty(0)}\,\alpha_\infty(x - x_{\mathrm{s}}) \tag{4.6}$$

is a multiple of the weight function centered at x_{s}. Because the plastic zone is now collapsed into a single point (representing one cross section of the bar), the nonlocal plastic strain rate does not need to be constant in a nonzero interval.

Such localized solution are possible solution for weight functions which attain their maximum at x_0. The localized solution is admissible only if the yield function is nowhere positive. Because the stress is constant, this means that the distribution of the current yield stress reaches its minimum at $x = x_{\mathrm{s}}$. Note that, in contrast to local plasticity, the yield stress changes not only inside the plastic region but also in its neighborhood, because $\bar{\kappa}$ can be positive at a certain point x_0 even if $\kappa(x_0) = 0$. For the linear softening model, the reduction of the yield stress is proportional to the nonlocal softening variable, and so the solution (4.5) is admissible only if the nonlocal field $\bar{\kappa}(x)$ has its maximum at $x = x_{\mathrm{s}}$. In view of Eq. (4.6), this means that the weight function $\alpha_\infty(r)$ must attain its maximum (not necessarily a strict one) at $r = 0$. Because this is the standard property of all nonlocal weight functions in common use, the solution is valid. So, even for weight functions that admit a bounded localized plastic strain, localization into a set of zero measure is possible.

As pointed out by Planas et al. (1993), the present basic nonlocal formulation is essentially equivalent to a cohesive zone model. The distribution of plastic strain (4.5) corresponds to a displacement jump

$$[[u]](x_s) = \frac{\sigma - \sigma_0}{H\alpha_\infty(0)} \tag{4.7}$$

at cross section x_{s}. Equation (4.7) can be interpreted as a cohesive traction-separation law

$$\sigma = \sigma_0 + H\alpha_\infty(0)[[u]] \tag{4.8}$$

This formulation is not a true localization limiter, because it does not prevent localization of the inelastic strain into a set of zero measure. The stress transmitted by the cohesive zone vanishes when the displacement jump $[[u]]$ reaches the critical value $u_f = -\sigma_0/(H\alpha_\infty(0))$.

Despite the fully localized character of local strain, the energy consumed by complete failure of the bar is nonzero. For linear softening, the consumed energy per unit area of the failed cross section can be evaluated as

$$G_{\mathrm{F}} = \frac{1}{2}\sigma_0 u_f = -\frac{\sigma_0^2}{2H\alpha_\infty(0)} \tag{4.9}$$

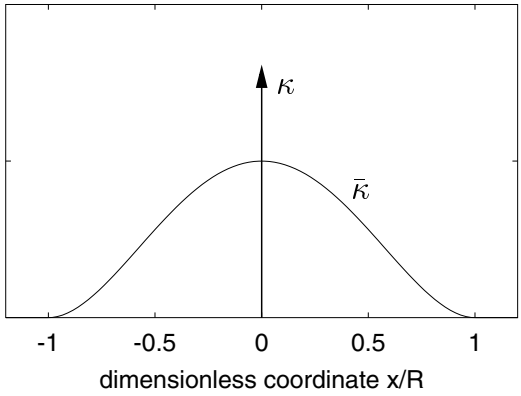

Figure 4.1: Localized plastic strain distribution.

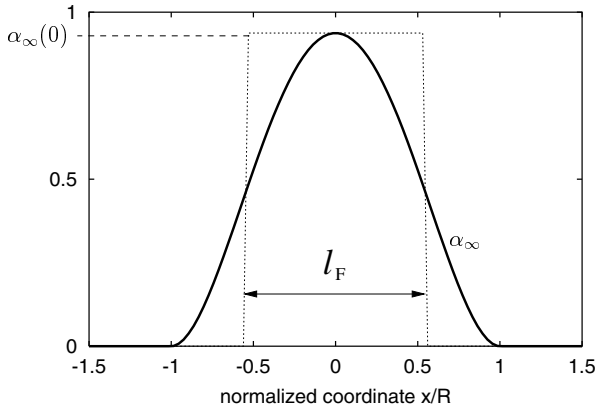

Figure 4.2: Illustration of the physical meaning of parameter $l_F = 1/\alpha_\infty(0)$.

The constant $\alpha_\infty(0)$ has the dimension of 1/length. Its inverse value, $l_\mathrm{F} = 1/\alpha_\infty(0)$, has the meaning of the width of a rectangle that has the same area and height as the graph of the weight function; see Fig. 4.2. Note that $G_\mathrm{F} = g_\mathrm{F} l_\mathrm{F}$ where $g_\mathrm{F} = \frac{1}{2}\sigma_0\varepsilon_f = -\sigma_0^2/(2H)$ is the area under the local stress-strain diagram. Therefore, l_F corresponds to the width of an equivalent localization band that would dissipate the same amount of energy if the material were governed by the local law with plastic modulus H.

4.2.3 Plastic region close to the boundary

It is interesting to note that the solution with plastic strain localized into a single cross section is not valid in those regions of a finite bar that are affected by the presence of a boundary. In such boundary layers of width R, the weight function is scaled according to Eq. (2.15) and a singular local field

$$\kappa(x) = \varepsilon_\mathrm{p}(x) = \frac{\sigma - \sigma_0}{H\alpha(x_\mathrm{s}, x_\mathrm{s})}\,\delta(x - x_\mathrm{s}) \tag{4.10}$$

is transformed into the nonlocal field

$$\bar{\kappa}(x) = \int_{\mathcal{L}} \alpha(x,\xi)\kappa(\xi)\mathrm{d}\xi = \frac{\sigma - \sigma_0}{H\alpha(x_\mathrm{s}, x_\mathrm{s})}\,\alpha(x, x_\mathrm{s}) \tag{4.11}$$

In contrast to the case of an infinite bar, for $0 < x_\mathrm{s} < R$ this function does not reach its maximum at $x = x_\mathrm{s}$. For a given local field $\kappa(\xi)$, $\alpha(x,\xi)$ in Eq. (4.11) is a function of x with fixed $\xi = x_\mathrm{s}$. The integral in the denominator of Eq. (2.15) decreases as x moves towards the boundary, and so the maximum of $\alpha(x, x_\mathrm{s})$ is between the point $x = x_\mathrm{s}$ and the physical boundary; see Fig. 4.3b. Consequently, the softening process in this intermediate layer between x_s and the boundary would be faster than at x_s, and the current yield stress would drop below the applied stress.

A solution exists only for x_s placed exactly on the boundary (Fig. 4.3a), because then, the condition $\bar{\kappa}(x) \le \bar{\kappa}(x_\mathrm{s})$ is satisfied in the entire interval $\mathcal{L}$. In physical terms this means that if the dominant imperfection is located in the boundary layer, the plastic zone starts forming there but, due to nonlocal softening effects, it later shifts to the boundary and eventually the plastic strain increments localize right at the boundary. Note that for $R \le x_\mathrm{s} < 2R$, the solution (4.5) remains valid but its nonlocal average becomes slightly unsymmetric, see Fig. 4.3c. This does not influence the size of the plastic zone and has no effect on the load-displacement response of the specimen.

The solution with plastic strain localized at the boundary results in a steeper load-displacement diagram and in a lower energy dissipation than the solution localized inside the bar. For this solution, $\alpha(x_\mathrm{s}, x_\mathrm{s})$ is amplified to the double of $\alpha_\infty(0)$, because the integral in the denominator of Eq. (2.15) is equal to $1/2$, provided that the other boundary is sufficiently far (i.e., that the bar is longer than the interaction radius). Consequently, the equivalent dissipation length $l_\mathrm{F} = 1/\alpha(x_\mathrm{s}, x_\mathrm{s})$ is reduced to one half of its value $1/\alpha_\infty(0)$, valid in an infinite bar or sufficiently far from the boundary.

For the Gaussian weight function and other weight functions with an unbounded support, the boundary effects decay with the distance from the boundary but are never exactly zero. Theoretically, the localized solution would always be attracted by the boundary, and localization inside the bar (at a finite distance from the boundary) would be impossible. This is of course true only in the strict mathematical sense, with exact arithmetics.

4.3 Vermeer–Brinkgreve model

4.3.1 Motivation

If properly regularized, a nonlocal plasticity model should give a plastic region of nonzero measure, with the plastic strain monotonically increasing from the boundary of the plastic region to its center. The static equilibrium condition and the yield condition imply that the drag stress (difference between the current and initial yield stress) is constant across the plastic region. However, for this expected plastic strain profile the nonlocal softening variable $\bar{\kappa}(x)$ cannot be constant across the plastic region, and thus the drag stress cannot be constant either. This is why the simplest nonlocal plasticity formulation with the drag stress proportional to the nonlocal softening variable does not act as a true localization limiter, as has been shown in the previous section.

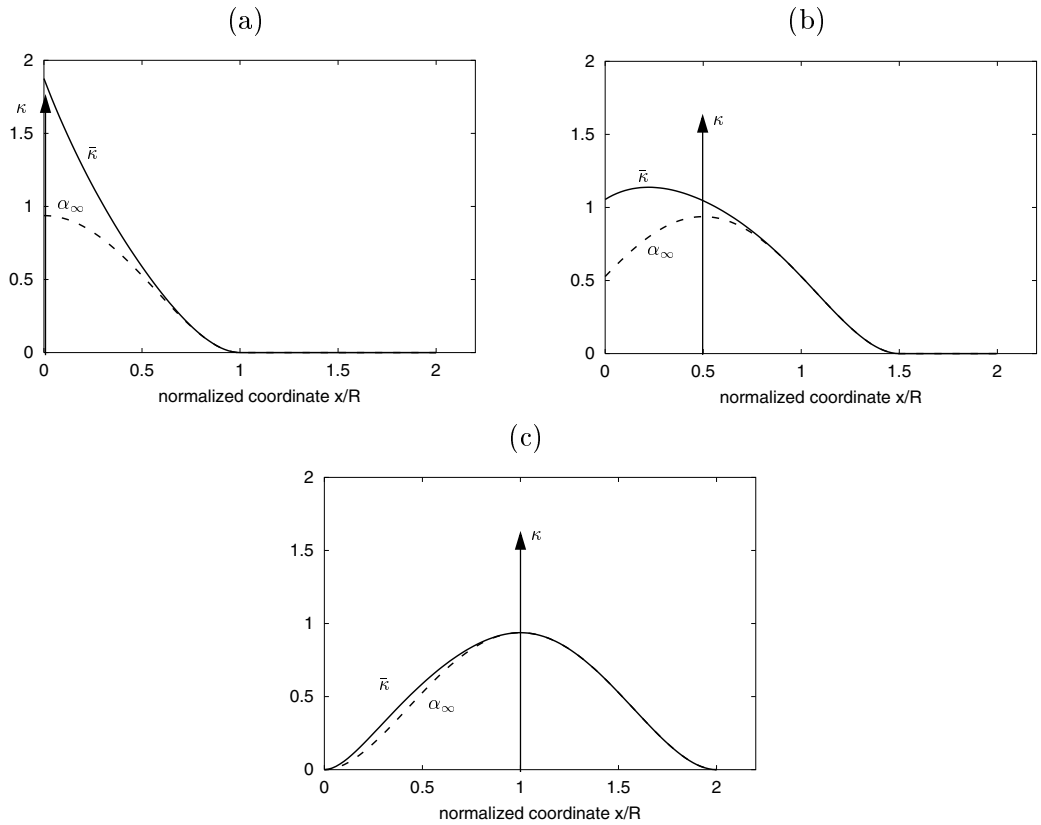

Figure 4.3: Distribution of nonlocal plastic strain $\bar{\kappa}(x)$ for hypothetical Dirac-like solutions $\kappa(x) = \delta(x - x_{\mathrm{s}})$ localized (a) directly at the boundary ($x_{\mathrm{s}} = 0$), (b) at distance $0.5R$ from the boundary, (c) at distance R from the boundary. The solution (b) localized at $x_{\mathrm{s}} = 0.5R$ is not admissible.

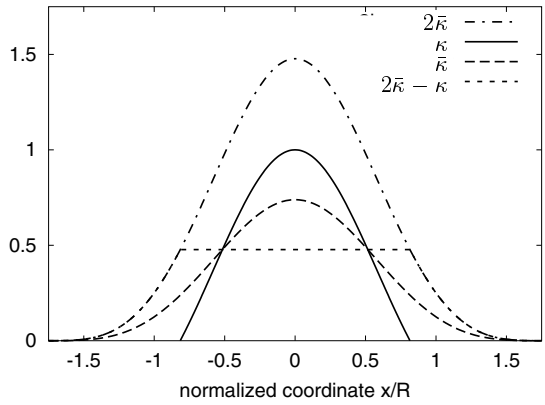

Figure 4.4: Vermeer–Brinkgreve model (parameter $m = 2$): κ and $\bar{\kappa}$ are such that $2\bar{\kappa}$ differs from κ by a constant inside the plastic region defined by $\kappa > 0$.

The behavior of the model in the one-dimensional localization test can be improved if the nonlocal softening variable is combined with the local one. In the simplest case, softening is assumed to be driven by a linear combination

$$\hat{\kappa} = m\bar{\kappa} + (1 - m)\kappa \tag{4.12}$$

where m is a suitably chosen parameter. The graph of $\bar{\kappa}(x)$ is expected to have a shape similar to the graph of $\kappa(x)$ but more flat and spread to the sides; see Fig. 4.4. The linear combination of $\kappa(x)$ and $\bar{\kappa}(x)$ with positive coefficients (parameter m between 0 and 1) cannot be constant across the plastic region, because both profiles have a negative curvature around the center of the plastic region. Taking into account that $\kappa''(x)$ is expected to be larger in magnitude than $\bar{\kappa}''(x)$, if follows that the value of m should be chosen larger than 1. For instance, for $m = 2$ the combined softening variable $\hat{\kappa}(x) = 2\bar{\kappa}(x) - \kappa(x)$ is the difference between the amplified nonlocal plastic strain and the local plastic strain. Fig. 4.4 shows that this difference can indeed be constant across the entire interval I_p in which $\kappa(x) > 0$.

4.3.2 Model description

The foregoing considerations motivate a nonlocal plasticity formulation with a linear softening law in the form

$$\sigma_\mathrm{Y} = \sigma_0 + H\hat{\kappa}, \qquad \hat{\kappa} = m\bar{\kappa} + (1 - m)\kappa \tag{4.13}$$

This formula could also be understood as the basic nonlocal softening law (4.1) with the nonlocal average evaluated using a special weight distribution

$$\alpha_m(x, \xi) = m\alpha(x, \xi) + (1 - m)\delta(x - \xi) \tag{4.14}$$

where α is a regular weight function and δ is the Dirac distribution. This refined nonlocal plasticity model, initially proposed by Vermeer and Brinkgreve (1994), includes the local model and the basic nonlocal model as special cases with $m = 0$ and $m = 1$, respectively.

Essentially the same model was later studied in Strömberg and Ristinmaa (1996), where it was called the mixed local and nonlocal model, and in Planas et al. (1996), where it was called the nonlocal model of the second kind, the case $m = 1$ being called the nonlocal model of the first kind; cf. also Bažant and Planas (1998, pp. 496–498).

4.3.3 Plastic region far from the boundary

For $0 \leq m \leq 1$, the model with softening law (4.13) has similar properties as the basic nonlocal model, i.e., the plastic strain localizes into a single cross section of the bar (set of zero measure). This has been rigorously proven (Planas et al. 1996). The plastic region has a nonzero measure if and only if $m > 1$. It is even possible to prove that the distribution of the softening variable (which is for tensile yielding identical with the plastic strain) is in this case continuous (Planas et al. 1996; Rolshoven and Jirásek 2001).

For a given state, the rate of the softening variable can be solved from the consistency condition $\dot{f} = \dot{\sigma} - \dot{\sigma}_{\mathrm{Y}} = 0$ in I_{p}, which is in the case of a linear softening law (4.13) equivalently written as

$$m \int_{I_{\mathrm{p}}} \alpha(x,\xi)\dot{\kappa}(\xi)\mathrm{d}\xi + (1-m)\dot{\kappa}(x) = \frac{\dot{\sigma}}{H} \qquad \forall x \in I_{\mathrm{p}} \tag{4.15}$$

The integration is carried out over the plastic region only, because $\dot{\kappa}(\xi) = 0$ for $\xi \notin I_{\mathrm{p}}$. For the infinite domain or at a sufficient distance from the boundary, the weight function does not need to be scaled according to Eq. (2.15), and $\alpha(x,\xi)$ can be replaced by $\alpha_\infty(x-\xi)$.

From the mathematical point of view, the important difference between Equations (4.2) and (4.15) is that the latter is a Fredholm integral equation of the *second kind*, which typically has a unique solution. A nonstandard feature of the problem is that the size of the interval I_{p} is not known in advance, and that the solution must satisfy additional admissibility conditions stemming from the loading-unloading conditions of plasticity.

The numerical solution procedure starts from an assumed interval I_{p} and computes the values of κ at the collocation points by solving a set of linear algebraic equations that approximate the integral equation. The formal solution is then tested for admissibility. First, the condition $\dot{\kappa} \geq 0$ implies that the values of $\dot{\kappa}$ at the collocation points are nonnegative. Second, if the yield condition $f = 0$ is satisfied at some points outside I_{p} at the beginning of the step (as is the case at the bifurcation from a perfectly uniform state), the rate of the yield function at those points must be nonpositive. This leads to the condition

$$m \int_{I_{\mathrm{p}}} \alpha(x,\xi)\dot{\kappa}(\xi)\mathrm{d}\xi \leq \frac{\dot{\sigma}}{H} \tag{4.16}$$

to be verified for those x outside I_{p} at which $\sigma(x) = \sigma_{\mathrm{Y}}(x)$. If any of the admissibility conditions is violated, the assumed plastic region is adapted accordingly, i.e., reduced if some computed values of $\dot{\kappa}$ are negative, and extended if Eq. (4.16) is violated. This is iteratively repeated until an admissible solution is found.

The size of the plastic zone and the shape of the plastic strain profile do not depend on the initial yield stress or the softening modulus, but they are strongly influenced by the parameter m; see the examples in Fig. 4.5a. The length of the plastic region monotonically increases with m, and for $m \to 1^+$ it approaches zero. Together with the nonlocal weight function, the newly introduced parameter $m > 1$ controls the size of the localized plastic

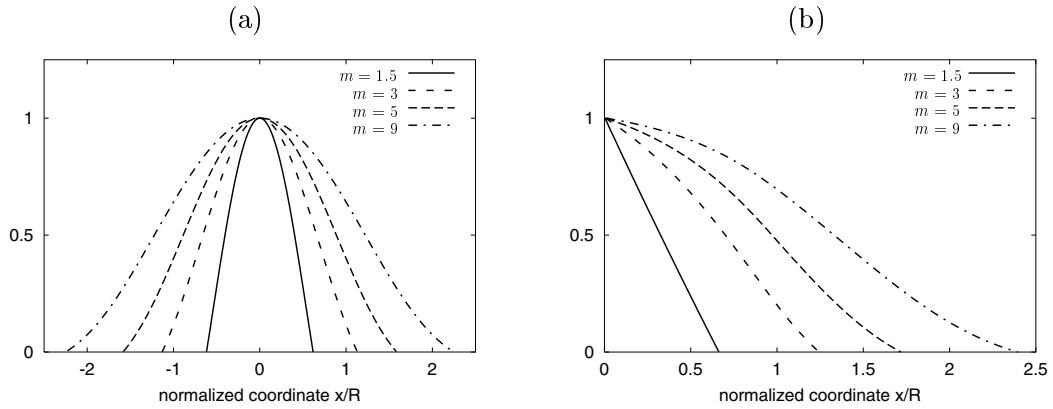

Figure 4.5: Vermeer–Brinkgreve model: The effect of parameter m on the plastic strain profiles localized (a) inside the bar, (b) at the boundary.

zone and the distribution of plastic strain. It can be expected that, for any given value of m, the radius of nonlocal interaction and the shape of the nonlocal weight function could be adjusted so as to match the desired plastic strain profile. Consequently, m could be chosen almost arbitrarily.

However, for numerical reasons it is wise to avoid the extremes. With m close to 1, the interaction radius would have to be much larger than the width of the plastic region, and this would increase the computational time needed for the evaluation of nonlocal averages. With very large values of m, the interaction radius would be much smaller than the width of the plastic region, and a dense set of integration points would be needed in order to capture the nonlocal interaction at all. In practice, a reasonable value of m seems to be 2.

4.3.4 Plastic region close to the boundary

Same as for the basic nonlocal model presented in Sec. 4.2, the one-dimensional localization problem has no admissible solution for which the plastic region would be separated from the boundary by an elastic layer of thickness a smaller than the interaction radius R. Inside the boundary layer of thickness R, the nonlocal weight function is scaled according to Eq. (2.15). If the assumed plastic region has a nonempty intersection with the boundary layer but does not touch the boundary, the formal solution of Eq. (4.15) becomes nonsymmetric and it is impossible to adjust the size of the plastic region such that the plastic strain would tend to zero on both elasto-plastic boundaries at the same time. This can be explained by the fact that for a fixed distance a, the problem has only one free parameter, L_p, but two conditions, $\kappa(a) = 0$ and $\kappa(a + L_\mathrm{p}) = 0$ must be satisfied.

But an admissible solution exists if the plastic region is assumed to start directly at the physical boundary, with no elastic layer interposed, which means that the condition $\kappa = 0$ must be respected only on one internal elasto-plastic boundary. For this solution, the plastic strain attains its maximum value at the physical boundary and monotonically decreases to zero as the elasto-plastic boundary is approached; see Fig. 4.5b. For values of m close to 1, the plastic strain distribution is almost linear.

The plastic region localized at the boundary consumes less energy than the plastic region inside the bar. For example, for $m = 2$ the energy consumed during failure with

localization at the boundary is about 62 % of the value that corresponds to localization inside the bar.

4.3.5 Nonlinear softening

Because the linear version of the Vermeer–Brinkgreve model has reasonable localization properties, it is interesting to explore how it could be extended to nonlinear softening. A natural generalization of Eq. (4.13) is

$$\sigma_{\mathrm{Y}} = \sigma_0 + h(\hat{\kappa}), \qquad \hat{\kappa} = m\bar{\kappa} + (1-m)\kappa \tag{4.17}$$

where h is a nonlinear function. If the plastic strain remains uniform in space, then $\bar{\kappa} = \kappa$ and the combined softening variable $\hat{\kappa} = m\bar{\kappa} + (1-m)\kappa$ is equal to κ, which means that Eq. (4.17) reduces to the local law (2.34).

The solution for the case of nonlinear softening is very similar to the one for linear softening. The rate of the current yield stress is given by

$$\dot{\sigma}_{\mathrm{Y}} = H_{\mathrm{t}}\left(\hat{\kappa}\right)\dot{\hat{\kappa}} = H_{\mathrm{t}}\left(\hat{\kappa}\right)\left[m\dot{\bar{\kappa}} + (1-m)\dot{\kappa}\right] \tag{4.18}$$

where $H_{\mathrm{t}} \equiv \mathrm{d}h/\mathrm{d}\hat{\kappa}$ is the tangent plastic modulus. From the consistency condition it follows that the rate of the softening variable satisfies Eq. (4.15) with the constant plastic modulus H replaced by the variable tangent plastic modulus H_{t}. This modulus is a function of the combined softening variable $\hat{\kappa}$, which is constant across the plastic region, and so H is also constant in space and varies only in time. Consequently, the width of the plastic region and the shape of the plastic strain profile are the same as for the model with linear softening, and the plastic region I_{p} does not change during the deformation process. The diagram showing the dependence of the load (reaction due to the imposed displacement at the bar end) on the plastic part of the bar extension (integral of the plastic strain across the plastic region) has the same shape as the selected softening curve.

For the softening function (2.36) that provides a complete description of linear softening, the complete loss of material resistance can be described without any artificial locking effects. The tangent plastic modulus becomes zero when the combined softening variable $\hat{\kappa}$ exceeds the critical value κ_{f}. The jump to a vanishing softening modulus occurs at all points of the plastic zone simultaneously, because the value of $\hat{\kappa}$ is constant across the plastic zone. This jump occurs when the current yield stress in the plastic zone vanishes, which means that the force transmitted by the bar vanishes as well. The subsequent evolution of plastic strain is not unique, because the current yield stress does not change any more and the consistency condition can be satisfied even if $\hat{\kappa}$ is not constant across the plastic zone. This would lead to numerical instabilities in a finite element solution, caused by the singularity of the tangent stiffness matrix. From the physical point of view, it is essential that no stresses are generated at increasing strain, which is guaranteed because yielding continues at zero stress. Thus the model can describe the complete loss of material resistance without any artificial locking effects. Numerical problems could be circumvented by transition to a discontinuous description (discrete crack), removal of fully softened elements from the model, or stabilization by a very small nonzero plastic modulus.

One could imagine another possible nonlinear extension of the Vermeer–Brinkgreve model. The linear softening law (4.13) can be rephrased as

$$\sigma_{\mathrm{Y}} = \sigma_0 + H\kappa + H_{\mathrm{m}}\left[\bar{\kappa} - \kappa\right] \tag{4.19}$$

where $H < 0$ is the constant plastic modulus and $H_{\mathrm{m}} = mH < H$ is another material parameter. The first two terms on the right-hand side, $\sigma_0 + H\kappa$, represent the local part of the softening law, and the last term, $H_{\mathrm{m}}\left[\bar{\kappa} - \kappa\right]$, is a nonlocal correction that is activated only in a nonuniform state. This interpretation has been suggested by Borino (2001). A possible nonlinear extension of Eq. (4.19) reads

$$\sigma_{\mathrm{Y}} = \sigma_0 + h(\kappa) + H_{\mathrm{m}}\left[\bar{\kappa} - \kappa\right] \tag{4.20}$$

where h is an appropriate nonlinear softening function. Note that the nonlocal correction has not been modified, and H_{m} is still considered as a constant. In a uniform state, Eq. (4.20) reduces to the usual local nonlinear softening law (2.34).

For this second nonlinear extension, the plastic zone is expanding and leads to locking on the global level. For the nonlocal law (4.20), the consistency condition gives

$$H_{\mathrm{m}}\dot{\bar{\kappa}} + \left[H_{\mathrm{t}}(\kappa) - H_{\mathrm{m}}\right]\dot{\kappa} = \dot{\sigma} \tag{4.21}$$

where the tangent plastic modulus $H_{\mathrm{t}} \equiv \mathrm{d}h/\mathrm{d}\kappa$ is a function of κ and is therefore variable in space. The ratio of the coefficients at the local and nonlocal term in the integral equation (4.21) is variable both in time and space, and so the solution of Eq. (4.15) is valid only at the bifurcation from a uniform state (when $H_{\mathrm{t}}(0) = H$ is constant in space), but later the distribution of plastic strain changes. The numerical solution reveals that the plastic zone expands (Fig. 4.6a) and the load-displacement diagram has a long tail (Fig. 4.6b). In fact, the load-displacement diagram corresponding to the localized solution would eventually cross the load-displacement diagram corresponding to the unstable solution with the strain remaining uniform, plotted for comparison by the dashed curve in Fig. 4.6b. This is certainly an undesired locking effect. Complete failure is possible only if the plastic zone extends over the entire bar. So it is clearly better to use Eq. (4.17) instead of Eq. (4.20).

4.4 Models motivated by ductile damage

One of the most important mechanisms leading to the reduction of the apparent yield stress in ductile metals is the growth and coalescence of voids. Even if the basic material between the voids is hardening, the reduction of the effective area due to the void growth can result into an overall softening, i.e., into a decrease of the nominal yield stress, taken per unit total area of the material including voids. This phenomenon is referred to as ductile damage, because the growth of defects is a damage process. The effect of ductile damage on the elastic properties is often neglected, unlike the effect of brittle damage, caused by the propagation of microcracks that reduce not only the strength but also the elastic stiffness.

This section will briefly present two nonlocal plasticity models that are motivated by the concept of ductile damage. Both models have been designed for applications in the finite-strain domain, but in the present study only their small-strain versions will be considered. This seems to be sufficient, because only the fundamental characteristics of the regularizing nonlocal terms are to be explored.

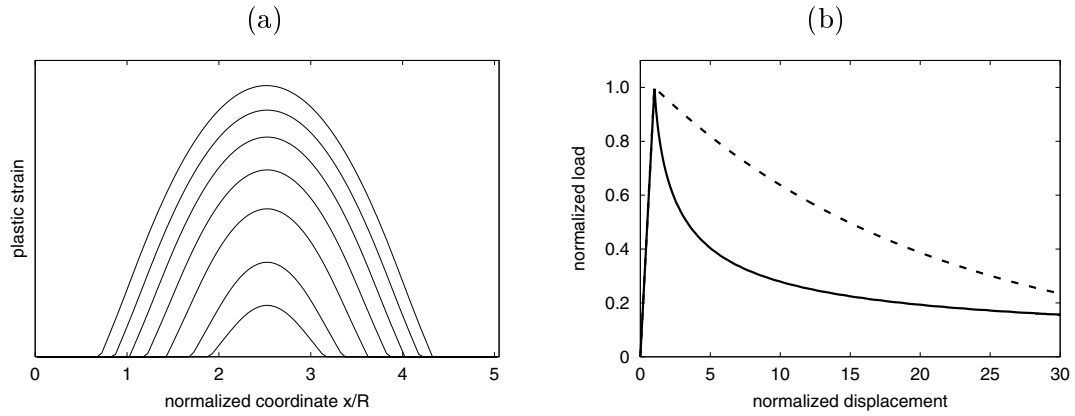

Figure 4.6: Alternative nonlinear version of the Vermeer–Brinkgreve model: (a) expansion of plastic strain profile, (b) load-displacement diagram with locking.

4.4.1 Ductile damage model of Geers and coworkers

Geers, Engelen and coworkers have recently advanced a nonlocal plasticity model (Geers et al. 2001; Engelen et al. 2003), in which the nonlocal softening variable $\bar{\kappa}$ is defined as the solution of a Helmholtz-type differential equation with Neumann-type boundary conditions. In Sec. 3.12, this model has been analyzed in its original implicit gradient format.

The implicit definition of $\bar{\kappa}$ through the Helmholtz-type differential equation and boundary conditions is equivalent to nonlocal averaging with the Green function of the corresponding boundary value problem playing the role of the weight function, cf. Peerlings et al. (2001). I propose to write this model as an integral-type nonlocal model, but using the bell-shaped polynomial function for the nonlocal averaging. The model equations presented in Sec. 3.12.1 remain essentially the same, but the Helmholtz-type differential equation and the boundary conditions are replaced by nonlocal averaging.

To illustrate the regularizing effect for the ductile damage model written in the integral-format, consider again the one-dimensional localization test. Differentiation of Eq. (3.96) leads to

$$\dot{\sigma}_{\mathrm{Y}} = (1-\omega_{\mathrm{p}})H_{\mathrm{L}0}\dot{\kappa} - \dot{\omega}_{\mathrm{p}}(\sigma_0 + H_{\mathrm{L}0}\kappa) \tag{4.22}$$

As long as the cumulative plastic strain remains smaller than the damage threshold, κ_{i}, $\omega_{\mathrm{p}} = 0$ and $\dot{\sigma}_{\mathrm{Y}} = H_{\mathrm{L}0}\dot{\kappa}$, which means that the material is hardening and the strain remains uniform. Localization can take place only after the ductile damage mechanism has been activated. In the range described by the second line in Eq. (3.97), Eq. (4.22) can be written as

$$\dot{\sigma}_{\mathrm{Y}} = \frac{\kappa_{\mathrm{c}} - \bar{\kappa}}{\kappa_{\mathrm{c}} - \kappa_{\mathrm{i}}} H_{\mathrm{L}0}\dot{\kappa} - \frac{\sigma_0 + H_{\mathrm{L}0}\kappa}{\kappa_{\mathrm{c}} - \kappa_{\mathrm{i}}}\dot{\bar{\kappa}} \tag{4.23}$$

The rate of the yield stress is a linear combination of the softening variable rate and its nonlocal average. Setting

$$H = \frac{H_{\mathrm{L}0}(\kappa_{\mathrm{c}} - \bar{\kappa} - \kappa) - \sigma_0}{\kappa_{\mathrm{c}} - \kappa_{\mathrm{i}}} \tag{4.24}$$

$$m = \frac{\sigma_0 + H_{\mathrm{L}0}\kappa}{\sigma_0 + H_{\mathrm{L}0}\kappa - H_{\mathrm{L}0}(\kappa_{\mathrm{c}} - \bar{\kappa})} \tag{4.25}$$

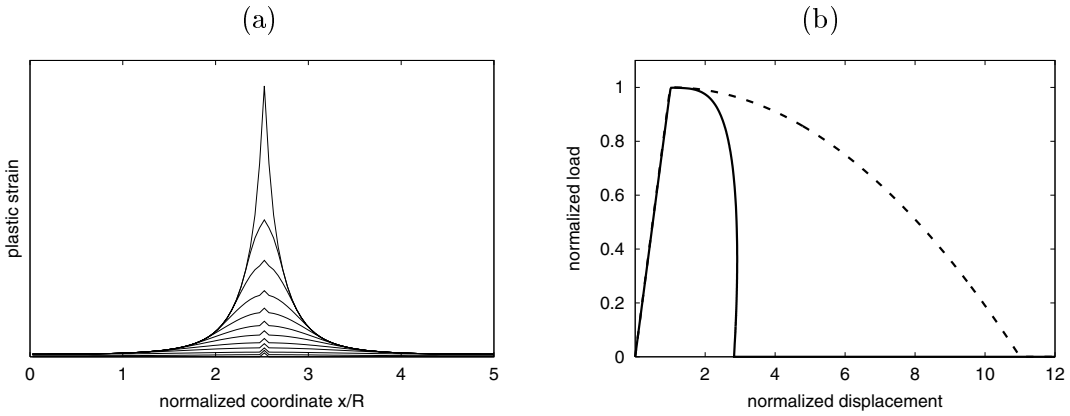

Figure 4.7: Ductile damage model of Geers and coworkers with linear damage law (3.97): (a) evolution of plastic strain profile, (b) load-displacement diagram.

Eq. (4.23) resembles the Vermeer–Brinkgreve model from Sec. 4.3,

$$\dot{\sigma}_{\mathrm{Y}} = (1-m)H\dot{\kappa} + mH\dot{\bar{\kappa}} \tag{4.26}$$

Note that the modulus H depends on the local and nonlocal softening variable.

Depending on the parameter values, bifurcation can take place either right at the onset of damage, i.e., at $\kappa = \kappa_{\mathrm{i}}$, or after κ has grown to a certain value $\kappa > \kappa_{\mathrm{i}}$. The first case occurs if $\kappa_{\mathrm{c}} < 2\kappa_{\mathrm{i}} + \sigma_0/H_{\mathrm{L}0}$. The initial profile of the plastic strain rate is the same as for the Vermeer–Brinkgreve model with parameters H and m evaluated from Equations (4.24)–(4.25) with $\kappa = \bar{\kappa} = \kappa_{\mathrm{i}}$. Because κ_{c} is larger than κ_{i} and $H_{\mathrm{L}0}$ is supposed to be positive, the equivalent parameter m is larger than 1, which means that the localized plastic zone has a nonzero size (see Sec. 4.3.3). After localization, the equivalence between both models breaks down, because m evaluated from Eq. (4.25) ceases to be uniform along the bar. The numerical solution shows that the size of the plastic zone decreases and approaches zero as the nonlocal plastic strain in the center of this zone tends to κ_{c}. This is illustrated in Fig. 4.7a. When $\bar{\kappa}$ in the center of the plastic zone reaches κ_{c}, the yield stress at that point vanishes, and so the applied stress must vanish as well. This means that the model can properly describe the failure process up to complete loss of residual strength. Because $\bar{\kappa}$ is nonuniform, there is initially only one cross section at which the yield stress vanishes. If the bar extension keeps increasing, the zone with zero yield stress expands and the distribution of the plastic strain rate becomes nonunique, but yielding can continue at zero stress level and no locking effects arise. Fig. 4.7b shows the load-displacement diagram for the localized solution (solid curve) and, for comparison, also the load-displacement diagram for the unstable solution with uniform strain (dashed curve), which is in fact just the rescaled local stress-strain law. Of course, this latter solution would apply only if the localization were artificially prevented. The dashed curve serves as a reference, to show the effect of localization on the structural response.

For the second case, i.e. if $\kappa_{\mathrm{c}} > 2\kappa_{\mathrm{i}} + \sigma_0/H_{\mathrm{L}0}$, the material is hardening even after the onset of damage, and the solution remains uniform up to the level of plastic strain at which H given by Eq. (4.24) vanishes. Afterwards, the solution can localize, but when this happens depends on the length of the bar. Theoretically, bifurcation in an infinite bar

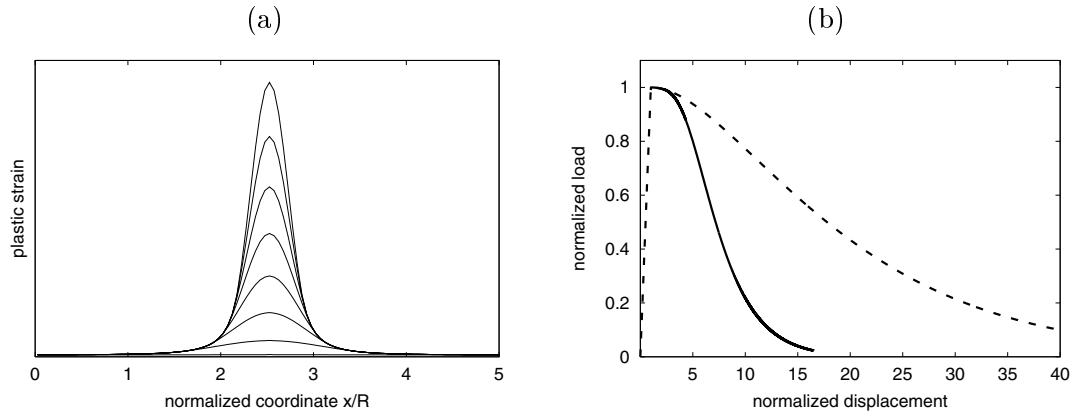

Figure 4.8: Ductile damage model of Geers and coworkers with exponential damage law (3.98): (a) evolution of plastic strain profile, (b) load-displacement diagram.

would take place at $\kappa = \bar{\kappa} = 0.5(\kappa_c - \sigma_0/H_{L0})$, but because the corresponding value of m according to Eq. (4.25) is infinite, the plastic zone would initially have an infinite size. As the plastic strain grows further, the equivalent value of m becomes finite and decreases, which leads to shrinking of the plastic zone, similar to the previous case. In a finite bar, localization is thus delayed until m becomes sufficiently small.

The results presented in Fig. 4.7 refer to the piecewise linear damage law (3.97), for which the softening curve has a negative curvature and the yield stress tends to zero at an increasing rate. To check how the shape of the softening curve affects the evolution of the plastic strain profile, the localization process has been simulated also for the exponential damage law, Eq. (3.98), for the special case $\kappa_i = 0$. This leads to a local stress-strain curve with a long tail, see Fig. 4.8. Shrinking of the plastic zone is in this case much less pronounced, but the stress transmitted by the specimen still tends to zero, and the model does not suffer by any locking effects.

4.4.2 Nonlocal Gurson model

Another model that shares common features with the Vermeer–Brinkgreve model is the nonlocal version of the modified Gurson model (Gurson 1977; Tvergaard 1981) proposed in Leblond et al. (1994) and exploited (with a viscoplastic extension) in Tvergaard and Needleman (1995) and Needleman and Tvergaard (1998). In the Gurson model, softening is considered to be a consequence of the increase of porosity p (void volume fraction), and the rate of porosity $\dot{p}$ is directly related to the plastic strain rate. The model has been formulated for large strains; the corresponding small-strain evolution law reads

$$\dot{p} = (1-p)\sum_{i=1}^{3} \dot{\varepsilon}_{ii}^{\mathrm{p}} + P(\kappa)\dot{\kappa} \tag{4.27}$$

The two terms on the right-hand side represent the increase of porosity due to the void growth and due to the nucleation of new voids, respectively. The first term is proportional to the volumetric part of the plastic strain rate ($\dot{\varepsilon}_{ii}^{\mathrm{p}}$, $i = 1, 2, 3$, are the rates of the normal plastic strain components) while the second term is proportional to the rate of the

cumulative plastic strain. The function $P(\kappa)$ describes the dependence of the nucleation rate on the cumulative plastic strain. Following Tvergaard and Needleman (1995), this function is approximated by a multiple of the normal distribution function,

$$P(\kappa) = \frac{p_{\mathrm{N}}}{s_{\mathrm{N}}\sqrt{2\pi}} \exp\left(-\frac{(\kappa-\kappa_{\mathrm{N}})^2}{2s_{\mathrm{N}}^2}\right) \tag{4.28}$$

where p_{N}, κ_{N} and s_{N} are constant parameters.

The modified Gurson yield condition reads

$$\frac{3J_2}{\sigma_{\mathrm{M}}^2} + 3p^* \cosh\left(\frac{I_1}{2\sigma_{\mathrm{M}}}\right) - 1 - (1.5p^*)^2 = 0 \tag{4.29}$$

where I_1 is the first stress invariant (three times the mean stress), J_2 is the second invariant of the stress deviator, σ_{M} is the yield stress of the matrix between the voids (linked by a hardening law to the cumulative plastic strain κ), and

$$p^*(p) = \begin{cases} p & \text{if } p \le p_{\mathrm{C}} \\ p_{\mathrm{C}} + \frac{p_{\mathrm{U}}^*-p_{\mathrm{C}}}{p_{\mathrm{F}}-p_{\mathrm{C}}}(p-p_{\mathrm{C}}) & \text{if } p_{\mathrm{C}} \le p \le p_{\mathrm{F}} \\ p_{\mathrm{U}}^* & \text{if } p_{\mathrm{F}} \le p \end{cases} \tag{4.30}$$

is the modified porosity that accounts for the effect of void coalescence (Tvergaard and Needleman 1984). The parameter values are taken e.g. as $p_{\mathrm{C}} = 0.08$, $p_{\mathrm{F}} = 0.25$ and $p_{\mathrm{U}}^* = 1/1.5 = 2/3$. Evolution of the plastic strain is governed by the associated flow rule.

In the nonlocal Gurson model, the porosity p in Eq. (4.30) is replaced by its nonlocal counterpart, $\overline{p}$, defined by the nonlocal version of the evolution equation (4.27),

$$\dot{\overline{p}}(\boldsymbol{x}) = \int_V \alpha(\boldsymbol{x},\boldsymbol{\xi})[1-\overline{p}(\boldsymbol{\xi})] \sum_{i=1}^{3} \dot{\varepsilon}_{ii}^{\mathrm{p}}(\boldsymbol{\xi})\,\mathrm{d}\boldsymbol{\xi} + \int_V \alpha(\boldsymbol{x},\boldsymbol{\xi}) P(\kappa(\boldsymbol{\xi}))\dot{\kappa}(\boldsymbol{\xi})\mathrm{d}\boldsymbol{\xi} \tag{4.31}$$

To illustrate the basic properties of the nonlocal Gurson model and to compare it to other nonlocal plasticity formulations, a simple localization problem that can be reduced to a one-dimensional description is analyzed. However, it is more convenient to look at the problem of localization in an infinite shear layer instead of the uniaxial tensile test, because the volumetric-deviatoric decomposition plays an important role for this model. If the material is subjected to a monotonically increasing shear strain, only a shear stress τ is generated. The volumetric stress invariant remains equal to zero, and the plastic flow is purely deviatoric. Consequently, the first integral on the right-hand side of Eq. (4.31) vanishes, and $\overline{p}$ can be interpreted as the nonlocal average of the local porosity p, which in this particular case becomes a unique function $p(\kappa)$ of the cumulative plastic strain. The specific form of this function can be obtained by integrating the evolution law $\dot{p} = P(\kappa)\dot{\kappa}$, rewritten as $\mathrm{d}p = P(\kappa)\mathrm{d}\kappa$. Introducing another function, $\omega_{\mathrm{p}}(p) = 1.5p^*(p)$, and taking into account that $I_1 = 0$ and $J_2 = \tau^2$, the yield condition (4.29) simplifies to

$$\frac{3\tau^2}{\sigma_{\mathrm{M}}^2} - [1-\omega_{\mathrm{p}}(\overline{p})]^2 = 0 \tag{4.32}$$

This is equivalent to

$$|\tau| - [1-\omega_{\mathrm{p}}(\overline{p})]\tau_{\mathrm{M}} = 0 \tag{4.33}$$

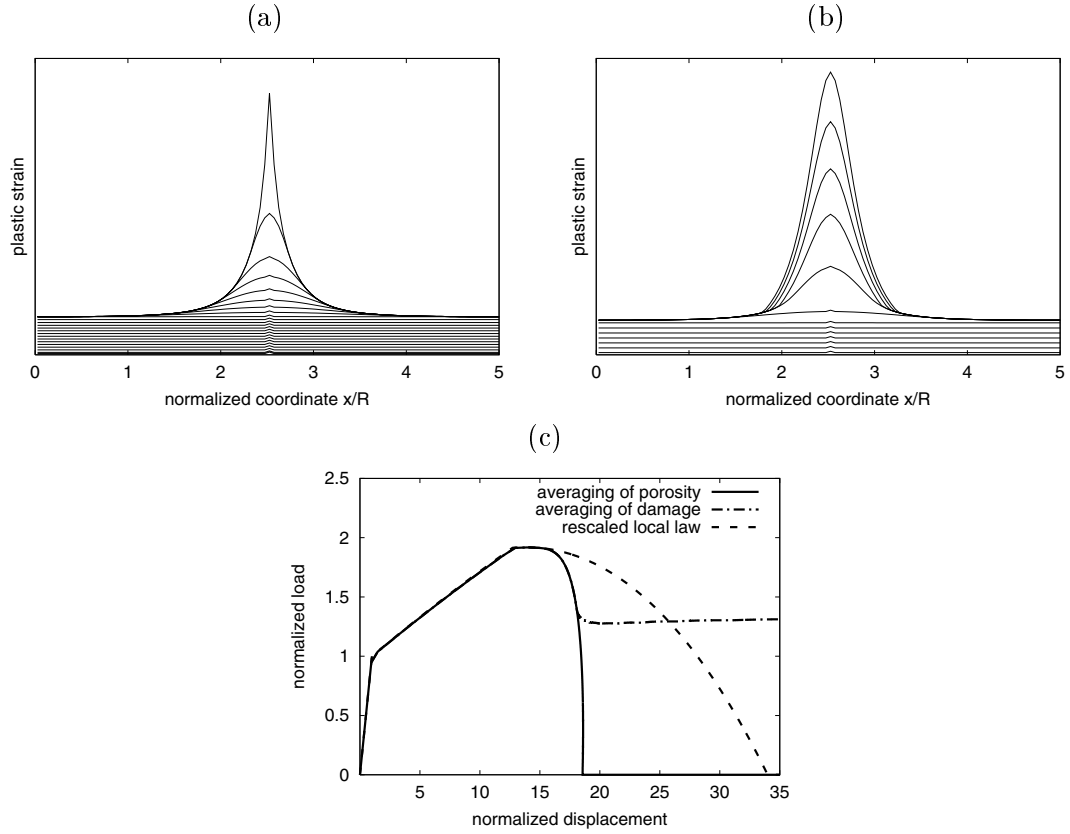

Figure 4.9: Nonlocal Gurson model: (a) shrinking of plastic strain profile for formulation with nonlocal porosity, (b) expansion of plastic strain profile for formulation with nonlocal damage parameter, (c) load-displacement diagrams.

where $\tau_{\mathrm{M}} = \sigma_{\mathrm{M}}/\sqrt{3}$ is the matrix yield stress in shear.

If the yield stress in the matrix is governed by a linear hardening law, $\tau_{\mathrm{M}} = \tau_0 + H\kappa$, the nominal yield stress in shear for the material weakened by voids is given by

$$\tau_{\mathrm{Y}} = [1 - \omega_{\mathrm{p}}(\overline{p(\kappa)})](\tau_0 + H\kappa) \tag{4.34}$$

which is very similar to the hardening-softening law (3.96) of the Geers model. The difference is that the Geers model evaluates the ductile damage parameter, ω_{p}, directly from the nonlocal cumulative plastic strain, while here the damage is evaluated from the nonlocal porosity, and the local porosity is a nonlinear function of the cumulative plastic strain. Despite this difference, the behavior of both models in a one-dimensional localization test is very similar.

Of course, the exact response depends on the selected material parameters, but the present results indicate that the softening process is reasonably reproduced until the complete loss of residual strength (due to the coalescence of voids), without any spurious locking effects, cf. Fig. 4.9c. As for Geers model, the plastic zone shrinks during the localization process, cf. Fig. 4.9a.

If the averaged quantity is the damage parameter ω_{p} instead of the porosity p, the material model locks. For this slightly different nonlocal formulation of Gurson's model,

the evolution of the plastic strain profile is shown in Fig. 4.9b, and the load-displacement diagram is plotted by the dash-dotted curve in Fig. 4.9c. During the initial stage of localization, both nonlocal formulations give almost identical results. However, the model based on damage averaging later leads to an expansion of the plastic zone, with the transmitted stress stabilized at a relatively high residual level. This locking effect is similar to that described for a nonlocal formulation of a quasi-brittle damage model based on averaging of the damage parameter (Jirásek 1998), and demonstrates the importance of such elementary tests.

4.5 Models with nonlocal stress and nonlocal strain

Historically the first nonlocal formulation of plasticity was proposed by Eringen in the early 1980s (Eringen 1981; Eringen 1983). He set up the framework for three classes of nonlocal plasticity models, based on the deformation theory, flow theory, and strain-space plasticity. Eringen did not consider the case of softening and did not intend his models to serve as localization limiters. He was rather interested in the continuum-based description of interacting dislocations and in the nonlocal effects on the distribution of stress around the crack tip in elastoplastic fracture mechanics. Nevertheless, for the sake of comparison it is useful to briefly comment on the behavior of his models after the onset of localization due to softening.

The first paper (Eringen 1981) contains a nonlocal formulation of the plasticity theory formulated in strain space (Green and Naghdi 1965; Naghdi and Trapp 1975), that does not act as a localization limiter. The stress is computed by averaging the 'local' stress that would be obtained from the local model. This is one possible extension of nonlocal elasticity. In one dimension, the stress-strain law (2.22) is replaced by

$$\sigma = \overline{E(\varepsilon - \varepsilon_{\mathrm{p}})} \tag{4.35}$$

If the elastic modulus is constant in space, Eq. (4.35) is equivalent to

$$\sigma = E(\bar{\varepsilon} - \bar{\varepsilon}_{\mathrm{p}}) \tag{4.36}$$

This particular nonlocal approach can be characterized as averaging of stress or averaging of elastic strain. It would be computationally very efficient, because the yield condition (written in strain space) remains local and the stress evaluation algorithm does not require any modifications, except for the weighted averaging of the locally computed stress. In the one-dimensional tensile test, all the solutions obtained with the corresponding local model would remain admissible, because the stress is constant due to the equilibrium condition, and a constant field is not modified by the averaging operator. As for the local model, strain can localize in a set of zero measure.

In a subsequent paper (Eringen 1983), nonlocal theories of plasticity were formulated in stress space. Again, the formulation cannot be used as a localization limiter, but this time the reason is different. In the flow theory, Eringen considered only perfect von Mises plasticity with an associated flow rule. In the one-dimensional case, the logic he followed would lead to a model with the stress-strain law

$$\sigma = \overline{E\varepsilon} - E\varepsilon_{\mathrm{p}} \tag{4.37}$$

For a spatially constant elastic modulus, this is equivalent to

$$\sigma = E(\overline{\varepsilon} - \varepsilon_{\mathrm{p}}) \tag{4.38}$$

Thus, one could say that the averaged quantity is the elastic stress or the total strain. This is another possible extension of nonlocal elasticity. While the previously mentioned model with nonlocal stress would not prevent localization into a set of zero measure, the present model with nonlocal strain would not allow any localization at all (in the one-dimensional test problem). At bifurcation from a uniform strain state, the nonlocal strain rate in the elastically unloading region would have to be equal to a negative constant, $\dot{\sigma}/E$, while in the plastically softening region it would have to be equal to a positive constant, $\dot{\sigma}(E^{-1} + H^{-1})$. However, the nonlocal strain obtained by weighted averaging with a continuous weight function is always continuous, even if the local strain is highly localized and contains a multiple of the Dirac distribution. Consequently, the nonlocal strain cannot have a jump at the elasto-plastic boundary, and the plastic strain cannot localize into any region smaller than the entire bar. Localization would be possible for uniform averaging over a finite neighborhood, i.e., for a discontinuous weight function equal to $1/(2R)$ for $|x - \xi| < R$ and to 0 for $|x - \xi| \geq R$. But this type of averaging would lead to instabilities already in the elastic regime, because periodic perturbations of the strain field with period $2R$ would not change the stress field. The same deficiency was detected in the context of models based on the imbricate continuum (Bažant and Chang 1984).

4.6 Model with nonlocal plastic strain

4.6.1 Model description

The first nonlocal formulation of softening plasticity was proposed by Bažant and Lin (1988) for a grouted soil; it was applied in finite element analysis of the stability of unlined excavation for a certain subway project.

The underlying cohesive-frictional plasticity model is based on the Mohr-Coulomb yield condition and on a linear softening law with the work-softening hypothesis. The averaged quantity is either the plastic strain or the plastic multiplier. In one dimension and for tensile yielding only, both formulations are equivalent. The local plastic strain, ε_{p}, is evaluated from the local consistency condition written in strain space. The plastic region is characterized by $E(\varepsilon - \varepsilon_{\mathrm{p}}) = \sigma_{\mathrm{Y}}$ and $\dot{\varepsilon} > 0$, and the consistency condition $E(\dot{\varepsilon} - \dot{\varepsilon}_{\mathrm{p}}) = \dot{\sigma}_{\mathrm{Y}}$ combined with the softening law $\dot{\sigma}_{\mathrm{Y}} = H\dot{\kappa} = H\dot{\varepsilon}_{\mathrm{p}}$ implies that, in the plastic region, the plastic strain rate is given by

$$\dot{\varepsilon}_{\mathrm{p}} = \frac{E\dot{\varepsilon}}{E + H} \tag{4.39}$$

The stress-strain law (2.22) is then replaced by

$$\sigma = E(\varepsilon - \bar{\varepsilon}_{\mathrm{p}}) \tag{4.40}$$

where $\bar{\varepsilon}_{\mathrm{p}}$ is the nonlocal average of ε_{p}.

The present interpretation of the Bažant–Lin model is not standard, but it follows from a systematic analysis of the algorithm and results published in Bažant and Lin (1988).

4.6.2 Localization analysis

Suppose that, at the bifurcation from a uniform strain state, the plastic strain localizes in an interval I_p. Equation (4.39) can be used to eliminate the strain rate from the rate form of Eq. (4.40). This leads to

$$(E+H)\dot{\varepsilon}_\mathrm{p} - E\dot{\bar{\varepsilon}}_\mathrm{p} = \dot{\sigma} \tag{4.41}$$

Dividing both sides by H and denoting $-E/H$ as m, exactly the same Fredholm integral equation (4.15) as for the Vermeer–Brinkgreve model from Sec. 4.3.2 is obtained. Because H is negative and $E+H$ must remain positive (to avoid a snapback in the local stress-strain diagram), the range of admissible values for $-E/H$ is the open interval $(1,\infty)$, which matches the range of values of parameter m that lead to a nonzero size of the plastic region. So, the model with nonlocal plastic strain acts as a localization limiter and, at bifurcation from a uniform strain state, it provides the same distribution of the plastic strain rate as the Vermeer–Brinkgreve model.

At later stages of the deformation process, the equivalence between both models remains valid only if the softening law is linear (with no cutoff at zero yield stress). For nonlinear softening laws, Eq. (4.15) still applies to the Vermeer–Brinkgreve model, provided that H is understood as the tangent plastic modulus. This modulus is evaluated from the combined softening variable $m\bar{\kappa}+(1-m)\kappa$, which is constant across the plastic region, and so H is also constant in space and varies only in time. In contrast to that, the model with nonlocal plastic strain applies the softening function to the local softening variable, and so the tangent plastic modulus becomes variable in space. This means that the right-hand side of Eq. (4.15) would be a function of x and, because parameter m corresponds to $-E/H$ and E remains constant, the coefficients at $\bar{\kappa}$ and κ on the left-hand side would also be functions of x. Thus, the shape of the plastic strain profile and the size of the plastic region are expected to vary during the deformation process.

For softening curves with a positive curvature (Fig. 2.4b), typically used for quasi-brittle materials such as concrete, the tangent plastic modulus decreases in magnitude, which corresponds to an increase of the equivalent parameter m. Because larger values of m lead to larger sizes of the plastic region, it can be expected that the plastic region expands. As the tail of the softening curve is approached, m tends to infinity and the plastic region would expand across the entire bar. This is no doubt a pathological behavior that would be accompanied by stress locking effects, i.e., by large residual stresses transmitted by the bar even at very large applied extensions.

For softening curves with a negative curvature (Fig. 2.4c), which could represent ductile materials with an acceleration of defect growth at large plastic strains, the tangent plastic modulus increases in magnitude and the plastic region would shrink. This is an acceptable behavior, physically interpreted as a gradual transition to a line crack. However, one should bear in mind that the nonlocal model cannot be used beyond the state at which the local yield stress at the center of the plastic region vanishes. It would not make sense to allow negative values of the local yield stress, because then a test with artificially enforced uniformity of strain would result into compressive stresses under large applied bar extensions. And if the local softening curve continues horizontally at zero current yield stress level, the tangent plastic modulus jumps from a large negative value to zero, and the equivalent value of parameter m tends to infinity. This would again produce stress

locking and a pathological expansion of the plastic region.

4.6.3 Locking mechanism

The reason for locking can be clearly explained using the example of a linear softening curve with a horizontal continuation at zero stress level after the critical plastic strain is exceeded; see Fig. 2.4a. Formally, the complete softening law can be written as

$$\sigma_{\mathrm{Y}} = \langle \sigma_0 + H\kappa \rangle \tag{4.42}$$

where $\langle \ldots \rangle$ is the positive part operator. This law describes the local yield stress, but the actual stress can be higher, due to the effect of nonlocal terms. Nevertheless, at a sufficiently large applied extension the stress transmitted by the bar should vanish. Let $x_{\max}$ be the point at which the strain attains its maximum value, $\varepsilon(x_{\max}) = \varepsilon_{\max}$. In a monotonic loading process, it is reasonable to expect that this maximum strain increases monotonically (even though certain parts of the bar experience elastic unloading at decreasing strain). This implies that $\varepsilon_{\mathrm{p}}(x) \leq \varepsilon_{\max}$ for all $x \in \mathcal{L}$, i.e., that the plastic strain can nowhere exceed the current maximum strain. According to Eq. (4.40), the stress at $x_{\max}$ can vanish only if $\bar{\varepsilon}_{\mathrm{p}}(x_{\max}) = \varepsilon_{\max}$. But if the nonlocal weight function is nonnegative (which is the case for all normally used weight functions), then

$$\begin{aligned} \bar{\varepsilon}_{\mathrm{p}}(x_{\max}) &= \int_{\mathcal{L}} \alpha(x_{\max},\xi)\varepsilon_{\mathrm{p}}(\xi)\mathrm{d}\xi \leq \int_{\mathcal{L}} \alpha(x_{\max},\xi)\varepsilon_{\max}\mathrm{d}\xi \\ &= \varepsilon_{\max}\int_{\mathcal{L}} \alpha(x_{\max},\xi)\mathrm{d}\xi = \varepsilon_{\max} \end{aligned} \tag{4.43}$$

This inequality can turn into an equality only if $\varepsilon_{\mathrm{p}}(\xi) = \varepsilon_{\max}$ at all points ξ for which $\alpha(x_{\max},\xi) > 0$, i.e., for all $\xi \in (x_{\max} - R, x_{\max} + R)$ where R is the interaction radius. This is in turn possible only if $\varepsilon(\xi) = \varepsilon_{\max}$ for all $\xi \in (x_{\max} - R, x_{\max} + R)$, which means that the strain would have to be uniform in an interval of size $2R$ centered at $x_{\max}$. But then the nonlocal plastic strain must be equal to $\varepsilon_{\max}$ at any point of this interval, and by a recursive application of the foregoing argument the interval of uniform strain can be shown to extend across the entire bar. Consequently, a complete loss of resistance of the bar must be preceded by an expansion of the plastic region over the entire bar.

In summary, the model with nonlocal plastic strain cannot properly describe the complete loss of material resistance. At later stages of softening it inevitably leads to spurious locking effects.

4.7 Thermodynamics with internal variables

Several recently emerged nonlocal plasticity models have been developed within the formalism of thermodynamics with internal variables. They have been conceived as nonlocal extensions of generalized standard materials, i.e., of material models derived from the postulate of maximum dissipation (Moreau 1970). In plasticity, such models are sometimes called fully associated, because all the evolution equations (flow rules and hardening laws) are formulated as normality rules associated with the yield surface.

Before discussing individual nonlocal formulations developed within this framework, it is useful to outline the general structure of such theories. The presentation exploits the

ideas of several articles (Svedberg 1996; Svedberg and Runesson 1998; Polizzotto et al. 1998; Borino et al. 1999), with some minor modifications and reinterpretations. For simplicity, the basic equations will be written in a scalar format valid for the one-dimensional case, but the generalization to a tensorial description would be straightforward.

4.7.1 Thermodynamic framework for local plasticity

A purely mechanical constitutive theory constructed within the framework of thermodynamics with internal variables requires the specification of appropriate expressions for the free energy density and for the dissipation density. The free-energy potential depends on the state variables (strain and internal variables), and the dissipation in general depends on the state variables and their rates, called the thermodynamic fluxes. The model satisfies the Second Law of thermodynamics if the dissipation is nonnegative for any process, i.e., for any admissible combination of the state variables and their rates. This is always true if the dissipation is written as a product of the thermodynamic fluxes and their conjugate quantities (dissipative thermodynamic forces), provided that the relation between the fluxes and the dissipative forces is derived from a dissipation (pseudo-)potential with appropriate properties; see e.g. Chapter 23 in Jirásek and Bažant (2002) for details.

In rate-independent one-dimensional elastoplasticity with isotropic hardening, the free energy depends on the strain, plastic strain and hardening variable, and is assumed to have the form

$$\psi(\varepsilon, \varepsilon_{\mathrm{p}}, \kappa) = \psi_{\mathrm{e}}(\varepsilon - \varepsilon_{\mathrm{p}}) + \psi_{\mathrm{p}}(\kappa) \tag{4.44}$$

where ψ_{e} is the elastically stored energy and ψ_{p} is the free energy blocked in the microstructure. For linear elasticity and linear hardening, the expressions for ψ_{e} and ψ_{p} are quadratic and the specific form of Eq. (4.44) is given by Eq. (2.28).

The dissipation is described by

$$\mathcal{D} = \sigma_{\mathrm{p}}\dot{\varepsilon}_{\mathrm{p}} + q\dot{\kappa} \tag{4.45}$$

where σ_{p} and q are the dissipative thermodynamic forces. In a fully associated theory, the dual dissipation potential is constructed as the indicator function of a convex yield function $f(\sigma_{\mathrm{p}}, q)$, and the resulting evolution laws have the form

$$\dot{\varepsilon}_{\mathrm{p}} = \dot{\lambda}\frac{\partial f(\sigma_{\mathrm{p}}, q)}{\partial \sigma} \tag{4.46}$$

$$\dot{\kappa} = \dot{\lambda}\frac{\partial f(\sigma_{\mathrm{p}}, q)}{\partial q} \tag{4.47}$$

$$\dot{\lambda} \geq 0, \qquad f(\sigma_{\mathrm{p}}, q) \leq 0, \qquad \dot{\lambda}\, f(\sigma_{\mathrm{p}}, q) = 0 \tag{4.48}$$

Local energy balance implies that the stress power must be equal to the sum of the free energy rate and the dissipation,

$$\sigma\dot{\varepsilon} = \rho\dot{\psi} + \mathcal{D} \tag{4.49}$$

This is a consequence of the First Law of thermodynamics. Substituting Eq. (4.45) and the rate form of Eq. (4.44) into Eq. (4.49), it follows that

$$\sigma\dot{\varepsilon} = \rho\psi'_{\mathrm{e}}\dot{\varepsilon} - \rho\psi'_{\mathrm{e}}\dot{\varepsilon}_{\mathrm{p}} + \rho\psi'_{\mathrm{p}}\dot{\kappa} + \sigma_{\mathrm{p}}\dot{\varepsilon}_{\mathrm{p}} + q\dot{\kappa} \tag{4.50}$$

where ψ'_{e} and ψ'_{p} are the derivatives of the potential functions ψ_{e} and ψ_{p} with respect to their arguments.

Strictly speaking, the validity of Eq. (4.50) is restricted to admissible processes, i.e., to those that can actually occur. In such processes, the rates of state variables are not totally independent; e.g., the plastic strain cannot spontaneously grow if the total strain is kept constant (at least not for the present rate-independent model). Still, it is reasonable to require that Eq. (4.50) be satisfied for an arbitrary combination of rates $\dot{\varepsilon}$, $\dot{\varepsilon}_{\mathrm{p}}$ and $\dot{\kappa}$. This means that the energy balance is extended to virtual processes, and Eq. (4.50) is interpreted as a virtual-work formulation of the conditions of thermodynamic equilibrium between dissipative forces and their quasi-conservative counterparts (see Chapter 23 in Jirásek and Bažant (2002) for a detailed explanation). If this line of reasoning is accepted, it can be inferred from Eq. (4.50) that

$$\sigma = \rho\psi'_{\mathrm{e}} \tag{4.51}$$

$$0 = \sigma_{\mathrm{p}} - \rho\psi'_{\mathrm{e}} \tag{4.52}$$

$$0 = q + \rho\psi'_{\mathrm{p}} \tag{4.53}$$

The first equation represents the stress-strain law, and the third equation provides the link between the dissipative force q and its quasi-conservative counterpart, defined as the derivative of the free-energy potential with respect to the hardening variable κ. Indeed, upon substituting the specific form of the free-energy potential (2.28), Equations (4.51) and (4.53) yield

$$\sigma = E(\varepsilon - \varepsilon_{\mathrm{p}}) \tag{4.54}$$

$$q = -H\kappa \tag{4.55}$$

Clearly, Eq. (4.54) is the linear elastic law (2.22), and Eq. (4.55) is the linear hardening law (2.23). Equation (4.52) combined with Eq. (4.51) indicates that the dissipative force σ_{p} is tied to the internal variables in the same way as the stress σ, and so σ_{p} and σ do not need to be distinguished. This is important because the yield function $f(\sigma_{\mathrm{p}}, q) \equiv f(\sigma, q)$ can now be written in terms of the actual stress (and not in terms of some mysterious dissipative force), which greatly facilitates its identification from physical measurements.

4.7.2 Thermodynamic framework for nonlocal plasticity

An attractive class of nonlocal plasticity theories can be derived from the assumption that the free energy density depends not only on the local values of the state variables but also on their weighted nonlocal averages. Thus the free-energy potential is written as $\psi(\varepsilon, \varepsilon_{\mathrm{p}}, \kappa, \bar{\varepsilon}, \bar{\varepsilon}_{\mathrm{p}}, \bar{\kappa})$, while the dissipation keeps the local form (4.45). If the energy balance were still enforced in the local sense of Eq. (4.49), the extended form of identity (4.50)

$$\sigma\dot{\varepsilon} = \rho\frac{\partial\psi}{\partial\varepsilon}\dot{\varepsilon} + \rho\frac{\partial\psi}{\partial\varepsilon_{\mathrm{p}}}\dot{\varepsilon}_{\mathrm{p}} + \rho\frac{\partial\psi}{\partial\kappa}\dot{\kappa} + \rho\frac{\partial\psi}{\partial\bar{\varepsilon}}\dot{\bar{\varepsilon}} + \rho\frac{\partial\psi}{\partial\bar{\varepsilon}_{\mathrm{p}}}\dot{\bar{\varepsilon}}_{\mathrm{p}} + \rho\frac{\partial\psi}{\partial\bar{\kappa}}\dot{\bar{\kappa}} + \sigma_{\mathrm{p}}\dot{\varepsilon}_{\mathrm{p}} + q\dot{\kappa} \tag{4.56}$$

would have to hold. However, for one isolated point, the nonlocal rate of a state variable is independent of its local rate at that point. This means that the terms multiplying $\dot{\bar{\varepsilon}}$, $\dot{\bar{\varepsilon}}_{\mathrm{p}}$ and $\dot{\bar{\kappa}}$ in Eq. (4.56) must vanish. Because these terms are the partial derivatives of free energy with respect to nonlocal state variables, the free energy cannot depend on the

nonlocal variables at all. Thus, within the present framework, local enforcement of energy balance in the standard sense inevitably leads to a standard local model.

A truly nonlocal theory can be constructed if it is admitted that nonlocal interaction results into some finite-distance energy exchange among individual material points. If this exchange is confined to the interior of the domain $\mathcal{L}$, i.e., if there is no nonlocal energy exchange across the boundary, the energy balance equation must be satisfied in the global sense,

$$\int_{\mathcal{L}} \sigma\dot{\varepsilon}\,\mathrm{d}x = \int_{\mathcal{L}} \rho\dot{\psi}\,\mathrm{d}x + \int_{\mathcal{L}} \mathcal{D}\,\mathrm{d}x \tag{4.57}$$

The integral on the left-hand side represents the total internal power (which is in the case of static equilibrium equal to the power supplied by the external forces), the first integral on the right-hand side is the global rate of change of internal energy, and the last integral is the global dissipation. In contrast to standard continuum mechanics, Eq. (4.57) is in general not valid for arbitrarily small subdomains of $\mathcal{L}$, and so it does not imply that Eq. (4.49) must hold pointwise. Due to spatial energy exchanges that occur at the microstructural level, the local energy balance equation must be enriched by the so-called nonlocal residual, $\mathcal{P}$, which represents the power density supplied to the given material point through nonlocal interactions with its neighborhood. Equation (4.49) is then replaced by

$$\sigma\dot{\varepsilon} + \mathcal{P} = \rho\dot{\psi} + \mathcal{D} \tag{4.58}$$

In a local continuum, $\mathcal{P}$ must vanish at all points. In a nonlocal continuum, the nonlocal residual is constrained by the so-called energy insulation condition

$$\int_{\mathcal{L}} \mathcal{P}\,\mathrm{d}x = 0 \tag{4.59}$$

which directly follows from Equations (4.57)–(4.58).

For both local and nonlocal models, the local dissipation $\mathcal{D}$ is required to be nonnegative, otherwise the model is not thermodynamically admissible. For local models, this condition is equivalent to the local form of the Clausius–Duhem inequality,

$$\sigma\dot{\varepsilon} - \rho\dot{\psi} \geq 0 \tag{4.60}$$

For nonlocal models, Eq. (4.60) remains valid only if the nonlocal residual $\mathcal{P}$ is added to the left-hand side. However, the global Clausius–Duhem inequality,

$$\int_{\mathcal{L}} \sigma\dot{\varepsilon}\,\mathrm{d}x - \int_{\mathcal{L}} \rho\dot{\psi}\,\mathrm{d}x \geq 0 \tag{4.61}$$

holds even for nonlocal models, provided that the insulation condition (4.59) is satisfied. It is therefore often stated that the nonlocal models satisfy the Clausius–Duhem inequality only in the global sense (Edelen and Laws 1971). One should bear in mind that the violation of the local Clausius–Duhem inequality (4.60) does not mean that the dissipation is locally allowed to be negative. The actual (local) dissipation, $\mathcal{D}$, is always required to be nonnegative but, due to the presence of the nonlocal residual, $\sigma\dot{\varepsilon} - \rho\dot{\psi}$ is not equal to $\mathcal{D}$. The *Clausius–Duhem inequality* (4.60) and the *dissipation inequality*, $\mathcal{D} \geq 0$, should be carefully distinguished.

The distribution of a state variable across the entire body uniquely determines the corresponding nonlocal field. So, in contrast to the case of local and nonlocal *values*, the local and nonlocal *fields* are not independent. Making use of the concept of dual averaging introduced in Sec. 2.3 and in particular of Eq. (2.18), the nonlocal rates can be eliminated from the expression for the rate of the global free energy:

$$\begin{aligned}\int_{\mathcal{L}} \rho\dot{\psi}\,\mathrm{d}x &= \int_{\mathcal{L}} \left(\rho\frac{\partial\psi}{\partial\varepsilon}\dot{\varepsilon} + \rho\frac{\partial\psi}{\partial\varepsilon_{\mathrm{p}}}\dot{\varepsilon}_{\mathrm{p}} + \rho\frac{\partial\psi}{\partial\kappa}\dot{\kappa} + \rho\frac{\partial\psi}{\partial\bar{\varepsilon}}\dot{\bar{\varepsilon}} + \rho\frac{\partial\psi}{\partial\bar{\varepsilon}_{\mathrm{p}}}\dot{\bar{\varepsilon}}_{\mathrm{p}} + \rho\frac{\partial\psi}{\partial\bar{\kappa}}\dot{\bar{\kappa}}\right)\,\mathrm{d}x \\ &= \int_{\mathcal{L}} \left(\rho\frac{\partial\psi}{\partial\varepsilon}\dot{\varepsilon} + \rho\frac{\partial\psi}{\partial\varepsilon_{\mathrm{p}}}\dot{\varepsilon}_{\mathrm{p}} + \rho\frac{\partial\psi}{\partial\kappa}\dot{\kappa}\right)\,\mathrm{d}x \\ &\quad + \int_{\mathcal{L}} \left[\left(\widetilde{\rho\frac{\partial\psi}{\partial\bar{\varepsilon}}}\right)\dot{\varepsilon} + \left(\widetilde{\rho\frac{\partial\psi}{\partial\bar{\varepsilon}_{\mathrm{p}}}}\right)\dot{\varepsilon}_{\mathrm{p}} + \left(\widetilde{\rho\frac{\partial\psi}{\partial\bar{\kappa}}}\right)\dot{\kappa}\right]\,\mathrm{d}x \end{aligned} \tag{4.62}$$

Recall that the tilde denotes the dual nonlocal average, constructed according to Eq. (2.20) where the order of arguments of the weight function is reversed. Substituting Eq. (4.62) and the dissipation expression (4.45) into Eq. (4.57), it follows that

$$\begin{aligned}\int_{\mathcal{L}} \sigma\dot{\varepsilon}\,\mathrm{d}x &= \int_{\mathcal{L}} \left[\rho\frac{\partial\psi}{\partial\varepsilon} + \left(\widetilde{\rho\frac{\partial\psi}{\partial\bar{\varepsilon}}}\right)\right]\dot{\varepsilon}\,\mathrm{d}x + \int_{\mathcal{L}} \left[\rho\frac{\partial\psi}{\partial\varepsilon_{\mathrm{p}}} + \left(\widetilde{\rho\frac{\partial\psi}{\partial\bar{\varepsilon}_{\mathrm{p}}}}\right) + \sigma_{\mathrm{p}}\right]\dot{\varepsilon}_{\mathrm{p}}\,\mathrm{d}x \\ &\quad + \int_{\mathcal{L}} \left[\rho\frac{\partial\psi}{\partial\kappa} + \left(\widetilde{\rho\frac{\partial\psi}{\partial\bar{\kappa}}}\right) + q\right]\dot{\kappa}\,\mathrm{d}x \end{aligned} \tag{4.63}$$

This identity is valid for an arbitrary distribution of rates $\dot{\varepsilon}$, $\dot{\varepsilon}_{\mathrm{p}}$ and $\dot{\kappa}$ if

$$\sigma = \rho\frac{\partial\psi}{\partial\varepsilon} + \left(\widetilde{\rho\frac{\partial\psi}{\partial\bar{\varepsilon}}}\right) \tag{4.64}$$

$$0 = \rho\frac{\partial\psi}{\partial\varepsilon_{\mathrm{p}}} + \left(\widetilde{\rho\frac{\partial\psi}{\partial\bar{\varepsilon}_{\mathrm{p}}}}\right) + \sigma_{\mathrm{p}} \tag{4.65}$$

$$0 = \rho\frac{\partial\psi}{\partial\kappa} + \left(\widetilde{\rho\frac{\partial\psi}{\partial\bar{\kappa}}}\right) + q \tag{4.66}$$

This is the nonlocal extension of Equations (4.51)–(4.53).

In the preceding section it has been shown that, for the specific choice of the free-energy potential (4.44), the dissipative force σ_{p} conjugate to the plastic strain turns out to be equal to the stress σ, which greatly facilitates the formulation of the yield condition. If follows from Equations (4.64)–(4.65), that the nonlocal extension has the same property if the free-energy potential is assumed to have the form

$$\psi(\varepsilon, \varepsilon_{\mathrm{p}}, \kappa, \bar{\varepsilon}, \bar{\varepsilon}_{\mathrm{p}}, \bar{\kappa}) = \psi_{\mathrm{e}}(\varepsilon - \varepsilon_{\mathrm{p}}, \bar{\varepsilon} - \bar{\varepsilon}_{\mathrm{p}}) + \psi_{\mathrm{p}}(\kappa, \bar{\kappa}) \tag{4.67}$$

which is a natural generalization of Eq. (4.44).

The yield condition can be formulated in stress space, because the dissipative force σ_{p} is equal to the stress σ. The yield function can still be kept in the simple form (2.27), i.e., the dissipative force q has the meaning of minus the drag stress. Because the dissipative

forces are conjugate to the *local* thermodynamic fluxes $\dot{\varepsilon}_\mathrm{p}$ and $\dot{\kappa}$, the evolution laws remain in the convenient form (2.24)–(2.26). One could envisage a more general theory with a nonlocal expression for the dissipation, but then it would be necessary to abandon the postulate of maximum dissipation, or to accept the evolution equations in an inconvenient nonlocal form. This issue will be further discussed in Sec. 4.9.1.

4.8 Models with double nonlocal averaging

4.8.1 Models with nonlocal elastic part

If the free energy depends on the nonlocal elastic strain, $\bar{\varepsilon}_\mathrm{e} = \overline{\varepsilon - \varepsilon_\mathrm{p}} = \bar{\varepsilon} - \bar{\varepsilon}_\mathrm{p}$, the model exhibits a nonlocal response already in the elastic range. For illustration, consider perfect elastoplasticity, for which the plastic part of the free energy potential, ψ_p, vanishes. Linear elastic behavior is obtained with the choice of a quadratic potential

$$\rho\psi(\varepsilon, \varepsilon_\mathrm{p}, \bar{\varepsilon}, \bar{\varepsilon}_\mathrm{p}) = \rho\psi_\mathrm{e}(\varepsilon - \varepsilon_\mathrm{p}, \bar{\varepsilon} - \bar{\varepsilon}_\mathrm{p}) = \tfrac{1}{2}E_\mathrm{L}(\varepsilon - \varepsilon_\mathrm{p})^2 + \tfrac{1}{2}E_\mathrm{N}(\bar{\varepsilon} - \bar{\varepsilon}_\mathrm{p})^2 \tag{4.68}$$

where E_L and E_N are material parameters playing the role of the 'local' and 'nonlocal' elastic moduli. The stress-strain law (4.64) then reads

$$\sigma = E_\mathrm{L}(\varepsilon - \varepsilon_\mathrm{p}) + E_\mathrm{N}(\widetilde{\bar{\varepsilon} - \bar{\varepsilon}_\mathrm{p}}) \tag{4.69}$$

If the nonlocal elastic modulus is uniform in space, it can be taken out of the dual averaging operator to simplify the stress-strain law to

$$\sigma = E_\mathrm{L}(\varepsilon - \varepsilon_\mathrm{p}) + E_\mathrm{N}(\widetilde{\bar{\varepsilon}} - \widetilde{\bar{\varepsilon}}_\mathrm{p}) \tag{4.70}$$

where $\widetilde{\bar{\varepsilon}}$ is the result of a double averaging of the strain field, first with the primal weight function and then with the dual weight function. The double average can be evaluated as

$$\begin{aligned} \widetilde{\bar{\varepsilon}}(x) &= \int_\mathcal{L} \alpha(\xi, x)\bar{\varepsilon}(\xi)\,\mathrm{d}\xi = \int_\mathcal{L} \alpha(\xi, x) \int_\mathcal{L} \alpha(\xi, \eta)\varepsilon(\eta)\,\mathrm{d}\eta\,\mathrm{d}\xi \\ &= \int_\mathcal{L}\int_\mathcal{L} \alpha(\xi, x)\alpha(\xi, \eta)\,\mathrm{d}\xi\,\varepsilon(\eta)\,\mathrm{d}\eta = \int_\mathcal{L} \beta(x, \eta)\varepsilon(\eta)\,\mathrm{d}\eta \end{aligned} \tag{4.71}$$

where

$$\beta(x, \eta) = \int_\mathcal{L} \alpha(\xi, x)\alpha(\xi, \eta)\,\mathrm{d}\xi \tag{4.72}$$

will be called the double weight function.

Note that the double weight function is always symmetric with respect to its arguments. In an infinite domain, is is given by

$$\begin{aligned} \beta(x, \eta) &= \int_{-\infty}^{\infty} \alpha_\infty(|x - \xi|)\alpha_\infty(|\xi - \eta|)\,\mathrm{d}\xi \\ &= \int_{-\infty}^{\infty} \alpha_\infty(|x - \eta - \zeta|)\alpha_\infty(|\zeta|)\,\mathrm{d}\zeta = \beta_\infty(|x - \eta|) = \beta_\infty(r) \end{aligned} \tag{4.73}$$

which means that the double weight function depends again only on the distance between the interacting points $r = |x - \eta|$. The double weight function β_∞ derived from the original bell-shaped function $\alpha_\infty^\mathrm{bell}$ given by Eq. (2.17) is plotted in Fig. 4.10.

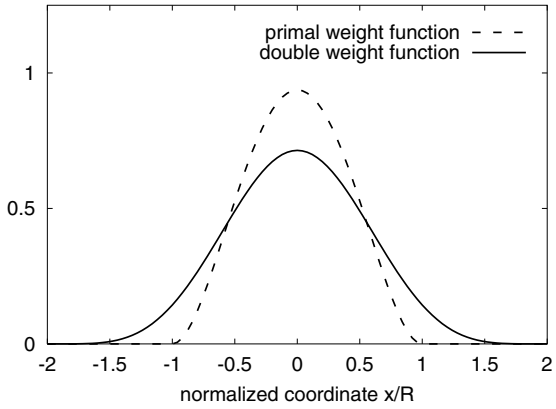

Figure 4.10: Double weight function β_∞ derived from the primal function $\alpha_\infty^{\rm bell}$ in an infinite domain.

In a finite domain, nonlocal averaging with the double weight function β transforms a uniformly distributed local variable into a nonlocal variable that is not uniform in the vicinity of the boundary. The reason is that even if α is constructed according to Eq. (2.15) so as to meet the normalizing condition $\int_{\mathcal{L}} \alpha(x,\xi)\,\mathrm{d}\xi = 1$, the weight function β defined by Eq. (4.72) does not meet this condition. Indeed,

$$\begin{aligned} \int_{\mathcal{L}} \beta(x,\eta)\,\mathrm{d}\eta &= \int_{\mathcal{L}}\int_{\mathcal{L}} \alpha(\xi,x)\alpha(\xi,\eta)\,\mathrm{d}\xi\,\mathrm{d}\eta \\ &= \int_{\mathcal{L}} \alpha(\xi,x)\int_{\mathcal{L}} \alpha(\xi,\eta)\,\mathrm{d}\eta\,\mathrm{d}\xi = \int_{\mathcal{L}} \alpha(\xi,x)\,\mathrm{d}\xi = \widetilde{1}(x) \end{aligned} \tag{4.74}$$

which is in general different from 1. Fig. 2.3 shows the integral $\int_{\mathcal{L}} \beta(x,\eta)\,\mathrm{d}\eta = \widetilde{1}(x)$ as a function of the dimensionless coordinate x/R for two different ratios L/R where R is the radius of nonlocal interaction and L is the total length of the bar. The weight function α is affected by scaling only in boundary layers of size R, and double averaging extends the influence of the boundary on the corresponding weight function β to the distance $2R$. If the length of the bar, L, is larger than $4R$, the weight function β in the central region between the boundary layers is the same as in an infinite body and satisfies the normalizing condition; see Fig. 2.3a. In the boundary layers of thickness $2R$, the integral $\int_{\mathcal{L}} \beta(x,\eta)\,\mathrm{d}\eta$ is variable. In the immediate vicinity of the boundary it is smaller than 1, and farther away it is larger than 1. If the length of the bar L is smaller than $4R$, the boundary layers merge and the normalizing condition is violated almost everywhere; see Fig. 2.3b.

In view of Eq. (4.71), the double averages in Eq. (4.70) can be interpreted as simple averages with a symmetrized weight function β given by Eq. (4.72). Even the local part of the stress-strain law can be included, simply by adding $E_{\rm L}/E_{\rm N}$ times the Dirac distribution $\delta(x-\eta)$ to the weight function $\beta(x,\eta)$. The resulting stress-strain law has the same format (4.36) as Eringen's first nonlocal model described in Sec. 4.5. Interestingly, even if the material parameters $E_{\rm L}$ and $E_{\rm N}$ vary in space, Eq. (4.69) can still be written in the form

(4.36) with the weight function given by

$$\beta(x,\eta) = \frac{E_{\mathrm{L}}(x)}{E}\delta(x-\eta) + \frac{1}{E}\int_{\mathcal{L}} E_{\mathrm{N}}(\xi)\alpha(\xi,x)\alpha(\xi,\eta)\,\mathrm{d}\xi \tag{4.75}$$

and with E = spatially constant reference modulus.

Even though the stress-strain law (4.69) can be presented in the form (4.36), the present model is not equivalent to the model proposed by Eringen (1981). The main difference is in the formulation of the yield conditions. The present model, constructed as a nonlocal extension of the concept of generalized standard materials, leads to a yield condition formulated in stress space. In contrast to that, Eringen (1981) decided to use a yield function formulated in strain space. These two formulations of the yield condition are not equivalent, because the stress-strain law is nonlocal.

4.8.2 Models with local elastic part

As already mentioned, nonlocal plasticity formulations that aim at regularizing the problem after the onset of localization due to softening are often constructed such that the nonlocal effects are not activated if the stress remains in the elastic range. In the present context, this can be achieved by neglecting the dependence of the free energy on the nonlocal elastic strain. For this reduced class of models, the free-energy potential (4.67) is further simplified to

$$\psi(\varepsilon,\varepsilon_{\mathrm{p}},\kappa,\bar{\kappa}) = \psi_{\mathrm{e}}(\varepsilon-\varepsilon_{\mathrm{p}}) + \psi_{\mathrm{p}}(\kappa,\bar{\kappa}) \tag{4.76}$$

with the elastic part usually given by a quadratic expression, $\rho\psi_{\mathrm{e}}(\varepsilon-\varepsilon_{\mathrm{p}}) = \frac{1}{2}E(\varepsilon-\varepsilon_{\mathrm{p}})^2$. Two such formulations will now be examined in more detail.

4.8.3 Model of Borino and coworkers

A simple thermodynamically motivated model with the plastic part of the free energy dependent only on the nonlocal softening variable was proposed by Borino et al. (1999). In the one-dimensional setting and for a model with a linear elastic part and with linear softening, the free energy density is written as

$$\rho\psi(\varepsilon,\varepsilon_{\mathrm{p}},\bar{\kappa}) = \tfrac{1}{2}E(\varepsilon-\varepsilon_{\mathrm{p}})^2 + \tfrac{1}{2}H\bar{\kappa}^2 \tag{4.77}$$

where $H < 0$ is the softening modulus. Evaluating the derivatives $\rho\,\partial\psi/\partial\kappa = 0$ and $\rho\,\partial\psi/\partial\bar{\kappa} = H\bar{\kappa}$ and substituting into Eq. (4.66), the dissipative force is $q = -\widetilde{H\bar{\kappa}}$, and the corresponding softening law reads

$$\sigma_{\mathrm{Y}} = \sigma_0 - q = \sigma_0 + \widetilde{H\bar{\kappa}} \tag{4.78}$$

The evaluation of the yield stress requires a two-fold evaluation of a nonlocal average.

As demonstrated in Sec. 4.8.1, double nonlocal averaging can be transformed into simple averaging with a modified weight function. Consequently, the softening law (4.78) can be written in the equivalent form

$$\sigma_{\mathrm{Y}} = \sigma_0 + H_0\widehat{\kappa} \tag{4.79}$$

where H_0 is a reference value of the softening modulus, and the superimposed hat has a different meaning than in Sec. 4.3 – here it denotes a nonlocal average with the modified weight function

$$\beta(x,\eta) = \frac{1}{H_0}\int_{\mathcal{L}} H(\xi)\alpha(\xi,x)\alpha(\xi,\eta)\,\mathrm{d}\xi \tag{4.80}$$

For a macroscopically homogeneous material with a spatially uniform softening modulus, $H(x) = H_0$, the weight function β is simply the double averaging function from Eq. (4.72).

The expression in Eq. (4.79) has the same structure as the softening law (4.1) used in the basic nonlocal model. In an infinite domain or sufficiently far from the boundary, the solutions of the one-dimensional localization problem obtained with the model from Borino et al. (1999) remain essentially the same as those obtained with the basic nonlocal model described in Sec. 4.2. If the weight function $\alpha_\infty(r)$ is a continuous bell-shaped function attaining its maximum value at $r = 0$, $\beta_\infty(r)$ defined in Eq. (4.73) has the same properties and the plastic region localizes into a single cross section.

The situation is slightly different in the boundary layers affected by scaling of the weight function. A solution with plastic strain fully localized at x_s is admissible only if $\beta(x, x_\mathrm{s})$ attains its maximum at $x = x_\mathrm{s}$. For the primary weight function $\alpha(x,\xi)$ scaled according to Eq. (2.15), this condition is satisfied if x_s is located right on the boundary. However, for the corresponding double weight function evaluated from Eq. (4.72), this is not the case. If x_s is placed on the boundary, $\beta(x, x_\mathrm{s})$ has its maximum at $x \approx 0.22R$; see Fig. 4.11a. Interestingly, there exists a point $x_\mathrm{s} \approx 0.34R$ such that $\beta(x, x_\mathrm{s})$ has its maximum at $x = x_\mathrm{s}$; see Fig. 4.11c. This means that the localization process triggered by an imperfection in the boundary layer is again attracted by one particular solution but, in contrast to the basic nonlocal model, the cross section at which the plastic strain increments eventually localize is now at a nonzero distance from the boundary.

4.8.4 Model of Svedberg and Runesson

The model described in Sec. 4.8.3 is theoretically appealing but does not act as a genuine localization limiter. As already discussed in Sections 4.2 and 4.3, a localized plastic region of nonzero measure is obtained only if the softening law combines in a suitable way the local and nonlocal softening variables. A thermodynamically consistent model of this kind was first proposed by Svedberg (1996) and Svedberg and Runesson (1998) and further investigated by Borino and Failla (2000). Its simplest version is based on the free-energy potential in the form

$$\rho\psi(\varepsilon,\varepsilon_\mathrm{p},\kappa,\bar\kappa) = \tfrac{1}{2}E(\varepsilon-\varepsilon_\mathrm{p})^2 + \tfrac{1}{2}H_\mathrm{L}\kappa^2 + \tfrac{1}{2}H_\mathrm{NL}(\bar\kappa-\kappa)^2 \tag{4.81}$$

where $H_\mathrm{L} < 0$ is the 'local' plastic modulus and H_NL is the 'nonlocal' plastic modulus that regularizes the model. For the sake of simplicity (but without any loss of generality), attention is restricted to the case of a macroscopically homogeneous material, for which the moduli H_L and H_NL are constant in space. Evaluating the derivatives $\rho\,\partial\psi/\partial\kappa = H_\mathrm{L}\kappa - H_\mathrm{NL}(\bar\kappa-\kappa) = (H_\mathrm{L}+H_\mathrm{NL})\kappa - H_\mathrm{NL}\bar\kappa$ and $\rho\,\partial\psi/\partial\bar\kappa = H_\mathrm{NL}(\bar\kappa-\kappa)$ and substituting into Eq. (4.66), the dissipative force turns out to be

$$q = -(H_\mathrm{L}+H_\mathrm{NL})\kappa + H_\mathrm{NL}\bar\kappa - H_\mathrm{NL}\widetilde{(\bar\kappa-\kappa)} = -(H_\mathrm{L}+H_\mathrm{NL})\kappa + H_\mathrm{NL}\widehat{\kappa} \tag{4.82}$$

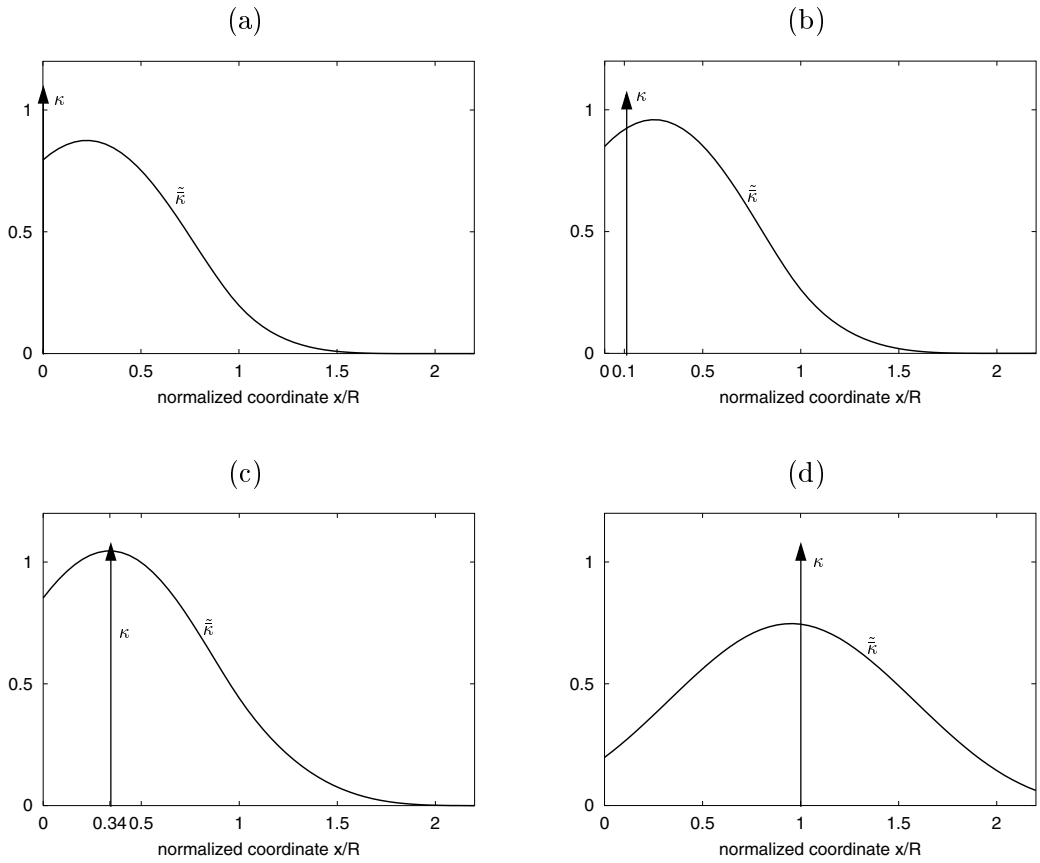

Figure 4.11: Model of Borino et al.: Double nonlocal average of plastic strain, $\widetilde{\widetilde{\kappa}}(x)$, for hypothetical Dirac-like solutions $\kappa(x) = \delta(x - x_\mathrm{s})$ localized in the vicinity of the boundary at (a) $x_\mathrm{s} = 0$, (b) $x_\mathrm{s} = 0.1R$, (c) $x_\mathrm{s} = 0.34R$, and (d) $x_\mathrm{s} = R$. Only the solution with $x_\mathrm{s} = 0.34R$ is admissible.

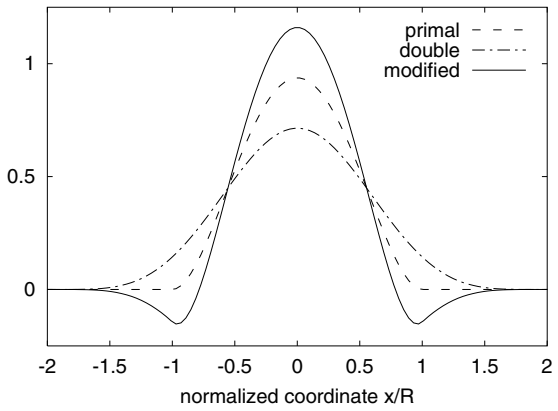

Figure 4.12: Svedberg–Runesson model: Modified weight function β derived from the primal weight function α according to (4.83).

where $\widehat{\kappa} = \bar{\kappa} + \widetilde{\kappa} - \widetilde{\bar{\kappa}}$, i.e., the hat denotes nonlocal averaging with a modified weight function

$$\beta(x,\eta) = \alpha(x,\eta) + \alpha(\eta,x) - \int_{\mathcal{L}} \alpha(\xi,x)\alpha(\xi,\eta)\,\mathrm{d}\xi \tag{4.83}$$

The resulting softening law

$$\sigma_{\mathrm{Y}} = \sigma_0 - q = \sigma_0 + (H_{\mathrm{L}} + H_{\mathrm{NL}})\kappa - H_{\mathrm{NL}}\widehat{\kappa} \tag{4.84}$$

has the same structure as the linear version of the Vermeer–Brinkgreve model (4.13) with $H_{\mathrm{L}} = H$ and $H_{\mathrm{NL}} = -mH$. The difference is that the standard weight function α used for the evaluation of the nonlocal average $\bar{\kappa}$ is nonnegative, while the modified weight function β given by Eq. (4.83) and used for the evaluation of the nonlocal average $\widehat{\kappa}$ has, in a certain range, also negative values, see Fig. 4.12. This follows from the fact that double averaging has a larger interaction radius than the original (primal) averaging. The first two terms on the right-hand side of Eq. (4.83) vanish for $|x-\xi| > R$ but the last term with a negative sign vanishes only for $|x-\xi| > 2R$, where R is the interaction radius of the weight function α.

Despite this unusual property of the modified weight function β, solutions of the one-dimensional localization problem are quite similar to the solutions constructed with the Vermeer–Brinkgreve model in Sec. 4.3. Some differences in the shape of the plastic strain profile can be observed if localization takes place at the boundary. Fig. 4.13 shows that for m larger than approximately 1.25, the maximum plastic strain is not attained at the boundary but at a certain distance that increases with increasing m. A nonzero size of the plastic zone is obtained with $m \equiv -H_{\mathrm{NL}}/H_{\mathrm{L}} > 1$, i.e., with $H_{\mathrm{L}} + H_{\mathrm{NL}} > 0$. This means that the nonlocal plastic modulus must be positive and larger in magnitude than the negative local plastic modulus.

In Sec. 4.3.5, two possible nonlinear extensions of the Vermeer–Brinkgreve model have been discussed:

- The nonlinear softening function is applied to the combination of the local and nonlocal softening variable, $m\bar{\kappa} + (1-m)\kappa$.

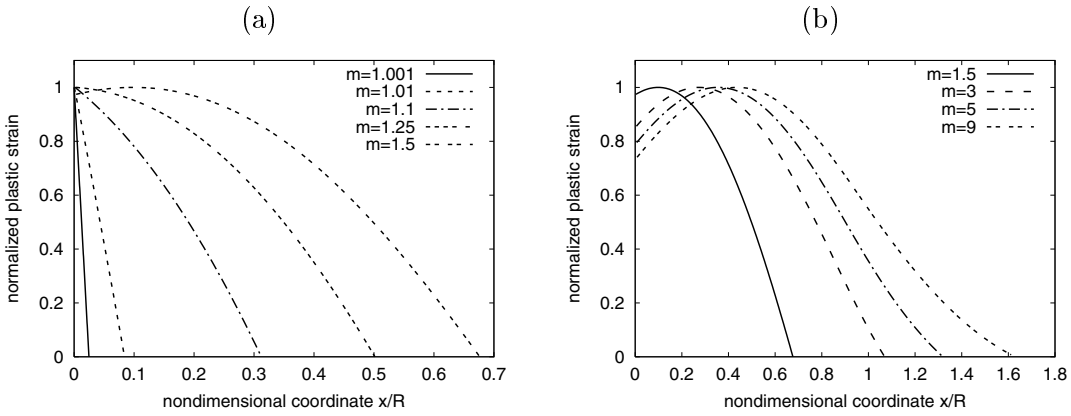

Figure 4.13: Svedberg–Runesson model: Distribution of plastic strain in the vicinity of a boundary at $x = 0$ for different values of parameter $m \equiv -H_{\mathrm{NL}}/H_{\mathrm{L}}$.

- The combined softening variable is split into the uniform part, κ, and the nonuniform part, $m(\bar{\kappa} - \kappa)$, and the nonlinear softening function is applied only to the uniform part while the modification of the yield stress due to the nonuniform part is kept linear.

The first extension gives a constant size of the plastic region during the softening process and the failure process is properly described up to the complete loss of residual strength, while the second extension gives an expanding plastic region and generates spurious stresses at late stages of the softening process.

Unfortunately, a consistent nonlinear formulation of the Svedberg–Runesson model leads rather to the second type of extension. The free energy potential (4.81) is in general written as

$$\rho\psi(\varepsilon, \varepsilon_{\mathrm{p}}, \kappa, \bar{\kappa}) = \tfrac{1}{2}E(\varepsilon - \varepsilon_{\mathrm{p}})^2 + \psi_{\mathrm{pL}}(\kappa) + \psi_{\mathrm{pNL}}(\bar{\kappa} - \kappa) \tag{4.85}$$

and the corresponding softening law reads

$$\sigma_{\mathrm{Y}} = \sigma_0 + h_{\mathrm{L}}(\kappa) + \widetilde{h_{\mathrm{NL}}}(\bar{\kappa} - \kappa) - h_{\mathrm{NL}}(\bar{\kappa} - \kappa) \tag{4.86}$$

where $h_{\mathrm{L}} = \rho\psi'_{\mathrm{pL}}$ and $h_{\mathrm{NL}} = \rho\psi'_{\mathrm{pNL}}$. In a test during which the strain is kept uniform (which is perhaps difficult to realize in a laboratory but can still be considered in a mind experiment), $\bar{\kappa} - \kappa$ remains equal to zero and the evolution of the yield stress is given by $\sigma_{\mathrm{Y}} = \sigma_0 + h_{\mathrm{L}}(\kappa)$. If the material is supposed to fail completely at a sufficiently large strain, $h_{\mathrm{L}}(\kappa)$ must tend to $-\sigma_0$ as $\kappa \to \infty$. In a test with strain localization, the corrective term $\widetilde{h_{\mathrm{NL}}} - h_{\mathrm{NL}}$ generates some residual yield stress, unless h_{NL} is constant inside the plastic region and in its neighborhood (to make $\widetilde{h_{\mathrm{NL}}}$ equal to h_{NL} inside the plastic region). For monotonic functions h_{NL}, this in turn implies that the argument $\bar{\kappa} - \kappa$ must be constant in and around the plastic region, and this is impossible unless κ is constant along the entire bar. Of course, the exact form of function h_{NL} is not prescribed, but the desired regularizing effect is achieved only if h_{NL} is an increasing function with a sufficiently large derivative, at least around the origin (recall the condition $H_{\mathrm{NL}} > -H_{\mathrm{L}} > 0$ derived for the linear softening case).

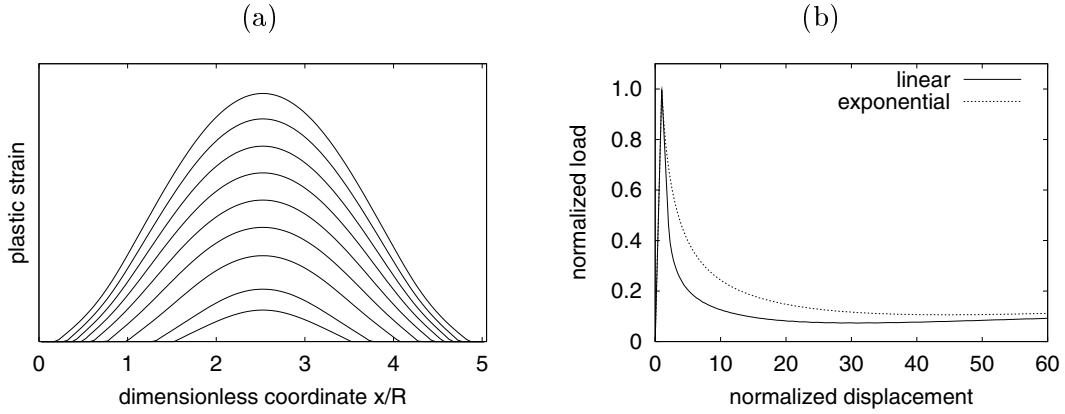

Figure 4.14: Svedberg–Runesson model: (a) evolution of plastic strain profile for exponential softening, (b) load-displacement diagram for linear and exponential softening laws.

The potential danger of locking, indicated by the foregoing theoretical analysis, is confirmed by numerical results. Fig. 4.14a shows the expanding plastic strain profile for an exponential softening law $h_{\mathrm{L}}(\kappa) = \sigma_0[\exp(-\kappa/\kappa_{\mathrm{c}}) - 1]$ and a linear stabilization law $h_{\mathrm{NL}}(\bar{\kappa} - \kappa) = H_{\mathrm{NL}}[\bar{\kappa} - \kappa]$ where $H_{\mathrm{NL}} > -h'_{\mathrm{L}}(0) = \sigma_0/\kappa_{\mathrm{c}}$. From the load-displacement diagram in Fig. 4.14b it is clear that stress locking appears at late stages of softening. For comparison, the dashed curve shows the load-displacement diagram for a linear softening law with a cutoff at zero stress, $h_{\mathrm{L}}(\kappa) = \langle \sigma_0 + H_{\mathrm{L}}\kappa \rangle - \sigma_0$. Even in this case, the locking stresses build up. If no cutoff is used, the stress would eventually become negative, which does not make sense in a tensile test.

4.9 Nilsson's model

4.9.1 Model description

In his thesis (Nilsson 1994) and a journal paper (Nilsson 1997), Nilsson proposed a thermodynamically motivated nonlocal plasticity model which shares many similar features with the model from Sec. 4.8.3. However, there are some important differences.

Nilsson started from the general thermodynamic framework similar to that presented in Sec. 4.7.2. In the most general version of his model, he considered all arguments of the free-energy potential as nonlocal. Because this would lead to a stress-strain law that is not easily invertible, Nilsson focussed his attention on what he called a model with restricted nonlocality, which incorporates the total strain only in its local form. In a one-dimensional setting and assuming linear elasticity and linear softening, the free energy density is written as

$$\rho\psi(\varepsilon, \bar{\varepsilon}_{\mathrm{p}}, \bar{\kappa}) = \tfrac{1}{2}E(\varepsilon - \bar{\varepsilon}_{\mathrm{p}})^2 + \tfrac{1}{2}H\bar{\kappa}^2 \tag{4.87}$$

In contrast to Eq. (4.77), the plastic strain that appears in the elastic part of the free energy is nonlocal. With this specific choice of the free-energy potential, Equations (4.64)–(4.66) are reduced to

$$\sigma = \rho\frac{\partial\psi}{\partial\varepsilon} = E(\varepsilon - \bar{\varepsilon}_{\mathrm{p}}) \tag{4.88}$$

$$\sigma_{\mathrm{p}} = -\left(\rho\widetilde{\frac{\partial\psi}{\partial\bar{\varepsilon}_{\mathrm{p}}}}\right) = E(\widetilde{\varepsilon - \bar{\varepsilon}_{\mathrm{p}}}) = \widetilde{\sigma} \tag{4.89}$$

$$q = -\left(\rho\widetilde{\frac{\partial\psi}{\partial\bar{\kappa}}}\right) = -\widetilde{H\bar{\kappa}} \tag{4.90}$$

So far, the model from Borino et al. (1999) presented in Sec. 4.8.3 could be considered as a special case of Nilsson's model with degenerated nonlocal averaging operators acting on the plastic strain and on the corresponding thermodynamic force. The main difference between the two models is in the evolution laws and the way they are derived from the postulate of maximum plastic dissipation. Borino et al. (1999) wrote the yield function f in terms of the dissipative forces conjugate to the local internal variables ε_{p} and κ. In their theory, ε_{p} enters the free energy by its local value, and the dissipative force conjugate to ε_{p} turns out to be equal to the stress σ. The dissipative force q conjugate to κ is the dual average $\widetilde{\chi}$ of the dissipative force $\chi \equiv -H\bar{\kappa}$ conjugate to $\bar{\kappa}$. If the yield function is written as $f(\sigma, \widetilde{\chi})$, the postulate of maximum plastic dissipation can be applied to the local dissipation $\mathcal{D} = \sigma\dot{\varepsilon}_{\mathrm{p}} + \widetilde{\chi}\dot{\kappa}$ and leads, in a straightforward way, to the associated evolution laws

$$\dot{\varepsilon}_{\mathrm{p}} = \dot{\lambda}\frac{\partial f}{\partial\sigma}, \qquad \dot{\kappa} = \dot{\lambda}\frac{\partial f}{\partial\widetilde{\chi}} \tag{4.91}$$

with the usual loading-unloading conditions.

For Nilsson's model, a direct extension would be to write the yield condition in terms of $\widetilde{\sigma}$ and $\widetilde{\chi}$, and the corresponding evolution laws would read

$$\dot{\varepsilon}_{\mathrm{p}} = \dot{\lambda}\frac{\partial f}{\partial\widetilde{\sigma}}, \qquad \dot{\kappa} = \dot{\lambda}\frac{\partial f}{\partial\widetilde{\chi}} \tag{4.92}$$

However, the yield condition would then contain the dual average of the stress, and its physical interpretation and numerical implementation would be quite difficult. Such considerations perhaps forced Nilsson to write the yield condition in terms of σ and χ, i.e., in terms of the forces conjugate to the nonlocal averages of internal variables, $\bar{\varepsilon}_{\mathrm{p}}$ and $\bar{\kappa}$. But, surprisingly, he stated that the corresponding evolution laws would read

$$\dot{\varepsilon}_{\mathrm{p}} = \dot{\lambda}\frac{\partial f}{\partial\sigma}, \qquad \dot{\kappa} = \dot{\lambda}\frac{\partial f}{\partial\chi} \tag{4.93}$$

This was later questioned in the discussion (Borino and Polizzotto 1999) of Nilsson's paper where it was argued that, if the yield function is written as $f(\sigma, \chi)$, it does not make sense to maximize locally $\mathcal{D} = \widetilde{\sigma}\dot{\varepsilon}_{\mathrm{p}} + \widetilde{\chi}\dot{\kappa}$ under the constraint $f(\sigma, \chi) \leq 0$, and one would have to resort to the maximization of the global dissipation

$$D = \int_{\mathcal{L}} \mathcal{D}\,\mathrm{d}x = \int_{\mathcal{L}} (\widetilde{\sigma}\dot{\varepsilon}_{\mathrm{p}} + \widetilde{\chi}\dot{\kappa})\,\mathrm{d}x = \int_{\mathcal{L}} (\sigma\dot{\bar{\varepsilon}}_{\mathrm{p}} + \chi\dot{\bar{\kappa}})\,\mathrm{d}x \tag{4.94}$$

over the set of all fields $\sigma(x)$ and $\chi(x)$ that satisfy the constraint $f \leq 0$ at all points x. This argument was accepted by Nilsson in his closure (Nilsson 1999), but he also pointed out that a strict application of this technique would lead to evolution laws for the nonlocal averages of internal variables, in the form

$$\dot{\bar{\varepsilon}}_{\mathrm{p}} = \dot{\lambda}\frac{\partial f}{\partial\sigma}, \qquad \dot{\bar{\kappa}} = \dot{\lambda}\frac{\partial f}{\partial\chi} \tag{4.95}$$

Consequently, the local internal variables ε_p and κ would completely disappear from all model equations, including the state laws and the evolution laws, and they would be everywhere replaced by their nonlocal averages. The resulting 'nonlocal' theory differs from the original local theory only formally: the internal variables are disguised under new symbols with an overbar. Such an extension would be empty and would make no sense. Nilsson (1999) concluded that his original evolution laws (4.93) cannot be derived from the postulate of maximum plastic dissipation, but they are still thermodynamically admissible as long as the global dissipation D remains nonnegative. Unfortunately, in some special cases the dissipation can become negative, as will be demonstrated in Sec. 4.9.3, just after the analysis of the one-dimensional localization problem.

4.9.2 Localization analysis

Even though Nilsson developed a relatively general framework for nonlocal plasticity models at finite strain (Nilsson 1994), the final application to one-dimensional localization analysis under small strain (Nilsson 1997) turns out to be very similar to the basic nonlocal plasticity model described in Sec. 4.2. The only difference is the elastic law (2.29), which is replaced by

$$\sigma = E(\varepsilon - \bar{\varepsilon}_\mathrm{p}) \tag{4.96}$$

where $\bar{\varepsilon}_\mathrm{p}$ is the nonlocal average of the plastic strain; all other equations remain unchanged.

Consequently, every solution valid for the basic nonlocal model can be transformed into a solution valid for Nilsson's model and vice versa. The transformation consists simply in adding the difference between the nonlocal and local plastic strain to the total strain. The stress level and the distribution of plastic strain are not affected by this transformation. Because the basic nonlocal model admits solutions with fully localized plastic strain, described by a multiple of the Dirac distribution, Nilsson's model has the same property.

In Sec. 4.2 it has been shown that, for a given stress level σ in the softening range, the distribution of the softening variable (which is, under tension, identical with the plastic strain) is given by Eq. (4.10). The distribution of the total strain can be described by

$$\varepsilon(x) = \varepsilon_\mathrm{e}(x) + \varepsilon_\mathrm{p}(x) = \frac{\sigma}{E} + \frac{\sigma - \sigma_0}{H\alpha(x_\mathrm{s}, x_\mathrm{s})}\delta(x - x_\mathrm{s}) \tag{4.97}$$

The corresponding solution of Nilsson's model at the same stress level is characterized by

$$\varepsilon^\mathrm{Nil}(x) = \varepsilon_\mathrm{e}(x) + \bar{\varepsilon}_\mathrm{p}(x) = \frac{\sigma}{E} + \frac{\sigma - \sigma_0}{H\alpha(x_\mathrm{s}, x_\mathrm{s})}\alpha(x, x_\mathrm{s}) \tag{4.98}$$

The plastic part of the total beam elongation is

$$\Delta L_\mathrm{p} = \int_\mathcal{L} \varepsilon_\mathrm{p}(x)\,\mathrm{d}x = \frac{\sigma - \sigma_0}{H\alpha(x_\mathrm{s}, x_\mathrm{s})} \int_\mathcal{L} \delta(x - x_\mathrm{s})\,\mathrm{d}x = \frac{\sigma - \sigma_0}{H\alpha(x_\mathrm{s}, x_\mathrm{s})} \tag{4.99}$$

for the basic nonlocal model, and

$$\Delta L_\mathrm{p}^\mathrm{Nil} = \int_\mathcal{L} \bar{\varepsilon}_\mathrm{p}(x)\,\mathrm{d}x = \frac{\sigma - \sigma_0}{H\alpha(x_\mathrm{s}, x_\mathrm{s})} \int_\mathcal{L} \alpha(x, x_\mathrm{s})\,\mathrm{d}x = \frac{\sigma - \sigma_0}{H\alpha(x_\mathrm{s}, x_\mathrm{s})}\widetilde{1}(x_\mathrm{s}) \tag{4.100}$$

for the Nilsson model.

If the point x_s at which the plastic strain has localized is far from the boundary, then $\widetilde{1}(x_\mathrm{s}) \equiv \int_\mathcal{L} \alpha(x, x_\mathrm{s})\,\mathrm{d}x$ is equal to 1. This means that the total elongation is not affected by the transformation from the solution of the basic nonlocal model to the solution of Nilsson's model, and the corresponding load-displacement diagrams are exactly the same. The transformation consists in this case in a redistribution of the total strain around the plasticized cross section, keeping the stress and the total elongation constant.

He stated that his model would lead to a finite size of the localization band, but this is true only if the localization band is defined as the region in which the total strain is growing. The actual plastic zone, in which the yield condition is satisfied (as an equality) and the local plastic strain is increasing, is confined to one single cross section, same as for the basic nonlocal model. So, Nilsson's model is again very similar to a cohesive zone model.

If localization starts in the vicinity of a boundary at $x = 0$, it is again attracted by the boundary. For $x_\mathrm{s} = 0$, the value of $\widetilde{1}(x_\mathrm{s})$ can be calculated analytically as $\widetilde{1}(0) = \int_\mathcal{L} \alpha(x, 0)\,\mathrm{d}x = \ln 2 \approx 0.69$. According to Equations (4.99)–(4.100), the plastic elongation at a given stress level, the total elongation at failure, and the energy consumed by the failure process are by 31 % smaller for Nilsson's model than for the basic nonlocal model.

4.9.3 Dissipation properties

In the one-dimensional case, the global dissipation of Nilsson's model is given by Eq. (4.93). Differentiating the yield function $f(\sigma, \chi) = |\sigma| - (\sigma_0 - \chi)$ and substituting the partial derivatives into Eq. (4.94), it follows that $\dot{\varepsilon}_\mathrm{p} = \dot{\lambda}\,\mathrm{sgn}\,\sigma$ and $\dot{\kappa} = \dot{\lambda}$. The global dissipation can then be expressed as

$$D = \int_\mathcal{L} (\sigma\dot{\bar{\varepsilon}}_\mathrm{p} + \chi\dot{\bar{\kappa}})\,\mathrm{d}x = \int_\mathcal{L} (\widetilde{\sigma}\,\mathrm{sgn}\,\sigma + \widetilde{\chi})\dot{\lambda}\,\mathrm{d}x = \int_\mathcal{L} \left(\widetilde{\sigma}\,\mathrm{sgn}\,\sigma - \widetilde{H\bar{\kappa}}\right)\dot{\lambda}\,\mathrm{d}x \tag{4.101}$$

For the solution described in Sec. 4.9.2, the rate of the local plastic multiplier, $\dot{\lambda} \equiv \dot{\kappa}$, is a positive multiple of the Dirac distribution centered at x_s, and so the sign of the global dissipation depends on the sign of $\widetilde{\sigma}\,\mathrm{sgn}\,\sigma - \widetilde{H\bar{\kappa}}$ at $x = x_\mathrm{s}$. Under tensile yielding, the stress at the yielding cross section, $\sigma(x_\mathrm{s})$, is positive, and so $\mathrm{sgn}\,\sigma(x_\mathrm{s}) = 1$. Therefore, it is sufficient to check the sign of $\widetilde{\sigma} - \widetilde{H\bar{\kappa}}$ at $x = x_\mathrm{s}$.

In the absence of body forces, the dissipation is positive. The stress is constant, i.e. $\sigma(x) = \sigma(x_\mathrm{s}) > 0$ for all $x \in \mathcal{L}$, and because $H < 0$ and $\bar{\kappa}(x) > 0$, it follows that $\sigma(x) - H\bar{\kappa}(x) > 0$. The dual average preserves this property, provided that the weight function is nonnegative.

However, in a general case the bar can be loaded by body forces that change the stress in the neighborhood of the plastic region without affecting the distribution of the plastic strain. From the condition of plastic admissibility, $|\sigma| - (\sigma_0 + H\bar{\kappa}) \leq 0$, it can be inferred only that the value of $\sigma - H\bar{\kappa}$ cannot exceed σ_0, but there is no reason why this value could not become negative. Only in the cross section that is yielding, $\sigma - H\bar{\kappa} = \sigma_0 > 0$ but, for a special distribution of body forces, other cross sections can be under compression high enough to make $\sigma - H\bar{\kappa}$ negative. Under such unfavorable circumstances, Nilsson's model violates the global form of the dissipation inequality. This shows that the model is not really thermodynamically admissible.

4.10 Dissipation properties of models with simple averaging

For models constructed within the thermodynamic framework, the expression for dissipation is readily available and the dissipation inequality can be checked. However, for models with constitutive equations postulated without any reference to thermodynamic potentials, it is not easy to check the thermodynamic admissibility. The reason is that the constitutive equations do not uniquely define the free energy, dissipation and nonlocal residual. Every thermodynamically admissible model must satisfy the global Clausius–Duhem inequality (4.61), which can be checked if the free-energy potential is given. If, for a certain choice of the free-energy potential, the inequality is satisfied during any admissible evolution of the state variables, there is a good chance that the local dissipation can be defined such that it remains always nonnegative, in which case the model is thermodynamically admissible. But to prove that a model is *not* thermodynamically admissible, it would be necessary to show that for *any* admissible choice of the free-energy potential, there exists an evolution of the state variables that violates the Clausius–Duhem inequality.

Note that the symmetric form of the nonlocal weight function for the model proposed by Borino et al. (1999) is not dictated by the basic requirements of thermodynamic admissibility but by an additional assumption—the postulate of maximum plastic dissipation, which provides a fully associated model. Consequently, unsymmetric models complying with the Second Law of thermodynamics may exist.

For example, the basic nonlocal model can be shown to satisfy the global Clausius–Duhem inequality. It suffices to assume the free-energy potential in the same form (4.77) as for the model from Borino et al. (1999). In the one-dimensional case, the global dissipation is evaluated as

$$D = \int_{\mathcal{L}} \left(\sigma\dot{\varepsilon} - \rho\dot{\psi}\right) \mathrm{d}x = \int_{\mathcal{L}} (\sigma\dot{\varepsilon}_{\mathrm{p}} - H\bar{\kappa}\dot{\bar{\kappa}})\, \mathrm{d}x = \int_{\mathcal{L}} \left(|\sigma| - \widetilde{H\bar{\kappa}}\right) \dot{\kappa}\, \mathrm{d}x \tag{4.102}$$

For the thermodynamically motivated model from Sec. 4.8.3, the yield condition reads $|\sigma| = \sigma_0 + \widetilde{H\bar{\kappa}}$. This condition is satisfied at all points where $\dot{\kappa} > 0$, and so the integrand in the last integral is always nonnegative. For the basic nonlocal model from Sec. 4.2, $|\sigma| - \widetilde{H\bar{\kappa}} \geq 0$ holds at all points where $\dot{\kappa} > 0$, because the dual weight function is nonnegative and $H < 0$ and $\bar{\kappa} \geq 0$, which implies that $\widetilde{H\bar{\kappa}} \leq 0$. Consequently, the global dissipation is always nonnegative. The derivation has been done for the one-dimensional case, but it can easily be extended to multiple dimensions. For an associated flow rule, $|\sigma|$ is replaced by $\boldsymbol{\sigma} : (\partial f / \partial \boldsymbol{\sigma})$, which is also nonnegative, provided that the yield function is convex and that the state of zero stress remains plastically admissible.

For the Vermeer–Brinkgreve model from Sec. 4.3, the foregoing verification of the Clausius–Duhem inequality cannot be directly reused, because the nonstandard weight function (4.14) is not nonnegative (due to the presence of a negative multiple of the Dirac distribution). Nevertheless, for the simplest case of uniaxial loading with vanishing body forces, it can be shown that the global Clausius–Duhem inequality is satisfied. Of course, this is not a complete proof of thermodynamic admissibility of the model.

model	section	stress-strain law	softening law
local	2.4	$\sigma = E(\varepsilon - \varepsilon_{\mathrm{p}})$	$\sigma_{\mathrm{Y}} = \sigma_0 + h(\kappa)$
basic nonlocal	4.2		$\sigma_{\mathrm{Y}} = \sigma_0 + h(\bar{\kappa})$
Vermeer–Brinkgreve	4.3		$\sigma_{\mathrm{Y}} = \sigma_0 + h(m\bar{\kappa} + (1-m)\kappa)$
	4.3.5		$\sigma_{\mathrm{Y}} = \sigma_0 + h(\kappa) + H_{\mathrm{m}}[\bar{\kappa} - \kappa]$
Geers et al.	4.4.1		$\sigma_{\mathrm{Y}} = [1 - \omega_{\mathrm{p}}(\bar{\kappa})](\sigma_0 + H\kappa)$
nonlocal Gurson	4.4.2		$\sigma_{\mathrm{Y}} = [1 - \omega_{\mathrm{p}}(\overline{p(\kappa)})](\sigma_0 + H\kappa)$
Eringen (strain space)	4.5	$\sigma = E(\bar{\varepsilon} - \bar{\varepsilon}_{\mathrm{p}})$	
Eringen (stress space)	4.5	$\sigma = E(\bar{\varepsilon} - \varepsilon_{\mathrm{p}})$	
Bažant–Lin	4.6	$\sigma = E(\varepsilon - \bar{\varepsilon}_{\mathrm{p}})$	
Borino et al.	4.8.3		$\sigma_{\mathrm{Y}} = \sigma_0 + \widetilde{h(\bar{\kappa})}$
Svedberg–Runesson	4.8.4		$\sigma_{\mathrm{Y}} = \sigma_0 + h_{\mathrm{L}}(\kappa) + \widetilde{h_{\mathrm{NL}}} - h_{\mathrm{NL}}$, where $h_{\mathrm{NL}} = h_{\mathrm{NL}}(\bar{\kappa} - \kappa)$
Nilsson	4.9	$\sigma = E(\varepsilon - \bar{\varepsilon}_{\mathrm{p}})$	$\sigma_{\mathrm{Y}} = \sigma_0 + h(\bar{\kappa})$

Table 4.1: Overview of integral-type nonlocal plasticity models

4.11 Overview of integral-type nonlocal model

A number of integral-type nonlocal formulations of softening plasticity have been scrutinized, with attention to their localization properties, boundary effects, and thermodynamic admissibility. The models are summarized in Table 4.1. Of course, this simple table provides only the basic orientation; it cannot cover all the specific details of different formulations. The names attached to the models are not always standard but they refer, to the best of the author's knowledge, to the first publication in which the key idea of the respective model appeared. The table displays only those stress-strain laws and softening laws that differ from the standard local equations given in the first row. The evolution equations (flow rule, evolution law for the softening variable, and loading-unloading conditions) usually keep the standard form (2.24)–(2.26), with the exception of Eringen's first model and the model due to Bažant and Lin, which work with the yield condition in strain space.

The main results can be summarized as follows:

1. The nonlocal plasticity models proposed by Eringen do not act as localization limiters. The first model does not prevent localization into a set of measure zero, and the second model does not allow any localization at all (in the one-dimensional setting).

2. Models with the yield stress dependent only on the nonlocal cumulative plastic strain (basic nonlocal formulation, model of Borino et al., and Nilsson's model) provide only a partial regularization and are essentially equivalent to a cohesive zone model. Plastic strain is localized into a set of zero measure but, in contrast to the local formulation, the global structural response in terms of the load-displacement diagram and work spent during the failure process is captured correctly. In finite element simulations in multiple dimensions, such models are likely to exhibit mesh-induced directional bias, because the plastic yielding would localize into one layer of elements.

3. Models that combine in a suitable way the effect of the local and nonlocal cumulative

plastic strain on the current yield stress act as true localization limiters and lead to a nonzero size of the localized plastic zone. This is true for the Vermeer–Brinkgreve model, models motivated by ductile damage (integral-type version of the implicit gradient plasticity model due to Geers et al. and nonlocal extension of the Gurson model), and the thermodynamically motivated model proposed by Svedberg and Runesson. The model proposed by Bažant and Lin has similar properties. At the first bifurcation from a uniform strain state, all these models are essentially equivalent. The subsequent evolution of the plastic strain profile and the stress transmitted by the plastic zone depend on the specific form of the softening law.

4. If the softening process needs to be simulated until the complete loss of material integrity (zero residual yield stress), the model should be selected with great care. At late stages of the softening process, certain formulations produce pathological effects such as stress locking or spatial expansion of the plastic zone. Such formulations have a limited scope. Only the Vermeer–Brinkgreve model and the ductile damage models seem to be suitable for the description of the complete failure process.

5. The models of Borino et al. and of Svedberg and Runesson comply with the postulate of maximum plastic dissipation (in a modified form for the entire body) and the dissipation is guaranteed to be nonnegative. An alternative formulation due to Nilsson, also motivated by thermodynamic considerations, is not really consistent. The evolution laws cannot be derived from a maximum dissipation postulate and, in some particular cases (e.g., in the presence of compressive stresses within the interaction distance from the plastic zone yielding under tension), the model can give negative dissipation.

6. Nonlocal extension of the postulate of maximum plastic dissipation leads to theoretically appealing models with a symmetric structure. These models require a double application of the nonlocal averaging operator, which complicates their numerical implementation. Also, at present there does not seem to be any model of this type that would act as a true localization limiter and at the same time could describe the complete failure process without any locking effects.

7. For nonlocal models formulated ad hoc, without any recourse to thermodynamics, it is not trivial to check their thermodynamic admissibility. For the basic nonlocal model, it is possible to prove that, if the free-energy potential is assumed in the same form as for the thermodynamically motivated model due to Borino et al., the dissipation is always nonnegative (but the evolution law for the softening variable is of course not associated).

8. If the nonlocal weight function is scaled in the proximity of boundaries, as is routinely done, the solution with a plastic region localized at the boundary usually dissipates much less energy than if the plastic region localizes inside the body. The boundary acts as a weak layer that attracts localization, because the solution that would actually occur is that with the steepest descent of the post-peak branch of the load-displacement diagram (Bažant and Cedolin 1991). Whether this is physically realistic depends on the actual structure of the material in the boundary layer. For the thermodynamically motivated models with double nonlocal averaging, the largest

plastic strain does not develop directly on the boundary but at a finite distance from it (for the Svedberg–Runesson model this is true if the nonlocal hardening modulus exceeds the magnitude of the local softening modulus by at least 25 %).

4.12 Choice of a nonlocal model

Based on the results for the gradient and integral-type nonlocal plasticity models, the Vermeer–Brinkgreve model and the ductile damage model are chosen for further development. For softening, these two models describe in an objective manner the initial bifurcation as well as the load-displacement response up to complete failure.

The analysis of the integral-type nonlocal formulation of these two models is extended to hardening and the two-dimensional plane strain setting. The main advantage compared to the implicit gradient approach is that the integral formulation does not need additional degrees of freedom, but uses standard finite elements. The disadvantage is that the stress-return algorithm is significantly more complex which makes the computation of the algorithmic tangent stiffness matrix practically impossible. The global iteration is performed with the elastic stiffness matrix, which is rather slow, but stable.

Chapter 5

Nonlocal models with hardening

5.1 Motivation

Until now, attention has been restricted to plasticity models with softening, but a realistic model should capture both hardening and softening. For local models, the hardening variable κ controls the evolution of the yield stress, and this variable grows during plastic deformation. The two regimes, hardening and softening, can be distinguished based on the current value of the hardening variable. For nonlocal models, the yield stress depends on both the local and the nonlocal hardening variable, which can in principle grow independently. Hardening and softening are respectively defined as the increase and decrease of the yield stress under homogeneous plastic deformation, for which $\kappa = \bar{\kappa}$.

For the two classes of models chosen for further development, the Vermeer–Brinkgreve model, Sec. 4.3, and the ductile damage models, Sec. 4.4, the extension to hardening and the complete bifurcation analysis is presented in this Chapter. The formal extension of the Vermeer–Brinkgreve model to hardening is straightforward (but the drawbacks will be detected in the bifurcation analysis). In the hardening law

$$\sigma_{\mathrm{Y}} = h_{\mathrm{NL}}(\kappa, \bar{\kappa}) = h(\hat{\kappa}) \tag{5.1}$$

the function h is replaced by a function that first increases (hardening) and later decreases (softening). The hardening law for ductile damage models written in the multiplicative format

$$\sigma_{\mathrm{Y}} = h_{\mathrm{NL}}(\kappa, \bar{\kappa}) = \sigma_0 h_1(\bar{\kappa}) h_2(\kappa) \tag{5.2}$$

naturally includes hardening and softening if the dimensionless functions $h_1 \geq 0$ and $h_2 \geq 0$ are chosen accordingly. Under uniform deformation, the yield stress increases for $h_1' h_2 + h_1 h_2' > 0$ and decreases for $h_1' h_2 + h_1 h_2' < 0$. The physical meaning of the stress parameter σ_0 depends on the specific choice of h_1 and h_2.

5.2 One-dimensional bifurcation analysis

The bifurcation analysis for a uniaxial tensile bar follows the same approach as in Chapters 3 and 4, but is limited to the rate problem at bifurcation from a uniform state. The analysis is performed for an infinite domain; cases where the boundary is separated from

the plastic region by more than the interaction radius R are automatically included, cf. Sec. 2.5. A solution of the rate problem is given by the distribution of the rate of the hardening variable, $\dot{\kappa}$, from which the other unknowns, i.e. $\dot{\bar{\kappa}}$, $\dot{\sigma}$, and $\dot{\varepsilon}$ can be computed.

In the plastic region I_p, $\dot{\kappa}$ can be solved from the consistency condition

$$H_\mathrm{NL}\dot{\bar{\kappa}} + H_\mathrm{L}\dot{\kappa} = \dot{\sigma} \tag{5.3}$$

with the nonlocal and local hardening moduli defined as

$$H_\mathrm{NL} = \frac{\partial h_\mathrm{NL}}{\partial \bar{\kappa}} \tag{5.4}$$

$$H_\mathrm{L} = \frac{\partial h_\mathrm{NL}}{\partial \kappa} \tag{5.5}$$

The solution is admissible if the loading-unloading conditions in the elastic region I_e, i.e. $\dot{\sigma} - H_\mathrm{NL}\dot{\bar{\kappa}} \leq 0$ and $\dot{\kappa} = 0$, are respected. The case $H_\mathrm{NL} + H_\mathrm{L} > 0$ corresponds to incremental hardening, and $H_\mathrm{NL} + H_\mathrm{L} < 0$ to incremental softening.

For the two classes of models, the analysis can be performed at once. For the Vermeer–Brinkgreve model, the nonlocal and local hardening moduli are

$$H_\mathrm{NL} = mH \tag{5.6}$$

$$H_\mathrm{L} = (1-m)H \tag{5.7}$$

with H defined as $H = \mathrm{d}h/\mathrm{d}\hat{\kappa}$. For the ductile damage models with the softening law written in the format (5.2), the moduli are

$$H_\mathrm{NL} = \sigma_0 h_1' h_2 \tag{5.8}$$

$$H_\mathrm{L} = \sigma_0 h_1 h_2' \tag{5.9}$$

The resulting equation for $\dot{\kappa}$ is identical if the parameters for the Vermeer–Brinkgreve model are chosen as

$$m = \frac{H_\mathrm{NL}}{H_\mathrm{NL} + H_\mathrm{L}} = \frac{h_1' h_2}{h_1' h_2 + h_1 h_2'} \tag{5.10}$$

$$H = H_\mathrm{NL} + H_\mathrm{L} = \sigma_0 \left(h_1' h_2 + h_1 h_2'\right) \tag{5.11}$$

In the following, the different bifurcation solutions are classified according to the signs of H_NL and H_L. For ductile damage models, the sign of h_1' is the same as the sign of H_NL and the sign of h_2' corresponds to the sign of H_L. The equivalent parameters of the Vermeer–Brinkgreve model are provided for each case.

In general, localization from a uniform state can take place only at nonpositive stress rate. In the part of the elastic region I_e that is separated from the plastic region by at least the interaction radius R, both $\dot{\kappa}$ and $\dot{\bar{\kappa}}$ are zero, and the loading-unloading conditions reduce to $\dot{\sigma} \leq 0$ (and $\dot{\kappa} = 0$). Since the stress and its rate are constant in the bar, the stress rate is nonpositive everywhere. This statement will be used repeatedly to demonstrate that no localized solution exists for specific cases.

For the case $H_{\mathrm{NL}} = 0$, the model is incrementally local. For hardening, $\dot{\kappa}$ is uniform, but for softening, irregular localized solutions are admissible. The subcase $H_{\mathrm{L}} > 0$ corresponds to a local model with hardening, which has only the regular homogeneous solution. For softening, i.e. $H_{\mathrm{L}} < 0$, the consistency condition in the plastic zone

$$H_{\mathrm{L}}\dot{\kappa} = \dot{\sigma} \tag{5.12}$$

admits the solution

$$\dot{\kappa} = \dot{\kappa}_0 \delta(x - x_0) \tag{5.13}$$

localized at an arbitrary position x_0 and described by a Dirac distribution, with an arbitrary constant $\dot{\kappa}_0$. The stress rate is negative and thus respects the loading-unloading conditions in the entire elastic region, where the rate of the yield stress $\dot{\sigma}_{\mathrm{Y}} = H_{\mathrm{NL}}\dot{\kappa}_0\alpha(x - x_0)$ is zero, because $H_{\mathrm{NL}} = 0$. Expressed in the parameters of the two models, this case covers $h_1' = 0$ and $m = 0$.

The case $H_{\mathrm{L}} = 0$ corresponds to the basic nonlocal model analyzed in Sec. 4.2 and covers $h_2' = 0$ and $m = 1$. For softening with $H_{\mathrm{NL}} < 0$, this case admits a solution with $\dot{\kappa}$ localized into a single cross section. This solution was classified as partially regular, because the global response of the model is regular. For hardening, i.e. $H_{\mathrm{NL}} > 0$, the rate of the yield stress is nonnegative everywhere,

$$\dot{\sigma}_{\mathrm{Y}} = H_{\mathrm{NL}}\bar{\dot{\kappa}} \geq 0 \tag{5.14}$$

and only the homogeneous solution exists.

The case $H_{\mathrm{L}} < 0$ always admits a localized solution with the plastic strain rate described by a Dirac distribution, Eq. (5.13), regardless of the sign of H_{NL}. This irregular solution respects the loading-unloading conditions, because in the plastic zone I_{p} (which is degenerated to a point), the rate of the yield stress is unbounded and negative

$$\dot{\sigma}_{\mathrm{Y}} = H_{\mathrm{L}}\dot{\kappa}_0\delta(0) < 0 \tag{5.15}$$

while it is bounded for the elastic zone I_{e}, where

$$\dot{\sigma}_{\mathrm{Y}} = H_{\mathrm{NL}}\dot{\kappa}_0\alpha(x - x_0) > H_{\mathrm{L}}\dot{\kappa}_0\delta(0) \tag{5.16}$$

If $H_{\mathrm{L}} < 0$ is combined with $H_{\mathrm{NL}} < 0$, this corresponds to $0 < m < 1$ and $H < 0$, and the solution has essentially the same properties as the basic nonlocal model, cf. Sec. 4.2 and Planas et al. (1996). If $H_{\mathrm{L}} < 0$ is combined with $H_{\mathrm{NL}} > 0$, and their sum is positive, i.e. $H_{\mathrm{L}} + H_{\mathrm{NL}} > 0$, the corresponding parameters of the Vermeer–Brinkgreve model are $m > 1$ and $H > 0$. This means that the proposed extension of the Vermeer–Brinkgreve model to hardening admits irregular solutions, see Fig. 5.1. For completeness, note that other localized solutions with a plastic region of nonzero size exist in this case. Finally, the case $H_{\mathrm{L}} < 0$, $H_{\mathrm{NL}} > 0$ and $H_{\mathrm{L}} + H_{\mathrm{NL}} < 0$ corresponds to $m < 0$ and $H < 0$ and admits the irregular localized solution.

The practically most important case is $H_{\mathrm{L}} > 0$, because $\dot{\kappa}$ is always regular in this case, both for hardening and softening. The proof that no localized solution exists for hardening is based on the fact that for any localized solution, a position x_0 with $\dot{\kappa} > \bar{\dot{\kappa}} > 0$ exists. The rate of the yield stress at this position x_0,

$$\dot{\sigma}_{\mathrm{Y}}(x_0) = H_{\mathrm{NL}}\bar{\dot{\kappa}}(x_0) + H_{\mathrm{L}}\dot{\kappa}(x_0) > (H_{\mathrm{NL}} + H_{\mathrm{L}})\,\bar{\dot{\kappa}}(x_0) > 0 \tag{5.17}$$

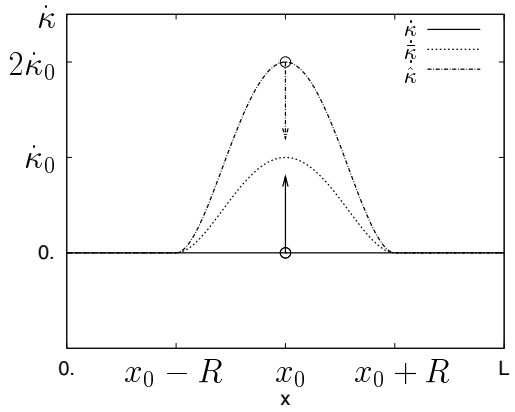

Figure 5.1: Plastic strain rate for a possible irregular solution of the Vermeer–Brinkgreve model with $m = 2$ during hardening.

would be positive. This is in contradiction with the result that the stress rate must be nonpositive for any localized solution, and it can be concluded that no localized solution exists. For hardening, the corresponding parameters of the Vermeer–Brinkgreve model are $m < 1$ and $H > 0$. The case of softening corresponds to $m > 1$ and $H < 0$, and it admits the typical regular solutions described in Sec. 4.3.

5.3 Consequences of the bifurcation analysis

In summary, a nonlocal plasticity model based on a nonlocal hardening law should satisfy

$$H_{\mathrm{L}} > 0 \tag{5.18}$$

for the rate of the hardening variable to be continuous, regardless of H_{NL}. The sign of the sum $H_{\mathrm{NL}} + H_{\mathrm{L}}$ determines whether the yield stress decreases or increases.

The straightforward extension of the Vermeer–Brinkgreve model cannot be used with a constant parameter m for hardening and softening. If $m > 1$, which is necessary to avoid irregular localization for softening, then the model admits localized solutions with decreasing yield stress for hardening. For $m < 1$, the solution is regular during hardening, but localizes into a set of zero measure during softening. The case $m = 1$ is regular during hardening, but only partially regular during softening. The overall response of the model is regular, but the plastic strain rate still localizes in a set of zero measure.

Models based on the ductile damage concept are a better choice for hardening and softening, if the function h_1 is chosen such that condition (5.18) is respected. This condition simply means $h_2'(\kappa) > 0$. Note that this restriction is sufficient for the one-dimensional case.

For hardening, i.e. $H_{\mathrm{NL}} + H_{\mathrm{L}} > 0$, the response is homogeneous, and for softening, i.e. $H_{\mathrm{NL}} + H_{\mathrm{L}} < 0$, *regular* localized solutions exist. The size of the localized plastic zone is controlled by $m = H_{\mathrm{NL}}/(H_{\mathrm{NL}} + H_{\mathrm{L}})$, so it depends only on the ratio of H_{L} and H_{NL}. Fig. 4.5a shows typical plastic strain profiles for different values of m. The profiles of κ and $\bar\kappa$ can be interpreted resp. as profiles of $\dot\kappa$ and $\dot{\bar\kappa}$ at bifurcation. The size of the plastic zone increases monotonically with m.

5.4 Bifurcation analysis under plane strain conditions

5.4.1 Plasticity model

For the purpose of the bifurcation analysis, the basic equations of the nonlocal extension of a standard local model are introduced, cf. Jirásek and Bažant (2002) for a detailed description of the standard local model. The general nonlocal plasticity model to be analyzed is based on the yield function

$$f(\boldsymbol{\sigma}, \kappa, \bar{\kappa}) = F(\boldsymbol{\sigma}) - h_{\mathrm{NL}}(\kappa, \bar{\kappa}) \tag{5.19}$$

where $\boldsymbol{\sigma}$ is the stress tensor, and $F(\boldsymbol{\sigma})$ is the equivalent stress. Material points for which the yield function is negative are elastic, while the yield function is zero for yielding points. The derivative of the yield function with respect to the stress is denoted as $\boldsymbol{f} = \partial f / \partial \boldsymbol{\sigma}$.

The flow rule

$$\dot{\boldsymbol{\varepsilon}}_{\mathrm{p}} = \dot{\lambda}\, \boldsymbol{g}(\boldsymbol{\sigma}) \tag{5.20}$$

prescribes the direction of plastic flow and depends on the current stress state through $\boldsymbol{g}$, and $\dot{\lambda}$ denotes the plastic multiplier. In many plasticity models, the flow direction is computed as the derivative of a scalar potential G with respect to $\boldsymbol{\sigma}$. For an associated flow rule, G is identified with f, which means that the yield function takes the role of the flow potential.

The yield stress h_{NL} depends on the hardening variable κ and its nonlocal average $\bar{\kappa}$. The evolution of κ is given by

$$\dot{\kappa} = \dot{\lambda}\, k(\boldsymbol{\sigma}) \tag{5.21}$$

where $k(\boldsymbol{\sigma})$ is a scalar factor which in general depends on the stress state. For certain models, e.g. the Drucker–Prager model studied in Chapter 6, $\boldsymbol{g}$ and k are constant.

The stress-strain relation is given by the elastic law

$$\boldsymbol{\sigma} = \boldsymbol{D} : (\boldsymbol{\varepsilon} - \boldsymbol{\varepsilon}_{\mathrm{p}}) \tag{5.22}$$

where : denotes the double-dot product. Compared to the elastic case, the strain is replaced by the difference of the strain and plastic strain, but the elastic stiffness tensor $\boldsymbol{D}$ remains unchanged.

Regarding the evolution equations for the internal variables $\boldsymbol{\varepsilon}_{\mathrm{p}}$ and κ, the loading-unloading conditions

$$\dot{\lambda} \geq 0, \quad f(\boldsymbol{\sigma}, \kappa, \bar{\kappa}) \leq 0, \quad \dot{\lambda}\, f(\boldsymbol{\sigma}, \kappa, \bar{\kappa}) = 0 \tag{5.23}$$

have to be respected. The last condition states that for a yielding material point, i.e. if $\dot{\lambda} > 0$, the yield function has to be zero, while for an elastic material point, it is negative. The special case $\dot{\lambda} = 0$ and $f(\boldsymbol{\sigma}, \kappa, \bar{\kappa}) = 0$ corresponds to neutral loading.

5.4.2 Analysis

The bifurcation analysis is performed for an infinite uniform domain under plane strain. The current (uniform) values of stress and strain are assumed to be known. Furthermore, the stress rates in the elastic part are prescribed as functions of one scalar unknown, so

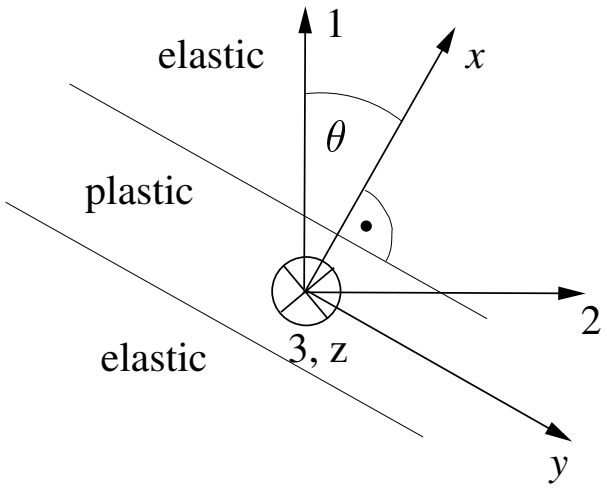

Figure 5.2: Localization plane.

their ratio, but not their value, is given. The principal unknowns are stress rate, strain rate, and plastic strain rate in the plastic region.

Under certain assumptions, possible bifurcations from the uniform solution in an infinite domain can be studied analytically. As depicted in Fig. 5.2, the localized solution in an infinite domain is assumed to have the form of a band inclined at an angle θ with respect to the horizontal axis. In the band, the deformation is plastic, and $\dot{\lambda} > 0$, while it is elastic outside, where $\dot{\lambda} = 0$. The axes of the global coordinate system are labeled 1, 2, and 3, the axes of the local system, which refers to the band, are labeled x, y, and z. The basic unknowns, i.e. the stress rate, strain rate and plastic strain rate, are assumed to be independent of the y- and z-coordinate.

To simplify the analysis, the special case of deformation under plane strain conditions is presented here, but the analysis could be extended to the general case. Under this assumption, the out-of-plane shear stress components τ_{xz} and τ_{yz} as well as the out-of-plane strain components ε_{xz}, ε_{yz}, and ε_z vanish. The tensorial components expressed with respect to a coordinate system are marked by two subscripts for the corresponding axis. For brevity, a double subscript is replaced by one, e.g. σ_{xx} is replaced by σ_x.

Since the localization problem is assumed to depend on the x-coordinate only, the unknown strain components ε_x, ε_y, and ε_{xy} as well as the unknown stress components σ_x, σ_y, σ_z, and τ_{xy} are functions of x only. Under these assumptions, the equilibrium equation $\mathrm{div}\boldsymbol{\sigma} = \mathbf{0}$ implies that σ_x and τ_{xy} are also independent of x

$$\sigma_x = \text{const.}, \qquad \tau_{xy} = \text{const.} \tag{5.24}$$

and thus constant in the entire domain. In the compatibility condition

$$2\,\frac{\partial^2 \varepsilon_{xy}}{\partial x \partial y} = \frac{\partial^2 \varepsilon_x}{\partial y^2} + \frac{\partial^2 \varepsilon_y}{\partial x^2} \tag{5.25}$$

the left-hand side as well as the first term on the right-hand side vanish, because all variables are independent of y. Under the assumption that ε_y remains bounded, Eq. (5.25) implies

$$\varepsilon_y = \text{const.} \tag{5.26}$$

in the entire domain.

In the elastic region, stress and strain are uniform. For a given stress state, the strain can be uniquely determined from the elastic law

$$\boldsymbol{\varepsilon}_{\mathrm{el}} = \boldsymbol{C} : \boldsymbol{\sigma} \tag{5.27}$$

where $\boldsymbol{C}$ is the elastic compliance tensor. Those components which are constant in the entire domain, i.e. σ_x, τ_{xy}, and ε_y, can be replaced by their values in the elastic region.

As in the one-dimensional case, the consistency condition for the plastic region

$$\dot{f}(\boldsymbol{\sigma}, \kappa, \bar{\kappa}) = \boldsymbol{f} : \dot{\boldsymbol{\sigma}} - H_{\mathrm{NL}} k \dot{\bar{\lambda}} - H_{\mathrm{L}} k \dot{\lambda} = 0 \tag{5.28}$$

provides an equation for the rate of the plastic multiplier $\dot{\lambda}$. The derivative $\boldsymbol{f} = \partial F / \partial \boldsymbol{\sigma}$ depends only on the given stress state. To write the consistency condition in the plastic region in terms of the stress state $\boldsymbol{\sigma}$ and the unknown plastic multiplier $\dot{\lambda}$, the stress rate needs to be expressed in terms of $\boldsymbol{\sigma}$ and $\dot{\lambda}$. Possible solutions have to be checked for admissibility, i.e. the loading-unloading conditions in the elastic region have to be respected.

Using Eq. (5.26), the strain rate $\dot{\varepsilon}_y$ in the plastic region can be identified with the strain rate in the elastic region

$$\dot{\varepsilon}_y = \dot{\varepsilon}_y^{\mathrm{E}} \tag{5.29}$$

Similarly, using Equations (5.24), two of the four unknown stress rates are equal to their values in the elastic region

$$\dot{\sigma}_x = \dot{\sigma}_x^{\mathrm{E}}, \quad \dot{\tau}_{xy} = \dot{\tau}_{xy}^{\mathrm{E}} \tag{5.30}$$

The remaining unknowns in the plastic region are the strain rates $\dot{\varepsilon}_x$ and $\dot{\varepsilon}_{xy}$, the stress rates $\dot{\sigma}_y$ and $\dot{\sigma}_z$, and the plastic multiplier $\dot{\lambda}$. These unknowns are functions of x only.

The flow rule, Eq. (5.20), relates the plastic strain rate to the given stress state. After inserting the flow rule into the stress-strain relation

$$\dot{\boldsymbol{\varepsilon}} = \boldsymbol{C} : \dot{\boldsymbol{\sigma}} + \dot{\lambda}\, \boldsymbol{g}(\boldsymbol{\sigma}) \tag{5.31}$$

the two scalar equations for $\dot{\varepsilon}_y$ and $\dot{\varepsilon}_z$ can be used to obtain the expressions

$$\dot{\sigma}_y(x) = \frac{\nu}{1-\nu}\, \dot{\sigma}_x^{\mathrm{E}} + \frac{E}{1-\nu^2}\, \dot{\varepsilon}_y^{\mathrm{E}} - \frac{E}{1-\nu^2}\, (g_y + \nu g_z)\, \dot{\lambda}(x) \tag{5.32}$$

$$\dot{\sigma}_z(x) = \frac{\nu}{1-\nu}\, \dot{\sigma}_x^{\mathrm{E}} + \frac{E}{1-\nu^2}\, \dot{\varepsilon}_y^{\mathrm{E}} - \frac{E}{1-\nu^2}\, (\nu g_y + g_z)\, \dot{\lambda}(x) \tag{5.33}$$

for the unknown stress rates in the plastic region. Here, g_y and g_z are components of $\boldsymbol{g}$ with respect to the local coordinate system.

Now, the consistency condition (5.28) can be written as

$$H_{\mathrm{NL}} k \dot{\bar{\lambda}}(x) + \left(\frac{F_\lambda}{k} + H_{\mathrm{L}} \right) k \dot{\lambda}(x) = \dot{f}^{\mathrm{E}} \tag{5.34}$$

with the abbreviations

$$F_\lambda = \frac{E}{1-\nu^2}\, (f_y g_y + f_z g_z + \nu f_y g_z + \nu f_z g_y) \tag{5.35}$$

$$\dot{f}^{\mathrm{E}} = \dot{\sigma}_x^{\mathrm{E}} \left[f_x + \frac{\nu}{1-\nu} \left(f_y + f_z \right) \right] + \frac{E}{1-\nu^2} \dot{\varepsilon}_y^{\mathrm{E}} \left(f_y + \nu f_z \right) + 2 f_{xy} \dot{\tau}_{xy}^{\mathrm{E}} \tag{5.36}$$

Eq. (5.34) is now written explicitly as a function of the known stress state, the prescribed stress rate, and the plastic multiplier only. For a given stress state, it provides a rate equation for the plastic multiplier $\dot{\lambda}$. For localized solutions, $\dot{f}^{\mathrm{E}} \leq 0$ must hold to satisfy the loading-unloading conditions in the elastic region. For $\dot{f}^{\mathrm{E}} > 0$, only the uniform solution is valid.

5.4.3 Discussion

First, the consistency condition and the loading-unloading conditions written at the elasto-plastic boundary are used to distinguish cases with irregular solutions from those which only admit regular solutions. For any given position x_{pl} in I_{p}, the consistency condition

$$\dot{f}^{\mathrm{E}} - H_{\mathrm{NL}} k \bar{\dot{\lambda}}(x_{\mathrm{pl}}) = \left(\frac{F_\lambda}{k} + H_{\mathrm{L}} \right) k \dot{\lambda}(x_{\mathrm{pl}}) \tag{5.37}$$

must hold. In the elastic region, inserting $\dot{\lambda} = 0$ into the loading-unloading condition $\dot{f} \leq 0$ implies

$$\dot{f}^{\mathrm{E}} - H_{\mathrm{NL}} k \bar{\dot{\lambda}}(x_{\mathrm{el}}) \leq 0 \tag{5.38}$$

for an arbitrary position x_{el}. The nonlocal average of the plastic multiplier is continuous, if common weight functions are used. For two positions x_{el} and x_{pl} right next to the elasto-plastic boundary, with x_{el} in the elastic and x_{pl} in the plastic region, this means $\bar{\dot{\lambda}}(x_{\mathrm{el}}) = \bar{\dot{\lambda}}(x_{\mathrm{pl}})$. From Eqs. (5.37) and (5.38), it then follows that

$$\left(\frac{F_\lambda}{k} + H_{\mathrm{L}} \right) \dot{\lambda}(x_{\mathrm{pl}}) \leq 0 \tag{5.39}$$

with $\dot{\lambda}(x_{\mathrm{pl}}) \geq 0$. Note that this condition is also valid for local models with $H_{\mathrm{NL}} = 0$, because the terms containing $\bar{\dot{\lambda}}$ vanish in this case.

Condition (5.39) has two important implications regarding the regularity of possible solutions. First, if

$$H_{\mathrm{L}} \leq -\frac{F_\lambda}{k} \tag{5.40}$$

holds, then $\dot{\lambda}(x_{\mathrm{pl}})$ may take nonzero values at the elasto-plastic boundary. This corresponds to a discontinuity in the plastic strain rate, which implies a discontinuity in the strain rate. The critical value of the local hardening modulus, $H^{\mathrm{crit}} = -F_\lambda / k$, can be expressed as

$$H^{\mathrm{crit}} = \frac{-E}{k(1-\nu^2)} \left(a \cos^4 \theta + b \cos^2 \theta + c \right) \tag{5.41}$$

where

$$a = (f_2 - f_1)(g_2 - g_1) \tag{5.42}$$

$$b = f_1 g_2 + f_2 g_1 - 2 f_1 g_1 + \nu (f_2 - f_1) g_3 + \nu f_3 (g_2 - g_1) \tag{5.43}$$

$$c = f_1 g_1 + f_3 g_3 + \nu (f_1 g_3 + f_3 g_1) \tag{5.44}$$

and f_i and g_i, $i = 1, 2, 3$, denote the components of $\boldsymbol{f}$ and $\boldsymbol{g}$ with respect to the global coordinate system. For the local plasticity model, this condition was obtained by bifurcation analysis under the assumption of a discontinuous solution (Rudnicky and Rice 1975; Ottosen and Runesson 1991; Runesson et al. 1991).

Second, discontinuous solutions can be excluded for a given stress state if

$$H_{\mathrm{L}} > H^{\mathrm{crit}} \tag{5.45}$$

where H^{crit} is the critical value of the hardening modulus for this stress state. If Eq. (5.45) holds, then $\dot{\lambda}(x_{\mathrm{pl}})$ must vanish at the boundary to fulfill condition (5.39), and consequently, $\dot{\lambda}$ is continuous. Since the value of the critical hardening modulus depends on the stress state, it is useful to evaluate, for a given plasticity model, the maximum of the critical hardening modulus over all stress states, denoted by $H^{\mathrm{crit}}_{\mathrm{max}}$. If the local hardening modulus is chosen such that the condition

$$H_{\mathrm{L}} > H^{\mathrm{crit}}_{\mathrm{max}} \tag{5.46}$$

holds, then no discontinuous solutions exist, regardless of the stress state. In the one-dimensional setting, this corresponds to the condition $H_{\mathrm{L}} > 0$. For a local model, only the uniform solution is admissible in this case.

For the Vermeer–Brinkgreve model, condition (5.45) restricts the choice of m even for softening. The local hardening modulus, $H_{\mathrm{L}} = (1 - m)H$, is positive for softening ($H < 0$ and $m > 1$), but it is larger than H^{crit} only for

$$m > \frac{H - H^{\mathrm{crit}}}{H} \tag{5.47}$$

Parameter m should be chosen accordingly for a two-dimensional simulation with the Vermeer–Brinkgreve model.

For a nonlocal plasticity model, *regular* localized solutions may exist for $H_{\mathrm{L}} > H^{\mathrm{crit}}$. Based on the results for the one-dimensional case, it follows that the rate equation (5.34) has such solutions if

$$H_{\mathrm{L}} + H_{\mathrm{NL}} < H^{\mathrm{crit}} \tag{5.48}$$

After the detailed description of the Drucker–Prager model and the nonlocal stress return algorithm in Chapter 6, examples demonstrating the capability of the nonlocal model to regularize localization in a two-dimensional setting will be presented in Chapter 7.

5.5 A convenient hardening law

The choice of a nonlocal hardening law should be based on the hardening law obtained under homogeneous plastic deformation. Experimentally, it is difficult to satisfy this condition. As an estimate, the results of tests with sufficiently small specimens can be taken, even though boundary effects may alter the response.

A nonlocal hardening law should respect

$$h_{\mathrm{NL}}(\kappa, \bar{\kappa} = \kappa) = \sigma_0 h_{\mathrm{hom}}(\kappa) \tag{5.49}$$

for a given homogeneous hardening law $\sigma_{\mathrm{Y}} = \sigma_0 h_{\mathrm{hom}}(\kappa)$. Here, σ_0 is introduced to make h_{hom} dimensionless. Even if the homogeneous hardening law is known, Eq. (5.49) does not uniquely define the nonlocal law.

The choice of a nonlocal hardening law should be simple and in accordance with the imposed restrictions. The simplest choice for h_2 is the linear function

$$h_2(\kappa) = 1 + H_2\kappa \tag{5.50}$$

with the (dimensionless) local hardening modulus H_2. This corresponds to the choice of the local hardening function in the ductile damage model of Geers et al. (2001). In the one-dimensional setting, it is sufficient to choose $H_2 > 0$ to satisfy condition (5.18). Under plane strain, the additional condition (5.46) written as

$$H_{\mathrm{L}} = \sigma_0 h_1(\bar{\kappa}) H_2 > H_{\max}^{\mathrm{crit}} \tag{5.51}$$

prohibits irregular solutions of the plastic strain rate regardless of the stress state (under the assumptions made for the analysis in Sec. 5.4.2).

A convenient choice of the nonlocal function h_1 is

$$h_1(\bar{\kappa}) = \frac{h_{\mathrm{hom}}(\bar{\kappa})}{h_2(\bar{\kappa})} \tag{5.52}$$

because for any given homogeneous hardening law h_{hom}, the nonlocal hardening law satisfies Eq. (5.49) automatically. No further restrictions on h_{hom} follow from the bifurcation analysis.

An additional condition may be used to guarantee that the nonlocal part of the model is always active. The model is incrementally local for $H_{\mathrm{NL}} = 0$, which can be excluded if h_2 is chosen such that

$$H_{\mathrm{NL}} < 0 \tag{5.53}$$

in the whole range of $\bar{\kappa}$. For softening, H_{NL} must be negative, so if H_{NL} is initially positive, it would be zero at some point of the deformation process, leading to an incrementally local model. Note that this condition is not necessary, because despite the incrementally local character, discontinuous solutions have already been excluded by respecting condition (5.46).

Inserting the expression for H_{NL}, Eq. (5.8), into condition (5.53), this condition can be written as

$$h'_{\mathrm{hom}}(1 + H_2\bar{\kappa}) - h_{\mathrm{hom}} H_2 < 0 \tag{5.54}$$

in terms of the given homogeneous hardening law and H_2 and requires that parameter H_2 be sufficiently large. Often, condition (5.54) is stricter than condition (5.46). A first estimate for H_2 can be obtained from a test at $\kappa = \bar{\kappa} = 0$. At this initial state, condition (5.54) simplifies to $H_2 > h'_{\mathrm{hom}}(0)/h_{\mathrm{hom}}(0)$. Nevertheless, it should be checked that condition (5.54) holds for all values of $\kappa = \bar{\kappa}$.

5.6 Uniaxial tensile test

To explore basic properties of this choice for the hardening law, a one-dimensional tensile test is performed for different values of H_2. The homogeneous hardening law

$$\sigma_0 h_{\mathrm{hom}}(\kappa) = \begin{cases} \sigma_{\mathrm{i}} + (\sigma_0 - \sigma_{\mathrm{i}}) \left[\left(\dfrac{\kappa}{\kappa_{\mathrm{peak}}} \right)^3 - 3 \left(\dfrac{\kappa}{\kappa_{\mathrm{peak}}} \right)^2 + 3 \dfrac{\kappa}{\kappa_{\mathrm{peak}}} \right] & \text{if} \quad 0 \le \kappa \le \kappa_{\mathrm{peak}} \\ \sigma_0 \exp\left(- \dfrac{\kappa - \kappa_{\mathrm{peak}}}{\kappa_{\mathrm{c}}} \right) & \text{if} \quad \kappa \ge \kappa_{\mathrm{peak}} \end{cases} \tag{5.55}$$

with a polynomial function for the pre-peak hardening, and an exponential function for post-peak softening is chosen as a test case. Here, $\sigma_{\mathrm{i}} < \sigma_0$ is the initial yield stress, σ_0 is the maximum yield stress, and κ_{peak} is the value of κ at the peak value of the yield stress, i.e. $\sigma_0 h_{\mathrm{hom}}(\kappa_{\mathrm{peak}}) = \sigma_0$.

The model parameters are chosen as $E = 25\,\mathrm{GPa}$, $\sigma_0 = 2.8\,\mathrm{MPa}$, $\sigma_{\mathrm{i}} = 0.5\,\sigma_0$, $\kappa_{\mathrm{peak}} = 3 \times 10^{-5}$, and $\kappa_{\mathrm{c}} = 9 \times 10^{-4}$, which are close to those realistic for concrete under uniaxial tension. The length of the bar is $L = 100\,\mathrm{mm}$, and the interaction radius of the bell function is set to $R = 10\,\mathrm{mm}$.

To comply with condition (5.54), it is sufficient to choose H_2 larger than

$$H_2^{\min} = \frac{3}{\kappa_{\mathrm{peak}}} \left(\frac{\sigma_0}{\sigma_{\mathrm{i}}} - 1 \right) = 10^5 \tag{5.56}$$

which ensures a negative slope of h_1 for all values of $\bar{\kappa}$. To detect the influence of H_2 on the response, the uniaxial tensile test is computed for the three values $H_2 = 2H_2^{\min}$, $4H_2^{\min}$, and $8H_2^{\min}$.

The normalized load-displacement diagram, see Fig. 5.3, shows the stress normalized by σ_0 as a function of the displacement normalized with the bar length L. The evolution of the size of the plastic zone (normalized with R) is shown in Fig. 5.4a as a function of the stress normalized with σ_0. The shape of a typical plastic strain profile, normalized with the plastic strain at peak load, is depicted in Fig. 5.4b.

The results show that H_2 has a negligible influence on the load-displacement response, the evolution of the plastic zone and the plastic strain profile. A partial explanation for this somewhat surprising result is that the initial size of the plastic zone L_{p}, controlled by $m = H_{\mathrm{L}}/(H_{\mathrm{L}} + H_{\mathrm{NL}})$, is similar for the three cases. For $H_2 = 2H_2^{\min}$, the initial size is $L_{\mathrm{p}} = 8.24R$, for $H_2 = 4H_2^{\min}$, $L_{\mathrm{p}} = 8.56R$, and for $H_2 = 8H_2^{\min}$, $L_{\mathrm{p}} = 8.72R$.

The length of the plastic zone reduces during the loading process and is approximately R in the late stages of the deformation process. Finite element meshes should be chosen accordingly.

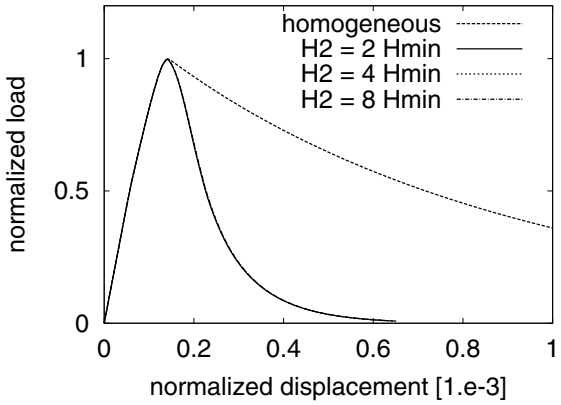

Figure 5.3: Load-displacement diagram for three values of H_2 and the homogeneous response for comparison.

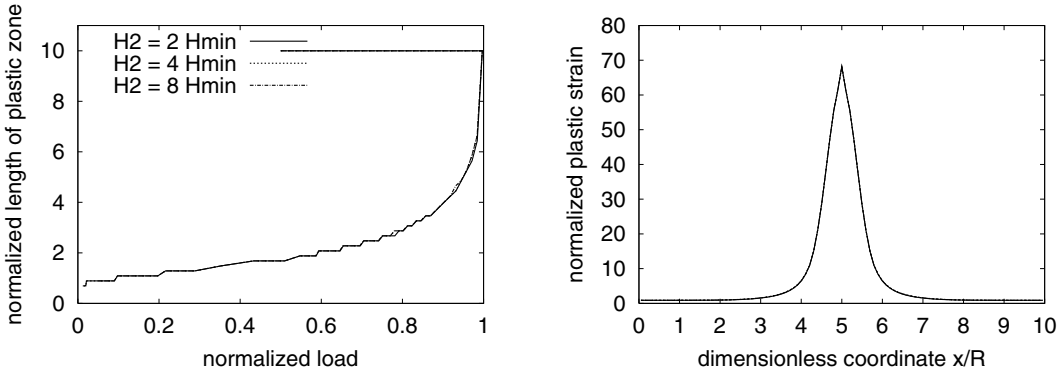

(a) (b)

Figure 5.4: Nonlocal model with hardening and softening: (a) Evolution of the size of the plastic zone, (b) Hardening variable κ at one third of peak load in the post-peak regime, for three values of H_2.

Chapter 6

Stress return for nonlocal plasticity

6.1 Motivation

The standard local stress return algorithm cannot be used for nonlocal plasticity models with the nonlocal hardening variable $\bar{\kappa}$ in the yield function. The yield function at one Gauss point depends on the value of the hardening variable at all other Gauss points, which causes coupling of the complementarity problem. From the previous analysis in the one-dimensional setting, two integral-type nonlocal models have been identified as suitable candidates for a regularized plasticity model: the Vermeer–Brinkgreve model and the ductile damage model. Common to both classes is a hardening law which depends on the local and nonlocal hardening variable, $\sigma_{\mathrm{Y}} = h_{\mathrm{NL}}(\kappa, \bar{\kappa})$.

In this chapter, a special nonlocal stress return algorithm is first developed in a rigorous way for the example of the Drucker–Prager plasticity model with linear softening regularized by the Vermeer–Brinkgreve approach, under the assumption that the trial stress state does not fall within the vertex region. Based on a physical interpretation of the resulting equations, a simple extension to nonlinear hardening, the vertex case and to more complex plasticity models is proposed.

6.2 Local Drucker–Prager plasticity model

6.2.1 Model equations

A simple plasticity model that takes into account the cohesive-frictional behavior of concrete can be based on the yield function

$$f\left(\boldsymbol{\sigma}, \tau_{\mathrm{Y}}\right) = F\left(\boldsymbol{\sigma}\right) - \tau_{\mathrm{Y}} \tag{6.1}$$

with the pressure-dependent equivalent stress

$$F\left(\boldsymbol{\sigma}\right) = c_{\phi} I_1 + \sqrt{J_2} \tag{6.2}$$

This special case of the Burzyński (1929) yield function was later made popular by Drucker and Prager (1952). The stress tensor is denoted by $\boldsymbol{\sigma}$, τ_{Y} is the yield stress under pure

shear, and I_1 and J_2 are the first invariant and second deviatoric invariant of the stress tensor. The friction coefficient c_ϕ is a positive parameter that controls the influence of the pressure $p = I_1/3$ on the yield limit, important for cohesive-frictional materials such as concrete, soils, or other geomaterials.

The non-associated flow rule is derived from the plastic potential

$$g\left(\boldsymbol{\sigma}\right) = c_\psi I_1 + \sqrt{J_2} \tag{6.3}$$

where c_ψ is the dilatancy coefficient. For concrete, an associated model with $c_\phi = c_\psi$ would overestimate the dilatancy, so the dilatancy coefficient is usually chosen smaller than the friction coefficient. For $c_\phi = c_\psi = 0$, the yield criterion and flow rule of the associated J_2-plasticity model are recovered as a special case.

In summary, the local small-strain plasticity model is described by the equations

$$\boldsymbol{\sigma} = \boldsymbol{D} : (\boldsymbol{\varepsilon} - \boldsymbol{\varepsilon}_\mathrm{p}) \tag{6.4}$$

$$\tau_\mathrm{Y} = h(\kappa) \tag{6.5}$$

$$\dot{\boldsymbol{\varepsilon}}_\mathrm{p} = \dot{\lambda}\frac{\partial g}{\partial \boldsymbol{\sigma}} = \dot{\lambda}\left(c_\psi \boldsymbol{\delta} + \frac{\boldsymbol{s}}{2\sqrt{J_2}}\right) \tag{6.6}$$

$$\dot{\kappa} = \sqrt{\tfrac{2}{3}}\,\|\dot{\boldsymbol{\varepsilon}}_\mathrm{p}\| \tag{6.7}$$

$$\dot{\lambda} \geq 0, \qquad f\left(\boldsymbol{\sigma}, \tau_\mathrm{Y}\right) \leq 0, \qquad \dot{\lambda}\, f\left(\boldsymbol{\sigma}, \tau_\mathrm{Y}\right) = 0 \tag{6.8}$$

which represent the linear elastic law, hardening law (linear or nonlinear), evolution laws for plastic strain and hardening variable, and the loading-unloading conditions. Note that the hardening law has a different meaning than in the preceding chapters, where $\tau_\mathrm{Y} = \tau_0 + h(\kappa)$ was used. In the above, $\boldsymbol{D}$ is the elastic stiffness tensor, $\boldsymbol{\varepsilon}$ is the strain tensor, $\boldsymbol{\varepsilon}_\mathrm{p}$ is the plastic strain tensor, $\dot{\lambda}$ is the rate of the plastic multiplier, $\boldsymbol{\delta}$ is the unit second-order tensor, $\boldsymbol{s}$ is the deviatoric stress tensor, κ is the hardening variable, Eq. (6.5) is the hardening law, and a superior dot marks the derivative with respect to time. The terms hardening variable and hardening law will be used in the general sense if both hardening and softening are included.

The flow rule has the form given in Eq. (6.6) at all points of the conical yield surface with the exception of its vertex, located on the hydrostatic axis. The special case of the stress return for trial stress states that fall within the vertex region will be handled separately.

For the Drucker–Prager model, the rate of the hardening variable is proportional to the rate of the plastic multiplier. Substituting the flow rule (6.6) into the evolution law for the hardening variable, Eq. (6.7), and computing the norm leads to

$$\dot{\kappa} = k\dot{\lambda} \tag{6.9}$$

with a constant parameter $k = \sqrt{1/3 + 2c_\psi^2}$.

6.2.2 Stress return algorithm for the regular case

Incremental finite element analysis requires the implementation of a procedure for the evaluation of the stress and plastic strain increments that correspond to a given increment of strain. In the local case, the algorithmic form of the elastic law and the hardening law

$$\boldsymbol{\sigma}_{(n+1)} = \boldsymbol{\sigma}_{(n)} + \boldsymbol{D} : (\Delta\boldsymbol{\varepsilon} - \Delta\boldsymbol{\varepsilon}_{\mathrm{p}}) \tag{6.10}$$

$$\tau_{\mathrm{Y}\,(n+1)} = h\left(\kappa_{(n)} + \Delta\kappa\right) \tag{6.11}$$

are simply obtained from Equations (6.4) and (6.5) if the values at the end of the step, denoted by subscript $n+1$, are expressed as the sum of the value at the end of the previous step, denoted by subscript n, and the increment, denoted by Δ. Using a backward Euler scheme for the time discretization of the flow rule, the increment of plastic strain is obtained from

$$\Delta\boldsymbol{\varepsilon}_{\mathrm{p}} = \Delta\lambda\, \boldsymbol{g}\left(\boldsymbol{\sigma}_{(n+1)}\right) \tag{6.12}$$

which is the algorithmic form of Eq. (6.6). This algorithmic form is valid for regular cases, i.e. for cases in which the stress $\boldsymbol{\sigma}_{(n+1)}$ does not lie on the hydrostatic axis. The so-called vertex case is described separately in Sec. 6.2.3. Under this assumption, the algorithmic form of the evolution law for the hardening variable

$$\Delta\kappa = k\Delta\lambda \tag{6.13}$$

is obtained from Eq. (6.9).

Since the flow rule is associated in the deviatoric plane, the yield function at the end of the step can be written as a function of the unknown increment of the plastic multiplier $\Delta\lambda$ only. The deviatoric stress at the end of the step $\boldsymbol{s}_{(n+1)}$ is a scalar multiple of the deviatoric 'trial' stress $\boldsymbol{s}_{\mathrm{trial}}$ computed from the trial stress state $\boldsymbol{\sigma}_{\mathrm{trial}} = \boldsymbol{\sigma}_{(n)} + \boldsymbol{D} : \Delta\boldsymbol{\varepsilon}$. This simplifies the expression for the flow direction at the end of the step,

$$\begin{aligned}
\boldsymbol{g}\left(\boldsymbol{\sigma}_{(n+1)}\right) &= c_\psi\boldsymbol{\delta} + \frac{\boldsymbol{s}_{(n+1)}}{2\sqrt{J_2(\boldsymbol{s}_{(n+1)})}} \\
&= c_\psi\boldsymbol{\delta} + \frac{\boldsymbol{s}_{\mathrm{trial}}}{2\sqrt{J_2\left(\boldsymbol{s}_{\mathrm{trial}}\right)}} \\
&= \boldsymbol{g}\left(\boldsymbol{\sigma}_{\mathrm{trial}}\right) = \boldsymbol{g}_{\mathrm{trial}}
\end{aligned} \tag{6.14}$$

which can be directly evaluated from the trial stress state. The value of the yield function at the end of the step,

$$\begin{aligned}
f\left(\boldsymbol{\sigma}_{(n+1)}, \tau_{\mathrm{Y}\,(n+1)}\right) &= F\left(\boldsymbol{\sigma}_{(n+1)}\right) - \tau_{\mathrm{Y}\,(n+1)} \\
&= F\left(\boldsymbol{\sigma}_{\mathrm{trial}} - \Delta\lambda\, \boldsymbol{D} : \boldsymbol{g}_{\mathrm{trial}}\right) - h\left(\kappa_{(n)} + k\Delta\lambda\right) \\
&= f_{(n+1)}(\Delta\lambda)
\end{aligned} \tag{6.15}$$

can now be written as a function of $\Delta\lambda$ only, because all other variables are known at the beginning of the step. The subscript at the yield function $f_{(n+1)}$ indicates the dependency of the function on the internal variables and the strain increment.

The numerical solution must satisfy the algorithmic form of the loading-unloading conditions

$$\Delta\lambda \geq 0, \quad f_{(n+1)}(\Delta\lambda) \leq 0, \quad \Delta\lambda\, f_{(n+1)}(\Delta\lambda) = 0 \tag{6.16}$$

This is in general a nonlinear complementarity problem (NLCP) for the unknown plastic multiplier $\Delta\lambda$. In the elastic region, characterized by $\Delta\lambda = 0$, the stress state must lie inside the elastic domain at the end of the step, i.e. $f_{(n+1)} < 0$. In the plastic region, characterized by $\Delta\lambda > 0$, the yield condition $f_{(n+1)} = 0$ must be fulfilled at the end of the step. For local plasticity models, the NLCP can be solved at each Gauss point independently using the conventional stress return algorithms, i.e. the NLCP is uncoupled.

For the Drucker–Prager model with a linear hardening law according to Eq. (2.36) and under the assumption that $\tau_0 + H\kappa_{(n+1)} > 0$, the value of the yield function at the end of the step, $f_{(n+1)}$, depends on the increment of the plastic multiplier $\Delta\lambda$ in a linear way, and Eq. (6.16) becomes a linear complementarity problem (LCP). Evaluating the equivalent stress that appears in the definition (6.15) of the yield function $f_{(n+1)}$ using Equations (6.2) and (6.14), the linear expression

$$\begin{aligned} F\left(\boldsymbol{\sigma}_{\text{trial}} - \Delta\lambda\, \boldsymbol{D} : \boldsymbol{g}_{\text{trial}}\right) &= F_{\text{trial}} - (9c_\phi c_\psi K + G)\Delta\lambda \\ &= F_{(n+1)}(\Delta\lambda) \end{aligned} \tag{6.17}$$

is obtained for sufficiently small increments $\Delta\lambda < \sqrt{J_2^{\text{trial}}}/G$. For larger increments, the stress state at the end of the step has a different Lode angle than the trial stress. In Eq. (6.17), $F_{\text{trial}} = F(\boldsymbol{\sigma}_{\text{trial}})$, K is the bulk modulus of elasticity, and G is the shear modulus. If the hardening function $h(\kappa)$ is linear as well, then the yield function can be expressed as

$$\begin{aligned} f_{(n+1)}(\Delta\lambda) &= F_{\text{trial}} - (9c_\phi c_\psi K + G)\Delta\lambda - \tau_0 - H\left(\kappa_{(n)} + k\Delta\lambda\right) \\ &= f_{\text{trial}} - (9c_\phi c_\psi K + G + Hk)\Delta\lambda \end{aligned} \tag{6.18}$$

where $f_{\text{trial}} = f\left(\boldsymbol{\sigma}_{\text{trial}}, \tau_{\text{Y}}(\kappa_{(n)})\right)$ is the trial value of the yield function, and this expression for $f_{(n+1)}$ is indeed linear in $\Delta\lambda$.

6.2.3 Stress return algorithm for the vertex case

The foregoing stress return algorithm is valid for trial stress states that do not fall within the vertex region. The vertex region is the part of the trial stress space for which a return to the yield surface respecting the regular algorithmic flow rule, Eq. (6.12), is impossible. In this case, a special vertex return must be used, where the stress state at the end of the step, $\boldsymbol{\sigma}_{(n+1)}$, lies on the vertex.

The two regions can be distinguished based on the fact that regular plastic flow is bounded. Indeed, for regular plastic flow, the increment of the plastic multiplier $\Delta\lambda$ may not exceed

$$\Delta\lambda_{\max} = \frac{\sqrt{J_2^{\text{trial}}}}{G} \tag{6.19}$$

for which $J_2\left(\boldsymbol{s}_{(n+1)}\right) = 0$. The trial stress state lies within the vertex region, if the yield function evaluated for the maximum value of regular plastic flow is positive, i.e.

$$f_{(n+1)}\left(\Delta\lambda_{\max}\right) > 0 \tag{6.20}$$

In the vertex case, the stress state at the end of the step lies on the hydrostatic axis, i.e. the deviatoric stress vanishes, $\boldsymbol{s}_{(n+1)} = \boldsymbol{0}$. The equivalent stress then depends only on the value of the first invariant at the end of the step, $I_{(n+1)}$, and the yield function at the end of the step can be written as

$$f\left(\boldsymbol{\sigma}, \tau_{\mathrm{Y}\,(n+1)}\right) = c_\phi \left(I_1^{\mathrm{trial}} + \Delta I_1\right) - h\left(\kappa_{(n)} + \Delta\kappa\right) \tag{6.21}$$

where $I_1^{\mathrm{trial}} = I_1(\boldsymbol{\sigma}_{\mathrm{trial}})$.

The simplification $\dot{\kappa} = k\dot{\lambda}$, Eq. (6.9), cannot be used in the vertex case, because the flow rule, Eq. (6.6), is not valid at the vertex. Instead, the evolution of the hardening variable is computed from the original evolution law, Eq. (6.7). Using the elastic law, the increment of the hardening variable is evaluated as

$$\begin{aligned} \Delta\kappa &= \sqrt{\tfrac{2}{3}}\,||\Delta\boldsymbol{\varepsilon}_{\mathrm{p}}|| \\ &= \sqrt{2(\Delta\varepsilon_{\mathrm{p}}^{\mathrm{v}})^2 + \tfrac{4}{3}J_2(\Delta\boldsymbol{e}_{\mathrm{p}})} \\ &= \sqrt{2\left(\frac{\Delta I_1}{9K}\right)^2 + \frac{J_2(\boldsymbol{s}^{\mathrm{trial}})}{3G^2}} \end{aligned} \tag{6.22}$$

where $\Delta\varepsilon_{\mathrm{p}}^{\mathrm{v}} = 1/3 I_1(\boldsymbol{\varepsilon}_{\mathrm{p}})$ is the volumetric plastic strain and $\Delta\boldsymbol{e}_{\mathrm{p}}$ is the deviatoric plastic strain. The increment of the hardening variable depends only on the known deviatoric trial stress and the volumetric stress increment.

Inserting the incremental evolution law for the hardening variable, Eq. (6.22), into the expression for the yield function at the end of the step, Eq. (6.21), a nonlinear function of the unknown ΔI_1 is obtained. The loading-unloading conditions are now expressed in terms of the increment of the hardening variable, $\Delta\kappa$ as

$$\Delta\kappa \geq 0, \quad f_{(n+1)}\left(\Delta\kappa\right) \leq 0, \quad \Delta\kappa\, f_{(n+1)}\left(\Delta\kappa\right) = 0 \tag{6.23}$$

Note that the plastic multiplier disappears from the stress return algorithm for the vertex case.

6.3 Nonlocal extension of the Drucker–Prager model

The nonlocal Drucker–Prager model is based on the nonlocal hardening law

$$\tau_{\mathrm{Y}} = h_{\mathrm{NL}}\left(\kappa, \bar{\kappa}\right) \tag{6.24}$$

where the yield stress depends in a suitable way on both the local hardening variable κ and its nonlocal counterpart $\bar{\kappa}$. This general form of the nonlocal hardening law includes both the model of Vermeer and Brinkgreve (1994) and the ductile damage model (Geers et al. 2001; Leblond et al. 1994). All other equations of the local model, including the loading-unloading conditions in the local format, remain the same.

The stress return algorithm is first developed for the nonlocal formulation of Vermeer and Brinkgreve (1994) and softening only. This formulation evaluates the yield stress from a linear combination of the local and nonlocal softening variable

$$\hat{\kappa}\left(\kappa, \bar{\kappa}\right) = m\bar{\kappa} + (1-m)\kappa \tag{6.25}$$

substituted into the softening law, which now reads

$$\tau_{\mathrm{Y}} = h_{\mathrm{NL}}\left(\kappa, \bar{\kappa}\right) = h(\hat{\kappa}(\kappa, \bar{\kappa})) \tag{6.26}$$

cf. Sec. 4.3 for a detailed analysis of this model in the one-dimensional setting.

Afterwards, the extension to the ductile damage model is presented. For this model, the hardening law

$$\tau_{\mathrm{Y}} = h_{\mathrm{NL}}(\kappa, \bar{\kappa}) = \tau_0 h_1(\bar{\kappa}) h_2(\kappa) \tag{6.27}$$

depends in a multiplicative fashion on two functions h_1 and h_2 (in the present format, they are dimensionless). The first function depends solely on the nonlocal hardening variable $\bar{\kappa}$, the second on the local hardening variable κ. The physical meaning of τ_0 depends on the particular form of these functions.

6.4 Stress return for the Vermeer–Brinkgreve model

For the nonlocal extension due to Vermeer & Brinkgreve, the algorithmic form of the softening law is

$$\tau_{\mathrm{Y}\,(n+1)} = h\left(\hat{\kappa}_{(n)} + \Delta\hat{\kappa}\right) \tag{6.28}$$

and the nonlocal softening variable $\Delta\bar{\kappa}$ in the expression for $\Delta\hat{\kappa} = m\Delta\bar{\kappa} + (1-m)\Delta\kappa$ leads to coupling of the CP. Indeed, the yield stress at one Gauss point now depends on the softening variable at the Gauss points in the neighborhood.

To develop the stress return algorithm for the nonlocal model, column matrices that collect the values of a quantity at all Gauss points of the structure are introduced. They are represented by bold face symbols, e.g. $\Delta\boldsymbol{\kappa}$ is a column matrix carrying the values of $\Delta\kappa$ of all Gauss points, and $\Delta\bar{\boldsymbol{\kappa}}$, $\Delta\hat{\boldsymbol{\kappa}}$, $\boldsymbol{h}_{\mathrm{NL}}$, $\boldsymbol{f}_{(n+1)}$, $\boldsymbol{f}_{\mathrm{trial}}$, $\boldsymbol{F}_{\mathrm{trial}}$ are defined in a similar fashion. The nonlocal averaging operator in Eq. (2.13) is discretized and represented by the square matrix $\boldsymbol{A}$, so the increment of the nonlocal softening variable is given by $\Delta\bar{\boldsymbol{\kappa}} = \boldsymbol{A}\,\Delta\boldsymbol{\kappa}$.

Because the increment of the softening variable, $\Delta\kappa$, is proportional to the increment of the plastic multiplier $\Delta\lambda$, Eq. (6.13), $\Delta\lambda$ can be replaced by $\Delta\kappa$ in the algorithmic form of the loading-unloading conditions

$$\Delta\boldsymbol{\kappa} \geq \boldsymbol{0}, \quad \boldsymbol{f}_{(n+1)}\left(\Delta\boldsymbol{\kappa}\right) \leq \boldsymbol{0}, \quad \Delta\boldsymbol{\kappa}^{\mathrm{T}}\boldsymbol{f}_{(n+1)}\left(\Delta\boldsymbol{\kappa}\right) = 0 \tag{6.29}$$

now written in a compact form for the whole body. Here, the operators $\leq$ and $\geq$ have to be interpreted for each component of the corresponding column matrices separately. Equation (6.29) is a coupled NLCP for the plastic multipliers of all Gauss points $\Delta\boldsymbol{\kappa}$, to be solved simultaneously for all Gauss points. Same as for the local model, the elastic region is characterized by $\Delta\kappa = 0$ and the stress state must lie inside the elastic domain at the end of the step, i.e. $f_{(n+1)} \leq 0$, while in the plastic region, characterized by $\Delta\kappa > 0$, the yield condition $f_{(n+1)} = 0$ must be fulfilled.

In the case of linear softening, and if the plastic zone is known, the increments of the softening variable can be solved from a linear system of equations. This is true for the initial linear part of the softening curve, i.e. for $\tau_0 + H\kappa_{(n+1)} > 0$. Similar to Eq. (6.18), but with the nonlocal softening law (6.26) and the constant $C = (9c_\phi c_\psi K + G)/k$, the yield condition can then be written as

$$f_{(n+1)}\left(\Delta\kappa, \Delta\hat{\kappa}\right) = f_{\mathrm{trial}} - C\Delta\kappa - H\Delta\hat{\kappa} = 0 \tag{6.30}$$

for one Gauss point in the plastic zone, and the yield function now depends also on $\Delta\hat{\kappa}$. In the compact format, this can be expressed as

$$\begin{aligned} \boldsymbol{f}_{(n+1)}\left(\Delta\boldsymbol{\kappa}\right) &= \boldsymbol{f}_{\text{trial}} - C\Delta\boldsymbol{\kappa} - H\Delta\hat{\boldsymbol{\kappa}} \\ &= \boldsymbol{f}_{\text{trial}} - C\Delta\boldsymbol{\kappa} - H\left[m\boldsymbol{A} + (1-m)\boldsymbol{I}\right]\Delta\boldsymbol{\kappa} \\ &= \boldsymbol{f}_{\text{trial}} - \boldsymbol{B}\Delta\boldsymbol{\kappa} = \boldsymbol{0} \end{aligned} \tag{6.31}$$

where the matrices are reduced such that they contain only entries corresponding to yielding Gauss points. Here,

$$\boldsymbol{B} = \left[C + (1-m)H\right]\boldsymbol{I} + mH\boldsymbol{A} \tag{6.32}$$

is a constant matrix, and $\boldsymbol{f}_{(n+1)}(\Delta\boldsymbol{\kappa})$ is a linear function of the increment of the softening variable at all Gauss points. Consequently, $\boldsymbol{\kappa}$ for the yielding Gauss points can be solved from the linear system of equations $\boldsymbol{B}\Delta\boldsymbol{\kappa} = \boldsymbol{f}_{\text{trial}}$.

For a nonlocal model, the size of the plastic zone is not known at the beginning of the step, and an iterative technique should be used. With a proper renumbering of the Gauss points, the matrix $\boldsymbol{B}$ is banded but typically has a large bandwidth, so a direct solution procedure would be quite expensive anyhow. The iterative technique is based on a criterion for selecting the presumably yielding Gauss points and repeated solution of the linear system for $\Delta\boldsymbol{\kappa}$.

In a typical iteration number $k+1$, the yield condition $\boldsymbol{f}_{(n+1)}^{(k+1)} = \boldsymbol{0}$ is solved for the set of Gauss points considered to be yielding. The superscript indicates the iteration of the stress return algorithm, and the subscript $n+1$ corresponding to the global incremental step will be omitted in the following for brevity. Of course, the set of yielding Gauss points may change from one iteration to the next. A Gauss point is considered to be yielding for iteration $k+1$, if the yield function is positive evaluated for the trial stress under the assumption that the point is not yielding, i.e. the local increment of iteration $k+1$ is set to zero, $\Delta\kappa^{(k+1)} = 0$. This condition can be written as

$$F_{\text{trial}} - h\left(\hat{\kappa}\left(\kappa_{(n)}, \bar{\kappa}_{(n)} + \Delta\bar{\kappa}^{(k)} - A^{\text{d}}\Delta\kappa^{(k)}\right)\right) > 0 \tag{6.33}$$

where A^{d} is the diagonal element of the discretized nonlocal averaging operator $\boldsymbol{A}$ for this Gauss point.

Instead of solving the system of equations $\boldsymbol{B}\Delta\boldsymbol{\kappa} = \boldsymbol{f}_{\text{trial}}$ directly, an iterative technique based on an additive split of the linear operator $\boldsymbol{B} = \boldsymbol{B}_1 + \boldsymbol{B}_2$, with an easy-to-invert matrix $\boldsymbol{B}_1$ is used. In each iteration of the nonlocal stress return algorithm, the equation

$$\boldsymbol{B}_1\Delta\boldsymbol{\kappa}^{(k+1)} = \boldsymbol{f}_{\text{trial}} - \boldsymbol{B}_2\Delta\boldsymbol{\kappa}^{(k)} \tag{6.34}$$

is solved for $\Delta\boldsymbol{\kappa}^{(k+1)}$. For a diagonal matrix $\boldsymbol{B}_1$, at each Gauss point and in each iteration, only a linear equation for $\Delta\kappa^{(k+1)}$ needs to be solved. The computed increment $\Delta\kappa^{(k+1)}$ is checked for admissibility, i.e. it is set to zero if $\Delta\kappa^{(k+1)} < 0$, because negative increments of the softening variable violate the loading-unloading conditions.

Convergence is achieved if each Gauss point fulfills the loading-unloading conditions at the end of the step. For elastic Gauss points with $\Delta\kappa^{(k+1)} = 0$, it is checked that the stress state lies inside the elastic domain, i.e. $f^{(k+1)} \leq 0$. For yielding Gauss points with $\Delta\kappa^{(k+1)} > 0$, the yield condition $f^{(k+1)} = 0$ does not need to be satisfied exactly, but only approximately with a small prescribed tolerance.

In a comparison of different splitting techniques and their convergence properties (Benvenuti and Tralli 2003) the split of $\boldsymbol{B}$ into its diagonal part

$$\boldsymbol{B}_1 = [C + (1-m)H]\,\boldsymbol{I} + mH\boldsymbol{A}^{\mathrm{d}} \tag{6.35}$$

and the remainder

$$\boldsymbol{B}_2 = mH\boldsymbol{A}^{\mathrm{r}} \tag{6.36}$$

where $\boldsymbol{A}^{\mathrm{d}}$ and $\boldsymbol{A}^{\mathrm{r}} = \boldsymbol{A} - \boldsymbol{A}^{\mathrm{d}}$ are the diagonal part and the remainder of $\boldsymbol{A}$, respectively, was found to be optimal. It performs significantly better than two previously proposed splits. In the context of J_2-plasticity, the split into $\boldsymbol{B}_1 = (C+H)\boldsymbol{I}$ and $\boldsymbol{B}_2 = mH(\boldsymbol{A} - \boldsymbol{I})$ had been used (Strömberg and Ristinmaa 1996). Even in the one-dimensional case, this split does not converge for all physically admissible values of the model parameters. If softening is too strong, convergence is lost. The split into the local part $\boldsymbol{B}_1 = [C + (1-m)H]\,\boldsymbol{I}$ and nonlocal part $\boldsymbol{B}_2 = mH\boldsymbol{A}$ had been proposed (Rolshoven and Jirásek 2001). For fine meshes, the numerical performance of this latter split is about the same as for the optimal split, Equations (6.35) and (6.36), but on coarse meshes, the optimal split is considerably faster and therefore used here.

6.5 General nonlocal stress return

To understand the physical meaning of this iterative technique and for an extension to the ductile damage model, nonlinear hardening as well as more complex yield criteria, it is useful to rewrite the equation that has to be solved for one Gauss point. Using the identity

$$\begin{aligned} \boldsymbol{A}^{\mathrm{r}}\Delta\boldsymbol{\kappa}^{(k)} &= \left(\boldsymbol{A} - \boldsymbol{A}^{\mathrm{d}}\right)\Delta\boldsymbol{\kappa}^{(k)} \\ &= \Delta\bar{\boldsymbol{\kappa}}^{(k)} - \boldsymbol{A}^{\mathrm{d}}\Delta\boldsymbol{\kappa}^{(k)} \end{aligned} \tag{6.37}$$

Eq. (6.34) can be written for the split (6.35)-(6.36) and one specific Gauss point as

$$f_{\mathrm{trial}} - C\Delta\kappa^{(k+1)} - H\left[m\Delta\bar{\kappa}^{\star(k+1)} + (1-m)\Delta\kappa^{(k+1)}\right] = 0 \tag{6.38}$$

where

$$\Delta\bar{\kappa}^{\star(k+1)} = \Delta\bar{\kappa}^{(k)} + A^{\mathrm{d}}\left(\Delta\kappa^{(k+1)} - \Delta\kappa^{(k)}\right) \tag{6.39}$$

The expression $\Delta\bar{\kappa}^{\star(k+1)}$ can be perceived as an approximation of $\Delta\bar{\kappa}^{(k+1)}$.

Comparing Eq. (6.38) to the yield condition at the end of the step, Eq. (6.30), the iterative scheme can be interpreted in the following manner: For each Gauss point that is assumed to be yielding, the updated approximation $\Delta\kappa^{(k+1)}$ of the increment of the hardening variable is computed from the yield condition at that point, assuming that the increments of the hardening variable at all other Gauss points are temporarily frozen (i.e., set equal to their values $\Delta\kappa^{(k)}$ determined in the previous iteration).

To include the ductile damage model and nonlinear hardening, the hardening law is explicitly expressed as a function of the local and nonlocal hardening variable, i.e. $\tau_{\mathrm{Y}} = h_{\mathrm{NL}}(\kappa, \bar{\kappa})$. For a yielding Gauss point, the yield condition at the end of the step

$$f_{(n+1)}\left(\Delta\kappa, \Delta\bar{\kappa}\right) = F_{\mathrm{trial}} - C\Delta\kappa - h_{\mathrm{NL}}\left(\kappa_{(n)} + \Delta\kappa,\, \bar{\kappa}_{(n)} + \Delta\bar{\kappa}\right) = 0 \tag{6.40}$$

is similar to Eq. (6.30). It can be written in the compact form

$$\boldsymbol{f}_{(n+1)}\left(\Delta\boldsymbol{\kappa}\right) = \boldsymbol{F}_{\mathrm{trial}} - C\Delta\boldsymbol{\kappa} - \boldsymbol{h}_{\mathrm{NL}}\left(\boldsymbol{\kappa}_{(n)} + \Delta\boldsymbol{\kappa},\, \bar{\boldsymbol{\kappa}}_{(n)} + \Delta\bar{\boldsymbol{\kappa}}\right) = \boldsymbol{0} \tag{6.41}$$

for all yielding Gauss points, but $\boldsymbol{h}_{\mathrm{NL}}$ is now a nonlinear function.

Clearly, for the ductile damage model or nonlinear hardening functions, the CP is nonlinear. The same is true for the case of the vertex return. A standard way to proceed would be to solve an iterative series of LCP's. Since each LCP again involves an iterative solution, this technique would be quite expensive.

In the spirit of the iterative technique developed for the case of linear softening, an alternative iterative technique for the solution of this nonlinear system of equations is proposed: Each equation of the system of equations is solved independently, i.e., the updated increment of the hardening variable at each Gauss point is computed from the yield condition at that point, with increments of the hardening variable at all other Gauss points temporarily frozen. The equation to be solved for one yielding Gauss point reads

$$F_{\mathrm{trial}} - C\Delta\kappa^{(k+1)} - h_{\mathrm{NL}}(\kappa_{(n)} + \Delta\kappa^{(k+1)}, \bar{\kappa}^{\star(k+1)}) = 0 \tag{6.42}$$

where

$$\bar{\kappa}^{\star(k+1)} = \bar{\kappa}^{(k)} + A^{\mathrm{d}}\left(\Delta\kappa^{(k+1)} - \Delta\kappa^{(k)}\right) \tag{6.43}$$

can again be interpreted as an approximation of $\bar{\kappa}^{(k+1)}$. This is a nonlinear equation for the unknown $\Delta\kappa^{(k+1)}$, and it can be solved by a Newton iteration.

This concept for the solution of the NLCP has been successfully implemented for the Drucker–Prager model extended in the spirit of the ductile damage model, including nonlinear hardening and the vertex stress return. The error in the yield criterion is typically reduced by one order of magnitude per iteration.

The same procedure can be used for the nonlocal extension of more complex plasticity models. For a quite general case, the stress return for yielding Gauss points is achieved by numerical solution of the nonlinear system of equations

$$\boldsymbol{\sigma}_{(n+1)} = \boldsymbol{D} : \left(\boldsymbol{\varepsilon}_{(n+1)} - \boldsymbol{\varepsilon}_{\mathrm{p},(n+1)}\right) \tag{6.44}$$

$$f\left(\boldsymbol{\sigma}_{(n+1)}, \kappa_{(n+1)}\right) = 0 \tag{6.45}$$

$$\Delta\boldsymbol{\varepsilon}_{\mathrm{p}} = \Delta\lambda\, \boldsymbol{g}\left(\boldsymbol{\sigma}_{(n+1)}, \kappa_{(n+1)}\right) \tag{6.46}$$

$$\Delta\kappa = N\left(\Delta\boldsymbol{\varepsilon}_{\mathrm{p}}\right) k\left(\boldsymbol{\sigma}_{(n+1)}\right) \tag{6.47}$$

which are the algorithmic form of elastic law, yield criterion, and evolution laws for plastic strain and hardening variable. In the above, the yield function f and the flow direction $\boldsymbol{g}$ are functions of stress and hardening variable, and the evolution law for the hardening variable depends on a function of the stress, $k(\boldsymbol{\sigma})$, and a given norm $N(\Delta\boldsymbol{\varepsilon}_{\mathrm{p}})$ of the plastic strain increment.

The nonlocal extension replaces the local yield function by a nonlocal one, f_{NL}, which depends also on the nonlocal average $\bar{\kappa}$. Following the iterative technique developed above and dropping the subscript $(n+1)$ for convenience, the nonlinear system of equations

$$\boldsymbol{\sigma}^{(k+1)} = \boldsymbol{D} : \left(\boldsymbol{\varepsilon}^{(k+1)} - \boldsymbol{\varepsilon}_{\mathrm{p}}^{(k+1)}\right) \tag{6.48}$$

$$f_{\mathrm{NL}}\left(\boldsymbol{\sigma}^{(k+1)}, \kappa^{(k+1)}, \bar{\kappa}^{\star(k+1)}\right) = 0 \tag{6.49}$$

$$\Delta\boldsymbol{\varepsilon}_{\mathrm{p}}^{(k+1)} = \Delta\lambda \boldsymbol{g}\left(\boldsymbol{\sigma}^{(k+1)}, \kappa^{(k+1)}\right) \tag{6.50}$$

$$\Delta\kappa^{(k+1)} = \frac{N\left(\Delta\boldsymbol{\varepsilon}_{\mathrm{p}}^{(k+1)}\right)}{d\left(\boldsymbol{\sigma}^{(k+1)}\right)} \tag{6.51}$$

is solved in the nonlocal case for iteration $k+1$. The nonlocal average of the hardening variable, $\bar{\kappa}^{(k+1)}$, is again replaced by the approximation $\bar{\kappa}^{\star(k+1)}$ according to Eq. (6.43).

Due to the complexity of the presented stress return algorithm, the global iteration for equilibrium is performed with the elastic stiffness matrix. The derivation of the consistent tangent stiffness matrix would be difficult and its use would not necessarily improve the computational efficiency. Nonlocal interaction increases the bandwidth of the stiffness matrix and makes the solution procedure more expensive.

6.6 Efficient implementation

The implementation of the nonlocal stress return algorithm is considerably simplified taking advantage of the fact that the yield condition, Eq. (6.42), resembles the yield condition in the standard stress return algorithm. The difference is the meaning of the variables and the modified hardening function. The implementation of this model is carried out in the finite element code OOFEM (Patzák and Bittnar 2001). Due to the object-oriented character of this code, the function that performs the stress return algorithm of the local model can be reused in its original format; it is simply called with different variables.

The effort of computing the nonlocal average $\bar{\kappa}$ in each iteration can be reduced if the operation is performed only for those points where this average actually changes. The nonlocal average of the hardening variable in a Gauss point that has at least one plastic 'neighbor' changes from one iteration to the next. Neighbors are those Gauss points which influence the nonlocal average at a given Gauss point, i.e. their distance to this point is less than the interaction radius. On the contrary, at elastic Gauss points without plastic neighbors, the nonlocal average of the hardening variable does not change. In the present implementation, this is used to speed up the algorithm: Elastic Gauss points without plastic neighbors are excluded from nonlocal averaging. In a typical simulation, the actual process zone is small compared to the structure, and the nonlocal average needs to be computed only in the process zone and at neighboring Gauss points.

Chapter 7

Examples with nonlocal Drucker–Prager model

7.1 Biaxial compression under plane strain

7.1.1 Test geometry and material parameters

As a first simple test case, biaxial compression under plane strain is simulated with the nonlocal Drucker–Prager model. Attention is restricted to regularization of the softening regime, and the material is assumed not to harden. Under these assumptions, both the ductile damage model and the Vermeer–Brinkgreve model could be used. Here, the Vermeer–Brinkgreve model is chosen.

A rectangular specimen with dimensions $B = 600$ mm and $L = 1200$ mm between smooth rigid plates is subjected to uniform displacement of the top, while the lateral displacement is unconstrained, see Fig. 7.1. In the out-of-plane direction, plane strain conditions are imposed. Initially, a homogeneous biaxial stress state develops in the specimen. At the onset of yielding, formation of a shear band is possible if ellipticity is lost. For the local model, this is the case if the hardening modulus is smaller than or equal to a certain critical value that can be determined by analysis of the acoustic tensor, cf. Rudnicky and Rice (1975).

For plane strain, the critical hardening modulus and the inclination of a possible shear band have been derived analytically by Runesson et al. (1991). The principal components of the deviatoric stress s_1, s_2, and s_3 are ordered such that s_3 corresponds to the out-of-plane direction and $s_1 \geq s_2$. The orientation of the shear band is specified by the angle θ between the second principal axis and the normal to the band, see Fig. 7.1. Under certain mild restrictions that are satisfied in the current examples, the critical hardening modulus normalized by the elastic modulus is

$$\frac{H^{\text{crit}}}{E} = \frac{1}{4k(1-\nu)} \left[2\left(c_\phi - c_\psi\right)^2 - (1-\nu)\left(\frac{s_3}{\sqrt{J_2}} + c_\phi + c_\psi \right)^2 \right] \tag{7.1}$$

According to this expression, the maximum value of the critical hardening modulus $H^{\text{crit}}_{\text{max}}$ over all stress states is

$$\frac{H^{\text{crit}}_{\text{max}}}{E} = \frac{(c_\phi - c_\psi)^2}{2k(1-\nu)} \tag{7.2}$$

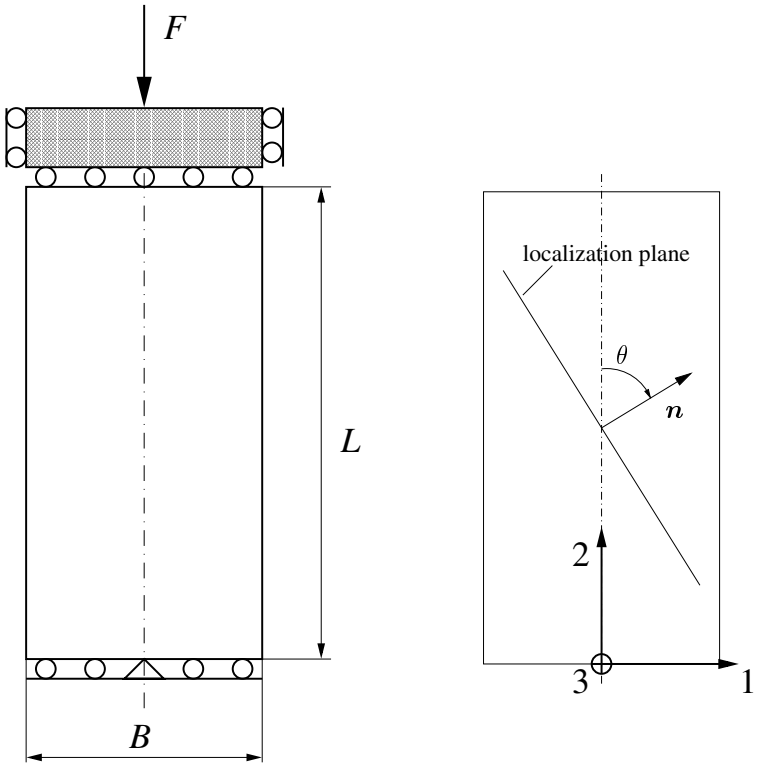

Figure 7.1: Structural model, coordinate system and definition of localization angle θ.

The orientation of the shear band can be determined from the relation

$$\tan^2\theta = -\frac{s_1 + \nu s_3 + (1+\nu)\sqrt{J_2}\,(c_\phi + c_\psi)}{s_2 + \nu s_3 + (1+\nu)\sqrt{J_2}\,(c_\phi + c_\psi)} \tag{7.3}$$

and it depends only on the sum of the friction and dilatancy coefficients and on the stress state.

In a plane strain simulation, plasticity models generally exhibit locking when standard low-order finite elements are used (de Borst and Groen 1995). For isochoric plasticity models such as J_2-plasticity, this phenomenon is known as volumetric locking. An effective technique to avoid volumetric locking for J_2-plasticity is reduced integration, but for the pressure-dependent plasticity models, it is not sufficient.

A simple way to avoid locking for a straight shear band is to use an oriented mesh. If the mesh lines in a triangular mesh are aligned with the direction of the shear band, the locking effect vanishes. For comparison, the simulation is performed both on these aligned meshes and on meshes with a misalignement between the mesh lines and the band orientation.

The finite element meshes consist of a region with an automatically generated mesh using T3D (Rypl 1998) and a region where the finite elements are arranged into layers, either oriented in the direction of the expected shear band, or deviating from that direction. The oriented region is chosen larger than the expected width of the localized plastic zone for the nonlocal model. Four different meshes are used: a coarse mesh with one layer of finite elements across the oriented region, a medium mesh with five layers, a fine mesh

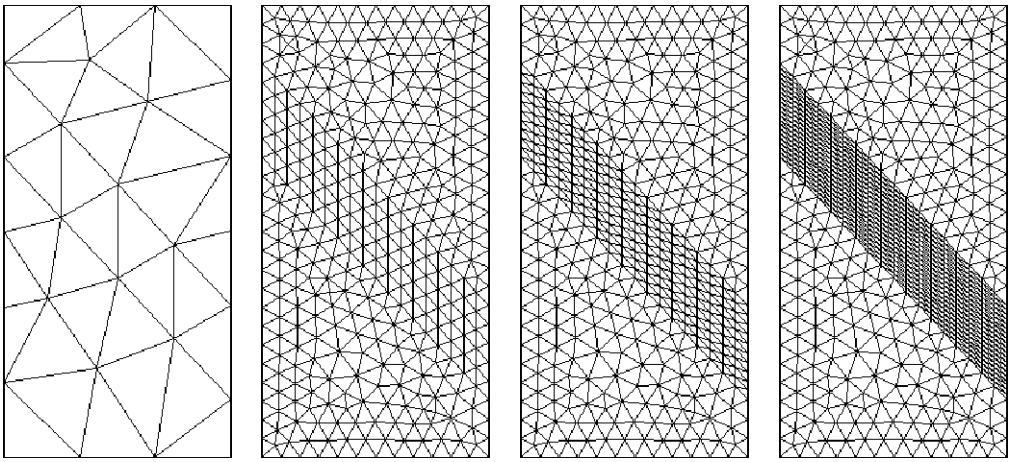

Figure 7.2: Four discretizations with linear plane strain triangular finite elements.

with ten layers, and a very fine mesh with twenty layers, see Fig. 7.2. The thickness of one layer of finite elements is respectively 170 mm, 34 mm, 17 mm and 8.5 mm. Along the oriented band, the number of elements is kept constant.

The material parameters adopted for the examples are: $E = 30$ GPa, $\nu = 0.2$, $\tau_0 = 20$ MPa, $c_\phi = 0.1$, $c_\psi = 0.05$, $\kappa_c = 5.7 \times 10^{-3}$, $R = 50$ mm, and $m = 2$. These parameters are close to those that characterize concrete under compression, but adapted so as to obtain bifurcation right at the onset of yielding. The adopted value of κ_c corresponds to the critical softening modulus of $H^{\text{crit}}/E = -0.12$, evaluated from Eq. (7.1) for the state at the onset of yielding. At the initial bifurcation, the selected value of m satisfies condition (5.47) for the most critical stress state, i.e.

$$2 = m > \frac{H - H^{\text{crit}}_{\max}}{H} = 1.022 \tag{7.4}$$

and this condition remains satisfied for the values of κ reached in this simulation.

To trigger the formation of a shear band, the yield stress of the central elements at the lower end of the oriented region is reduced by 2.5% (in two elements for the coarse and medium meshes and in four for the fine and very fine meshes).

At the onset of yielding, the stress state in the specimen is homogeneous. Denoting by σ the nominal stress in the vertical direction (negative for compression), the principal values of the deviatoric stress can be evaluated as $s_1 = -(1+\nu)\,\sigma/3$, $s_2 = (2-\nu)\,\sigma/3$, and $s_3 = (2\nu - 1)\,\sigma/3$, and the second deviatoric invariant is $J_2 = (1 - \nu + \nu^2)\,\sigma^2/3$. For the given set of material parameters, the direction of the shear band obtained from Eq. (7.3) is $\theta = 0.82$, which is approximately 47°.

For all load-displacement diagrams, the load is normalized by the product of the width of the specimen and the initial yield stress, $B\tau_0$, and the top displacement by the height of the specimen, L.

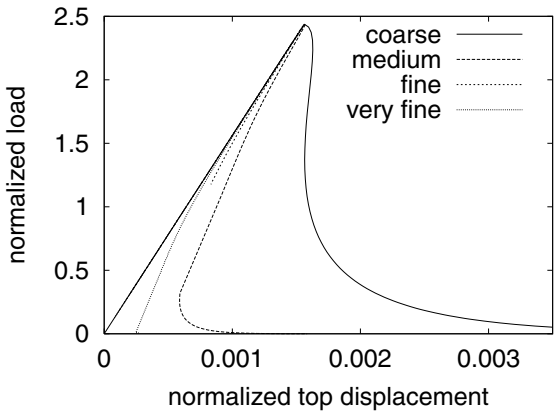

Figure 7.3: Load-displacement diagram for the local model on four aligned meshes.

7.1.2 Discussion of results for aligned meshes

In a first series of simulations, the orientation of the refined zone is chosen so as to coincide with the expected bifurcation angle. On these meshes, local and nonlocal formulation can be compared without the influence of locking effects.

As amply documented in the literature, a local plasticity model leads to a strongly mesh-dependent load-displacement response, see Fig. 7.3. Upon mesh refinement, the numerical response becomes excessively brittle, because the boundary value problem is ill-posed in the local case. Fig. 7.4 compares the distribution of the local softening variable κ for the local and the nonlocal model obtained on the medium mesh. It demonstrates the well-known fact that, for the local model, the plastic zone tends to localize into one layer of finite elements.

The load-displacement curves obtained with the nonlocal model show good convergence upon mesh refinement, see Fig. 7.5. For the coarse mesh, the distance of the Gauss points is larger than the interaction radius, and the result is the same as for the local model. This shows that a certain minimum mesh density is necessary to activate the nonlocal interaction. For the other meshes, medium, fine and very fine, the load-displacement curves are practically identical at early stages of the softening process, but some deviation is observed at later stages. During the loading process, the stress state of the specimen changes, and the bifurcation angle can deviate from the angle valid for the elastic limit state. The shear band is then no longer perfectly aligned with the computational grid, and mesh locking effects, though small, are present. These lead to a slightly more rigid response of the coarser meshes.

Except for the coarse mesh, for which plastic strain localizes in one layer of finite elements, the size and shape of the plastic zone exhibit no spurious dependence on the mesh density, see Fig. 7.6 for the distribution of the local softening variable κ. The plastic zone extends over approximately 85 mm. The three finer meshes give practically the same results. For practical applications, it is thus sufficient to design the finite element mesh so as to obtain a plastic zone that extends over three to four elements.

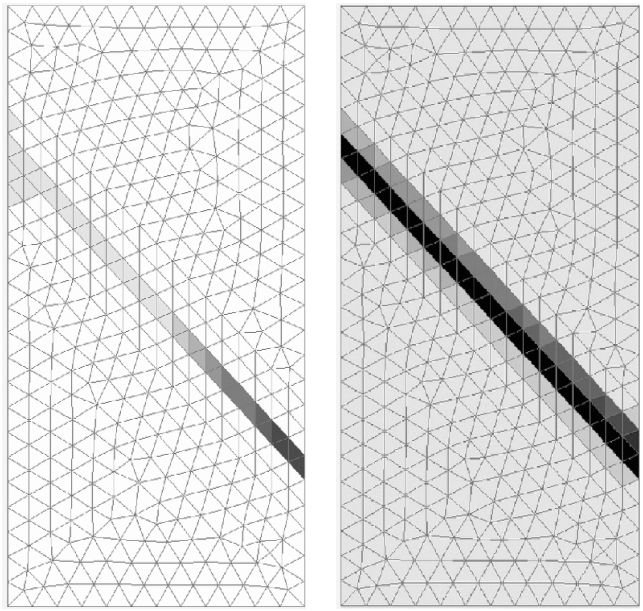

Figure 7.4: Distribution of the local softening variable κ for the local and nonlocal model on the aligned medium mesh.

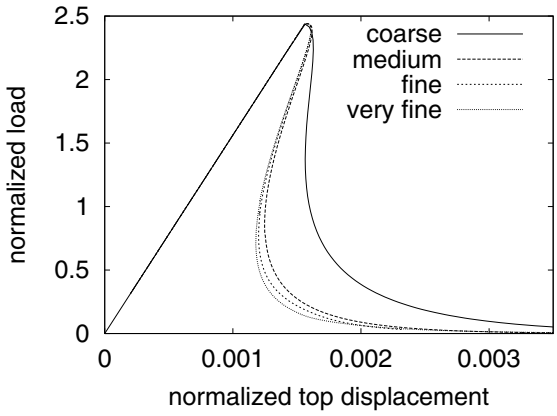

Figure 7.5: Load-displacement diagram for the nonlocal model on four aligned meshes.

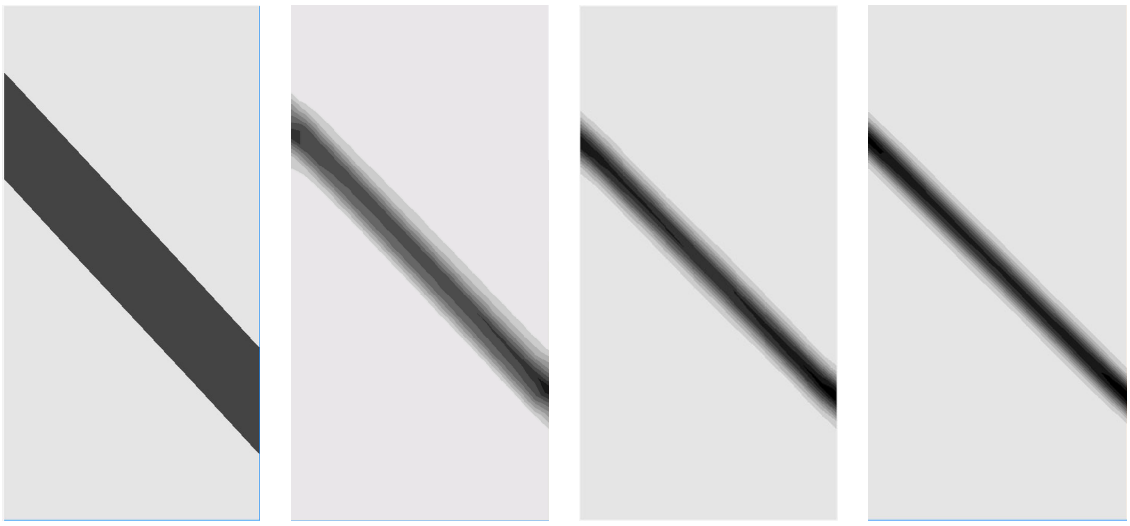

Figure 7.6: Distribution of the local softening variable κ for the nonlocal model on aligned meshes, at two thirds of the peak load (in the post-peak range).

7.1.3 Discussion of results for misaligned meshes

In the second example, both the local and the nonlocal model are tested on the medium mesh with the oriented region deviating by 8^o from the expected shear band. The imperfection is now located in the topmost layer of the refined region, so that the shear band can evolve within the oriented region.

For the nonlocal model, the load-displacement response is initially quite similar, see Fig. 7.7. At later stages of the loading process the misaligned mesh gives a stiffer response, presumably caused by the locking effect of the finite elements.

The influence of the mesh on the orientation of the shear band is negligible for the nonlocal model, see Fig. 7.8. The direction of the shear band is still captured correctly. In contrast to that, for the local model, the plastic zone is still confined to one layer of finite elements, and follows the prescribed direction of the grid.

Two effects are at the origin of mesh-induced directional bias. First, in a mesh of standard finite elements without any remedy for locking, the mesh lines are preferential directions for weak discontinuities. Second, even for elements without locking, a local model tends to localize in one layer of finite elements because the dissipated energy is smaller in this case.

7.2 Triaxial compression under plane strain

7.2.1 Motivation

Localization under hardening due to nonassociated flow can hardly occur in biaxial compression under plane strain conditions if the Drucker–Prager model is used with realistic material parameters for concrete. The customary calibration based on failure under equibiaxial compression and uniaxial compression leads to a yield criterion and flow rule which

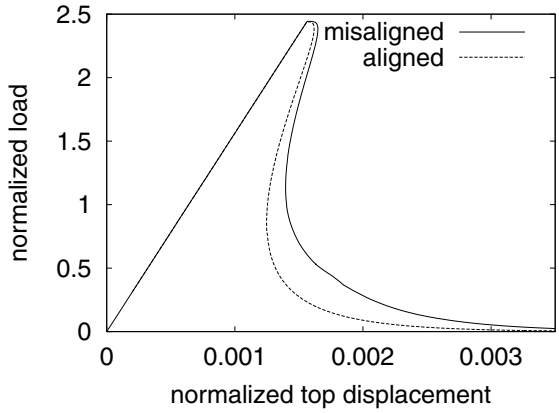

Figure 7.7: Load-displacement diagram for the nonlocal model on the misaligned and the aligned medium mesh.

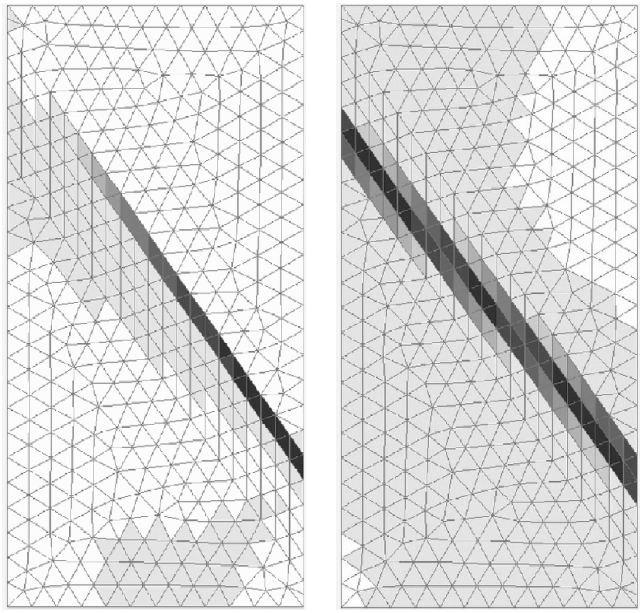

Figure 7.8: Distribution of the local softening variable κ for the local and nonlocal model on the misaligned medium mesh.

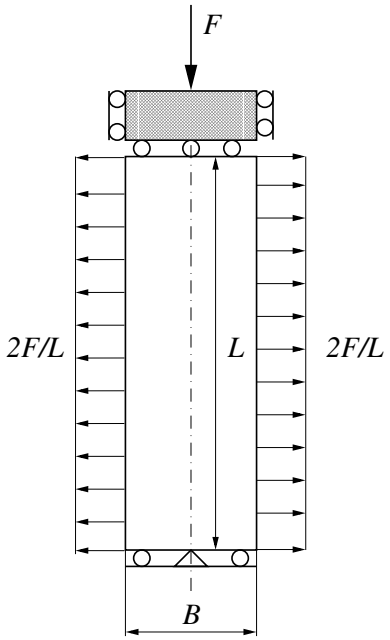

Figure 7.9: Structural model.

are only slightly nonassociated. The critical hardening modulus H^{crit} is typically negative, which means that localization can occur only after the onset of softening.

To test the capability of the nonlocal material model to correctly regularize localization due to nonassociated flow, a triaxial stress state under plane strain conditions is more appropriate. In this case, the critical hardening modulus is negative for values which are closer to those realistic for concrete.

7.2.2 Test geometry and material parameters

A rectangular specimen of length $L = 1800\,\text{mm}$ and width $B = 600\,\text{mm}$ is subjected to an applied displacement generated by a compressive load F at the top and a tensile load of magnitude $2F$ in the lateral direction, as depicted in Fig. 7.9. The structural model is discretized with three different meshes, called coarse, medium, and fine, see Fig. 7.10. As explained in the Sec. 7.1, it is advantageous to use a mesh with a region aligned with the expected inclination of the shear band. Here, this region has a thickness of 350 mm, and consists of 5 layers of elements for the coarse mesh, 10 layers for the medium, and 20 layers for the fine mesh.

To trigger the localization, the initial yield stress τ_0 in a small region slightly off center is reduced. The region of constant size and location consists of two elements for the coarse mesh, eight for the medium, and 32 for the fine mesh. The yield stress is reduced by 5 %.

The nonlocal material model with a hardening law in the multiplicative format

$$h_{\text{NL}}(\kappa, \bar{\kappa}) = \tau_0 \frac{h_{\text{hom}}(\bar{\kappa})}{h_2(\bar{\kappa})} h_2(\kappa) \tag{7.5}$$

is used in this simulation. The two factors of the multiplicative law are chosen according

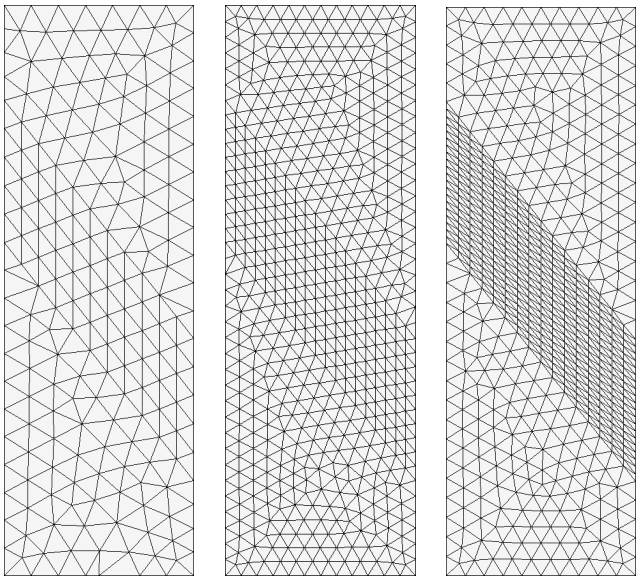

Figure 7.10: Three discretizations with linear plane strain triangular finite elements.

to the concept outlined in Sec. 5.5. A simple linear hardening law

$$h_{\text{hom}}(\kappa) = 1 + H_{\text{hom}}\kappa \tag{7.6}$$

is used for the homogeneous hardening law, and h_2 is chosen as the linear function

$$h_2(\kappa) = 1 + H_2\kappa \tag{7.7}$$

The dimensionless hardening modulus H_2 is chosen such that the derivative of $h_1 = h_{\text{hom}}/h_2$ is negative everywhere. In the present case, the minimum value for H_2 is H_{hom}.

The material parameters used in this simulation are chosen so that the critical hardening modulus according to Eq. (7.1) is positive, i.e. bifurcation can occur during hardening. They are set to $E = 20\,\text{GPa}$, $\tau_0 = 20\,\text{MPa}$, $\nu = 0.2$, $c_\phi = 0.3$, and $c_\psi = 0.05$. For these parameters, the critical hardening modulus for the homogeneous stress state at the onset of yielding is $H^{\text{crit}}/E = 0.0468$, and the critical bifurcation angle is $\theta = 51^{\text{o}}$.

The hardening modulus in the homogeneous hardening law is chosen smaller than the critical hardening modulus, but still positive. The maximum value of H_{hom} that would theoretically allow bifurcation is $H_{\text{hom}} = H^{\text{crit}}/\tau_0 = 46.8$. Preliminary studies showed that bifurcation did not occur for hardening moduli close to this value, and the hardening modulus is set to $H_{\text{hom}} = 5$ instead. One should keep in mind that the difference between the adopted value of the hardening modulus and the critical hardening modulus is still very small, because $H^{\text{crit}} - H_{\text{hom}}\tau_0 = 0.0418E$. To comply with conditions (5.46) and (5.54) H_2 is set to 100. This is larger than the minimum value needed, which is $H^{\text{crit}}_{\text{max}}/\tau_0 = 67.2$ in this case.

For the load-displacement diagram in Fig. 7.12, the load is normalized by the product of the width of the specimen and the initial yield stress, $B\tau_0$. The top displacement is normalized by the height of the specimen, L. The plots for the local hardening variable

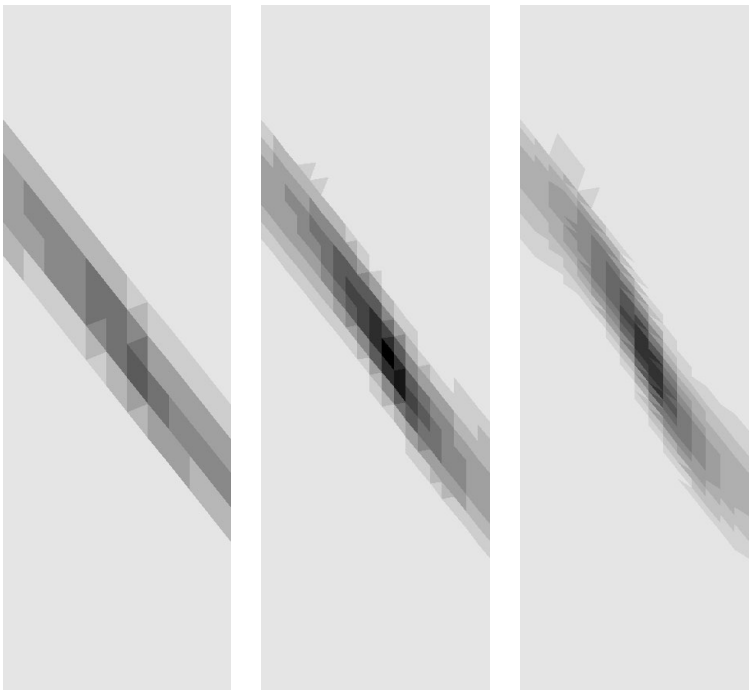

Figure 7.11: Distribution of the local hardening variable κ in the post-peak range (normalized top displacement is 1×10^{-3}) for the three meshes, plotted in the range 1×10^{-4} to 6×10^{-3}.

κ, see Fig. 7.11, are presented in an unsmoothened format, because this allows to detect possible localization into one layer of finite elements more easily.

7.2.3 Discussion

The load-displacement response and the distribution of the hardening variable κ show no spurious dependence on the computational grid. The distribution of the softening variable shows that the deformation localizes, as it is expected from the bifurcation analysis. The size of the plastic zone is practically the same for all three meshes.

7.3 Eccentric compression

7.3.1 Motivation

Properly formulated nonlocal models reproduce the experimentally observed transition from ductile to brittle response when the size of geometrically similar structures is increased. For simple loading cases such as biaxial compression, the pre-peak response and especially the structural strength, defined as the load divided by a suitable area of the structure, do not depend on the size of the structure. The differences appear solely in the post-peak behavior, often of less practical interest.

For complex structures, the differences in the local post-peak response may change

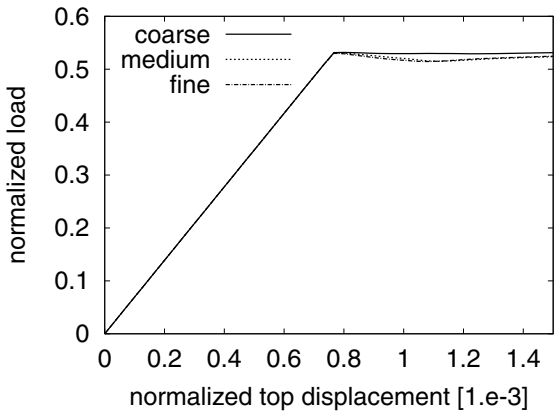

Figure 7.12: Load-displacement diagram for the three meshes.

label	L [mm]	D [mm]	$e = D/6$ [mm]
XS	100	25	4.167
S	200	50	8.333
M	400	100	16.67
L	800	200	33.33
XL	1600	400	66.67
XXL	3200	800	133.33

Table 7.1: Dimensions of the eccentric compression series.

the pre-peak response of the structure and produce a so-called size effect on structural strength. Typical examples for which size effect on structural strength is experimentally observed are single-edge notched three-point bending tests (Walsh 1972), double-edge notched tension and compression tests, and double-edge notched shear tests (Bažant and Pfeiffer 1986; Bažant and Pfeiffer 1987). Recently, an experimental size effect series for eccentric compression of unnotched cylindrical columns has been performed by Burtscher (2002). Because the nonlocal plasticity model is designed mainly for concrete under compression, eccentric compression of a column is chosen as an application example.

7.3.2 Test series

A series of six plain concrete columns with quadratic cross section of geometrically similar sizes are simulated to explore the size effect on structural strength. In comparison to the test series studied by Burtscher (2002), the eccentricity is increased to enhance the size effect, the cross section is chosen quadratic instead of circular, and an additional smaller and larger specimen is added to the series. The different sizes are labeled extra small (XS), small (S), medium (M), large (L), extra large (XL) and extra extra large (XXL). The aspect ratio of length L to width (equal to depth) D is $L/D = 4$ for all specimens, and the eccentricity is set to $e = D/6$, cf. Table 7.1 for the dimensions of all specimens. The parameters of the material model are roughly calibrated to the plain concrete used in the experimental series by Burtscher (2002).

For geometric description, an orthogonal coordinate system is used. The x-coordinate

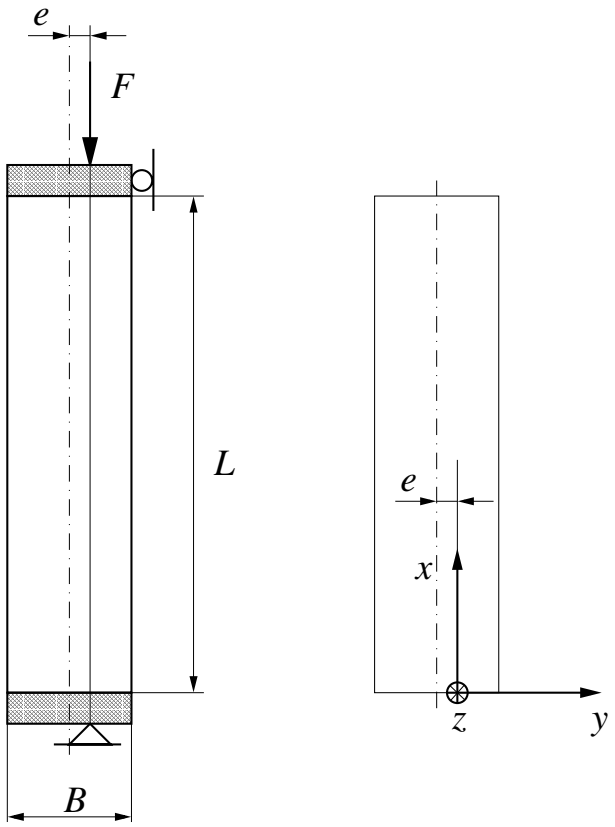

Figure 7.13: Structural model of column under eccentric compression.

is parallel to the longitudinal axis of symmetry of the column, the y-coordinate lies in the plane of interest, and the z-coordinate describes the out-of-plane direction, see Fig. 7.3.2. The columns are loaded along the x-axis in eccentric compression. At the bottom and top, the column is fixed with no-slip conditions to a stiff metal plate. This plate can rotate around an axis parallel to the z-axis, but with the prescribed eccentricity of $e = D/6$. At the bottom, the axis is fixed in x- and y-direction, while a load is applied in the x-direction at the top.

7.3.3 Numerical model

The simulation is performed under plane strain conditions, because three-dimensional simulations are prohibitively expensive in terms of computational effort. A relatively fine discretization is necessary to ensure the correct resolution of potential localized material failure patterns. From one-dimensional examples, their width can be expected to be approximately R. Furthermore, a fine resolution is necessary to minimize spurious effects due to locking of the finite elements. The ratio of element length over R is kept constant for all specimens, leading to meshes with an increasing number of finite elements. The mesh for XS is an exception, because it has the same structure as the mesh for the S case; compared to the other meshes, it is finer.

For the discretization, an automatically generated mesh of linear plane strain triangles

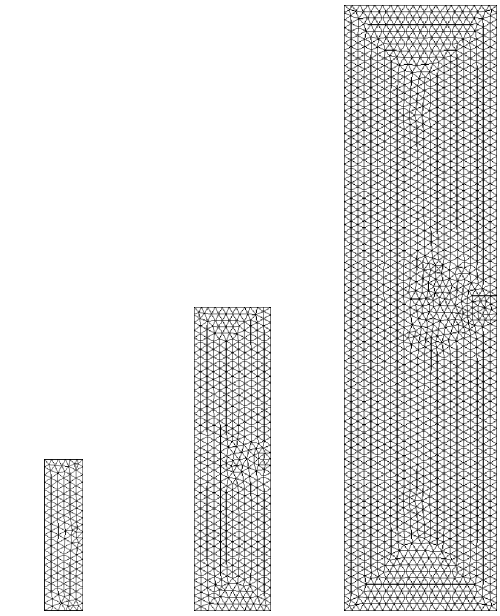

Figure 7.14: Three of six meshes with linear plane strain triangular finite elements.

is used, see Fig. 7.14. The mesh density is uniform, and the mesh is designed such that the interaction radius R extends over approximately five elements for all sizes. Physically, this plane strain simulation can also be interpreted as the eccentric compression of a long wall, for which plane strain conditions are a realistic approximation.

In preliminary simulations, a localized failure mode developed for larger structures in the post-peak range. For uniform material properties, this mode was initiated typically close to the center, but since the exact location was unknown, the control of the simulation was difficult. To avoid this control problem, and to study the post-peak failure mode along with the size effect in structural strength, a small imperfection is introduced on the compressive side in the central cross section of the column. In a quadratic region of size $L/25 \times L/25$, the yield stress is reduced by 1 %. The mesh is adapted so that the imperfection always has the desired size, see Fig. 7.14. The central cross section is the weakest link of the column, if second-order geometric effects were taken into account. So this is where the plastic deformation would initiate even for a perfectly homogeneous column.

7.3.4 Material model and calibration

The nonlocal Drucker–Prager plasticity model with hardening and softening is used for the column compression examples. For the nonlocal model, the concept of ductile damage is used. The Vermeer–Brinkgreve model is not applicable, because hardening is taken into account.

The nonlocal hardening law is constructed from a given local hardening law for the homogeneous case as explained in detail in Sec. 5.5. For concrete under compression, the

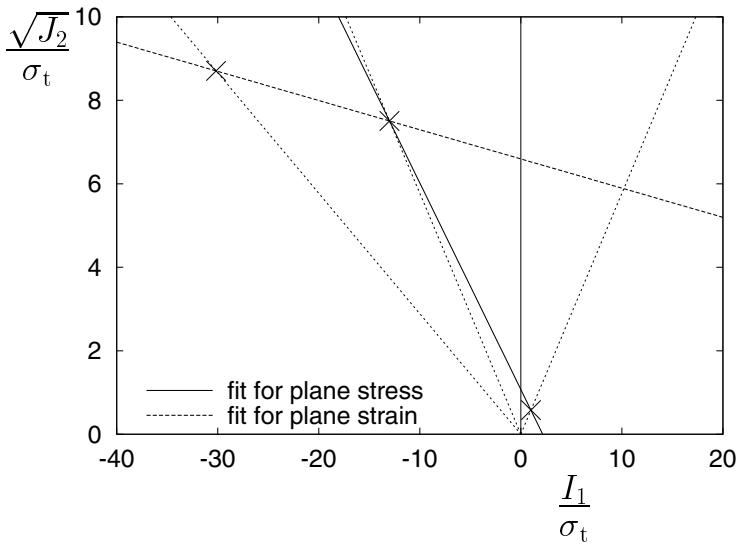

Figure 7.15: Two possible fits of the Drucker–Prager yield surface: The fit for the plane strain case (under compression) uses the yield stress in uni- and biaxial compression, while the fit for the plane stress case uses uniaxial tension and uniaxial compression. σ_t denotes the yield stress in uniaxial tension. The three dotted lines mark the three standard loading cases, the crosses the corresponding yield stress.

homogeneous hardening law

$$\tau_0 h_{\text{hom}}(\kappa) = \begin{cases} \tau_i + (\tau_0 - \tau_i)\left[\left(\dfrac{\kappa}{\kappa_{\text{peak}}}\right)^3 - 3\left(\dfrac{\kappa}{\kappa_{\text{peak}}}\right)^2 + 3\dfrac{\kappa}{\kappa_{\text{peak}}}\right] & \text{if} \quad 0 \le \kappa \le \kappa_{\text{peak}} \\ \tau_0 \exp\left[-\left(\dfrac{\kappa - \kappa_{\text{peak}}}{\kappa_c}\right)^2\right] & \text{if} \quad \kappa \ge \kappa_{\text{peak}} \end{cases} \tag{7.8}$$

is a realistic approximation.

The material parameters for plain concrete are calibrated in a rough manner. First, only a limited range of experimental data exists for the concrete modeled here. For the estimation of material parameters that cannot be fitted from the available experimental data for this specific concrete, data from experiments with other concrete is used. Second, the Drucker–Prager model is only a rough approximation of concrete, and a sophisticated calibration of material parameters for specific loading cases does not make sense. Finally, the aim of this simulation series are qualitative results regarding size effect and failure modes in eccentric compression. Nonetheless, the concept for the calibration of different material parameters is presented in order to show the general limitations.

A fundamental problem of the Drucker–Prager model applied to concrete is that the yield surface cannot be fitted at the same time to the three standard loading cases uniaxial tension, uniaxial compression and biaxial compression with good accuracy, cf. Fig. 7.15. It is customary to fit the material parameters depending on the predominant loading case.

For eccentric compression under plane strain, uniaxial and biaxial compression are

used for the fit, because the plane strain condition generates considerable stresses in the out-of-plane direction. In this case, the yield stress in uniaxial tension is overestimated, see Fig. 7.15.

The hardening law of the model is calibrated from small-size one-dimensional compressive tests, where the deformation is assumed to be uniform. The initial yield stress is set to $\tau_\mathrm{i} = 0.5\tau_0$, and the value of κ at peak load is $\kappa_\mathrm{peak} = 0.9 \times 10^{-3}$. Calibrated from the fracture energy of uniaxial compressive test, κ_c is set to 9×10^{-3}.

The dilatancy angle c_ψ is calibrated from experimental data of uniaxial compression. The slope of the curve of compressive stress over volumetric strain can be adjusted with the dilatancy angle. Following this approach, $c_\psi = 0.065$ is obtained. This value of the dilatancy angle crucially underestimates the volumetric expansion at peak load, which is positive in uniaxial compression experiments, but turns out to be negative for this value of the dilatancy angle. Because the main interest here is the size effect in structural strength, $c_\psi = 0.015$ is adopted.

The bell-shaped polynomial function, Eq. (2.17), is used for nonlocal averaging of the hardening variable κ. Its interaction radius is set to $R = 24\,\mathrm{mm}$, which corresponds to three times the maximum aggregate size of the concrete used. This choice of the interaction length can be based on heuristic arguments. The interaction length could be calibrated from the size effect in fracture energy under compression. Such a calibration has been performed for a tension dominated experiment simulated with an isotropic nonlocal damage model (Jirásek et al. 2003).

In summary, the material parameters are: $E = 25$ GPa, $\nu = 0.2$, $\tau_0 = 17\,\mathrm{MPa}$, $\tau_\mathrm{i} = 0.5\tau_0$, $\kappa_\mathrm{peak} = 0.9 \times 10^{-3}$, $\kappa_\mathrm{c} = 9 \times 10^{-3}$, $R = 24\mathrm{mm}$, $c_\phi = 0.07$, and $c_\psi = 0.015$.

For the normalized load-displacement diagrams, the nominal stress, i.e. load divided by the cross-sectional area of the column, $A = D^2$, is plotted as a function of the nominal strain, i.e. displacement of the point where the load is applied divided by the length L of the column.

7.3.5 Discussion

To validate the discretization, the same physical case, eccentric compression of size M, is computed on a mesh with twice the mesh density of the original mesh. The results show no significant difference in the peak load computed on the medium and fine mesh, see Fig. 7.16. In the post-peak response, small differences appear.

For all sizes, nonlinearities appear at about half of the peak load in the pre-peak regime, see the load-displacement response in Fig. 7.17. This is due to the adopted nonlinear hardening law. The computed part of the post-peak response shows the typical trend from ductile to brittle with increasing size.

The double-logarithmic size effect plots, Fig. 7.18, show a strong influence of the size of the structure on the structural strength, defined as the nominal stress at peak load. For small specimen, the structural strength increases, while it changes only slightly for larger sizes. The structural strength of the smallest specimen (XS) is approx. 41 % bigger than for the largest specimen (XXL). Qualitatively, the increase of the structural strength for smaller specimens corresponds to the experimental findings of Burtscher (2002), see Fig. 7.18.

At peak load, the distribution of the (local) hardening variable κ is nonuniform in y-

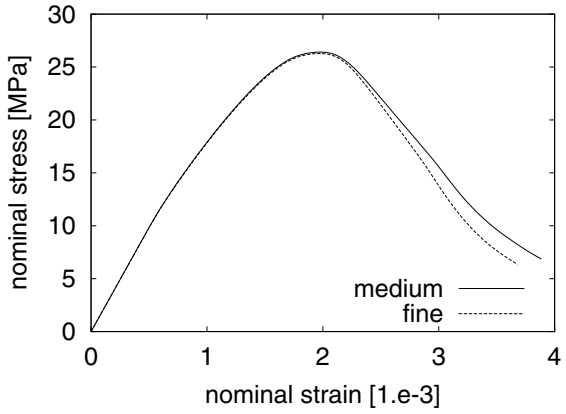

Figure 7.16: Influence of mesh refinement on the load-displacement response for size M.

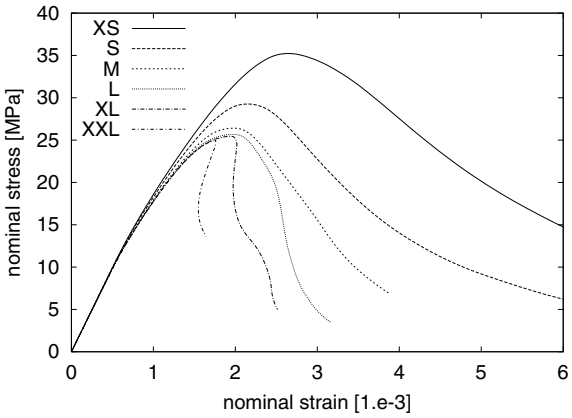

Figure 7.17: Normalized load-displacement diagram for size effect series.

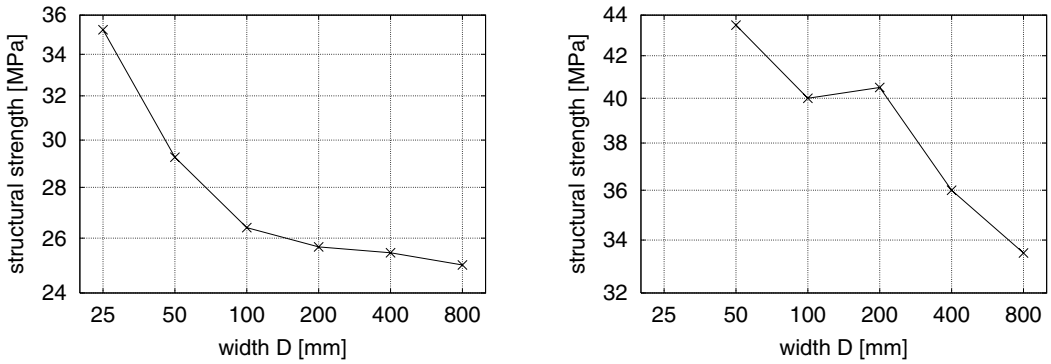

Figure 7.18: Size effect on structural strength: (a) plane strain simulation, (b) three-dimensional experiments performed by Burtscher (2002).

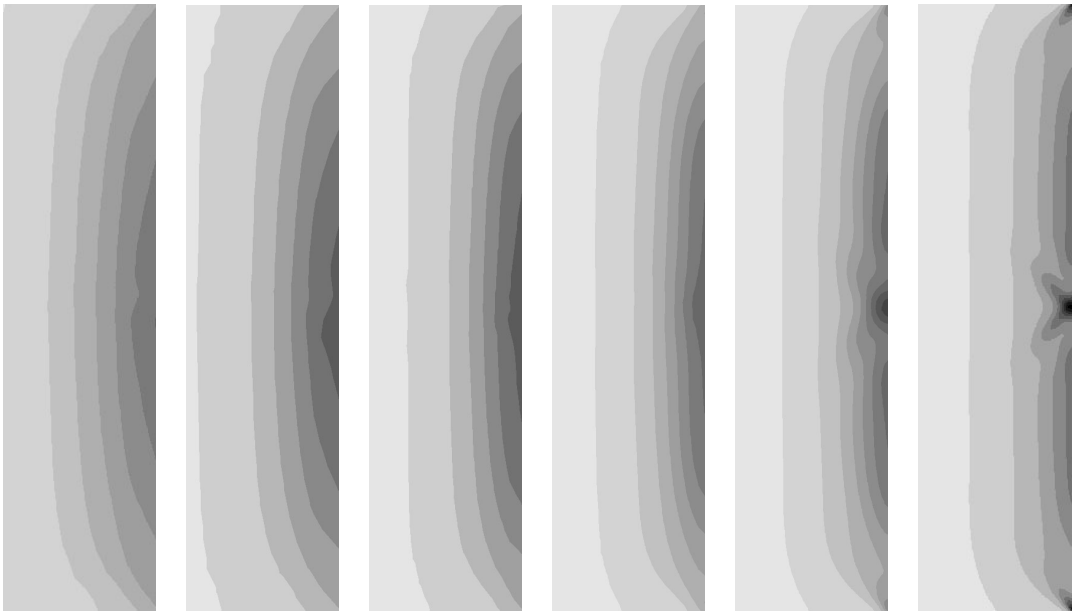

Figure 7.19: Local hardening variable κ at peak load, plotted in the range 5×10^{-5} to 4×10^{-3}.

direction, see Fig. 7.19. Due to the eccentric loading, its maximum lies on the compressive side, while the tensile side is not yielding. In x-direction, κ is constant, with the exception of the boundaries. Here, the no-slip condition repulses plastic deformation. For the smaller specimens, the plastic strain penetrates deeper in the y-direction, a larger domain of the specimen undergoes plastic deformation. It is the nonlocal interaction that causes the plastic region to widen in the y-direction for the smaller specimen. For the two largest specimens, the differences in the penetration depths are negligible, which corresponds well to the similar peak load for these two sizes.

Highly localized failure modes are observed for the two largest sizes in the post-peak part of the deformation process, see Fig. 7.20. These failure patterns are localized shear bands that initiate at the weak spot and extend over approximately one half of the specimens' width D at two thirds of peak load (in the post-peak range). The width of these shear bands is approximately the same for the two largest specimens, which is why the post-peak response is more brittle for the XXL specimen.

The four smaller sizes show some narrowing of the plastic zone, which initially extends over the whole specimen length, but a clear localized failure mode cannot be observed. The interaction radius R and the possible localized failure mode is too big compared to the size of the specimen.

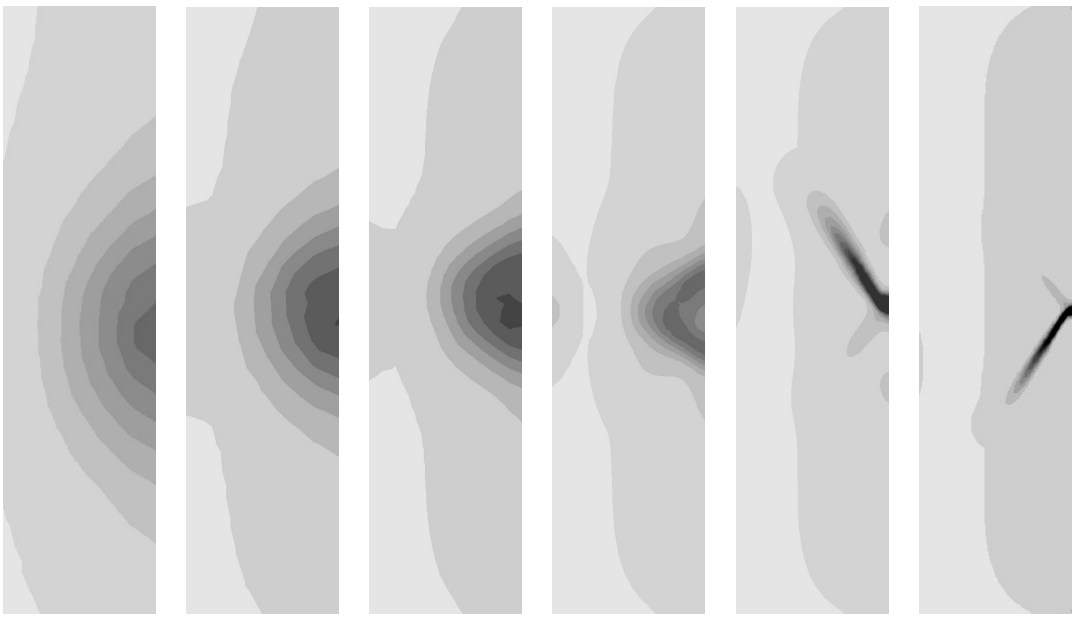

Figure 7.20: Local hardening variable κ at two thirds of peak load in the post-peak regime, plotted in the range 1×10^{-4} to 2×10^{-2}.

Chapter 8

Nonlocal Rankine plasticity with examples

8.1 Nonlocal Rankine plasticity model

This chapter explores basic properties of the nonlocal extension due to Vermeer and Brinkgreve (1994) applied to a plasticity model based on the Rankine yield function (Rankine 1858). The Rankine plasticity model is chosen as a test case, because it is the simplest plasticity model for tensile failure. The model is formulated for *plane stress* conditions, which simplifies the stress return algorithm.

The Rankine yield surface plotted in principal stress space has a corner, see Fig. 8.1, which complicates the formulation of the flow rule in the common plasticity format using one yield function. It is advantageous to formulate the yield surface as the intersection of two yield surfaces; for a detailed description of multi-surface plasticity, refer to Jirásek and Bažant (2002, Chapter 20).

For plane stress, the two yield functions

$$f_1(\boldsymbol{\sigma}, \sigma_{\mathrm{Y}}) = \sigma_1(\boldsymbol{\sigma}) - \sigma_{\mathrm{Y}} \tag{8.1}$$

$$f_2(\boldsymbol{\sigma}, \sigma_{\mathrm{Y}}) = \sigma_2(\boldsymbol{\sigma}) - \sigma_{\mathrm{Y}} \tag{8.2}$$

describe the Rankine yield function in a two-surface format. In the above, σ_1 and σ_2 are the principal values of the stress tensor $\boldsymbol{\sigma}$. Plastic yielding is initiated when the maximum principal stress reaches the tensile stress σ_{Y}. Except for the case of equibiaxial stress, when both principal values are equal, the value of the second principal stress does not have any influence on the yielding process. Compressive failure cannot be modeled with the Rankine yield surface.

An associated plasticity model uses the yield function as the flow potential, i.e. the flow direction is the derivative of the yield function with respect to the stress. In the context of multi-surface plasticity, the associated flow rule reads

$$\dot{\boldsymbol{\varepsilon}}_{\mathrm{p}} = \sum_{k=1}^{n} \dot{\lambda}_k \frac{\partial f_k(\boldsymbol{\sigma}, \sigma_{\mathrm{Y}})}{\partial \boldsymbol{\sigma}} \tag{8.3}$$

In general, a multi-surface plasticity model with n independent yield functions contains n plastic multipliers $\dot{\lambda}_k$ and the same number of sets of loading-unloading conditions. Here,

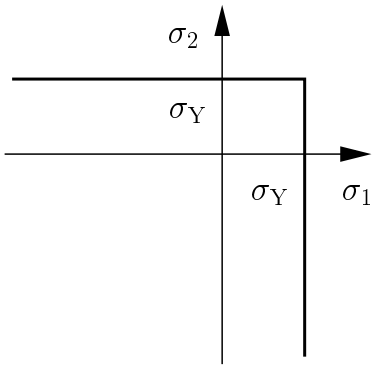

Figure 8.1: Rankine yield surface in principal stress space.

the model has two yield functions, and the associated flow rule gives

$$\begin{aligned} \dot{\boldsymbol{\varepsilon}}_{\mathrm{p}} &= \dot{\lambda}_1 \frac{\partial f_1}{\partial \sigma_1} \frac{\partial \sigma_1}{\partial \boldsymbol{\sigma}} + \dot{\lambda}_2 \frac{\partial f_2}{\partial \sigma_2} \frac{\partial \sigma_2}{\partial \boldsymbol{\sigma}} \\ &= \dot{\lambda}_1 \, \boldsymbol{n}_1 \otimes \boldsymbol{n}_1 + \dot{\lambda}_2 \, \boldsymbol{n}_2 \otimes \boldsymbol{n}_2 \end{aligned} \tag{8.4}$$

where $\boldsymbol{n}_1$ and $\boldsymbol{n}_2$ are the two normalized eigenvectors of the stress tensor, and $\otimes$ denotes the dyadic product of two vectors. Since the model has two plastic multipliers, the two sets of loading-unloading conditions

$$\dot{\lambda}_1 \geq 0, \qquad f_1(\boldsymbol{\sigma}, \sigma_{\mathrm{Y}}) \leq 0, \qquad \dot{\lambda}_1 f_1(\boldsymbol{\sigma}, \sigma_{\mathrm{Y}}) = 0 \tag{8.5}$$

$$\dot{\lambda}_2 \geq 0, \qquad f_2(\boldsymbol{\sigma}, \sigma_{\mathrm{Y}}) \leq 0, \qquad \dot{\lambda}_2 f_2(\boldsymbol{\sigma}, \sigma_{\mathrm{Y}}) = 0 \tag{8.6}$$

must be respected.

The evolution of the hardening variable κ that controls the yield stress $\sigma_{\mathrm{Y}} = h(\kappa)$ in the local model is given by the norm of the plastic strain rate

$$\dot{\kappa} = \|\dot{\boldsymbol{\varepsilon}}_{\mathrm{p}}\| = \sqrt{\left(\dot{\lambda}_1\right)^2 + \left(\dot{\lambda}_2\right)^2} \tag{8.7}$$

which, for the adopted flow rule, depends only on the rates of the plastic multipliers. The yield surface evolves isotropically in both directions of the principal stress space. The linear elastic stress-strain relation

$$\boldsymbol{\sigma} = \boldsymbol{D} : (\boldsymbol{\varepsilon} - \boldsymbol{\varepsilon}_{\mathrm{p}}) \tag{8.8}$$

where $\boldsymbol{D}$ is the elastic stiffness tensor for plane stress, completes the description of the local model.

The nonlocal extension of the Rankine plasticity model is based on the modified softening law (Vermeer and Brinkgreve 1994)

$$\sigma_{\mathrm{Y}} = h(\hat{\kappa}) \tag{8.9}$$

with the softening variable $\hat{\kappa}$ defined as

$$\hat{\kappa} = m\bar{\kappa} + (1 - m)\kappa \tag{8.10}$$

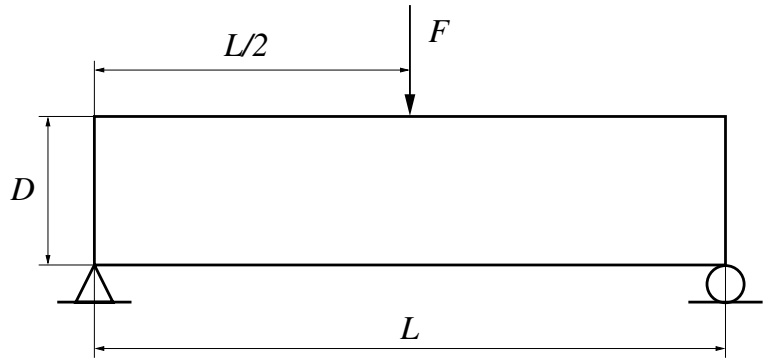

Figure 8.2: Structural model for the three-point bending test.

For a detailed analysis in the one-dimensional setting, cf. Sec. 4.3. With this approach, only a pure softening law can be used, i.e. combined hardening and softening is excluded. Regarding parameter m, the three cases $m = 0$ (local model), $m = 1$ (basic nonlocal model), and $m = 2$ (nonlocal model) are compared. Softening is modeled with the exponential function

$$\sigma_{\mathrm{Y}} = h(\hat{\kappa}) = \sigma_0 \exp\left(-\frac{\hat{\kappa}}{\kappa_{\mathrm{c}}}\right) \tag{8.11}$$

where σ_0 is the initial tensile yield stress and κ_{c} controls the slope of the softening curve, see Fig. 2.4b.

The stress return algorithm uses a backward Euler difference scheme for the time discretization and follows the concept described in Chapter 6.

8.2 Three-point bending test

8.2.1 Test geometry and model parameters

As a simple test case, a beam under three-point bending is analyzed. The beam of length $L = 850\,\mathrm{mm}$ and depth $D = 200\,\mathrm{mm}$ is supported and loaded as depicted in Fig. 8.2. Three-point bending of concrete is dominated by tensile failure, which can be correctly captured by the Rankine yield criterion. The beam is modeled as a plane stress problem, assuming that the out-of-plane stresses can be neglected. This assumption is valid if the width of the beam is small compared to the other dimensions.

For the numerical solution, the structure is discretized by linear quadrilateral finite elements. The discretization is refined in the center of the beam, where plastic yielding is expected to start. To detect possible mesh-induced directional bias, the mesh lines in the refined region are not oriented in the direction of the expected process zone, but inclined at an angle of 14^{o}, see Fig. 8.3. The density is chosen such that the interaction radius R covers approximately one element for the coarse mesh, three elements for the medium, and nine for the fine mesh.

Since the aim of this simulation series are qualitative results, the material parameters are not fitted to a specific concrete, but simply chosen as realistic values. The elastic constants are set to $E = 25\,\mathrm{GPa}$ and $\nu = 0.2$. The parameters of the softening law are set to $\sigma_0 = 2.8\,\mathrm{MPa}$ (the uniaxial tensile strength) and $\kappa_{\mathrm{c}} = 6 \times 10^{-4}$. The weighted average is

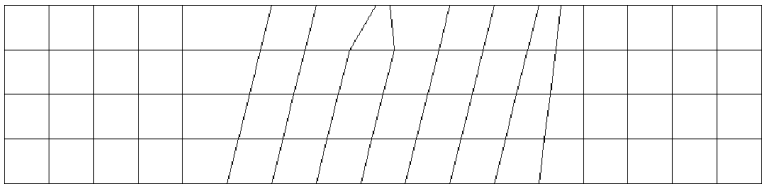

coarse

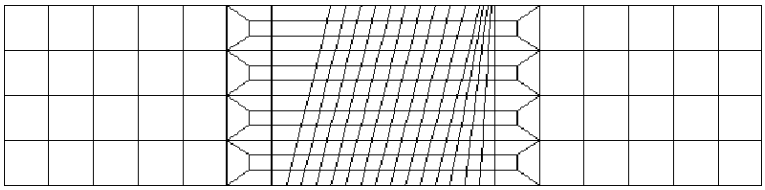

medium

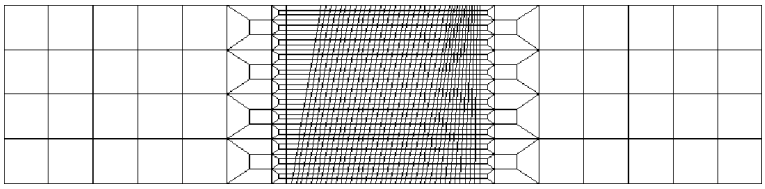

fine

Figure 8.3: Three discretizations with linear plane stress quadrilateral finite elements.

computed with the bell-shaped polynomial function, Eq. (2.17), with an interaction radius of $R = 50\,\mathrm{mm}$. For $m = 2$, the fracture energy in uniaxial tensile failure is realistic for these parameters of the softening law; for $m = 1$ and for the local model with $m = 0$, the response is expected to be more brittle.

For the load-displacement diagrams, load and displacement are normalized with their values at the elastic limit load, computed with the beam theory. The applied load per unit thickness is divided by the elastic limit load per unit thickness $F_{\mathrm{el}} = 2\sigma_0 D^2/(3L)$. The displacement of the point where the load is applied is normalized with its value at the elastic limit, $d_{\mathrm{el}} = \sigma_0 L^2/(6ED)$. The load-displacement response and the distribution of κ for the local model are presented in Figures 8.4 and 8.5; for the nonlocal model with $m = 1$, see Figures 8.6 and 8.7; for the nonlocal model with $m = 2$, see Figures 8.8 and 8.9. The local softening variable κ is plotted in a raw fashion, i.e. the value at one Gauss point determines the uniform grey shade of the corresponding quarter of the quadrilateral. This is preferred to the application of a smoothing algorithm, because localization of κ into one layer of finite elements can be easily recognized.

8.2.2 Discussion

For the local material model ($m = 0$), the load-displacement response depends strongly on the discretization, see Fig. 8.4. With mesh refinement, the response tends from ductile to brittle. This is due to the fact that the plastic strain localizes into one layer of finite elements, see Fig. 8.5, and the total fracture energy decreases when the size of this finite element layer is reduced. The mesh lines constitute preferential directions for the evolution

of the process zone. Plastic strain clearly develops along these mesh lines, and the global failure mode is wrongly predicted.

The basic nonlocal model ($m = 1$) gives significantly better results. With mesh refinement, the load-displacement response converges, see Fig. 8.6. The slightly more ductile response of the medium mesh compared to the fine mesh is probably due to the fact that the linear finite elements introduce nonnegligible constraints. As expected on the grounds of the one-dimensional analysis, plastic strain is highly localized, see Fig. 8.7. Regarding the numerical solution, this leads to a poor convergence rate in the global iteration for equilibrium. Compared to the local model, plastic flow is nevertheless much less attracted by the mesh lines.

For the regularized nonlocal model ($m = 2$), the mesh refinement has little influence on the load-displacement response for the medium and fine mesh, see Fig. 8.8. The coarse mesh is not sufficiently fine to fully activate the nonlocal interaction, and leads to results which are too stiff. The response is significantly more ductile than for the basic nonlocal model with $m = 1$, due to the fact that κ_c is the same for both models, but the equivalent width of the plastic zone is not. To dissipate the same energy, the models should use different values of κ_c.

Regarding the distribution of κ, there is no significant difference between the results obtained on the two finer meshes, see Fig. 8.9, but the coarse mesh gives almost the same response as the local material model. For the two finer meshes, the width of the plastic region is approximately $1.5\,R$ and does not depend in a spurious manner on the discretization.

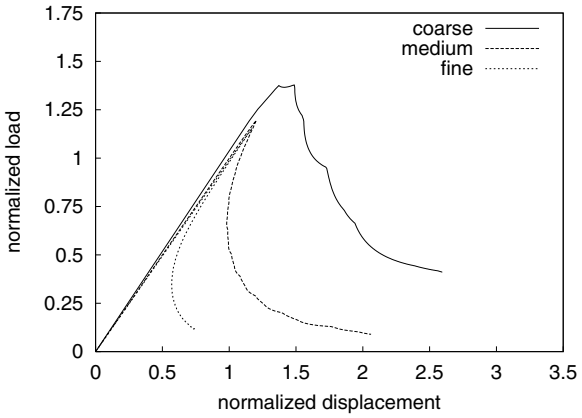

Figure 8.4: Load-displacement diagram for the local model ($m = 0$).

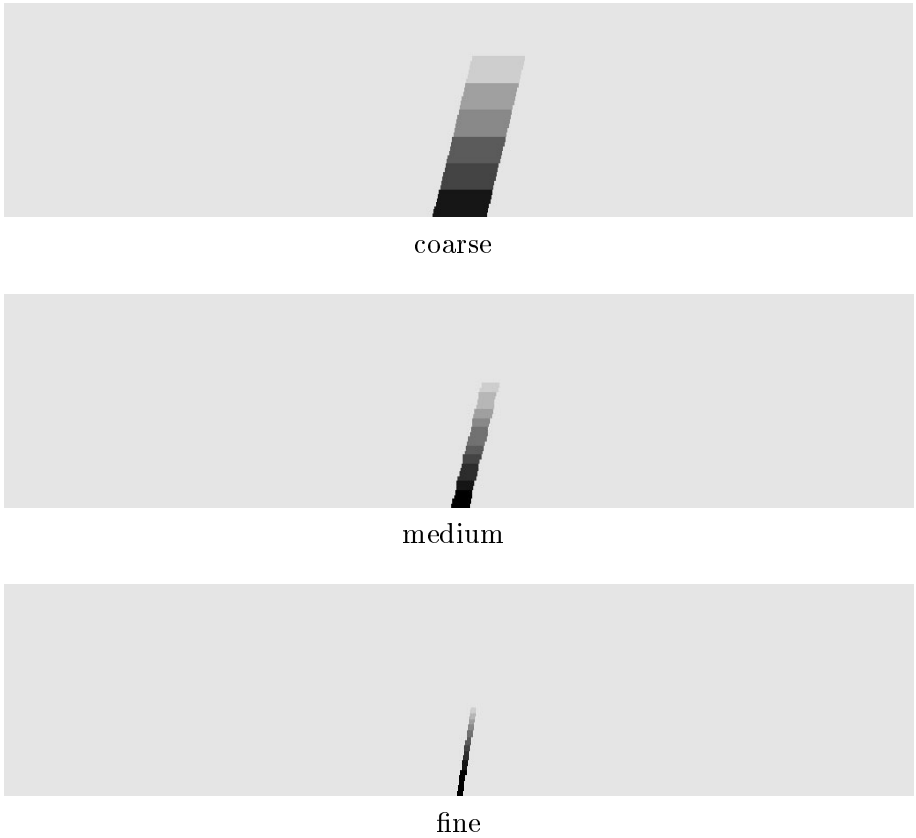

Figure 8.5: Local model: Distribution of the local softening variable κ at one third of peak load in the post-peak regime, plotted in the range 1×10^{-4} to 3×10^{-3}.

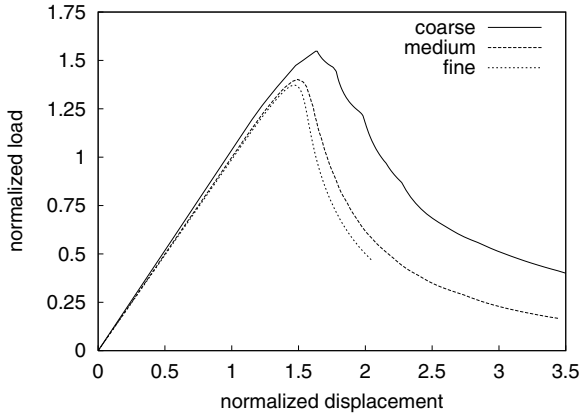

Figure 8.6: Load-displacement diagram for the basic nonlocal model ($m = 1$).

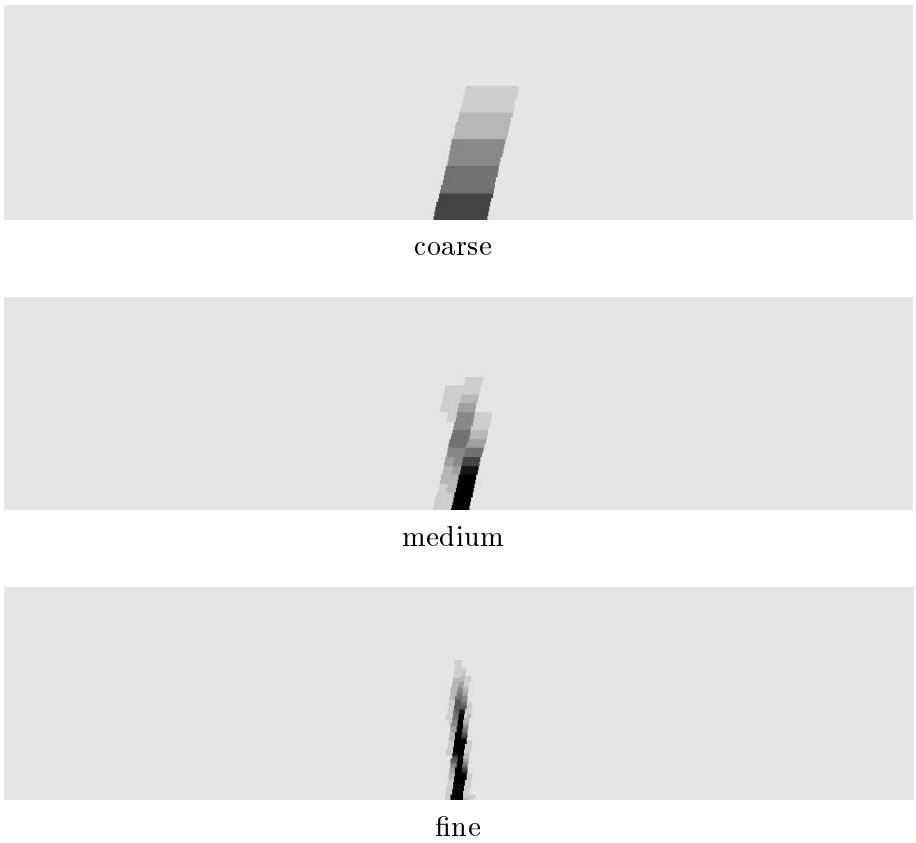

Figure 8.7: Basic nonlocal model ($m = 1$): Distribution of the local softening variable κ at one half of peak load in the post-peak regime, plotted in the range 1×10^{-4} to 3×10^{-3}.

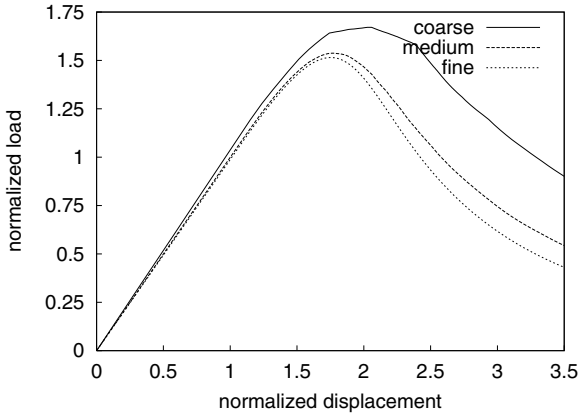

Figure 8.8: Load-displacement diagram for the nonlocal model ($m = 2$).

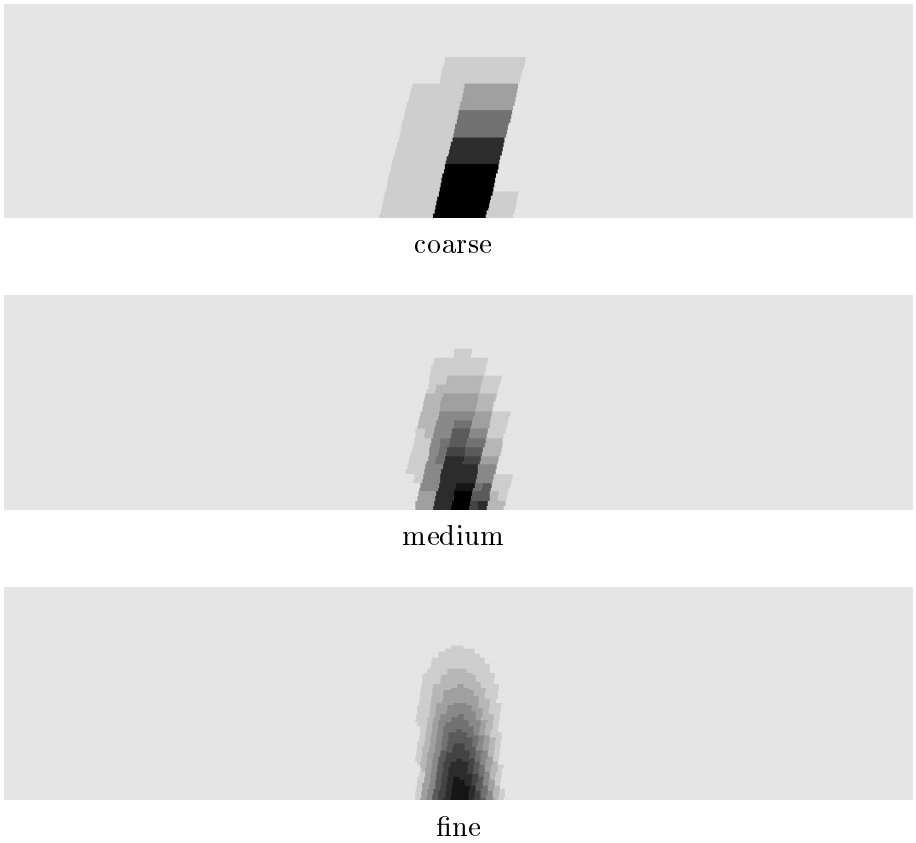

Figure 8.9: Nonlocal model ($m = 2$): Distribution of the local softening variable κ at one half of peak load in the post-peak regime, plotted in the range 1×10^{-4} to 3×10^{-3}.

Chapter 9

Conclusions

Localized failure is a common phenomenon in engineering practice. For concrete structures, failure is typically preceded by macroscopic cracking. In geomaterials, compressive failure is accompanied by the formation of shear bands. Metals can develop adiabatic shear bands under fast inelastic deformation. The characteristic size of the deformation patterns is a material property related to the size and spacing of major heterogeneities.

Physical modeling of localized failure is a difficult task because it involves the description of these zones of highly localized deformations. The localization of strain is caused by the fact that the stress transmitted by the material reduces with increasing deformation. This so-called strain softening has to be taken into account by the material model.

A continuum model for the description of materials that experience strain softening must contain a parameter with the dimension of length. This length scale is related to the size and spacing of major heterogeneities, which control the typical size of the localized patterns. The length scale can be incorporated into a continuum model by the use of higher-order gradients or weighted spatial averages.

In the context of plasticity, it is particularly attractive to introduce the nonlocality through gradients or weighted spatial averages of the hardening variable. The initial elastic response remains unchanged, because the nonlocality is linked to the inelastic deformation. The nonlocal part of the model is activated only after the onset of yielding, which is appropriate for typical engineering applications.

A detailed one-dimensional analysis of a large number of existing nonlocal models in Chapters 3 and 4 shows that a model suitable for the complete failure process should be selected with great care. At the initial bifurcation, most models predict the response in a physically reasonable manner. But for certain models, the localized zone of plastic deformation expands at later stages of the loading process, which leads to high residual stresses. For these models, failure of the bar is achieved only when the whole bar is yielding, which is physically inappropriate.

Two models sharing similar features are selected for further development: the integral-type formulation of the ductile damage model and the Vermeer–Brinkgreve model. Both models introduce nonlocality by use of a yield stress that depends in a suitable way on the local and nonlocal hardening variable. For softening, both models lead to a plastic zone of finite size controlled by the length scale. In the original format of the ductile damage model, the nonlocal quantity was obtained as the solution of a Helmholtz-type differential equation. Such implicit gradient models can be written in a mathematically

equivalent format as integral-type nonlocal models. In the integral format, which was used by the Vermeer–Brinkgreve model, the nonlocal hardening variable is obtained as the weighted spatial average of the local hardening variable. Despite these similarities, the implementation in a finite element program differs significantly for implicit gradient and integral-type nonlocal models. For the latter, the weighted spatial averages need to be computed at the Gauss points, and for plasticity models, the stress-return algorithm has to be modified. For implicit gradient models, additional degrees of freedom must be introduced for the solution of the weak form of the Helmholtz-type differential equation. In this thesis, the numerical solution is constructed using an integral format.

A bifurcation analysis for hardening revealed that the Vermeer–Brinkgreve model admits irregular solutions in this case, while the ductile damage model is regular under certain mild conditions. These conditions concern additional parameters introduced by the nonlocal hardening law, and they can be respected without limiting the range of application. Only the ductile damage model can be used for the description of both hardening and softening.

For two-dimensional deformation under plane strain conditions, localization can occur due to non-associated flow even in the hardening range. A bifurcation analysis for this case resulted in necessary conditions for regular solutions. The size and shape of the initial plastic profile were obtained from a scalar rate equation, which has a similar structure as in the one-dimensional case.

The application of the proposed nonlocal enhancement to two- or three-dimensional plasticity models is straightforward, because the only equation that changes compared to the local model is the hardening law used to compute the yield stress. To illustrate the technique, the concept was applied to Rankine plasticity and Drucker–Prager plasticity This choice includes tensile and compressive failure.

For nonlocal plasticity models written in an integral format, the key part of the numerical algorithm is the stress return, because it involves the solution of a nonlinear complementarity problem. It is solved by a Jacobi-like iterative technique, which is developed in a rigorous manner for the special case of the Drucker–Prager model with softening, and extended to the general nonlinear case with hardening and complex yield criteria based on a physical interpretation of the resulting equations. In an object-oriented programming environment, the format of the algorithm makes it possible to reuse the implementation for the local stress return in its original format. The experience acquired with the employed material models shows that the algorithm is robust and efficient.

Simulations of laboratory tests with the different nonlocal plasticity models include biaxial, triaxial, and eccentric compression under plane strain conditions, and three-point bending under plane stress. The tests were chosen to demonstrate the main features of the nonlocal concept:

- Regular description of localization due to softening and non-associated flow.
- No spurious dependence of dissipated energy or size of the plastic zone on the computational grid.
- Prediction of size effect on structural strength and on post-peak response.
- Suitability for tension and compression.

Several aspects of this nonlocal model could be explored in future work. The concept of nonlocal enhancement could be applied to a more realistic material model for concrete, such as the modified Leon-model (Etse and Willam 1994). Regarding the additional parameters introduced by the nonlocal model, a rigorous procedure for their calibration to the results of standard experiments should be developed. Another challenge would be to apply the integral-type nonlocal enhancement to a local plasticity model formulated for finite deformations.

References

Aifantis, E. C. (1984). On the microstructural origin of certain inelastic models. *Journal of Engineering Materials and Technology, ASME 106*, 326–330.

Aifantis, E. C. (1992). On the role of gradients in the localization of deformation and fracture. *International Journal of Engineering Science 30*, 1279–1299.

Aifantis, E. C. (1995). Pattern formation in plasticity. *International Journal of Engineering Science 33*, 2161–2178.

Aifantis, E. C. and J. B. Serrin (1983). Equilibrium solutions in the mechanical theory of fluid microstructures. *Journal of Colloid and Interface Science 96*, 530–547.

Baker, C. T. H. (1977). *The Numerical Treatment of Integral Equations*. Oxford: Clarendon Press.

Bažant, Z. P. (1976). Instability, ductility, and size effect in strain-softening solids. *Journal of the Engineering Mechanics Division, ASCE 102*, 331–344.

Bažant, Z. P. (1988). Stable states and paths of structures with plasticity or damage. *Journal of Engineering Mechanics, ASCE 114*, 2013–2034.

Bažant, Z. P. and L. Cedolin (1991). *Stability of Structures*. New York and Oxford: Oxford University Press.

Bažant, Z. P. and T.-P. Chang (1984). Instability of nonlocal continuum and strain averaging. *Journal of Engineering Mechanics, ASCE 110*, 2015–2035.

Bažant, Z. P. and M. Jirásek (2002). Nonlocal integral formulations of plasticity and damage: Survey of progress. *Journal of Engineering Mechanics, ASCE 128*(10).

Bažant, Z. P. and F.-B. Lin (1988). Nonlocal yield-limit degradation. *International Journal for Numerical Methods in Engineering 26*, 1805–1823.

Bažant, Z. P. and P. A. Pfeiffer (1986). Shear fracture tests of concrete. *Materials and Structures 19*, 111–121.

Bažant, Z. P. and P. A. Pfeiffer (1987). Determination of fracture energy from size effect and brittleness number. *ACI Materials Journal 84*, 463–480.

Bažant, Z. P. and J. Planas (1998). *Fracture and Size Effect in Concrete and Other Quasibrittle Materials*. Boca Raton: CRC Press.

Benvenuti, E. and A. Tralli (2003). Iterative LCP solvers for nonlocal loading-unloading conditions. *International Journal for Numerical Methods in Engineering*. Submitted.

Borino, G. (2001, August). Private communication to M. Jirásek.

Borino, G. and B. Failla (2000). Thermodynamically consistent plasticity models with local and nonlocal internal variables. In *European Congress on Computational Methods in Applied Sciences and Engineering*, Barcelona, pp. 1–11. ECCOMAS. CD-ROM.

Borino, G., P. Fuschi, and C. Polizzotto (1999). A thermodynamic approach to nonlocal plasticity and related variational approaches. *Journal of Applied Mechanics, ASME 66*, 952–963.

Borino, G. and C. Polizzotto (1999). Comments on Nonlocal bar revisited by Christer Nilsson. *International Journal of Solids and Structures 36*, 3085–3091.

Brinkgreve, R. B. J. (1994). *Geomaterial Models and Numerical Analysis of Softening*. Ph. D. thesis, Delft University of Technology, The Netherlands.

Burtscher, S. (2002). *Size effect of concrete and sandstone in compression*. Ph. D. thesis, Technical University Vienna, Vienna, Austria.

Burzyński, W. (1929). Über die Anstrengungshypothesen. *Schweizerische Bauzeitung, Zürich 94*, 259.

Chambon, R., D. Caillerie, and N. E. Hassan (1998). One-dimensional localisation studied with a second grade model. *European Journal of Mechanics/A: Solids 17*, 637–656.

Coleman, B. D. and M. L. Hodgdon (1985). On shear bands in ductile materials. *Archive for Rational Mechanics and Analysis 90*, 219–247.

Comi, C. and U. Perego (1996). A generalized variable formulation for gradient dependent softening plasticity. *International Journal for Numerical Methods in Engineering 39*, 3731–3755.

de Borst, R. and A. E. Groen (1995). Some observations on element performance in isochoric and dilatant plastic flow. *International Journal for Numerical Methods in Engineering 38*, 2887–2906.

de Borst, R. and H. B. Mühlhaus (1992). Gradient-dependent plasticity: Formulation and algorithmic aspects. *International Journal for Numerical Methods in Engineering 35*, 521–539.

de Borst, R. and J. Pamin (1996). Some novel developments in finite element procedures for gradient-dependent plasticity. *International Journal for Numerical Methods in Engineering 39*, 2477–2505.

Dillon, O. W. and J. Kratochvil (1970). A strain gradient theory of plasticity. *International Journal of Solids and Structures 6*, 1513–1533.

Drucker, D. C. and W. Prager (1952). Soil mechanics and plasticity analysis of limit design. *Quarterly of Applied Mathematics 10*, 157–162.

Duhem, P. (1893). Le potentiel thermodynamique et la pression hydrostatique. *Annales Scientifiques de l'Ecole Normale Supérieure 10*, 183–230.

Edelen, D. G. B. and N. Laws (1971). On the thermodynamics of systems with nonlocality. *Archive for Rational Mechanics and Analysis 43*, 24–35.

Engelen, R. A. B., M. G. D. Geers, and F. P. T. Baaijens (2003). Nonlocal implicit gradient-enhanced elasto-plasticity for the modelling of softening behaviour. *International Journal of Plasticity 19*, 403–433.

Eringen, A. C. (1966). A unified theory of thermomechanical materials. *International Journal of Engineering Science 4*, 179–202.

Eringen, A. C. (1981). On nonlocal plasticity. *International Journal of Engineering Science 19*, 1461–1474.

Eringen, A. C. (1983). Theories of nonlocal plasticity. *International Journal of Engineering Science 21*, 741–751.

Eringen, A. C. and N. Ari (1983). Nonlocal stress field at a Griffith crack. *Crystal Lattice Defects and Amorphous Materials 10*, 33–38.

Etse, G. and K. J. Willam (1994). A fracture-energy based constitutive formulation for inelastic behavior of plain concrete. *Journal of Engineering Mechanics, ASCE 120*, 1983–2011.

Fleck, N. A. and J. W. Hutchinson (1993). A phenomenological theory for strain gradient effects in plasticity. *Journal of the Mechanics and Physics of Solids 41*, 1825–1857.

Fleck, N. A. and J. W. Hutchinson (1997). Strain gradient plasticity. In J. W. Hutchinson and T. Y. Wu (Eds.), *Advances in Applied Mechanics*, Volume 33, pp. 295–361. New York: Academic Press.

Fleck, N. A., G. M. Muller, M. F. Ashby, and J. W. Hutchinson (1994). Strain gradient plasticity: theory and experiment. *Acta Metallurgica et Materialia 42*, 475–487.

Gao, H., Y. Huang, W. D. Nix, and J. W. Hutchinson (1999). Mechanism-based strain gradient plasticity—I. Theory. *Journal of the Mechanics and Physics of Solids 47*, 1239–1263.

Geers, M. (2003). Finite strain logarithmic hyperelasto-plasticity with softening: a strongly nonlocal implicit gradient framework. *Computer Methods in Applied Mechanics and Engineering*. in press.

Geers, M., R. Ubachs, and R. Engelens (2003). Strongly nonlocal gradient-enhanced finite strain elastoplasticity. *International Journal for Numerical Methods in Engineering 56(14)*, 2039–2068.

Geers, M. G. D., R. A. B. Engelen, and R. J. M. Ubachs (2001). On the numerical modelling of ductile damage with an implicit gradient-enhanced formulation. *Revue européenne des éléments finis 10*, 173–191.

Görtler, H. (1975). *Dimensionsanalyse*. Berlin: Springer.

Green, A. E. and P. M. Naghdi (1965). A general theory of an elastic-plastic continuum. *Archive for Rational Mechanics and Analysis 18*, 251–281.

Gurson, A. L. (1977). Continuum theory of ductile rupture by void nucleation and growth—I. Yield criteria and flow rules for porous ductile media. *Journal of Engineering Materials and Technology, ASME 99*, 2–15.

Huang, Y., H. Gao, W. D. Nix, and J. W. Hutchinson (2000). Mechanism-based strain gradient plasticity—II. Analysis. *Journal of the Mechanics and Physics of Solids 48*, 99–128.

Jirásek, M. (1998). Nonlocal models for damage and fracture: Comparison of approaches. *International Journal of Solids and Structures 35*, 4133–4145.

Jirásek, M. and Z. P. Bažant (2002). *Inelastic Analysis of Structures*. Chichester: John Wiley and Sons.

Jirásek, M. and S. Rolshoven (2003). Comparison of integral-type nonlocal plasticity models for strain-softening materials. *International Journal of Engineering Science 41*, 1553–1602.

Jirásek, M., S. Rolshoven, and P. Grassl (2003). Numerical modeling of size effect of fracture energy of concrete. *International Journal of Numerical and Analytical Methods in Geomechanics*. Accepted.

Kröner, E. (1966). Continuum mechanics and range of atomic cohesion forces. In T. Yokobori, T. Kawasaki, and J. Swedlow (Eds.), *Proceedings of the First International Conference on Fracture*, Sendai, Japan, pp. 27–?? Japanese Society for Strength and Fracture of Materials.

Kunin, I. A. (1966). Theory of elasticity with spatial dispersion (in Russian). *Prikladnaja Matematika i Mechanika 30*, 866–??

Lakes, R. S. (1986). Experimental microelasticity of two porous solids. *International Journal of Solids and Structures 22*, 55–63.

Leblond, J. B., G. Perrin, and J. Devaux (1994). Bifurcation effects in ductile metals with nonlocal damage. *Journal of Applied Mechanics, ASME 61*, 236–242.

Li, X. and S. Cescotto (1996). Finite element method for gradient plasticity at large strains. *International Journal for Numerical Methods in Engineering 39*, 619–633.

Ma, Q. and D. R. Clarke (1995). Size dependent hardness in silver single crystals. *Journal of Materials Research 10*, 853–863.

Mindlin, R. D. (1964). Micro-structure in linear elasticity. *Archive for Rational Mechanics and Analysis 16*, 51–78.

Mindlin, R. D. (1965). Second gradient of strain and surface tension in linear elasticity. *International Journal of Solids and Structures 1*, 417–438.

Moreau, J. J. (1970). Sur les lois de frottement, de viscosité et de plasticité. *Comptes Rendus de l'Académie des Sciences, Paris 271*, 608–611.

Morrison, J. L. M. (1939). The yield of mild steel with particular reference to the effect of size of specimen. *Proceedings of the Institute of Mechanical Engineers 142*, 193–223.

Mühlhaus, H. B. and E. C. Aifantis (1991). A variational principle for gradient plasticity. *International Journal of Solids and Structures 28*, 845–858.

Naghdi, P. M. and J. A. Trapp (1975). The significance of formulating plasticity theory with reference to loading surfaces in strain space. *International Journal of Engineering Science 13*, 785–797.

Needleman, A. and V. Tvergaard (1998). Dynamic crack growth in a nonlocal progressively cavitating solid. *European Journal of Mechanics/A: Solids 17*, 421–438.

Nilsson, C. (1994). *On nonlocal plasticity, strain softening and localization.* Report TVSM-1007, Division of Structural Mechanics, Lund Institute of Technology, Lund, Sweden.

Nilsson, C. (1997). Nonlocal strain softening bar revisited. *International Journal of Solids and Structures 34*, 4399–4419.

Nilsson, C. (1999). Author's closure. *International Journal of Solids and Structures 36*, 3093–3100.

Nix, W. D. (1989). Mechanical properties of thin films. *Metallurgical Transactions 20A*, 2217–2245.

Nix, W. D. and H. Gao (1998). Indentation size effects in crystalline materials: A law for strain gradient plasticity. *Journal of the Mechanics and Physics of Solids 46*, 411–425.

Noll, W. (1972). A new mathematical theory of simple materials. *Archive for Rational Mechanics and Analysis 48*, 1–50.

Ottosen, N. and K. Runesson (1991). Properties of bifurcation solutions in elasto-plasticity. *International Journal of Solids and Structures 27*, 410–421.

Pamin, J. (1994). *Gradient-dependent plasticity in numerical simulation of localization phenomena.* Ph. D. thesis, Delft University of Technology, Delft, The Netherlands.

Patzák, B. and Z. Bittnar (2001). Design of object oriented finite element code. *Advances in Engineering Software 32*, 759–767.

Peerlings, R. H. J., R. de Borst, W. A. M. Brekelmans, and J. H. P. de Vree (1996). Gradient-enhanced damage for quasi-brittle materials. *International Journal for Numerical Methods in Engineering 39*, 3391–3403.

Peerlings, R. H. J., R. de Borst, W. A. M. Brekelmans, and M. G. D. Geers (1998). Gradient enhanced damage modelling of concrete fracture. *Mechanics of Cohesive-Frictional Materials 3*, 323–342.

Peerlings, R. H. J., M. G. D. Geers, R. de Borst, and W. A. M. Brekelmans (2001). A critical comparison of nonlocal and gradient-enhanced softening continua. *International Journal of Solids and Structures 38*, 7723–7746.

Pijaudier-Cabot, G. and Z. P. Bažant (1987). Nonlocal damage theory. *Journal of Engineering Mechanics, ASCE 113*, 1512–1533.

Planas, J., M. Elices, and G. V. Guinea (1993). Cohesive cracks versus nonlocal models: Closing the gap. *International Journal of Fracture 63*, 173–187.

Planas, J., M. Elices, and G. V. Guinea (1994). Cohesive cracks as a solution of a class of nonlocal models. In Z. P. Bažant, Z. Bittnar, M. Jirásek, and J. Mazars (Eds.), *Fracture and Damage in Quasibrittle Structures*, London, pp. 131–144. E&FN Spon.

Planas, J., G. V. Guinea, and M. Elices (1996). Basic issues on nonlocal models: uniaxial modeling. Technical Report 96-jp03, Departamento de Ciencia de Materiales, ETS de Ingenieros de Caminos, Universidad Politécnica de Madrid, Ciudad Universitaria sn., 28040 Madrid, Spain.

Polizzotto, C., G. Borino, and P. Fuschi (1998). A thermodynamic consistent formulation of nonlocal and gradient plasticity. *Mechanics Research Communications 25*, 75–82.

Poole, W. J., M. F. Ashby, and N. A. Fleck (1996). Microhardness of annealed and work-hardened copper polycrystals. *Scripta Metallurgica et Materialia 34*, 559–564.

Qiu, X., Y. Huang, Y. Wei, H. Gao, and K. C. Hwang (2003). The flow theory of mechanism-based strain gradient plasticity. *Mechanics of Materials*. in press.

Ramaswamy, S. and N. Aravas (1998). Finite element implementation of gradient plasticity models. Part I: Gradient-dependent yield functions. *Computer Methods in Applied Mechanics and Engineering 163*, 11–32.

Rankine, W. J. M. (1858). *Manual of Applied Mechanics*. Glasgow.

Richards, C. W. (1958). Effects of size on the yielding of mild steel beams. *Proceedings of the American Society for Testing and Materials 58*, 955–970.

Rogula, D. (1965). Influence of spatial acoustic dispersion on dynamical properties of dislocations. I. *Bulletin de l'Académie Polonaise des Sciences. Série des sciences techniques 13*, 337–343.

Rogula, D. (1982). Introduction to nonlocal theory of material media. In D. Rogula (Ed.), *Nonlocal Theory of Material Media*, Number 268 in CISM Courses and Lectures, pp. 125–222. Wien and New York: Springer Verlag.

Rolshoven, S. and M. Jirásek (2001). Numerical aspects of a regularized plasticity model for strain-softening materials. In K. J. Bathe (Ed.), *Computational Fluid and Solid Mechanics*, Amsterdam. Elsevier. Proceedings of the first MIT Conference on Computational Fluid and Solid Mechanics, held in Cambridge, Massachusetts, USA, 12–15 June 2001.

Rudnicky, J. W. and J. R. Rice (1975). Conditions for the localization of deformation in pressure-sensitive dilatant materials. *Journal of the Mechanics and Physics of Solids 23*, 371–394.

Runesson, K., N. S. Ottosen, and D. Perić (1991). Discontinuous bifurcations of elastic-plastic solutions at plane stress and plane strain. *International Journal of Plasticity 7*, 99–121.

Rypl, D. (1998). *Sequential and Parallel Generation of Unstructured 3D Meshes*. Ph. D. thesis, Czech Technical University, Prague, Czech Republic.

Schreyer, H. and Z. Chen (1986). One-dimensional softening with localization. *Journal of Applied Mechanics, ASME 53*, 791–797.

Schreyer, H. L. (1990). Analytical solutions for nonlinear strain-gradient softening and localization. *Journal of Applied Mechanics, ASME 57*, 522–528.

Shi, M. X., Y. Huang, and K. C. Hwang (2000). Plastic flow localization in mechanism-based strain gradient plasticity. *International Journal of Mechanical Sciences 42*, 2115–2131.

Stolken, J. S. and A. G. Evans (1998). A microbend test method for measuring the plasticity length scale. *Acta Metallurgica et Materialia 46*, 5109–5115.

Strömberg, L. and M. Ristinmaa (1996). FE-formulation of a nonlocal plasticity theory. *Computer Methods in Applied Mechanics and Engineering 136*, 127–144.

Svedberg, T. (1996). A thermodynamically consistent theory of gradient-regularized plasticity coupled to damage. Licentiate thesis, Chalmers University of Technology.

Svedberg, T. and K. Runesson (1997). A thermodynamically consistent theory of gradient-regularized plasticity coupled to damage. *International Journal of Plasticity 13*, 669–696.

Svedberg, T. and K. Runesson (1998). Thermodynamically consistent nonlocal and gradient formulations of plasticity. In A. Brillard and J. F. Ganghoffer (Eds.), *Nonlocal Aspects in Solid Mechanics, EUROMECH Colloquium 378*, Mulhouse, France, pp. 32–37.

Toupin, R. A. (1962). Elastic materials with couple-stresses. *Archive for Rational Mechanics and Analysis 11*, 385–414.

Tvergaard, V. (1981). Influence of voids on shear band instabilities under plain strain conditions. *International Journal of Fracture 17*, 389–407.

Tvergaard, V. and A. Needleman (1984). Analysis of the cup-cone fracture in a round tensile bar. *Acta Metallurgica 32*, 157–169.

Tvergaard, V. and A. Needleman (1995). Effects of nonlocal damage in porous plastic solids. *International Journal of Solids and Structures 32*, 1063–1077.

van Mier, J. G. M. (1984). *Strain-softening of concrete under multiaxial loading conditions*. Ph. D. thesis, Technical University of Eindhoven, Eindhoven, The Netherlands.

Vardoulakis, I. and E. C. Aifantis (1991). A gradient flow theory of plasticity for granular materials. *Archives of Mechanics 87*, 197–217.

Vermeer, P. A. and R. B. J. Brinkgreve (1994). A new effective non-local strain measure for softening plasticity. In R. Chambon, J. Desrues, and I. Vardoulakis (Eds.), *Localisation and Bifurcation Theory for Soils and Rocks*, Rotterdam, pp. 89–100. Balkema.

Walsh, P. F. (1972). Fracture of plain concrete. *Indian Concrete Journal 46*, 469–470 and 476.

Zauderer, E. (1989). *Partial Differential Equations of Applied Mathematics* (2nd ed.). Chichester, U.K.: Wiley.

Zervos, A., P. Papanastasiou, and I. Vardoulakis (2001). A finite element displacement formulation for gradient elastoplasticity. *International Journal for Numerical Methods in Engineering 50*, 1369–1388.

Curriculum vitae

Simon ROLSHOVEN
May 4, 1973, Freiburg i.B., Germany

Work experience

Sep. 00 – Dec. 03	Research assistant and doctoral student at the *Laboratory of Structural and Continuum Mechanics*, *EPF Lausanne*, Switzerland.
Mar. 99 – Apr. 99	Two–month internship in Research & Development at *Hilti AG*, Schaan, Liechtenstein.
Apr. 97 – Mar. 99	Teaching assistant at the *Institute of Mechanics, Technical University Berlin (TU)*, Germany.
Feb. 95 – July 95	Six–month internship at *AN Maschinenbau*, Bremen, Germany.

University studies

Oct. 95 – July 00	Physikalische Ingenieurwissenschaft, *TU Berlin*, Germany. Specialized in continuum and structural mechanics, fluid dynamics.
Oct. 99 – July 00	Exchange student at the *Ecole Polytechnique*, Paris, France. Diplomarbeit "A mechanism of transition to turbulence in a three-dimensional boundary layer" at *LADHYX*.

Scholarships and Awards

Jan. 01	*Erwin–Stephan–Award* of *TU Berlin*.
Sep. 99 – July 00	Scholarship of *Dr.–Jürgen–Ulderup–Stiftung* and of *Fondation de l'X*.
Apr. 97 – July 00	Scholarship of *Studienstiftung (German National Merit Foundation)*.